



University of Kentucky  
UKnowledge

---

Theses and Dissertations--Chemical and  
Materials Engineering

Chemical and Materials Engineering

---

2013

## The Effects of Ceria Addition on Aging and Sulfation of Lean NO<sub>x</sub> Traps for Stand Alone and LNT-SCR Applications

Vencon G. Easterling  
*University of Kentucky*, [vencon23@aol.com](mailto:vencon23@aol.com)

[Right click to open a feedback form in a new tab to let us know how this document benefits you.](#)

---

### Recommended Citation

Easterling, Vencon G., "The Effects of Ceria Addition on Aging and Sulfation of Lean NO<sub>x</sub> Traps for Stand Alone and LNT-SCR Applications" (2013). *Theses and Dissertations--Chemical and Materials Engineering*. 17.

[https://uknowledge.uky.edu/cme\\_etds/17](https://uknowledge.uky.edu/cme_etds/17)

This Doctoral Dissertation is brought to you for free and open access by the Chemical and Materials Engineering at UKnowledge. It has been accepted for inclusion in Theses and Dissertations--Chemical and Materials Engineering by an authorized administrator of UKnowledge. For more information, please contact [UKnowledge@lsv.uky.edu](mailto:UKnowledge@lsv.uky.edu).

## **STUDENT AGREEMENT:**

I represent that my thesis or dissertation and abstract are my original work. Proper attribution has been given to all outside sources. I understand that I am solely responsible for obtaining any needed copyright permissions. I have obtained and attached hereto needed written permission statements(s) from the owner(s) of each third-party copyrighted matter to be included in my work, allowing electronic distribution (if such use is not permitted by the fair use doctrine).

I hereby grant to The University of Kentucky and its agents the non-exclusive license to archive and make accessible my work in whole or in part in all forms of media, now or hereafter known. I agree that the document mentioned above may be made available immediately for worldwide access unless a preapproved embargo applies.

I retain all other ownership rights to the copyright of my work. I also retain the right to use in future works (such as articles or books) all or part of my work. I understand that I am free to register the copyright to my work.

## **REVIEW, APPROVAL AND ACCEPTANCE**

The document mentioned above has been reviewed and accepted by the student's advisor, on behalf of the advisory committee, and by the Director of Graduate Studies (DGS), on behalf of the program; we verify that this is the final, approved version of the student's dissertation including all changes required by the advisory committee. The undersigned agree to abide by the statements above.

Vencon G. Easterling, Student

Dr. Stephen Rankin, Major Professor

Dr. Stephen Rankin, Director of Graduate Studies

THE EFFECTS OF CERIA ADDITION ON AGING AND SULFATION OF  
LEAN NO<sub>x</sub> TRAPS FOR STAND ALONE AND LNT-SCR APPLICATIONS

---

DISSERTATION

---

A dissertation submitted in partial fulfillment of the  
requirements for the degree of Doctor of Philosophy in the  
College of Engineering  
at the University of Kentucky

By  
Vencon Glenn Easterling

Lexington, Kentucky

Co-Directors: Dr. Mark Crocker, Professor of Chemistry and  
Dr. Stephen Rankin, Professor of Chemical and Materials Engineering

Lexington, Kentucky

2013

Copyright © Vencon Glenn Easterling 2013

## ABSTRACT OF DISSERTATION

### THE EFFECTS OF CERIA ADDITION ON AGING AND SULFATION OF LEAN NO<sub>x</sub> TRAPS FOR STAND ALONE AND LNT-SCR APPLICATIONS

Model powder and fully formulated monolithic lean NO<sub>x</sub> trap (LNT) catalysts were used to investigate the effect of ceria on desulfation behavior. Temperature-programmed reduction (TPR) experiments (model catalysts) showed each of the oxide phases present is able to store sulfur and possesses distinct behavior (temperature at which desulfation occurs). La-CeO<sub>2</sub> or CeO<sub>2</sub>-ZrO<sub>2</sub>-containing samples (monoliths) showed a greater resistance to deactivation during sulfation and required lower temperatures to restore the NO<sub>x</sub> storage efficiency to its pre-sulfation value.

Fully formulated monolithic LNT catalysts containing varying amounts of Pt, Rh and BaO were subjected to accelerated aging to elucidate the effect of washcoat composition on LNT aging. Elemental analysis revealed that residual sulfur, associated with the Ba phase, decreased catalyst NO<sub>x</sub> storage capacity and that sintering of the precious metals resulted in decreased contact between the Pt and Ba phases.

Spatially-resolved inlet capillary mass spectrometry (SpaciMS) was employed to understand the factors influencing the selectivity of NO<sub>x</sub> reduction in LNT catalysts (degreened and thermally aged) containing Pt, Rh, BaO and Al<sub>2</sub>O<sub>3</sub>, and in one case contained La-stabilized CeO<sub>2</sub>. Stretching of the NO<sub>x</sub> storage and reduction zone (NSR) zone resulted in increased selectivity to NH<sub>3</sub> due to the fact that less catalyst was available to consume NH<sub>3</sub> by either the NH<sub>3</sub>-NO<sub>x</sub> SCR reaction or the NH<sub>3</sub>-O<sub>2</sub> reaction. Additionally, the loss of oxygen storage capacity (OSC) and NO<sub>x</sub> storage sites, along with the decreased rate of NO<sub>x</sub> diffusion to Pt/Rh sites, led to an increase in the rate of propagation of the reductant front after aging, in turn, resulting in increased H<sub>2</sub>:NO<sub>x</sub> ratios at the Pt/Rh sites and consequently increased selectivity to NH<sub>3</sub>.

Finally, a crystallite scale model was used to predict selectivity to NH<sub>3</sub> from the LNT catalysts during rich conditions after a fixed amount of NO<sub>x</sub> was stored during lean conditions. Both the experimental and model predicted data showed that the production

of  $\text{NH}_3$  is limited by the rate of diffusion from the Ba storage sites to the Pt particles at  $200^\circ\text{C}$ . At  $300^\circ\text{C}$ , the process is limited by the rate at which  $\text{H}_2$  is fed to the reactor.

KEYWORDS: Lean  $\text{NO}_x$  Trap, Desulfation, Ceria, SpaciMS, Ammonia

Vencon Glenn Easterling

---

December 12th, 2012

---

THE EFFECTS OF CERIA ADDITION ON AGING AND SULFATION OF  
LEAN NO<sub>x</sub> TRAPS FOR STAND ALONE AND LNT-SCR APPLICATIONS

By

Vencon Glenn Easterling

Prof. Mark Crocker

---

Co-Director of Dissertation

Prof. Stephen Rankin

---

Co-Director of Dissertation  
and  
Director of Graduate Studies

December 12, 2012

---

Date

To My Family

## ACKNOWLEDGEMENTS

First and foremost I would like to thank Prof. Mark Crocker for his support and direction during the pursuit of my doctorate. I would also like to state my appreciation to him for encouraging me to change from master's to doctoral degree during my graduate studies.

I would also like to express my gratitude to Prof. Dibakar Bhattacharyya, Prof. Richard Kermode, Prof. Barbara Knutson, Prof. Stephen Rankin, and Mr. Bruce Cole for their help while I was considering returning to school after working in industry.

I would also like to recognize and credit the other members of my advisory committee: Prof. Yang-Tse Cheng and Prof. John Selegue both for their time and their helpful insight.

Thanks to Dr. Robert McCabe, Dr. Mark Dearth, Dr. Joseph Theis, Mr. Justin Ura, and others in the Research and Innovation Center (RIC) at the Ford Motor Company and Dr. Todd Toops, Dr. Jae-Soon Choi, and Dr. William Partridge, and others at the Fuels, Engines and Emissions Research Center (FEERC) at Oak Ridge National Laboratory. I was extremely fortunate to have the opportunity to conduct the majority of my research at these facilities. The experience I gained at both of these centers is immeasurable.

I would like to thank Prof. Michael Harold at the University of Houston for his support during my work on the modeling portion of my research and for allowing me to visit Houston's campus.

I would like to recognize Dr. Robert McCabe and his wife for opening their house to me for some of my visits to Ford. I cannot say how much I appreciated a nice bed and home-cooked meal after working long hours in the laboratory.

I would like to thank the Department of Energy (DOE) and Ford Motor Company for the funding of this research.



I would like to thank my co-workers at the University of Kentucky Center for Applied Energy Research (CAER) for their support and friendship. The Biofuels and Environmental Catalysis research group has grown with me during the pursuit of this degree.

I consider myself extremely gifted to have met and made many friends over the course of my studies. Especially, I would like to thank Dr. Scott Lewis, Dr. Vinod Kanniah, and Dr. Harry Hunter for many fun experiences and keeping things light during the most demanding parts of my graduate school education.

I owe a special thanks to Miss Elizabeth Kidd for all of the emotional support she has provided me. It has been a long journey, and she was always standing beside me, ready to help me in whatever means was necessary.

Lastly and most importantly, I would like to express my appreciation to my parents, sister, and other family for their support during this educational journey. I would like to thank my sister, Mrs. Glenna Bianchin, for always setting the bar high in our sibling rivalry. I would also like to thank my cousin, Mr. Trey Hieneman, for being part of my support system when I was traveling for school and for providing at least a few opportunities to attend the UK basketball games every year. I cannot express my gratitude to my parents, Mr. Glenn Easterling and Mrs. Sharon Easterling, for their support and for the providing me a chance to make this change in my life. The lessons they have taught me have helped me get to where I am today.

## TABLE OF CONTENTS

Acknowledgements.....	iii
LIST OF TABLES .....	IX
LIST OF FIGURES .....	X
CHAPTER 1. GENERAL INTRODUCTION.....	1
1.1. Air Pollutants and Their Effect on Human Health.....	1
1.2. Response to Air Pollution: Clean Air Act and its Amendments.....	2
1.2.1. Tier I .....	3
1.2.2. Tier II .....	4
1.3. Current State and Future of NO <sub>x</sub> Emissions .....	6
1.4. The Role of Fuel Economy on Emissions Regulations .....	7
1.5. Automobile Manufacturers' Response to Emissions Regulations.....	8
1.6. Viable Solutions to Obtain Improved Fuel Efficiency and Meet Emissions Regulations .....	10
1.6.1. Three-Way Catalysts.....	11
1.6.2. Diesel Emission Control Systems.....	13
1.6.3. Selective Catalytic Reduction (SCR) Catalysts .....	14
1.6.4. Lean NO <sub>x</sub> Trap (LNT) Catalysts.....	17
1.7. Synergy of LNT+SCR Systems.....	18
1.8. Scope of the Dissertation .....	18
1.9. References.....	20
CHAPTER 2. LEAN NO <sub>x</sub> TRAP CATALYSTS: DESIGN AND OPERATIONAL CONSIDERATIONS .....	23
2.1. Components of LNT Catalysts.....	23
2.1.1. Cordierite Substrate .....	23
2.1.2. Catalyst Support.....	24
2.1.3. NO <sub>x</sub> Storage Materials .....	25
2.1.4. Platinum Group Metals (PGM).....	28
2.2. Mechanisms Involved LNT Catalysis.....	28
2.2.1. Oxidation of NO to NO <sub>2</sub> .....	29
2.2.2. Storage of NO <sub>x</sub> at BaO Sites .....	33
2.2.2.1. Effects of Components in the Engine Exhaust .....	34
2.2.2.2. Identity of Ba Storage Component .....	34
2.2.2.3. Mechanisms of NO <sub>x</sub> Storage.....	36
2.2.2.4. Proximity of Pt and Ba Components .....	40
2.2.2.5. Summary of NO <sub>x</sub> Adsorption.....	41
2.2.3. Reductant Evolution.....	41
2.2.4. Factors Influencing NO <sub>x</sub> Release.....	42
2.2.5. Rich phase product selectivity .....	43
2.2.5.1. Mechanisms of NO <sub>x</sub> reduction.....	43
2.2.5.2. NH <sub>3</sub> as an Intermediate .....	47
2.3. Drawbacks to LNT Utilization.....	50
2.3.1. Sulfur.....	50

2.3.2. Additional Concerns of LNT Utilization .....	55
2.4. LNT-SCR.....	55
2.5. References.....	59
CHAPTER 3. EFFECT OF CERIA ON THE DESULFATION CHARACTERISTICS OF MODEL LEAN NO <sub>x</sub> TRAP CATALYSTS .....	84
3.1. Introduction.....	84
3.2. Experimental.....	86
3.2.1. Preparation of Powder Catalyst Samples.....	86
3.2.2. Temperature Programmed Sulfation-Desulfation Experiments.....	87
3.2.3. Preparation of Monolith Catalyst Samples .....	88
3.2.4. Monolith Catalyst Sulfation and Desulfation .....	89
3.2.5. Measurement of Total Sulfur Release During Desulfation.....	91
3.3. Results and Discussion .....	92
3.2.1. Powder Model Catalysts .....	92
3.3.1.1. Temperature Programmed Reduction.....	92
3.3.1.2. Effect of Platinum Location on Desulfation Efficiency ..	99
3.3.2. Monolith Catalysts.....	102
3.3.2.1. Effects of Sulfur on NO <sub>x</sub> Storage Efficiency and Regeneration Temperature.....	102
3.3.2.2. Effect of Precious Metal Loading on NO <sub>x</sub> Storage Efficiency and Regeneration Temperature .....	107
3.4. Conclusions.....	111
3.5. References.....	113
CHAPTER 4. EFFECT OF AGING ON THE NO <sub>x</sub> STORAGE AND REGENERATION CHARACTERISTICS OF FULLY FORMULATED LEAN NO <sub>x</sub> TRAP CATALYSTS .....	119
4.1. Introduction.....	119
4.2. Experimental.....	123
4.2.1. Catalyst Preparation .....	123
4.2.2. Aging Protocol.....	125
4.2.3. Catalyst Evaluation .....	126
4.2.4. N <sub>2</sub> Physisorption .....	127
4.2.5. Pulsed H <sub>2</sub> Chemisorption.....	127
4.2.6. HRTEM-EELS.....	128
4.2.7. Postmortem Sulfur Analysis .....	128
4.3. Results and Discussion .....	128
4.3.1. Characterization .....	128
4.3.2. Oxygen Storage Capacity .....	134
4.3.3. NO <sub>x</sub> Storage .....	135
4.3.4. NO <sub>x</sub> Release and Reduction.....	141
4.3.5. Selectivity of NO <sub>x</sub> Reduction.....	143
4.3.6. Effects of Aging on Specific Catalyst Functions.....	148
4.3.7. Interfacial Pt-Support Perimeter .....	151
4.4. Conclusions.....	153
4.5. References.....	155

CHAPTER 5. APPLICATION OF SPACIMS TO THE STUDY OF AMMONIA FORMATION IN LEAN NO <sub>x</sub> TRAP CATALYSTS .....	166
5.1. Introduction.....	166
5.2. Experimental.....	169
5.2.1. Catalyst Preparation.....	169
5.2.2 Catalyst Aging .....	170
5.2.3. Catalyst Characterization .....	171
5.2.3.1. N <sub>2</sub> Physisorption .....	171
5.2.3.2. Pulsed H <sub>2</sub> Chemisorption.....	171
5.2.4. SpaciMS Measurements.....	171
5.2.4.1. Determination of the Amount of Reductant Required for Catalyst Regeneration .....	171
5.2.4.2. NO <sub>x</sub> Storage and Reduction Measurements.....	173
5.3. Results and Discussion .....	174
5.3.1. Catalyst Characterization .....	174
5.3.2. Amount of Reductant Required for Complete NO <sub>x</sub> Reduction during Rich Purging .....	175
5.3.3. Non-Ceria Containing Catalyst.....	177
5.3.3.1. NO <sub>x</sub> Storage .....	177
5.3.3.2. NO <sub>x</sub> Reduction.....	182
5.3.4. Ceria-containing Catalyst.....	193
5.3.4.1. NO <sub>x</sub> Storage .....	193
5.3.4.2. NO <sub>x</sub> Reduction .....	196
5.4. Conclusions.....	202
5.5. References.....	204
CHAPTER 6. AN INVESTIGATION INTO THE VALIDITY OF A CRYSTALLITE-SCALE MODEL TO PREDICT THE NH <sub>3</sub> REGENERATION OF A PT/RH/BAO/AL <sub>2</sub> O <sub>3</sub> LEAN NO <sub>x</sub> TRAP CATALYST .....	210
6.1. Introduction.....	210
6.2. Experimental.....	213
6.2.1. Catalyst Aging .....	214
6.2.2 Pulsed H <sub>2</sub> Chemisorption.....	214
6.2.3 SpaciMS and H-Sense Mass Spectrometers .....	215
6.2.4. Determination of the Amount of NO <sub>x</sub> Stored .....	216
6.2.5. NH <sub>3</sub> Selectivity .....	217
6.3. Model Development.....	218
6.4. Results and Discussion .....	224
6.4.1. Determination of the Amount of NO <sub>x</sub> Stored on the Catalysts.....	224
6.4.2 Experimental Results: NH <sub>3</sub> , N <sub>2</sub> O, H <sub>2</sub> .....	227
6.4.2.1 B-225 DG.....	227
6.4.2.2. B-225 AD.....	231
6.4.3 Modeling Results .....	232
6.4.3.1 Model vs. Experimental Results: B-225 DG .....	232
6.4.3.2. MODEL VS. EXPERIMENTAL RESULTS: B-225 AD.....	237
6.5. Conclusions.....	241
6.6. References.....	243

CHAPTER 7. SIGNIFICANT FINDINGS AND RECOMMENDATIONS FOR FUTURE WORK .....	257
7.1. Significant Findings .....	257
7.1.1. Effect of Ceria on the Desulfation Characteristics of Model Lean NO <sub>x</sub> Trap Catalysts .....	257
7.1.2. Effect of Aging on the NO <sub>x</sub> storage and Regeneration Characteristics of Fully Formulated Lean NO <sub>x</sub> Trap Catalysts ...	258
7.1.3. Application of SpaciMS to the Study of Ammonia Formation in Lean NO <sub>x</sub> Trap Catalysts.....	258
7.1.4. An Investigation into the Validity of a Crystallite-Scale Model to Predict the NH <sub>3</sub> Regeneration of a Pt/Rh/BaO/Al <sub>2</sub> O <sub>3</sub> Lean NO <sub>x</sub> Trap Catalyst.....	259
7.2 Suggestions for Future Research .....	260
APPENDIX A.1. – LIST OF ABBREVIATIONS .....	262
APPENDIX A.2. DEVELOPMENT OF THE MATERIAL BALANCES USED THE DISPERSION MODEL.....	266
A.2.1. Parameter Development .....	266
A.2.2. Species Balance.....	271
A.2.2.1. Gas Phase Species Balance (Diffusion from the Bulk to the Interface) .....	272
A.2.2.2. Washcoat Species Balance.....	273
A.2.2.3. Interface between the Fluid Phase and Washcoat.....	273
A.2.2.4. The Species Balance for the Component j in the Fluid Phase .....	274
A.2.3. Washcoat Species Balance.....	276
A.2.3.1. Hydrogen Surface Balance.....	276
A.2.3.2. NH <sub>3</sub> Surface Balance .....	277
A.2.3.3. N <sub>2</sub> Surface Balance .....	279
A.2.3.4. Vacant Site Balance .....	279
A.2.4. Dimensionless Expressions for Use in the Model .....	280
A.2.5. Determination of the Overall Mass Transfer Coefficient .....	282
A.2.6. References.....	284
BIBLIOGRAPHY .....	285
VITA .....	307

## LIST OF TABLES

Table 1.1. Tier 2 Emission Standards, FTP 75 cycle, g/mi.	5
Table 3.1. Feed composition for experiments utilizing powder catalysts.....	87
Table 3.2. Composition of monolith catalysts .....	89
Table 3.3. Feed gas composition during determination of NO <sub>x</sub> storage efficiency .....	91
Table 3.4. Feed gas composition during determination of fraction of sulfur released/stored.....	92
Table 3.5. Relative amounts of H <sub>2</sub> S released from different storage components during temperature-programmed reduction.....	94
Table 4.1. Composition of catalysts subjected to simulated road aging.....	124
Table 4.2. Nominal Pt loading in the three different powders used for washcoat preparation .....	124
Table 4.3. Gas compositions used for rapid aging, oxygen storage-reduction and NO <sub>x</sub> storage-reduction cycling experiments .....	126
Table 4.4. Physical properties and oxygen storage capacity of fresh and aged catalysts .....	129
Table 4.5. Summary of elemental analysis data for aged catalysts .....	130
Table 4.6. Comparison of NO <sub>x</sub> storage and release during lean-rich cycling .....	137
Table 4.7. Total Pt-support interfacial perimeter as a function of Pt particle size, assuming hemispherical particle morphology .....	153
Table 5.1. Composition of catalysts used in this study.....	170
Table 5.2. Physical properties of degreened and aged catalysts .....	175
Table 5.3. Comparison of cycle-averaged NO <sub>x</sub> conversion and NH <sub>3</sub> selectivity during lean-rich cycling for degreened and aged catalysts .....	185
Table 6.1. Composition of catalysts used in this study.....	214
Table 6.2. Amount of NO <sub>x</sub> for each of catalysts.....	226
Table 6.3 a. Values of N <sub>c</sub> , R <sub>c</sub> , and R <sub>eff</sub> for various Pt dispersions .....	233
Table 6.3 b. Parameter values to estimate N <sub>c</sub> and R <sub>eff</sub> .....	233
Table 6.3 c. Variation of M <sub>NO<sub>x</sub></sub> (mol) with monolith length, assuming uniform, axial NO <sub>x</sub> storage.....	233

## LIST OF FIGURES

Figure 1.1. Sources of air pollution in the United States for the physical year 2006 .....	2
Figure 1.2. The FTP-75 cycle .....	4
Figure 1.3. $\text{NO}_x$ emission standards for automobiles and light trucks from 1966 to 2008....	6
Figure 1.4. Impact of control programs on mobile source nitrogen oxide emissions.....	7
Figure 1.5. Crude oil prices in 2010 dollars from 1947 to October 2011 .....	8
Figure 1.6. Three-way catalyst (TWC) performance determined by engine air to fuel ratio .....	10
Figure 1.7. Comparison of three different catalysts for $\text{NO}_x$ reduction with $\text{NH}_3$ .....	16
Figure 3.1. Sulfur species released from $\text{Pt}/\text{Al}_2\text{O}_3$ sulfated to 2.5 g sulfur/L of catalyst equivalent during TPR. Gas composition: 2% $\text{H}_2$ , 5% $\text{CO}_2$ and 5% $\text{H}_2\text{O}$ , balance Ar, GHSV=30,000 $\text{h}^{-1}$ .....	93
Figure 3.2. Comparison of $\text{H}_2\text{S}$ released from $\text{Pt}/\text{Al}_2\text{O}_3$ sulfated to 1.0, 2.5, and 7.5 g sulfur/L of catalyst during TPR. Gas composition as for Figure 3.1 .....	95
Figure 3.3. Comparison of $\text{H}_2\text{S}$ released from $\text{Pt}/\text{CeO}_2$ sulfated to 1.0, 2.5, and 7.5 g sulfur/L of catalyst during TPR. Gas composition as for Figure 3.1 .....	96
Figure 3.4. Comparison of $\text{H}_2\text{S}$ released from PBA sulfated to 1.0, 2.5, 6.0, and 7.5 g sulfur/L of catalyst during TPR. Gas composition as for Figure 3.1 .....	97
Figure 3.5. Comparison of $\text{H}_2\text{S}$ released from PBAC sulfated to 1.0, 2.5, 6.0, and 7.5 g sulfur/L of catalyst during TPR. Gas composition as for Figure 3.1 .....	99
Figure 3.6. Comparison of $\text{H}_2\text{S}$ released from PBA and 1:1 physical mixture of $\text{Pt}/\text{Al}_2\text{O}_3$ and $\text{BaO}/\text{Al}_2\text{O}_3$ sulfated to 1.0 and 2.5 g sulfur/L of catalyst during TPR. Gas composition as for Figure 3.1. Note that for clarity the plots have been stacked .....	101
Figure 3.7. Comparison of lean $\text{NO}_x$ storage efficiency values for fresh and sulfated monolith samples. Samples were sulfated with 9 ppm $\text{SO}_2$ for 16 h at 350 °C under 1 min lean/1 min rich conditions .....	103
Figure 3.8. Comparison of normalized lean $\text{NO}_x$ storage efficiency values ( $\text{NO}_x$ storage efficiency after desulfation divided by the $\text{NO}_x$ storage efficiency after clean-off) for samples 30-0, 30-50, 30-100, 30-50z, and 30-100z. Desulfation conditions: 1.2% $\text{CO}$ , 0.4% $\text{H}_2$ , 10% $\text{CO}_2$ , 10% $\text{H}_2\text{O}$ , balance $\text{N}_2$ , GHSV=30000 $\text{h}^{-1}$ .....	104
Figure 3.9. Comparison of fraction of sulfur released/stored after sulfation with 90 ppm $\text{SO}_2$ for 1 h for samples 30-0, 30-50, 30-100, 30-50z and 30-100z. Desulfation conditions as for Figure 3.8 .....	105
Figure 3.10. Comparison of normalized lean $\text{NO}_x$ storage efficiency values ( $\text{NO}_x$ storage efficiency after desulfation divided by the $\text{NO}_x$ storage efficiency after clean-off) for samples 30-50, Pt-50, Pt-100. Desulfation conditions as for Figure 3 .....	109
Figure 3.11. Comparison of fraction of sulfur released/stored after sulfation with 90 ppm $\text{SO}_2$ for 1 h for samples 30-50, Pt-50 and Pt-100. Desulfation conditions as for Figure 3.8 .....	111
Figure 4.1. Schematic showing the functions of the three different powders contained in the prepared catalysts. In addition, alumina powder was added to the washcoat as a balance.....	125
Figure 4.2(a-c). Illustration of fresh catalyst sample 45-50 using STEM imaging .....	132

Figure 4.3. Rod-shaped Al <sub>2</sub> O <sub>3</sub> crystals in aged 45-50 with local agglomeration of dense Ba-rich phase. (b) Al <sub>2</sub> O <sub>3</sub> support with large, sintered Pt nanoparticles .....	133
Figure 4.4. STEM imaging of aged 45-50 and EELS spectrum imaging. (a) Aged catalyst with area of EELS line scan (red line). (b) STEM insert showing area of (sintered) La-stabilized CeO <sub>2</sub> after aging process. The red spot indicates the area of the EELS measurement shown in (b). (c) Relative elemental concentration obtained during EELS spectrum imaging for the line-scan shown in (a).....	134
Figure 4.5. NO <sub>x</sub> storage and release during lean-rich cycling for fresh catalysts .....	136
Figure 4.6. NO <sub>x</sub> storage and release during lean-rich cycling for aged catalysts .....	137
Figure 4.7. Comparison of NO <sub>x</sub> storage efficiency during the first cycle and during subsequent lean-rich cycling for fresh and aged catalysts .....	139
Figure 4.8. Selectivity to N <sub>2</sub> O (top), NH <sub>3</sub> (middle) and N <sub>2</sub> (bottom) for NO <sub>x</sub> reduction during lean-rich cycling .....	144
Figure 4.9. Comparison of integrated outlet CO concentration before and after aging (T = 350 °C) .....	147
Figure 4.10. Correlation of the change in cycle-averaged NO <sub>x</sub> conversion after aging with the change in cycle-averaged lean phase NSE.....	150
Figure 5.1. Required amount of H <sub>2</sub> during 60 s lean – 5 s rich cycling for catalyst regeneration. Solid colors represent values for degreened catalysts and patterned colors represent values for aged catalysts. The blue or top values in the columns represent the oxygen storage capacities, and the red or bottom values represent the NO <sub>x</sub> storage capacities .....	176
Figure 5.2. Lean NO <sub>x</sub> storage efficiency as a function of position for degreened (DG) and aged (AD) catalyst B-225 .....	178
Figure 5.3. a) Lean phase NO concentration and b) lean phase NO <sub>2</sub> concentration as a function of position during NO <sub>x</sub> storage on degreened (DG) and aged (AD) catalyst B-225 .....	179
Figure 5.4. Schematic showing NO and NO <sub>2</sub> concentrations along the length of the catalyst and the mechanism of NO <sub>x</sub> storage under lean conditions. Note that the relative concentrations depicted correspond to actual data collected at 200 °C for catalyst B-225 .....	181
Figure 5.5. Comparison of cycled-averaged NO <sub>x</sub> conversion (solid bars) and NO <sub>x</sub> storage efficiency (checkered bars) as a function of position for degreened catalysts: a) B-225 at 200 °C, b) B-225 at 300 °C, c) BC-175 at 200 °C, and d) BC-175 at 300 °C.....	183
Figure 5.6. Rich phase NO <sub>x</sub> release as a function of position during regeneration of degreened (DG) and aged (AD) catalyst B-225.....	184
Figure 5.7. Rich phase NH <sub>3</sub> selectivity as a function of position for degreened (DG) and aged (AD) catalyst B-225 .....	186
Figure 5.8. Schematic showing NO <sub>x</sub> and NH <sub>3</sub> concentrations along the length of the catalyst and the mechanism of NO <sub>x</sub> reduction under rich conditions (after Pihl et al. [38]). Note that the relative concentrations depicted correspond to actual data collected at 200 °C for catalyst B-225 .....	189
Figure 5.9. NH <sub>3</sub> concentration vs. time at each sampling location at 200°C for a) degreened B-225 and b) aged B-225 .....	191



Figure 5.10. NO <sub>x</sub> concentration profiles measured at the 16.4 mm position for degreened (DG) and aged (AD) B-225 as a function of time for regeneration events at 200°C and at 300°C. The dashed vertical lines indicate the time at which NH <sub>3</sub> breaks through at the 25.4 mm position .....	193
Figure 5.11. Lean NO <sub>x</sub> storage efficiency as a function of position for degreened (DG) and aged (AD) catalyst BC-175 .....	194
Figure 5.12. a) Lean phase NO concentration and b) lean phase NO <sub>2</sub> concentration as a function of position during NO <sub>x</sub> storage on degreened (DG) and aged (AD) catalyst BC-175.....	195
Figure 5.13. Percent change in NO <sub>x</sub> storage efficiency (NSE) after aging as a function of position for: B-225 at 300 °C (solid bars) and BC-175 at 300 °C (checkered bars). Percent change in NSE is defined as: 100 x (degreened NSE - aged NSE)/degreened NSE.....	196
Figure 5.14. Rich phase NO <sub>x</sub> release as a function of position during regeneration of degreened (DG) and aged (AD) catalyst BC-175 .....	197
Figure 5.15. Rich phase NH <sub>3</sub> selectivity as a function of position for degreened (DG) and aged (AD) catalyst BC-175.....	198
Figure 5.16. NH <sub>3</sub> concentration vs. time at each sampling location at 200°C for a) degreened BC-175 and b) aged BC-175 .....	199
Figure 5.17. NO <sub>x</sub> concentration profiles measured at the 16.4 mm position for degreened (DG) and aged (AD) BC-175 as a function of time for regeneration events at 200 °C and at 300 °C. The dashed vertical lines indicate the time at which NH <sub>3</sub> breaks through at the 25.4 mm position .....	200
Figure 6.1. Description of the Measurement Locations Along the Length of the Monolith Catalyst .....	216
Figure 6.2. Illustration of down-looking view of Pt on exposed BaO supported on Al <sub>2</sub> O <sub>3</sub> .....	220
Figure 6.3. Transition from a linear to exponential relationship occurring during NO <sub>x</sub> storage on the B-225 DG catalyst. Feed gas: 500 ppm NO, 5% O <sub>2</sub> , bal. Ar at 200 °C .....	225
Figure 6.4. Relationship between the break-through times of H <sub>2</sub> , NH <sub>3</sub> , and N <sub>2</sub> O for: a) B-225 DG at 200 °C, b) B-225 DG at 300 °C, c) B-225 AD at 200 °C, and d) B-225 AD at 300 °C.....	228
Figure 6.5. Comparison of yield and selectivity for B-225 DG and AD catalysts. a) NH <sub>3</sub> Yield, %, b) N <sub>2</sub> O Yield, %, c) NH <sub>3</sub> Selectivity, %, d) N <sub>2</sub> O Selectivity .....	230
Figure 6.6. Comparison between the a) experimental data and b) model predicted data for the B-225 DG catalyst at 200 °C .....	234
Figure 6.7. Comparison between the a) experimental data and b) model predicted data for the B-225 DG catalyst at 200 °C with k <sub>1</sub> = 1 x 10 <sup>-5</sup> m <sup>4</sup> /mol*s instead of 1 x 10 <sup>-3</sup> m <sup>4</sup> /mol*s .....	235
Figure 6.8. Comparison between the a) experimental data and b) model predicted data for the B-225 DG catalyst at 300 °C .....	236
Figure 6.9. Comparison between the a) experimental data and b) model predicted data for the B-225 DG catalyst at 300 °C with k <sub>1</sub> = 1 x 10 <sup>-5</sup> instead of 1 x 10 <sup>-3</sup> .....	236
Figure 6.10. Comparison between the a) experimental data and b) model predicted data for the B-225 AD catalyst at 200 °C with D <sub>A</sub> = 9 x 10 <sup>-18</sup> m <sup>2</sup> /s.....	237

Figure 6.11. Comparison between the a) experimental data and b) model predicted data for the B-225 AD catalyst at 200 °C with $D_A = 9 \times 10^{-16} \text{ m}^2/\text{s}$ .....	238
Figure 6.12. Comparison between the a) experimental data and b) model predicted data for the B-225 AD catalyst at 200 °C .....	239
Figure 6.13. Comparison between the a) experimental data and b) model predicted data for the B-225 AD catalyst at 300 °C .....	240

## **Chapter 1. General Introduction.**

During the past 40 years, two interrelated changes in our society, environmental awareness and the desire for improved fuel economy, have increasingly impacted the lives of the population of the United States of America. On July 9, 1970, the Environmental Protection Agency was created as a response to growing concern over environmental protection and conservation [1]. Also during the 1970's, two oil crises occurred in response in disruptions to global oil supply. These trends of increased environmental awareness and efforts towards decreased fuel consumption have continued into the present day. Although not necessarily obvious, the desire for increased fuel economy and reduced emissions are problems with solutions that involve a common feature: lean-burn engine operation.

### *1.1. Air Pollutants and Their Effect on Human Health.*

To understand the need for automobile emissions control, one has to look no further than the major components present in automotive emissions and their negative effects on humans and the environment. While air pollution can be associated with natural sources such as volcanic eruptions, forest fires, or dust storms, the major sources of air pollution are from human activities [2]. A large portion from human activity corresponds to the tailpipe emissions from automobiles as shown in Figure 1.1. The major components of this pollution are carbon monoxide (CO), hydrocarbons (HC), particulate matter (PM) and oxides of nitrogen (NO<sub>x</sub>). CO is a colorless and odorless gas that is poisonous to humans. Some HCs are linked to cancer in humans while others contribute to the greenhouse effect. PM is the term given to the fine particles that are present as aerosols during combustion processes, which have been linked to heart disease and lung cancer. Likewise, NO<sub>x</sub> has many negative effects on our environment, including the smog that is present in many cities across the United States. Another derives from the reaction of NO<sub>x</sub> with HCs to produce ground level ozone that can cause breathing complications. NO<sub>x</sub> also reacts in the atmosphere to create acid rain. Acid rain is detrimental to vegetation and aquatic species. The impact exerted by these air pollutants on human health is evident in the Centers for Disease Control (CDC) estimate that exposure to air pollution

results in \$40 to \$50 billion dollars in health care costs per year and 50,000 to 120,000 premature deaths per year [4].

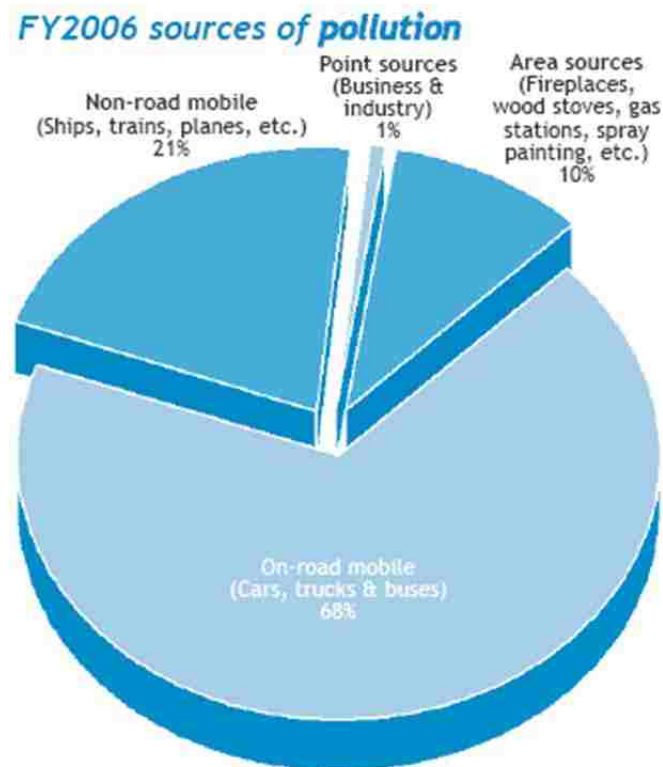


**Figure 1.1. Sources of air pollution in the United States for fiscal year 2006. [3]**  
**Source: ps-cleanair.org. Figure reprinted with permission.**

### *1.2. Response to Air Pollution: Clean Air Act and its Amendments.*

In response to rising concerns over the health effects attributed to these pollutants, the United States government has established legislation to determine and set limits on these different pollutants. These targets for air emissions are the result of regulations that have evolved over the past half century. The origin of air quality standards can be traced to 1955 with the passing of the Air Pollution Control Act that empowered states to control air pollution. These standards continued with the Clean Air Act in 1963, the Air Quality Act in 1967, the Clean Air Act Extension of 1970, and the Clean Air Act Amendments of 1977. Subsequent additions were made in the 1990s which are particularly important

when considering automobile exhaust. Programs for the control of acid rain were added in 1990, and the National Ambient Air Quality Standards lowered the levels of ground-level ozone that make up smog as well as the fine airborne particulate matter that makes up soot.

### *1.2.1. Tier 1.*

The origin of today's automotive emission standards originated with the Clean Air Act Amendments in 1990. These amendments established more stringent Tier 1 standards that were phased in between 1994 and 1997. These standards assigned emission levels to all vehicles under 8500 lbs. gross vehicle weight rating (GVWR) [5]. The standards were comprised of two milestones: 5 years/50,000 mi. and 10 years/100,000 mi. These standards divided personal vehicles such as cars, light trucks, minivans, and sport utility vehicles into categories based on the GVWR. Also the  $\text{NO}_x$  standard was dependent on whether the vehicles used gasoline or diesel as fuel.

Tier 1 standards are enforced using the federal testing procedure (FTP) 75 cycle [5]. The FTP-75 cycle has been used since 1978 and is divided into three segments as shown in Figure 1.2. Emissions are measured after the engine is started; this is referred to as the cold start. Emissions continue to be measured during the transient phase and during the last phase, in which the engine is turned off and restarted. The total cycle is 11.04 miles total, lasting 1874 s, and using an average speed of 21.2 mph.

While this procedure is effective in measuring emissions, there exist some shortcomings when trying to capture real world driving conditions. In response to this issue, supplemental federal testing procedures (SFTP) were instituted. The US06 is a representation of aggressive, high speed, and/or high acceleration driving behavior [5]. This test is comprised of an 8.01 miles loop, average speed of 42.4 mph with a maximum speed of 80.3 mph, and a duration of 596 s. The other supplement test accounts for the emissions associated with the use of air conditioning in a vehicle. This test is 3.6 miles in length with an average speed of 21.6 mph, maximum speed of 54.8 mph, and duration of 596 s.

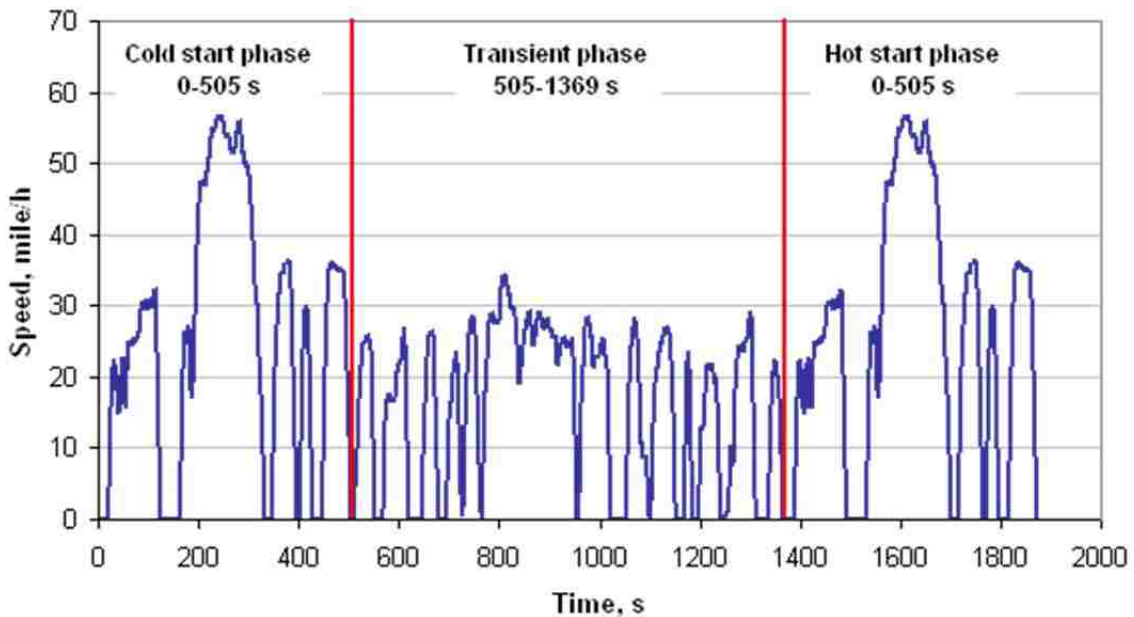


**Figure 1.2. FTP-75 Cycle [5]. Source: DieselNet.com. Figure reprinted with permission.**

### 1.2.2. Tier II.

As part of the Tier 1 initiative, a study on the effectiveness of reducing emissions even further and the economic impact of those more stringent standards was conducted. The study resulted in the adoption of the Tier II standards in 2007 after a phase in period beginning in 2004. The main difference between Tier I and Tier II standards is that the standards in Tier II apply to all vehicles, regardless of weight up to 8500 lbs. GVWR. Also, the standards are the same irrespective of the fuel type. The Tier II standards are structured into different emissions levels referred to as bins, as shown in Table 1.1 [6]. On account of HC and CO levels being inherently lower from diesel engines as compared to stoichiometric engines, the abatement of  $\text{NO}_x$  emissions will be the focus of this dissertation. Tier II mandates that every manufacturer must average a  $\text{NO}_x$  standard of 0.07 g/mi as tested on the FTP 75 cycle for the full useful life of either 10 years or 120,000 miles. As with Tier I, SFTP standards exist to correct for the aforementioned shortcomings of the FTP test.

In addition to the emission standards, Tier II also mandates that sulfur levels in gasoline be reduced to an average of 30 ppm with a cap of 80 ppm and in diesel be reduced to 15 ppm. As will be discussed later in this dissertation, sulfur interferes with the effectiveness of emission control systems.

**Table 1.1. Tier 2 emission standards, FTP 75 cycle, g/mi [6]. Source: DieselNet.com.**

Bin#	Intermediate life (5 years / 50,000 mi)					Full useful life				
	NMOG	CO	NO <sub>x</sub>	PM	HCHO	NMOG	CO	NO <sub>x</sub>	PM	HCHO
8	0.1	3.4	0.14	-	0.015	0.125	4.2	0.2	0.02	0.018
7	0.075	3.4	0.11	-	0.015	0.09	4.2	0.15	0.02	0.018
6	0.075	3.4	0.08	-	0.015	0.09	4.2	0.1	0.01	0.018
5	0.075	3.4	0.05	-	0.015	0.09	4.2	0.07	0.01	0.018
4	-	-	-	-	-	0.07	2.1	0.04	0.01	0.011
3	-	-	-	-	-	0.055	2.1	0.03	0.01	0.011
2	-	-	-	-	-	0.01	2.1	0.02	0.01	0.004
1	-	-	-	-	-	0	0	0	0	0

An interesting feature of Tier II concerns whether or not a vehicle meets, exceeds, or fails to meet the Tier II, Bin 5 standard. If the manufacturer exceeds Tier II, bin 5, a credit is earned that can be used later or traded to another manufacturer. If bin 5 is not met, the manufacturer must obtain sufficient credits no more than 3 years after the violation occurred. This is where credit trading or redemption occurs.

Figure 1.3 is effective in summarizing the preceding discussion on the degree to which tailpipe emissions have been tightened by ever increasing governmental regulations. Every drop in NO<sub>x</sub> levels as shown in the figure represents new standards coming into effect. The 0.07 g/mi. value achieves Tier II, Bin 5 levels for the full useful life of the vehicle. From 1966, beginning with the original Clean Air Act, to the enactment of Tier II, NO<sub>x</sub> limits have been reduced by slightly more than 98%. To illustrate how stringent the emissions standards have become, in order to achieve Tier II, Bin 2 status (0.02 g/mi.), a further 71% reduction in NO<sub>x</sub> tailpipe emissions would be required.

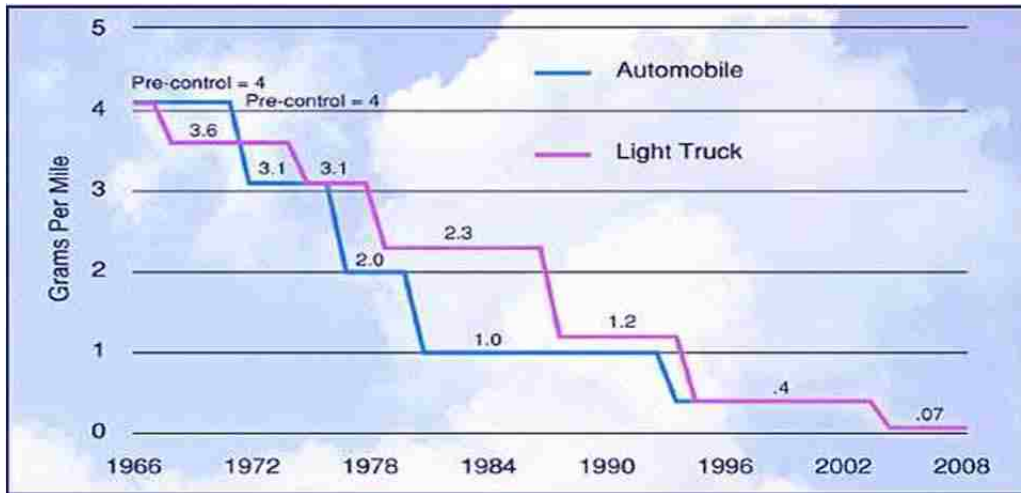


**Figure 1.3. NO<sub>x</sub> emission standards for automobiles and light trucks from 1966 to 2008 [7,8,9]. Source: fhwa.dot.gov and cta.ornl.gov. Figure reprinted with permission.**

*1.3. Current State and Future of NO<sub>x</sub> Emissions.*

Despite these legislative efforts, NO<sub>x</sub> emissions now are actually greater than they were in 1970. This increase is not an indictment of the failure of governmental regulation, but a result of more vehicles being driven more miles on American highways. Figure 1.4 demonstrates that these regulations have reduced NO<sub>x</sub> levels to one-fifth of the levels that would exist without emissions controls in place [10].



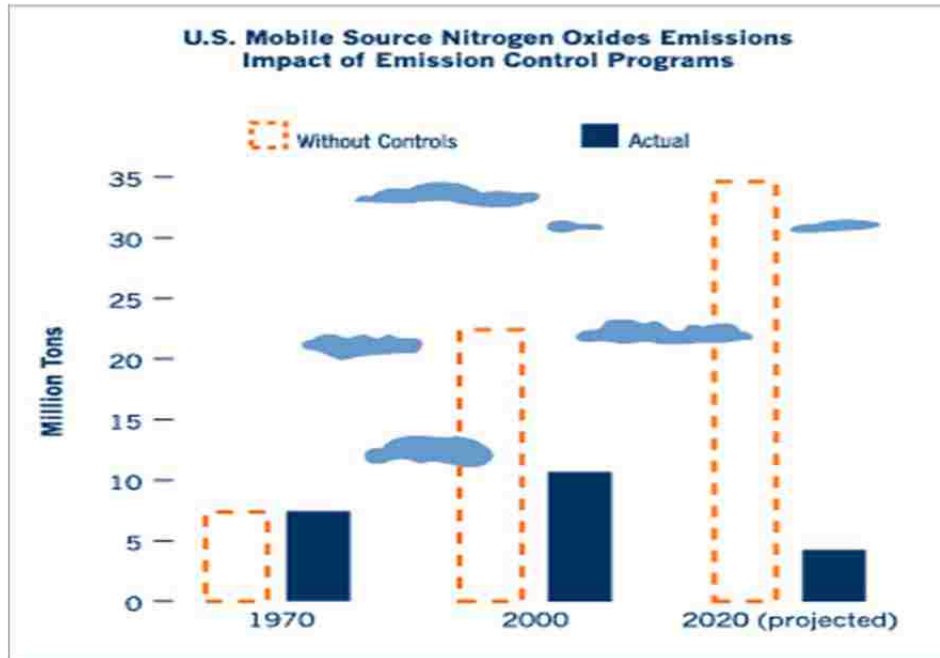


**Figure 1.4. Impact of control programs on mobile source nitrogen oxide emissions [10]. Source epa.gov. Figure reprinted with permission.**

*1.4. The Role of Fuel Economy on Emissions Regulations.*

While environmental awareness and the subsequent responses were occurring, another trend was also driving the response of suppliers to consumer demand. Twice during the 1970's, an oil crisis occurred in the United States, leading to increased gasoline prices and shortages. Since then global events (as shown in Figure 1.5), such as government volatility in oil producing countries (e.g. Iran, Venezuela), wars (both Gulf Wars) and terrorist attacks (the events of 9/11) have resulted in increased fuel prices [11]. These events, along with decreasing oil supplies, have contributed to a public desire for more fuel-efficient automobiles. In this context, the most recent Corporate Average Fuel Economy (CAFE) standards hold significant implications for vehicle emissions. The CAFE standards are applicable from 2012 to 2016, and the standards state that all vehicles with a GVWR of 10,000 lbs. or less must average 35.5 mpg. The average is subdivided into an average of 42 mpg for cars and 26 mpg for trucks, which must be met by 2016. Failure to meet this regulation will result in the manufacturer being charged \$5 per vehicle for every tenth of a mile that the vehicle is short of the standard. However, as engine operation becomes more efficient, the additional changes to engine operation are

necessitated as a part of the vehicle design implemented to meet the CAFE standard might increase NO<sub>x</sub> emissions to levels above Tier II, bin 5.

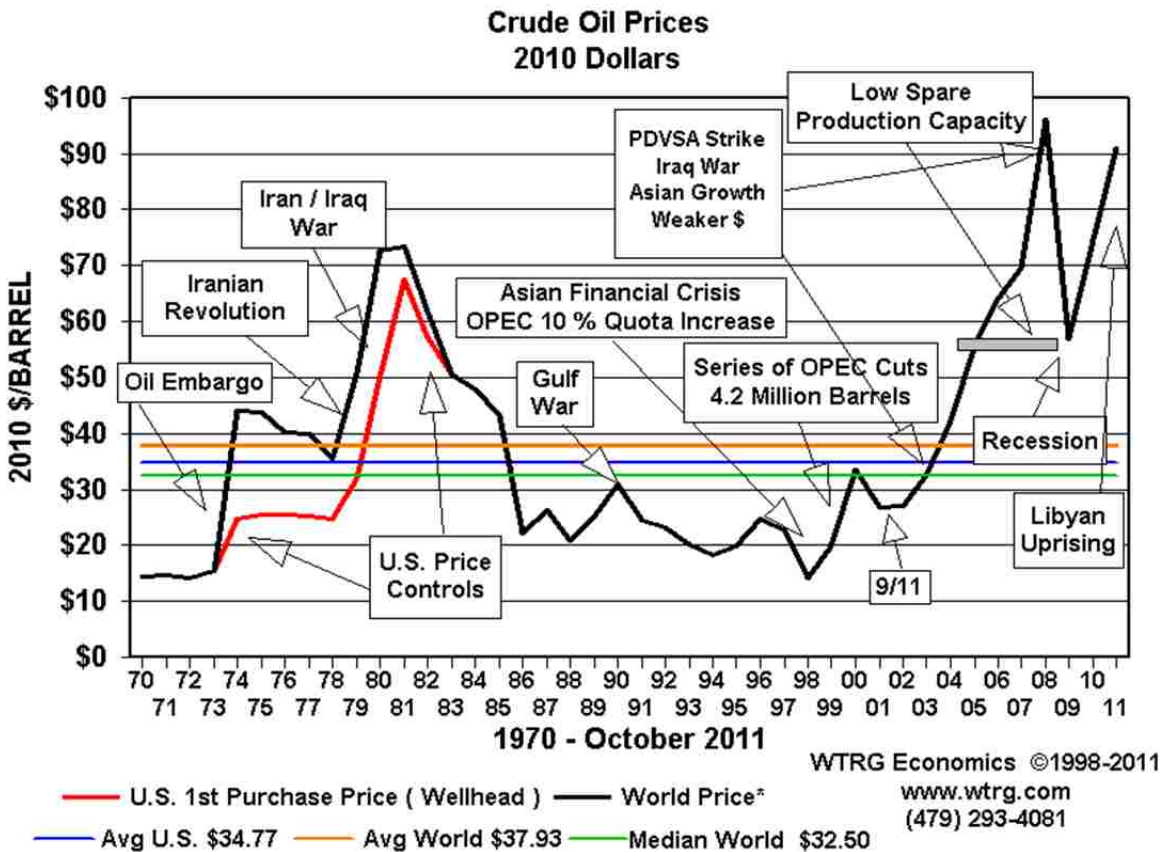


Figure 1.5. Crude oil prices in 2010 dollars from 1947 to October 2011 [11]. Source: [www.wtrg.com](http://www.wtrg.com). Figure reprinted with permission.

*1.5. Automobile Manufacturers’ Response to Emissions Regulations.*

In response to these government standards, the automobile industry has sought solutions to decrease vehicle emissions. The first measures involved “de-tuning” engine operation in which variables such as air to fuel ratios, valve timing, etc., were modified to produce exhaust gases that meet the emission standards. Some of these methods include excess air injection and exhaust gas recirculation. In both of these methods the exhaust gas is diluted and more complete combustion is obtained. Over time, though, the standards could not be met, while at the same time they reduced fuel efficiency. The next measure taken in combating emission levels was the development of the catalytic converter. The

catalytic converter is comprised of a ceramic or metal honeycomb monolith upon which a washcoat is applied. The washcoat contains a high surface material such as alumina or titanium oxide that provides a high surface area for the platinum group metals (PGM) (i.e., platinum, rhodium and or palladium) which catalyze the reaction of the exhaust gases to more desirable products. The first catalytic converters were two-way or oxidation converters that converted CO and HC into CO<sub>2</sub> and water. In a response to lower NO<sub>x</sub> emission standards, three-way or oxidation-reduction converters were developed to also reduce NO<sub>x</sub> to nitrogen. The three-way converters are still in use to this day.

This desire for increased fuel efficiency helped spur the development of the catalytic converter because as mentioned previously, changing engine operation tends to decrease the efficiency of the engine. How an engine operates can be described by the ratio of air to fuel fed to the cylinder. The three possible modes of engine operation are stoichiometric, rich, and lean. Stoichiometric engine operation occurs when the weight ratio of air to fuel is equal to 14.7. This value corresponds to the point at which sufficient air is present to just consume all of the fuel (assuming that combustion of the fuel goes to completion). If the ratio is less than 14.7, the mixture is considered to be fuel-rich, while values greater than 14.7 are considered to be fuel-lean. Figure 1.6 shows how the conversion of pollutant species can vary depending on the air to fuel ratio. Under stoichiometric to rich conditions, high conversions for HC, CO, and NO are possible albeit at the cost of reduced fuel efficiency. Looking at these conversions in the lean range, CO and HC values are still very high while NO conversion plunges to levels well below 50%. This low level of conversion is due to the fact that NO and NO<sub>2</sub> cannot be reduced in an environment containing an excess of oxygen. As the demand from consumers for more fuel efficient vehicles increases and emission regulations concerning NO<sub>x</sub> tailpipe levels become more stringent, the problem of NO<sub>x</sub> reduction during lean burn engine operation will present a larger obstacle for manufacturers to overcome.

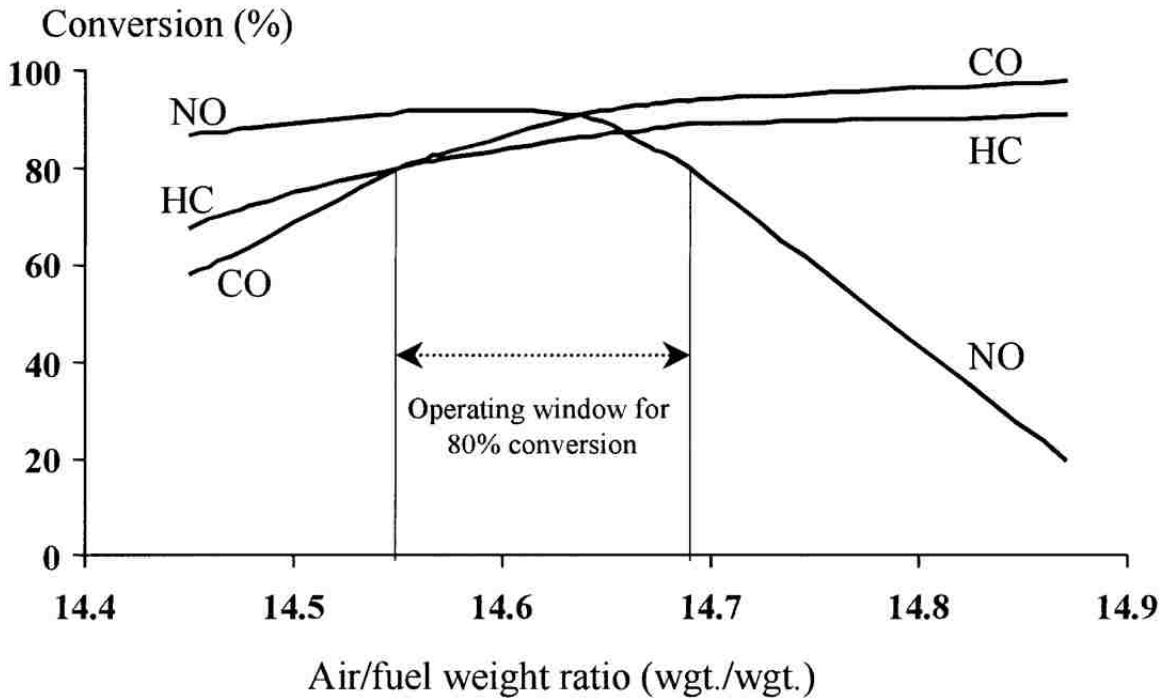


**Figure 1.6. Three-way catalyst (TWC) performance determined by engine air to fuel ratio. Reprinted from Applied Catalysis A: General, Vol. 221, R.H. Heck, R.J. Farrauto, Automobile exhaust catalysts, Pages No. 443-457, Copyright (2001), with permission from Elsevier [12].**

*1.6. Viable Solutions to Obtain Improved Fuel Efficiency and Meet Emissions Regulations.*

The above discussion gives one an idea of what should be expected from an automobile in terms of emissions and fuel efficiency. Currently there are many ultra-low emission vehicles available to the public. These are vehicles that meet the emission standard for Tier 2 Bin 5 for NO<sub>x</sub> levels of less than 0.07 g/mi over the full useful life of the vehicle. For the 2012 model year, there are over 250 spark injected (gasoline) vehicle available that meet or exceed the Tier 2 Bin 5 standard [13]. In addition, several hybrids, electric, and natural gas powered vehicles meet this standard. However, each of these options has drawbacks. Hybrids have the looming cost to replace the battery sets over the useful life of the vehicle. Electric vehicles are limited by driving range. Natural gas vehicles do not yet have the infrastructure to support them.

Light duty diesels (LDDs) present an interesting option due to their high fuel efficiency (up to a 30% increase compared to gasoline engines) [13], while producing significantly lower levels of HC and CO compared to stoichiometric gasoline engines. Due to the air to fuel ratios of  $\sim 22$  (and even as high as 50) at which diesel engines operate, almost none of the  $\text{NO}_x$  is converted in the oxygen-rich exhaust which is disappointing considering the advantages (i.e., greater torque and durability) of diesel engines as compared to spark-injected gasoline engines. But what if there were a way to meet  $\text{NO}_x$  emission standards while retaining the benefits of diesel engines?

#### *1.6.1. Three-Way Catalysts.*

The development of current three way catalysts was the result of the initial efforts by manufacturers to reduce emissions as required by the adoption of the Clean Air Act in 1970 [14]. The first control systems were oxidation catalysts that converted HC and CO to  $\text{CO}_2$  and  $\text{H}_2\text{O}$  to levels mandated by the Clean Air Act. These catalysts consisted of a combination of Pt and Pd supported on either  $\gamma$ -alumina beads or a honeycomb monolith with a washcoat containing the Pt and Pd supported on  $\gamma\text{-Al}_2\text{O}_3$  applied to the channels present. This system performed well in oxidizing the desired pollutants but also suffered from sintering of the precious metals due to high operating temperatures and poisoning by Pb that was present in gasoline formulations at the time. For this reason unleaded fuels were developed in the 1970s. Stabilizers such as  $\text{CeO}_2$  and  $\text{La}_2\text{O}_3$  were added to the washcoat to address the sintering problem.

Towards the end of the 1970s,  $\text{NO}_x$  emission standards were lowered further to less than 1.0 g/mi [12]. A new control strategy was needed because  $\text{NO}_x$  could not be reduced to  $\text{N}_2$  in the present oxidizing system. The initial design consisted of a two stage catalyst in the exhaust manifold with the ability to inject air in between the stages. An upstream catalyst would use CO and HC present to reduce  $\text{NO}_x$  to  $\text{N}_2$ , and a downstream catalyst would then oxidize the remaining CO and HC remaining in the exhaust. Here additional oxygen would be supplied by air to convert the remaining CO and HC species present after the upstream catalyst.

The next step in the development of the three-way catalyst was the development of oxygen sensors that could provide feedback to the engine during operation. Designers discovered that if the air to fuel ratio was held to stoichiometric conditions (14.7 as shown in Figure 1.6) throughout the engine cycle,  $\text{NO}_x$  could be reduced by CO and HC [12]. This system was made possible by the development of sophisticated oxygen sensors that could control engine operation and air input into the exhaust stream. Because the catalyst could convert all three pollutants simultaneously, the name three-way catalytic (TWC) converter was adopted. The components were similar to the first generation converter. Pt oxidized CO and HC while Rh reduced  $\text{NO}_x$ . Because of the modulation of the air to fuel ratio around the stoichiometric point, an oxygen storage component was added. High surface area  $\text{CeO}_2$  acted as a buffer in the three-way catalyst.  $\text{CeO}_2$  provided additional oxygen when remaining reductants (e.g., CO and HC) were present after the  $\text{NO}_x$  had been reduced to  $\text{N}_2$  and acted as an oxygen storage material when conditions were lean. Again using  $\gamma\text{-Al}_2\text{O}_3$  as a support material, these components were applied as a washcoat to a ceramic, honeycomb material.

From the mid-1980s to the present, the third and then fourth generation catalytic converters were developed [12]. The third generation was necessitated by the desire for increased fuel economy and higher operating speeds. To address fuel economy, fuel was shut off during deceleration events. This change in operation, combined with the higher operating speeds, led to the exposure of the catalyst to highly oxidizing, high temperature conditions. Catalysts were modified by adjusting the locations of the precious metals on the  $\text{CeO}_2$  and  $\gamma\text{-Al}_2\text{O}_3$  support, and by adding additional stabilizing materials such as  $\text{ZrO}_2$  and  $\text{La}_2\text{O}_3$  to reduce the interactions that lead to deactivation at high temperatures. Pd was added to the fourth generation of catalyst in an effort to reduce the cost of using Pt and Rh. While Pd was more cost effective, Pd usage requires separation of the Pd and Rh due the risk of Pd-Rh formation at high temperature, an alloy which displays diminished activity for  $\text{NO}_x$  reduction.

In summary, the development of three way converters led to the use of:

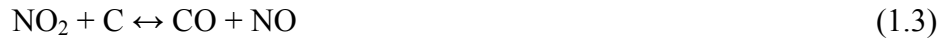
- ceramic, honeycomb supports
- precious metals such as Pt, Rh, Rd for the required oxidation and reduction reactions
- addition of stabilizers such as  $\text{La}_2\text{O}_3$  and  $\text{ZrO}_2$
- addition of  $\text{CeO}_2$  to act as an oxygen buffer during engine operation
- washcoat utilizing  $\gamma\text{-Al}_2\text{O}_3$  as a support

These innovations would subsequently lead to the catalysts used in current lean-burn applications.

#### *1.6.2. Diesel Emission Control Systems.*

The attractiveness of diesel engine applications is attributed to their fuel efficiency relative to gasoline spark-ignited engines. This increased efficiency is a result of the very lean engine operation at air to fuel ratios of greater than 22. While diesel exhaust contains less  $\text{NO}_x$ , CO, and HC species due to lean operating conditions as compared to gasoline engines, high particulate emissions exist. The particulate matter is comprised of dry soot, inorganic oxides, and liquids. If the operation of a diesel engine is changed to lower particulate emissions by increasing the combustion temperatures, more  $\text{NO}_x$  is produced.

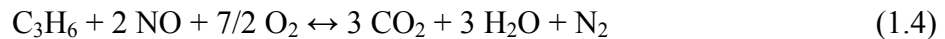
As a response to the initial adoption of the Tier II standards, diesel oxidation catalysts (DOC) and diesel particulate filters (DPF) were added to the exhaust system. The dry soot present as particulate matter is oxidized by  $\text{NO}_2$  in the exhaust stream. Since NO is the predominate  $\text{NO}_x$  species from the engine, the NO is oxidized upstream by a DOC such as Pt or Pd on  $\gamma\text{-Al}_2\text{O}_3$ . The reaction sequence is as follows [13]:



The first reaction occurs in the DOC, and the last two reactions occur in the DPF.

### *1.6.3. Selective Catalytic Reduction (SCR) Catalysts.*

As the Tier II standards were instituted, the more relaxed standards for NO<sub>x</sub> from diesel engines disappeared, as standards for gasoline and diesel had become the same. Once diesel exhaust was treated by the DOC and DPF, most of the CO and HC had been converted to CO<sub>2</sub> and H<sub>2</sub>O, whereas the NO<sub>x</sub> had been oxidized to NO<sub>2</sub> and reduced back to NO as the gases passed through the tailpipe. The exhaust gas at this point was a mixture of NO and NO<sub>2</sub> in an oxidized atmosphere. However, the catalytic converters utilized for spark-injected applications were not capable of reducing NO<sub>x</sub> in the oxygen-rich environment. The first solutions to this quandary involved using the hydrocarbons that were present in diesel fuel as a reductant. After an extensive search, several candidate catalysts were proposed. For example, using propene as the HC, NO can be converted to CO<sub>2</sub>, H<sub>2</sub>O and N<sub>2</sub> over an appropriate catalyst:



Unfortunately, the reductant can be consumed by oxygen, and incomplete reduction of the NO can result in N<sub>2</sub>O formation:



Pt and Al<sub>2</sub>O<sub>3</sub> is effective in reducing the NO<sub>x</sub> over the Pt sites but only in a very narrow operating window of 180°C to 275°C. This limits the effectiveness of the catalyst as the exhaust temperature can vary from about 150°C to 450°C in diesel exhaust depending on the engine speed and load requirements. Another problem with using Pt/Al<sub>2</sub>O<sub>3</sub> in this



application is that Pt catalyzes the reduction of NO<sub>x</sub> to N<sub>2</sub>O, which is a powerful greenhouse gas.

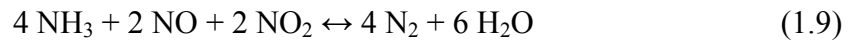
The other approach to NO<sub>x</sub> reduction under lean conditions involves the use of NH<sub>3</sub> as a reductant, the NH<sub>3</sub> being generated on board the vehicle via the hydrolysis of urea. Researchers at Engelhard in 1957 [15] discovered that NH<sub>3</sub> reacts with NO over Pt even in the presence of oxygen, in a reaction termed selective catalytic reduction (SCR). NH<sub>3</sub> is hydrolyzed from urea by:



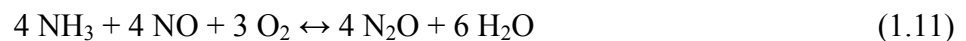
NH<sub>3</sub> is stored on the catalyst and reacts with NO<sub>x</sub> as it is adsorbed from the exhaust stream. How NH<sub>3</sub> reacts with NO<sub>x</sub> is dependent on the exhaust temperature and the ratio of NH<sub>3</sub> and NO<sub>x</sub> on the catalyst surface. The standard SCR reaction involves a 1:1 ratio for NH<sub>3</sub> and NO:



Comparatively without the presence of oxygen, this reaction is much slower and is not relevant under these conditions [16]. Another reaction involving both NO and NO<sub>2</sub> with NH<sub>3</sub> is called “fast” SCR [17,18]:



NO<sub>x</sub> conversions resulting from these reactions are typically in the range of 80% to 90%. Some deNO<sub>x</sub> performance is lost due to the consumption of NH<sub>3</sub> by oxygen and the conversion of NO<sub>x</sub> to N<sub>2</sub>O as follows [19]:



Because diesel exhaust has a broad temperature window due to the variation in engine speed and load, it has proven difficult to find a catalyst which can span the entire operating range; as shown in Figure 1.7, different catalysts tend to operate in different temperature regions.

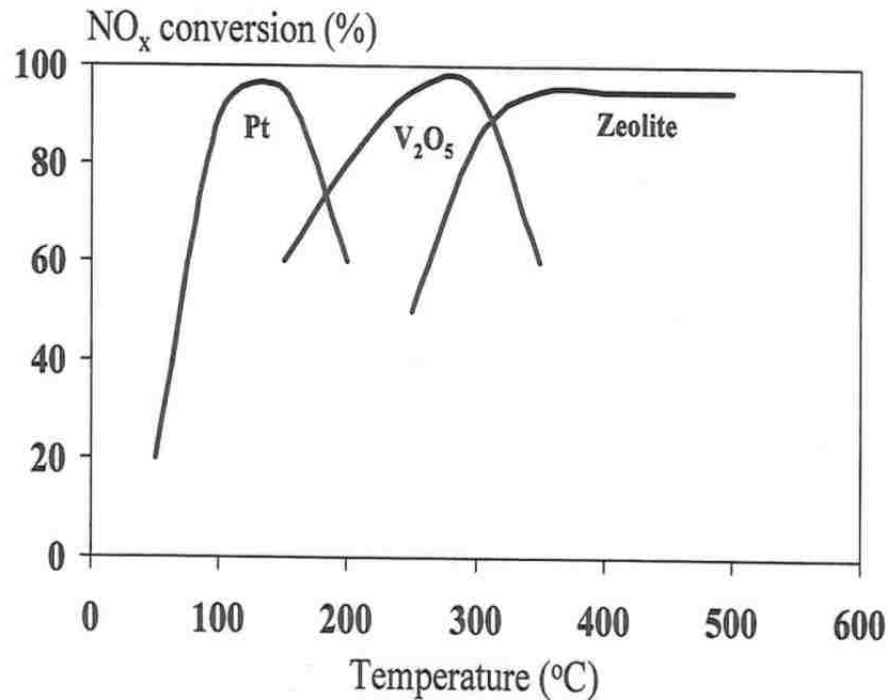


**Figure 1.7. Comparison of three different catalysts for NO<sub>x</sub> reduction with NH<sub>3</sub>. Reprinted from R.H. Heck, R.J. Farrauto, Catalytic Air Pollution Control: Commercial Technology, 2<sup>nd</sup> Edition, John Wiley and Sons, Inc. New York 2002. Page 206. [13].**

Regarding concerns arising from the use of SCR catalysts in this application, NH<sub>3</sub> slip from the catalyst is possible if the correct NO<sub>x</sub>:NH<sub>3</sub> ratios are not maintained on the catalyst, while there is also the possibility of N<sub>2</sub>O production. NH<sub>3</sub> is a respiratory irritant and N<sub>2</sub>O is a well-known greenhouse gas. Finally, the use of a SCR catalyst requires installation of the catalyst, injection and control system, and urea storage tank. All of these add weight to the vehicle which decreases fuel efficiency numbers and adds to the purchase price and maintenance costs.

#### *1.6.4. Lean NO<sub>x</sub> Trap (LNT) Catalysts.*

An alternative to SCR catalyst is the NO<sub>x</sub> storage and reduction (NSR) or Lean NO<sub>x</sub> trap (LNT) catalyst. This type of catalyst was developed in the mid-1990s by Toyota and consists of a washcoat containing platinum group metals (PGM), storage materials (alkali or alkaline-earth metals) and a high surface area support ( $\gamma$ -Al<sub>2</sub>O<sub>3</sub>) [20,21]. The LNT is able to reduce NO<sub>x</sub> to N<sub>2</sub> by operating under two modes of engine operation: lean and periodic switches to rich. The LNT operates by storing NO<sub>2</sub> which is formed from NO oxidation on PGM sites during normal lean operating conditions. Before the storage capacity of the trap is reached, the engine operation is switched to net rich conditions upon which the stored NO<sub>x</sub> is released and reduced at the PGM sites to N<sub>2</sub>. The LNT has an advantage over SCR in that an external supply of reductant is not required, since the necessary reducing agents are supplied by modifying the engine operation. This advantage does not add weight or require space on the vehicle.

Although LNTs show great promise as a technology to reduce NO<sub>x</sub> emissions from diesel engines to levels that would allow their use in all 50 states, the LNT does have some problems associated with its use. While Tier II standards reduced the amount of sulfur present in diesel fuel from 500 to 15 ppm as previously mentioned, sulfur still presents a hindrance to LNT operation. The most common storage material for LNTs is BaO. Under lean conditions, NO<sub>x</sub> is stored at the Ba sites as a mixture of barium nitrates and barium nitrites, the form depending on conditions such as temperature and gas composition at the time of storage. Herein lies the problem. While Ba is an excellent storage material for nitrates and nitrites, Ba has a greater affinity for sulfur. Upon exposure to sulfur that is created during the combustion cycle from the sulfur present in the fuel, SO<sub>2</sub> is formed. The resulting BaSO<sub>4</sub> is thermodynamically more stable than Ba(NO<sub>3</sub>)<sub>2</sub> [22]. What this means to LNT operation is that high temperatures and long rich durations are required to desulfate the trap. This requirement means that the engine must operate under rich conditions for longer periods, which can negate the fuel savings associated with lean burn engine operation inherent in diesel engines. These higher temperatures can also lead to sintering of the PGMs and side reactions within the washcoat that will reduce the storage capacity of the catalyst. Finally, the cost of the

PGMs render LNT catalysts sometimes cost prohibitive as compared to other emission control technologies.

### *1.7. Synergy of LNT- SCR Systems.*

What if these problems could be solved by modifying the composition and application of LNTs? The scope of this dissertation is to address these issues by suggesting the addition of ceria to the LNT and to use this LNT formulation in conjunction with a SCR catalyst to meet the upcoming emission standards. As will be discussed, this configuration provides a means to deal with the presence of sulfur in the exhaust stream by using ceria to preferentially store  $\text{SO}_2$  at ceria sites instead of barium sites. The LNT-SCR system has the potential to eliminate the external supply of reductant by forming  $\text{NH}_3$  over the LNT and to reduce the amount of PGM required for the LNT since the end result of the LNT will not be complete conversion of  $\text{NO}_x$  to  $\text{N}_2$ , but rather to supply  $\text{NH}_3$  for the SCR catalyst. The addition of the SCR catalyst also solves the problem of  $\text{NH}_3$  slipping from the LNT. The most attractive attribute of this synergistic system is that for a given level of  $\text{NO}_x$  reduction (with the addition of the SCR) the volume of the LNT catalyst, and hence the amount of PGMs and their associated cost, can be reduced.

### *1.8. Scope of the Dissertation.*

The research reported in this dissertation has three aims: 1) to gauge the effectiveness of ceria to act as a sulfur sink and to reduce the sintering of PGM in LNT catalysts; 2) to demonstrate the effects of catalyst composition on the  $\text{NH}_3$  selectivity of LNT catalysts during regeneration; and finally 3) to test a model designed to predict product selectivity from a LNT catalyst loaded with a fixed amount of stored  $\text{NO}_x$ . Since HC and CO emissions are already low in lean burn applications, the focus of this dissertation will be on technologies capable of reducing  $\text{NO}_x$  levels in lean burn engine exhaust.

The next chapter in this dissertation provides the essential background information concerning LNT composition and the chemistry involved during their operation.

Chapter 3 examines the effect of ceria incorporation on sulfation and aging of LNT catalysts. The addition of ceria to LNTs is a response to the problems that the sulfur content in fuels and engine oil presents. Ceria provides an alternative to Ba storage sites for sulfur adsorption during lean operation thereby helping to preserve NO<sub>x</sub> storage capacity. Additionally, ceria has the ability to reduce sintering of the PGM sites by limiting agglomeration of the precious metals that occurs during high temperature events, i.e., during desulfation of the catalyst.

Chapter 4 examines at the effects of washcoat composition on LNT aging characteristics. LNT catalysts with varying amounts of precious metals and storage components are exposed to sulfur and to high temperatures to see how NO<sub>x</sub> conversion and selectivity to NH<sub>3</sub> change in response to aging.

The objective of chapter 5 was to understand the factors governing NH<sub>3</sub> formation (and consumption) in LNTs, including the state of catalyst with respect to aging and the oxygen storage capacity (OSC) of the catalyst.

In chapter 6, the results of an experiment studying the reduction selectivity obtained from a fixed amount of NO<sub>x</sub> stored on a LNT are compared to a model derived to predict these results. Modeling is essential in the design of a LNT-SCR system that promotes NH<sub>3</sub> formation in the LNT while reducing PGM content.

Finally, in chapter 7, all of the significant findings from this work are summarized along with suggestions for future work on this subject. Additionally, the most common abbreviations used throughout this dissertation are included in Appendix 1. Lastly, Appendix 2 contains the derivation of the balances used by the model.

### *1.9. References.*

- [1] Summary of the Clean Air Act 42 U.S.C. §7401 et seq. (1970)  
<http://www.epa.gov/lawsregs/laws/caa.html>. Downloaded 5/23/12.
- [2] ARB's Community Health Program: What is Air Pollution?  
<http://www.arb.ca.gov/ch/educational/definition.htm>. Downloaded 5/23/12.
- [3] Where Does Pollution Come From?  
[http://www.pscleanair.org/images/chart\\_sources.gif](http://www.pscleanair.org/images/chart_sources.gif). Downloaded 5/23/12
- [4] J. Price, L. Ansah, J. Huber, Evaluation Report: EPA and States Not Making Sufficient Progress in Reducing Ozone Precursor Emissions In Some Major Metropolitan Areas Report No. 2004-P-00033 OFFICE OF INSPECTOR GENERAL September 29, 2004 <http://www.epa.gov/oig/reports/2004/20040929-2004-P-00033.pdf>. Downloaded 5/23/12
- [5] Emission Test Cycles: FTP-75 <http://www.dieselnet.com/standards/cycles/ftp75.php>. Downloaded 5/25/12.
- [6] Emission Standards » United States Cars and Light-Duty Trucks—Tier 2  
[http://dieselnet.com/standards/us/ld\\_t2.php](http://dieselnet.com/standards/us/ld_t2.php). Downloaded 5/25/12.
- [7] U.S. Department of Transportation Federal Highway Administration Transportation Air Quality Facts and Figures January 2006 Publication No. FHWA-HEP-05-045 HEP/12-05(8M)E  
[http://www.fhwa.dot.gov/environment/air\\_quality/publications/fact\\_book/page14.cfm](http://www.fhwa.dot.gov/environment/air_quality/publications/fact_book/page14.cfm). Downloaded 5/23/12.
- [8] S.C. Davis, S.W. Diegel, R.G. Boundy. Transportation Energy Data Book, 31<sup>st</sup> ed., U.S. Department of Energy, Office of Energy Efficiency and Renewal Energy, 2012. <http://cta.ornl.gov/data/chapter12.shtml>. Downloaded 5/23/12.

- [9] S.C. Davis, S.W. Diegel. U.S. Department of Energy, Office of Energy Efficiency and Renewal Energy. *Transportation Energy Data Book: Edition 24*, ORNL-6973. December 2004. Downloaded 5/23/12.
- [10] <http://epa.gov/otaq/invntory/overview/results/longdesc-all.htm#hc>. Downloaded 5/25/12.
- [11] J.L. Williams, Oil Price History and Analysis WTRG Economics <http://www.wtrg.com/prices.htm>. Downloaded 5/25/12.
- [12] R.M. Heck, R.J. Farrauto, Automobile Exhaust Catalysts. *Applied Catalysis A: General*, 221 (2001) 443-457.
- [13] R.M. Heck, R.J. Farrauto. *Catalytic Air Pollution Control: Commerical Tehcnology*, 2nd ed., John Wiley and Sons, Inc., New York, 2002.
- [14] [www.epw.senate.gov/enlaws/cleanair.pdf](http://www.epw.senate.gov/enlaws/cleanair.pdf). Downloaded 2/5/13.
- [15] [www.greenercars.org/LEED2012.xls](http://www.greenercars.org/LEED2012.xls). Downloaded 10/24/12.
- [16] J.G.E. Cohn, D.R. Steele and H.C. Andersen, Selective Removal of Nitrogen Oxides from Oxygen-Containing Gases, Especially from Nitric Acid Production from Ammonia. US Patent No. 2975025 (1961).
- [17] M. Koebel, M. Elsener, G. Madia, Reaction Pathways in the Selective Catalytic Reduction Process with NO and NO<sub>2</sub> at Low Temperatures. *Industrial and Engineering Chemistry Research* 40 (2001) 52-59.
- [18] A. Kato, S. Matsuda, T. Kamo, F. Nakajima, H. Kuroda, T. Narita, Reaction between NO, and NH<sub>3</sub> on Iron Oxide-Titanium Oxide Catalyst. *Journal of Physical Chemistry* 85 (1981) 4099-4102.

- [19] G. Tuentler, W.F. van Leeuwen, L.J. Snepvangers, Kinetics and Mechanism of the  $\text{NO}_x$  Reduction with  $\text{NH}_3$  on  $\text{V}_2\text{O}_5$ - $\text{WO}_3$ - $\text{TiO}_2$  Catalyst. *Industrial & Engineering Chemistry Product Research and Development* 25 (1986) 633-636.
- [20] N. Takahashi, H. Shinjoh, T. Iijima, T. Suzuki, K. Yamazaki, K. Yokota, H. Suzuki, N. Miyoshi, S. Matsumoto, T. Tanizawa, T. Tanaka, S. Tateishi, K. Kasahara, The New Concept 3-Way Catalyst for Automotive Lean-Burn Engine:  $\text{NO}_x$  Storage and Reduction Catalyst. *Catalysis Today* 27 (1996) 63-69.
- [21] N. Miyoshi, S. Matsumoto, K. Katoh, T. Tanaka, J. Hardara, N. Takashi, K. Yokota, M. Sugiura, K. Kasahara, Development of New Concept Three-Way Catalyst for Automotive Lean-Burn Engines. *SAE Technical Paper Series* 950809 (1995).
- [22] L. Lietti, P. Forzatti, I. Nova, E. Tronconi,  $\text{NO}_x$  Storage Reduction Over Pt-Ba/ $\gamma$ - $\text{Al}_2\text{O}_3$  Catalyst. *Journal of Catalysis* 204 (2001) 175-191.



## Chapter 2. Lean NO<sub>x</sub> Trap Catalysts: Design and Operational Considerations.

Lean NO<sub>x</sub> Traps (LNTs) were developed by Toyota in the mid-1990s as a means to achieve higher fuel efficiency while reducing NO<sub>x</sub> (NO + NO<sub>2</sub>) emissions that are inherent in the use of lean burn, diesel engines [1,2]. The amount of CO<sub>2</sub> emitted from a diesel engine is less than a similar sized spark-injected gasoline engine (in terms of power output) due to the increased thermodynamic efficiency the diesel possesses [3]. The principle behind the use of these LNT catalysts is that NO<sub>x</sub> is stored during lean operation (the engine exhaust contains stoichiometrically excess oxygen). Concurrently, any hydrocarbons (HCs) and CO in the exhaust are oxidized over the platinum group metals (PGMs) to CO<sub>2</sub> and H<sub>2</sub>O. Before the maximum NO<sub>x</sub> storage capacity of the LNT catalyst is reached, the engine operating conditions are adjusted such that the engine exhaust is net rich. At this point the stored NO<sub>x</sub> is released and then reduced to nitrogen. Other N-species, such as NH<sub>3</sub> and N<sub>2</sub>O, are also potential products depending on the temperature and composition of the exhaust and duration of the rich event. The length of the lean and rich phase is dependent on the operating regime of the engine, the quality of the fuel, and the operational history of the LNT catalyst.

### *2.1. Components of LNT Catalysts.*

#### *2.1.1. Cordierite Substrate.*

The design of the LNT catalyst is comprised of four main components: substrate, support, storage material, and PGMs. The LNT may also include certain additives to improve catalyst performance. The main function of the substrate is to provide a high surface area material that possesses mechanical and thermal durability upon which a washcoat containing the other ingredients can be applied. The most common substrate used today is synthetic cordierite, 2MgO·2Al<sub>2</sub>O<sub>3</sub>·5SiO<sub>2</sub>. Cordierite mainly consists of kaolin (Al<sub>2</sub>O<sub>3</sub>·SiO<sub>2</sub>·2H<sub>2</sub>O), talc (3MgO·4SiO<sub>2</sub>·H<sub>2</sub>O) and alumina (Al<sub>2</sub>O<sub>3</sub>) that are ground, blended, and extruded into a paste. The cordierite is usually configured as a honeycomb monolith which provides a high surface area to volume ratio (e.g., 852 ft<sup>2</sup>/ft<sup>3</sup>) [4]. The honeycomb monolith also has a low pressure drop across the catalyst which eliminates the risk of creating a back pressure to the engine. Cordierite also possesses the

necessary mechanical and thermal properties required for operation of a catalyst located down-stream of an internal combustion engine. The low thermal expansion coefficient of cordierite ( $10 \times 10^{-7}/^{\circ}\text{C}$ ) makes it resistant to cracking when cycled over a wide temperature range [4]. The mechanical axial strength of over 3000 psi is required for operation underneath an automobile. Moreover, the melting point of greater than  $1300^{\circ}\text{C}$  is well above the operating range of a LNT [5].

### *2.1.2. Catalyst Support.*

A washcoat that contains PGMs,  $\text{NO}_x$  storage materials, and catalyst support is applied to the cordierite monolith. Different types of supports, such as  $\text{TiO}_2$ ,  $\text{SiO}_2$ ,  $\text{ZrO}_2$ ,  $\text{CeZrO}_2$ ,  $\text{TiO}_2\text{-ZrO}_2$ ,  $\text{CeO}_2$ , and  $\gamma\text{-Al}_2\text{O}_3$ , have been studied by several groups. Each of these materials behaves differently with the other catalyst components with regards to performance under different operating regimes. Johnson et al. stated a simple goal for all catalyst supports: to provide a durable, high surface area to aid in the maintenance of the dispersion of the metallic promoters or PGMs [7]. Using this as a metric,  $\gamma\text{-Al}_2\text{O}_3$  was used as the support in all of the catalysts studied for this dissertation. Since the goal of this research effort was to look at the addition and the variation of different catalyst components, the use of  $\gamma\text{-Al}_2\text{O}_3$  as a support is ideal because  $\gamma\text{-Al}_2\text{O}_3$  is a well-known support material that has been utilized in three-way catalytic (TWC) converters, oxidation catalysts, and even in the first SCR catalysts. Additionally, the results of a study by Fekete et al. [8] studying  $\text{TiO}_2$ ,  $\text{ZrO}_2$ , and  $\gamma\text{-Al}_2\text{O}_3$  revealed that  $\gamma\text{-Al}_2\text{O}_3$  is the most suitable support because  $\text{TiO}_2$  and  $\text{ZrO}_2$  have high reactivity with the Ba storage component which can lead to unwanted side reactions within the washcoat.

The properties of  $\gamma\text{-Al}_2\text{O}_3$  (surface area, pore size distribution, surface acidic properties and crystal structure) depend on its preparation, purity, and thermal history [4]. A high surface area is created by heat-treating or calcining in air, typically at about  $500^{\circ}\text{C}$ , where a network is formed from  $\text{Al}_2\text{O}_3$  particles 20-50Å in diameter which bond together, forming polymer-type chains. As temperature is increased between the ranges in which a given  $\text{Al}_2\text{O}_3$  crystal structure is stable, there is gradual dehydration, which causes an irreversible loss in physical surface area and loss in its surface hydroxyl or Brønsted acid

sites. Continued heating causes a complete transformation to another crystal structure with a continuing loss in physical surface area and surface OH<sup>-</sup> groups. This transformation is shown by the following [3]:

Boehmite:  $\gamma$ -monohydrate (500-850 °C), internal surface area 100-200 m<sup>2</sup>/g →  
 $\delta$ -monohydrate (850-1050 °C) →  $\theta$ -monohydrate (1050-1150 °C) →  
 $\alpha$ -monohydrate (>1150 °C), 1-5 m<sup>2</sup>/g

As shown,  $\gamma$ -Al<sub>2</sub>O<sub>3</sub> is the structure that is most attractive for use as a support for an LNT because it exists in the operating temperature window of diesel engine operation (150 °C to 500 °C) and possesses the highest surface area.  $\gamma$ -Al<sub>2</sub>O<sub>3</sub> with Pt and Ba species impregnated on the surface has a surface area of ~150 m<sup>2</sup>/g [4]. The surface of  $\gamma$ -alumina is covered in OH<sup>-</sup> groups onto which storage material and precious metals are applied.

To improve certain properties such as thermal durability and bonding with the support and PGM materials, different additives have been added to  $\gamma$ -Al<sub>2</sub>O<sub>3</sub>. This addition is also known as doping. Schaper et al. and Pijolat et al. [9,10] pointed to two phenomena as being responsible for the loss of surface area at high temperatures (>900 °C): initial sintering due to the collapse of micropores and phase transformation from  $\gamma$ -Al<sub>2</sub>O<sub>3</sub> into  $\alpha$ -Al<sub>2</sub>O<sub>3</sub>. Schaper et al. [11] believed the transformation from the  $\gamma$  to the  $\alpha$  phase proceeded via a surface diffusion of the oxygen ions changing the crystal lattice from a cubic to a hexagonal closed packed structure. To add additional thermal stability to the  $\gamma$ -Al<sub>2</sub>O<sub>3</sub> support, lanthanum was added. Lanthanum oxide, La<sub>2</sub>O<sub>3</sub>, decreases the sintering of  $\gamma$ -Al<sub>2</sub>O<sub>3</sub> by formation of lanthanum aluminate, LaAlO<sub>3</sub>, on the  $\gamma$ -Al<sub>2</sub>O<sub>3</sub> surface [11,12]. The addition of the La<sub>2</sub>O<sub>3</sub> was found to postpone the phase transformation by 100°C by promoting the rate of nucleation of cubic LaAlO<sub>3</sub> on the  $\gamma$ -Al<sub>2</sub>O<sub>3</sub> surface and thereby inhibiting the surface diffusion of species responsible for sintering [13].

### 2.1.3. NO<sub>x</sub> Storage Materials.

As the name suggests, the main function of the NO<sub>x</sub> storage material in LNTs is to store NO<sub>x</sub> during lean engine operation. NO<sub>2</sub> has been shown to be preferential to NO for

storage; this will be discussed later in this chapter in the section describing the mechanisms inherent in LNT operation. As the basicity of the storage material increases, so does its ability to store NO<sub>x</sub> [14-19]. For this reason, either alkali metals (Na, K, Cs) or alkaline earth metals (Mg, Ca, Sr, Ba) or combinations of these are used as storage materials. The criteria for determining which material is the best choice include a number of factors such as NO<sub>x</sub> storage capacity, NO<sub>x</sub> conversion, stability in the washcoat, and sulfur resistance. Many of these desired properties are determined by the basicity of the storage material. In order of increasing basicity, the metals follow the order: Mg ≤ Li < Ca < Na ≤ Sr < Ba < K < Cs [19,20]. While Cs has the highest basicity of this list of metals, the HC conversion performance is the worst, which eliminates it as a suitable choice [19]. Han et al. compared Pt/Al<sub>2</sub>O<sub>3</sub> catalysts that contained BaO, CaO, or SrO. Overall, BaO and SrO showed the highest NO<sub>x</sub> storage capacity, but BaO showed the best NO<sub>x</sub> conversion [21].

Although most of the literature uses BaO as the storage component, K has been the subject of increasing research. For diesel exhaust applications, the use of K has some drawbacks. Light duty diesels (passenger cars and light trucks) have exhaust temperatures between 100 and 500 °C depending on operating load and engine speed. Looking at the NO<sub>x</sub> storage capacity, Ba and K have two different temperature ranges for maximum efficiency. BaO has a higher NO<sub>x</sub> storage capacity below 400 °C, and K has a higher capacity above 400 °C [19]. Gill et al. postulated that the increased performance of K at a higher temperature was attributed to the increased stability of the nitrates formed by alkali metals [22]. Conversely, the low temperature NO<sub>x</sub> conversion was less than that of BaO due to K inhibiting the formation of NO<sub>2</sub>. Another factor in determining whether K is suitable as a storage material is the water solubility of KNO<sub>3</sub>. Moreover, K has the potential to react with the cordierite substrate that is common in most auto catalyst applications. The mobility of K due to its affinity for water makes maintaining K sites in the desired location on the catalyst support problematic. Additionally, as will be discussed, the formation of sulfates follows the same general mechanism as nitrates with the resulting sulfates having a greater thermodynamic stability on the LNT. On account of this, the nitrates stored at K sites are more stable than the ones stored at Ba sites;

similarly, the sulfate stored on K sites is more difficult to remove than sulfates associated with Ba. The results of the increased efforts required to remove sulfates from K are longer rich periods and/or the necessity of increased reductant concentrations. This change decreases the potential fuel savings gained by the selection of a diesel engine. The implications of sulfur for LNTs will be discussed shortly.

Lastly, it is worth mentioning that the choice of the storage component will affect the product selectivity during regeneration of the LNT. Studies by Castoldi et al [23] and Lesage et al. [24] have shown that the selectivity to  $N_2$  is higher while the  $NO_x$  “puff” is smaller from catalysts using K versus Ba (the  $NO_x$  “puff” phenomenon will be discussed below).

In light of the above discussion and following the suggestions from Miyoshi et al [1], BaO seems to be the best choice for use a  $NO_x$  storage material. As with the choice of  $\gamma$ - $Al_2O_3$  as the catalyst support, because Ba-based storage materials have been thoroughly researched, they represent a good choice when studying the addition of other components and the modification of the PGMs. Ba is present in the LNT as BaO,  $Ba(OH)_2$ , and/or  $BaCO_3$ , depending on the composition of the exhaust stream [14]. In most of the experiments discussed in this dissertation,  $CO_2$  and  $H_2O$  were present, so all three types of Ba-compounds would be expected to be present on the catalyst surface at the end of the rich phase. During the subsequent lean phase as  $NO_x$  is preferentially stored at the BaO and  $Ba(OH)_2$  sites, the majority of the sites available for storage will be  $BaCO_3$ . An exception was a set of the experiments described later in this dissertation which deal with the modeling of the release of a fixed amount of  $NO_x$  from different catalysts, in which  $CO_2$  and  $H_2O$  were excluded. Because of that, the form of Ba could be identified as  $Ba(OH)_2$  (due to the use of hydrogen during the rich phase). According to Lietti et al [14],  $NO_x$  storage occurs first at the BaO sites, followed by  $Ba(OH)_2$  and  $BaCO_3$ , in line with the higher basicity of the former compound.

#### *2.1.4. Platinum Group Metals (PGM).*

The final ingredient of LNTs consists of the PGM component: platinum, rhodium, and palladium. While there have been many different studies on PGMs in three-way catalysts and LNTs, one common finding is that these metals behave differently under varying feed gas streams and reaction conditions. The choice of which PGM to use depends on the metal's chemistry during lean and rich operation. During the lean phase, the PGM must be able to oxidize NO to NO<sub>2</sub> that will subsequently spillover to the storage sites. Under rich conditions, the PGMs must adsorb reductants such as CO, H<sub>2</sub>, and HC as well as to provide sites close to the stored nitrates and nitrites which can dissociatively adsorb NO<sub>x</sub> as part of a reverse spillover mechanism. Pt is the primary choice for oxidation of NO, but Rh and Pd are more active for NO<sub>x</sub> reduction [25-28]. Moreover, Kobayashi et al. showed that a combination of Pt/Rh had a higher trapping activity than either Pd/Rh or Pd [20]. Additionally, Theis et al. reported that a combination of Pt and Rh had the best overall NO<sub>x</sub> conversion at low temperatures (250°C) for fresh and aged catalysts as compared to Pt only samples [29]. Theis proposed the Rh increased reduction capability and also enhanced the purging of the trap by creating a concentration gradient between the catalyst surface and the exhaust that promoted the decomposition of the stored NO<sub>x</sub> and a more thorough purge [29]. The gradient was created by the ability of Rh to promote the thermodynamic instability of NO<sub>3</sub><sup>-</sup> stored on the catalyst at the Ba sites by more efficiently removing the NO<sub>x</sub> in the gas phase. Lastly, Amberntsson et al. showed that an alloy of Pt and Rh increased the overall efficiency of the NO<sub>x</sub> storage catalyst despite storing a lower amount of NO<sub>x</sub> than a Pt-only catalyst [27].

#### *2.2. Mechanisms Involved LNT Catalysis.*

Although a large number of experimental studies have focused on determining the mechanisms involved when using a LNT catalyst to convert NO<sub>x</sub> to N<sub>2</sub>, a precise, definitive mechanism still proves elusive. Fortunately, the following series of steps are both accepted in the catalysis community and provide enough description to enable one to gain a well-informed idea of how an LNT catalyst is operated. The discussion will be focused on the type of catalysts used in the experiments that will be presented in the later chapters, rather than involving all of the different combinations of PGMs, storage

materials, supports, and reductants that have been presented in the literature. Arguments have already been made for why different catalyst components are preferred, and the effects of gases present in the exhaust during the lean and rich phases will be presented as the different steps are explained.

The steps involved in the operation of LNTs are [30,32]:

1. NO oxidation to NO<sub>2</sub> on Pt,
2. NO<sub>x</sub> (NO+NO<sub>2</sub>) storage on BaO on the catalyst surface
3. Reductant evolution,
4. NO<sub>x</sub> release from the trapping site,
5. NO<sub>x</sub> reduction to N<sub>2</sub>.

Although many authors agree on these five steps, the details about each step, particularly steps 1 and 2, are subject to debate.

### *2.2.1. Oxidation of NO to NO<sub>2</sub>.*

The oxidation of NO to NO<sub>2</sub> is a very important step in the operation of most aftertreatment systems. LNTs are based on NO<sub>x</sub> present in the form of NO<sub>2</sub> for efficient trapping to occur [6,33-38]. As will be discussed in section 2.2.2., most trapping metals as described previously more effectively adsorb NO<sub>2</sub> as compared to NO [6]. Therefore, the more efficiently a LNT can oxidize NO to NO<sub>2</sub>, the greater the potential NO<sub>x</sub> storage capacity.

The oxidation of NO to NO<sub>2</sub> is affected by the temperature and composition of the exhaust stream and the state of the PGMs on the catalyst. The oxidation reaction is subject to limitations based on temperature. At low temperatures (below 250 °C), the reaction is kinetically limited from reaching equilibrium. As the temperature is increased (> 200 °C), the process changes from one that is limited by kinetics to one that is limited by the thermodynamic equilibrium that exists between NO, O<sub>2</sub>, and NO<sub>2</sub>. Where the equilibrium occurs is dependent on the temperature, oxygen concentration, and space velocity of the LNT. The space velocity can create kinetic limitations that prevent the

reaction from reaching equilibrium. The equilibrium will shift to higher temperatures as the concentration of  $O_2$  increases. Mahzoul et al. [32] noticed that the  $NO_x$  storage capacity of a Pt/BaO/ $Al_2O_3$  catalyst increased as  $O_2$  concentration was increased from 0 to 3%, but above 3% no additional effect was observed. As the space velocity or residence time of the system increases, not only does the temperature required to reach equilibrium increase (the increase in temperature is required to overcome limited kinetics), but the equilibrium conversion at that temperature decreases. Above this temperature, the oxidation of NO is under thermodynamic control, and below it, the process is kinetically controlled. The integral nature of LNTs presents an additional factor influencing when or if equilibrium can be reached, since as  $NO_2$  is produced and stored on the catalyst, the equilibrium is shifted towards additional  $NO_2$  production [39].

As previously discussed, Pt has unparalleled NO oxidation capacity [25-27,35]. In the literature, NO oxidation is studied using Pt and a support ( $\gamma-Al_2O_3$ ) or with a model or fully formulated LNT containing Pt and a storage material such as Ba on a support ( $\gamma-Al_2O_3$ ). The amount and dispersion of Pt and the interaction between Pt and  $\gamma-Al_2O_3$  impacts the kinetics of NO oxidation. Lee et al. [40] noted that higher dispersions (i.e., smaller particles) did not always lead to higher NO oxidation rates. Indeed, Pt particles with lower exposed surface areas generally exhibit increased catalytic activity for NO oxidation. Olsson et al. [41] similarly noted that after aging while the onset of oxidation was unaffected, the rate of NO oxidation increased. This is consistent with Lee, given that thermal aging results in Pt particle sintering [42-44]. Pt oxides are present as a surface layer on the Pt particles [41]. Smaller particles of Pt are more likely to form  $PtO_x$  relative to larger particles [45]. This occurrence is one reason why catalysts are subjected to slightly elevated temperatures ( $\geq 500$  °C) under neutral conditions before using them in experiments and real-world applications. After the particles become larger, it is less likely that  $PtO_x$  will form, and catalyst performance is improved. Mulla et al. observed a 4-fold increase in the NO oxidation turnover rate (TOR) for a sintered catalyst as compared to a fresh one [46]. This observation, TOR increasing with increasing Pt particle size, is supported in the literature [40,41,47-49].



The presence of Ba has the ability to reduce the activity of the Pt particles due to the potential for increased formation of Pt oxides during lean periods of operation. Many authors have reported that the presence of Ba in a Pt/BaO/Al<sub>2</sub>O<sub>3</sub> LNT decreases the rate of oxidation reactions over Pt as compared to a Pt/Al<sub>2</sub>O<sub>3</sub> catalyst [30,41,50-53]. The high surface coverage by oxygen prevents the adsorption of NO on Pt. Indeed, the presence of Ba decreases the NO oxidation activity of Pt as compared to a Ba-free catalyst for the following possible reasons. First, during the preparation by impregnation of the catalyst, some of the Pt might dissolve into the Ba phase. If the Pt dispersion is decreased due to Ba masking Pt, the activity for the oxidation of NO will decrease. Second, as NO<sub>x</sub> is stored at the Ba sites, some of the Pt sites might become sterically hindered by the resulting Ba(NO<sub>3</sub>)<sub>2</sub>, since the molar volume of Ba(NO<sub>3</sub>)<sub>2</sub> is 3 times larger than that of BaO [30]. The final possible reason for the decrease in activity caused by the presence of Ba is proposed by Yoshia et al. Yoshia considered the acidity or alkalinity of the support by noting that if the support was acidic, Pt oxide formation was suppressed [52]. In a Pt/Al<sub>2</sub>O<sub>3</sub> catalyst, the  $\gamma$ -Al<sub>2</sub>O<sub>3</sub> is electrophilic and electrons are donated from the outer band in the Pt atoms to the support. When Pt oxides are formed, electrons are transferred from the Pt to the oxygen. With an acidic support, there is a lower electron density in the Pt present, and the formation of the oxides is suppressed. When added, the alkalinity of BaO decreases some of the acidic nature of the support so that there are more available electrons for the formation of PtO<sub>x</sub> [52]. Olsson and Fridell [41] did indeed observe from XPS data that after exposure to NO<sub>2</sub>, Pt/BaO/Al<sub>2</sub>O<sub>3</sub> had a higher occurrence of PtO<sub>x</sub> than Pt/ $\gamma$ -Al<sub>2</sub>O<sub>3</sub>.

An additional source of chemisorbed oxygen is NO<sub>2</sub> itself. NO<sub>2</sub> is an effective source of atomic oxygen because of its high sticking coefficient. The chemisorbed oxygen prevents the adsorption of other species thereby inhibiting the NO oxidation reaction [54,55].

The different components, Pt, NO, NO<sub>2</sub>, and O<sub>2</sub>, have been discussed in terms of their contributions to the oxidation of NO over Pt. Turning to the mechanism involved on the catalyst surface, some debate exists in the literature as to which type of mechanism is

occurring. Olsson et al. [39] first proposed the oxidation of NO over Pt followed an Eley-Rideal (ER) mechanism that contained the following adsorption and desorption steps:



and the reversible oxidation step [56]



Olsson noted that ER was preferred to a Langmuir-Hinshelwood (LH) NO oxidation step:

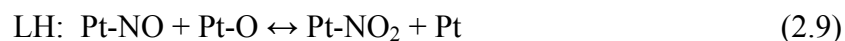


since a high oxygen coverage in (2.5) hinders a high NO<sub>2</sub> formation rate, and Olsson's experimental results did not indicate that NO oxidation will be self-poisoned by a high coverage. Conversely, Mahzoul et al [32] suggested a LH mechanism occurring at Pt sites close to the Ba storage sites as follows:



The actual oxidation of NO<sub>x</sub> is discussed in section 2.2.2.3.

Later, Olsson et al. [30] considered that either ER, LH, or a combination of ER and LH mechanisms might be occurring. The initial adsorption steps for NO, NO<sub>2</sub>, and O<sub>2</sub> are the same as in the previous report, but now Olsson considers the LH and ER mechanisms for adsorbed NO and NO<sub>2</sub> reacting with chemisorbed oxygen on the Pt sites:



For the model using LH and ER mechanisms, both of the above reactions (2.9 and 2.10) would be involved. Although all 3 of these possibilities provided satisfactory fits for their data, Olsson decided that a LH mechanism would be more probable based on reasoning by Bartram [57]. Bartram stated that  $\text{NO}_2$  should be bridge bonded to decompose to NO and oxygen on the Pt surface. This implies that  $\text{NO}_2$  would require two Pt sites to decompose, making a LH mechanism most probable. Nova et al. [58] also favored  $\text{NO}_x$  adsorption and oxygen dissociation over Pt (LH), while Muncrief et al. [46] also used Langmuir-Hinshelwood and Eley-Rideal mechanisms for these steps.

From the literature, evidence is given in support of each of these scenarios that describe NO oxidation over Pt. The LH mechanism is probably the most likely to occur for the reasons suggested by Bartram. The most important aspect of this step is that  $\text{NO}_2$  is formed and adsorbed at the Pt sites.

### 2.2.2. Storage of $\text{NO}_x$ at BaO Sites.

Mechanisms presented in the literature agree on the following:

1.  $\text{NO}_2$  is preferred to NO for storage at the BaO sites.
2. BaO,  $\text{Ba(OH)}_2$ , and  $\text{BaCO}_3$  are present on the catalyst surface.
3.  $\text{NO}_x$  stored as  $\text{Ba(NO}_3)_2$  is more stable than  $\text{Ba(NO}_2)_2$ ; as temperatures and storage times increase,  $\text{Ba(NO}_2)_2$  is eventually oxidized to  $\text{Ba(NO}_3)_2$  as the oxidation state of N is increased from  $3^+$  to  $5^+$ .
4. Proximity of Pt to Ba is critical for efficient storage on the LNT.

In general, there is no consensus on the following:

1. After NO is oxidized over Pt, does it travel to the Ba sites on the catalyst surface as an adsorbed species or does it desorb from Pt and readsorb onto Ba from the gas stream?
2. While chemisorbed oxygen is necessary in every mechanism, is the oxygen supplied by spillover from the Pt sites, or is it supplied by NO<sub>2</sub> or through BaO<sub>2</sub>? This point will be discussed later in this chapter.

#### *2.2.2.1. Effects of Components in the Engine Exhaust.*

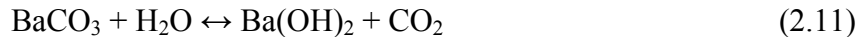
The components present in the engine exhaust influence the storage of NO<sub>x</sub> and the phase of the Ba storage component. Two potentially reactive components that are present in large quantities (5 to 10 vol%) in the exhaust gases from diesel engines are CO<sub>2</sub> and H<sub>2</sub>O. Although  $\gamma$ -Al<sub>2</sub>O<sub>3</sub> is capable of NO<sub>x</sub> storage [32,36,59-62], the presence of H<sub>2</sub>O in the gas stream reduces NO<sub>x</sub> storage on the  $\gamma$ -Al<sub>2</sub>O<sub>3</sub> support. Without H<sub>2</sub>O present, researchers [32,59-63] have estimated that between 1% and 8% of the NO<sub>x</sub> stored on the LNT is stored on the  $\gamma$ -Al<sub>2</sub>O<sub>3</sub> support. Toops [64] reported a decrease of 92% of NO<sub>x</sub> stored on  $\gamma$ -Al<sub>2</sub>O<sub>3</sub> when H<sub>2</sub>O was present. The reason for this decrease is due to the presence of molecular H<sub>2</sub>O on the  $\gamma$ -Al<sub>2</sub>O<sub>3</sub> which hinder the NO<sub>x</sub> sorption process by limiting the amount of storage sites available. Since H<sub>2</sub>O is present in the experiments that will be discuss in the later chapters in this dissertation, the remaining summary on NO<sub>x</sub> adsorption and desorption will focus on the Ba component.

#### *2.2.2.2. Identity of Ba Storage Component.*

Although the Ba component in most mechanisms is assumed to be BaO, when H<sub>2</sub>O and CO<sub>2</sub> are present, Ba(OH)<sub>2</sub> and BaCO<sub>3</sub> co-exist on the catalyst support. The impact of these three phases can be realized by comparing their basicities. Lietti [14,65] ranked the following compounds involving Ba in order of increasing basicity, which is also a ranking of the stability of the Ba component on the catalyst.



BaSO<sub>4</sub> is formed when sulfur is present in the gas stream and will be discussed later in this chapter. NO<sub>x</sub> adsorption occurs at the Ba components that are the least stable first. As such, NO<sub>x</sub> is stored preferentially at the BaO sites, followed by Ba(OH)<sub>2</sub>, and finally at BaCO<sub>3</sub> sites. Evidence for the type of Ba compound present is provided by Lietti et al. [14] from NO<sub>x</sub> storage experiments. A LNT was regenerated with varying amounts of CO<sub>2</sub> and H<sub>2</sub>O present in the gas feed. Whether or not CO<sub>2</sub> or H<sub>2</sub>O was present during the regeneration determined the duration of the delay before NO<sub>x</sub> slip occurred. NO<sub>x</sub> slip occurred the earliest when regeneration was performed in dry air (CO<sub>2</sub>, no H<sub>2</sub>O). Under these conditions, the Ba storage component would be expected to be BaCO<sub>3</sub>. This was in line with the negative effect that CO<sub>2</sub> has on NO<sub>x</sub> storage [14,64,66,67]. When the LNT was regenerated with H<sub>2</sub> only, NO<sub>x</sub> slip occurred later with less CO<sub>2</sub> produced as the stored NO<sub>x</sub> displaced the OH<sup>-</sup> and CO<sub>3</sub><sup>2-</sup> species present in the Ba compounds. During this step the BaCO<sub>3</sub> compounds are gradually becoming Ba(OH)<sub>2</sub>. As this transition occurred, the increase in the amount of Ba(OH)<sub>2</sub> accounted for an increase in NO<sub>x</sub> storage. Finally (once again with H<sub>2</sub> only) NO<sub>x</sub> slip occurred even later with more H<sub>2</sub>O and almost no CO<sub>2</sub> produced. At this point in the experiment, nearly all of the BaCO<sub>3</sub> sites had become Ba(OH)<sub>2</sub>. In the last two cases, H<sub>2</sub>O reduced the impact of CO<sub>2</sub> by converting the BaCO<sub>3</sub> species into Ba(OH)<sub>2</sub>.



The trends seen in this set of experiments follow the reported thermodynamic predictions in the literature [2,14, 20,66,68]. Although not present during regeneration, CO has a similar effect as CO<sub>2</sub> is produced, according to eqn. (2.12) [31]



The presence of CO results in an increase in the concentration of NO according to (2.12). This reaction reduces the trapping efficiency of the LNT. The ratio of the two depends on the duration and temperature of NO<sub>x</sub> storage.

The increased stability of  $\text{Ba}(\text{NO}_2)_2$  and  $\text{Ba}(\text{NO}_3)_2$  compared to  $\text{BaO}$  and  $\text{Ba}(\text{OH})_2$  is a desired result because  $\text{NO}_x$  stored as nitrites and nitrates will remain at the Ba sites during lean conditions, rather than being replaced by other species; conversely, the stability of  $\text{BaSO}_4$  means that sulfur compounds will preferentially store at the Ba sites. As discussed later,  $\text{BaSO}_4$  leads to a decrease in the available Ba sites for  $\text{NO}_x$  storage over time. Ultimately, the storage capacity of the LNT is compromised.

In summary,  $\text{NO}_x$  is stored as nitrites and nitrates at  $\text{BaO}$ ,  $\text{Ba}(\text{OH})_2$  and  $\text{BaCO}_3$  sites, in that order. Individually,  $\text{CO}_2$  and  $\text{H}_2\text{O}$  have a negative effect on  $\text{NO}_x$  storage because the resulting Ba phase is more stable than  $\text{BaO}$ ; this degrades  $\text{NO}_x$  storage efficiency. When  $\text{CO}_2$  and  $\text{H}_2\text{O}$  are both present in the exhaust stream, the negative effects of  $\text{CO}_2$  are reduced because the  $\text{BaCO}_3$  sites can be hydrolyzed to  $\text{Ba}(\text{OH})_2$ .

#### *2.2.2.3. Mechanisms of $\text{NO}_x$ Storage.*

Based on the preceding discussion, only  $\text{BaO}$  storage sites will be considered hereafter in order to simplify the discussion of the mechanisms in operation during the storage of  $\text{NO}_x$  on a LNT. Additionally, it should be noted that the formation of nitrates is favored over nitrites given that the range of temperatures studied in the experiments discussed in later chapters was 200 °C to 300 °C. Nitrites are reported to be present from 150 °C to 200 °C [62,68] and at the beginning of the storage process [32,69-72]. The likelihood of the presence of nitrates at higher temperatures is due either to oxidation of the nitrites being easier as temperatures increase or to nitrites being more unstable than nitrates at these temperatures with respect to decomposition [32,36,62,69-74].

The storage of  $\text{NO}$  and  $\text{NO}_2$  formed from the oxidation of  $\text{NO}$  over Pt is thought to be a sequential process [5,30,75-77]. Fridell et al. [39] described the  $\text{NO}_x$  adsorption process in 3 steps.  $\text{NO}_2$  formed at the Pt sites is at first loosely adsorbed on  $\text{BaO}$  as a  $\text{BaO}\text{-NO}_2$  species, and then  $\text{BaO}\text{-NO}_2$  decomposes to  $\text{BaO}_2$ , a peroxide, and  $\text{NO}$  which is released to the gas phase:



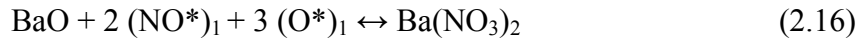
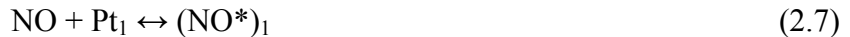
The BaO<sub>2</sub> would ultimately react with NO<sub>2</sub> in the gas phase to produce Ba(NO<sub>3</sub>)<sub>2</sub>



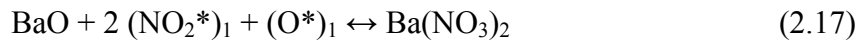
While this mechanism does explain the NO<sub>x</sub> slip that is seen during storage and has been suggested by other authors as an intermediate step [71,78-80], direct experimental evidence for the Ba-peroxide has yet to be found [81].

Mahzoul et al. proposes that two kinds of sites are present [32]. Pt particles close to BaO crystallites (sites 1) are responsible for nitrate formation (\* denotes adsorbed species).

Continuing from the previous discussion of Mahzoul's study, eqn. (2.6) through (2.8):



Or

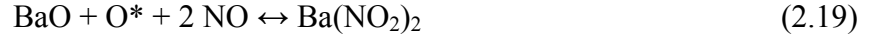


Pt sites far from the Ba crystallites (sites 2) allow the Pt to behave as an oxidation catalyst, forming nitrites.

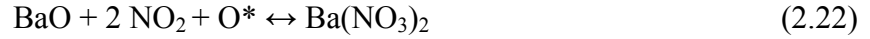


Kabin et al. 77, Kromer et al.84, Bhatia et al.85, Cant el al. and Kwak et al 86 have also postulated proximity theories [75, 82-84].

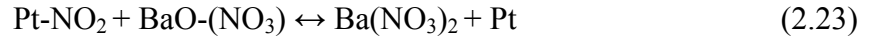
Lietti et al. [14] also proposed two pathways for this series of reactions to occur but differed from Mahzoul by exploring whether or not NO is adsorbed or is first oxidized to NO<sub>2</sub>. If NO is adsorbed at Pt sites close to BaO, then the following occurs with oxygen again being dissociated over Pt:



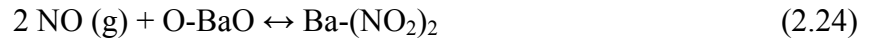
If NO is oxidized to NO<sub>2</sub> at Pt sites close to BaO sites first, then:



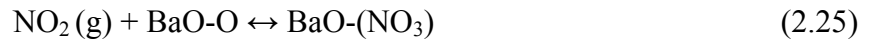
If the reaction sequence provided by Olsson [30] is continued (in which NO oxidation occurs either by ER, LH, or ER-LH mechanisms), then NO<sub>x</sub> is stored on the Ba component by NO or NO<sub>2</sub> spilling over from the Pt sites as opposed to adsorbing on the surface directly from the gas phase:



The other possibility of NO<sub>x</sub> storage would involve NO being adsorbed on the oxidized BaO sites:

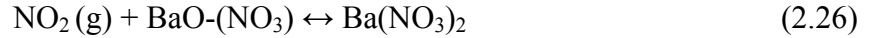


Similarly, adsorbed NO<sub>2</sub> can react with an adsorbed oxygen atom and nitrate formed:





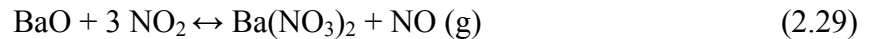
with the nitrate localized on the Ba part of BaO. Another NO<sub>2</sub> (g) molecule is then adsorbed on the oxide part and Ba(NO<sub>3</sub>)<sub>2</sub> is formed:



Probably the most accepted views on NO oxidation and subsequent storage as Ba(NO<sub>3</sub>)<sub>2</sub> or Ba(NO<sub>2</sub>)<sub>2</sub> are provided by Nova et al. and Forzatti et al [58,73,74,85-87]. Nova et al. presented a mechanism involving NO<sub>x</sub> adsorption and oxygen dissociation over Pt [58]:



Nitrites are stored at BaO sites in close proximity to Pt sites, whereas the nitrate is formed on the catalyst surface and NO is released. This is described by the disproportionation reaction:

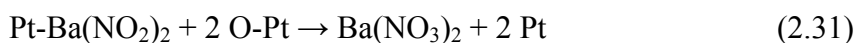
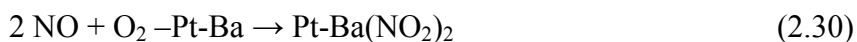


In this reaction, NO<sub>2</sub> is the source of adsorbed oxygen needed for NO<sub>3</sub><sup>-</sup> formation to occur. The NO released into the gas stream is available to be oxidized again over a Pt site located downstream in the catalyst. As the catalyst becomes saturated with NO<sub>x</sub>, there is less opportunity for NO to be oxidized and readsorbed and therefore would pass unreacted through the rear of the LNT. The stoichiometry for (2.29) has been proved by several research groups. Nova et al. [74] monitored the ratio of moles of NO evolved at the reactor outlet to moles of NO<sub>2</sub> consumed. Nova found as NO<sub>x</sub> storage approached saturation, this ratio approached 0.33 which corresponds to 1 mole of NO released for every 3 moles of NO<sub>2</sub> consumed.

Forzatti et al. [74,85-87] also supports the inclusion of the disproportionation reaction. Using FTIR under *In Operando* conditions, Forzatti also observed that 1 mol of NO was released for every 3 mol of NO<sub>2</sub> adsorbed [85]. Forzatti postulates two parallel routes for NO<sub>x</sub> storage in the presence of oxygen. In the nitrate route, NO<sub>2</sub>, from NO oxidation on

Pt, spills over to Ba sites in close proximity to Pt to form Ba(NO<sub>3</sub>)<sub>2</sub> with the evolution of NO into the gas phase, eqn. (2.29).

In the other route, NO is directly oxidized on Pt to form Ba(NO<sub>2</sub>)<sub>2</sub> that is oxidized by oxygen that spills over from Pt to form Ba(NO<sub>3</sub>)<sub>2</sub> (as shown in eqn. 2.31).



The ratio of nitrites to nitrates formed is dependent on the Ba loading on the catalyst and the temperature. Forzatti found more nitrites were formed as the Ba loading increased due to enhancement of the interface existing between Pt and Ba [74,85,86]. Kumar et al. [88] demonstrated the dependence of temperature by measuring the ratio of oxygen to nitrogen stored on BaO. Using Ba(NO<sub>3</sub>)<sub>2</sub> and Ba(NO<sub>2</sub>)<sub>2</sub> standards, Kumar determined the theoretical ratio of O:N to be 2.5 and 1.5, respectively. Using NO pulse experiments, at 350 °C the ratio was calculated to be 2.3 corresponding to NO<sub>x</sub> stored as Ba(NO<sub>3</sub>)<sub>2</sub>. As the temperature was reduced to 250 °C, the ratio decreased to 1.8, indicating a mixture of Ba(NO<sub>3</sub>)<sub>2</sub> and Ba(NO<sub>2</sub>)<sub>2</sub>.

#### 2.2.2.4. Proximity of Pt and Ba Components.

The proximity of the Pt and Ba phases has been well researched in the literature [31,32,49,58,66,74,77,82,89,90-108]. The effect of their proximity was confirmed in powder experiments that revealed that NO<sub>x</sub> storage was decreased when Pt and BaO were not on the same nanoparticle [89]. The proximity is considered in terms of either the type of Ba or the type of Pt. At Ba sites close to Pt, a rapid uptake of NO<sub>x</sub> occurs, while at Ba sites far from Pt, NO<sub>x</sub> uptake still occurs but at much slower rate [1,6,37]. If one considers Pt sites, the following remarks can be made. Pt in contact with Ba is thought to be responsible for NO<sub>x</sub> storage pathways involving the dissociative adsorption of O<sub>2</sub> on Pt that could provide the proximal Pt and Ba sites with a source of O-atoms for the oxidation of NO<sub>2</sub> to NO<sub>3</sub><sup>-</sup> [31]. Pt far from Ba is thought to play an important role in NO oxidation [32,109,110]. At these far sites, NO<sub>2</sub> formed is likely to be involved as the

oxidant in the disproportion reaction, eqn. (2.32). The proximity of Pt and Ba also helps to explain the changes in the rate of  $\text{NO}_x$  uptake with  $\text{NO}_x$  loading [87]. At the beginning of  $\text{NO}_x$  uptake, the spillover of  $\text{NO}_x$  from Pt to the Ba sites is fast and complete uptake of  $\text{NO}_x$  is observed in the LNT. Uptake of  $\text{NO}_x$  decreases as the formation of  $\text{Ba}(\text{NO}_3)_2$  or  $\text{Ba}(\text{NO}_2)_2$  creates a diffusion barrier for  $\text{NO}_2$ . The development of this diffusion barrier increases the likelihood of  $\text{NO}_x$  slip.

#### 2.2.2.5. Summary of $\text{NO}_x$ Adsorption.

Even though there appear to be several pathways for the oxidation and adsorption of  $\text{NO}_x$ , three distinct pathways have been suggested by Epling et al. [6] which can summarize the oxidation and adsorption steps and which are based on the topology of the active sites.

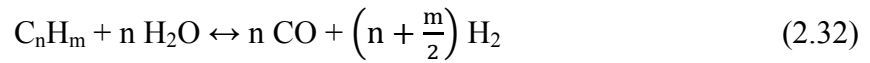
1. When Pt and Ba are close to one another, a rapid uptake of  $\text{NO}_x$  occurs.  $\text{O}_2$  and  $\text{NO}_2$  act as the oxygen source for oxidation of nitrite species to nitrate. The sites further away trap  $\text{NO}_2$  from the phase exclusively via the  $\text{NO}_2$  disproportion mechanism with no  $\text{O}_2$  participation.
2. Pt close to Ba sites are involved in NO oxidation, trapping of NO, and further oxidation to nitrates. Pt sites far from Ba are only involved in NO oxidation.
3. A  $\text{NO}_3^-$  spillover type mechanism describes the migration of  $\text{NO}_3^-$  species away from the Pt sites as they become saturated from the rapid uptake of  $\text{NO}_2$  and adsorbed atomic oxygen. This is similar to a two-dimensional shrinking core mechanism.

#### 2.2.3. Reductant Evolution.

As reported by Epling [6], three means exist to change the exhaust from a diesel engine from lean to rich conditions. If fuel is injected into the exhaust, reductants are produced from hydrocarbons (HC) present reacting with PGM in the LNT. The reductants are also produced by fuel reacting over a partial oxidation catalyst or reformer located upstream of the LNT. Lastly, the engine operation is manipulated to produce rich exhaust gases that will contain reductants.

The most common reductants utilized to reduce the stored  $\text{NO}_x$  on the LNT are  $\text{H}_2$ ,  $\text{CO}$ , and HC such as  $\text{C}_3\text{H}_6$  or  $\text{C}_3\text{H}_8$ . Studies on the effectiveness of these reductants have shown that  $\text{H}_2$  is the most effective at reducing  $\text{NO}_x$  and facilitating the release of  $\text{SO}_2$  from Ba storage sites (to be discussed shortly) and regenerating the LNT [28,63,111-117].  $\text{CO}$  itself or from the partial oxidation of HC is known to poison the Pt sites at low temperatures ( $\leq 200\text{ }^\circ\text{C}$ ) and limit the regeneration of the Ba sites in the LNT [28,118].  $\text{H}_2$  is supplied directly in the case of experiments or in real world scenarios.  $\text{H}_2$  is produced from the other reductants by means of:

steam reforming ( $> 300\text{ }^\circ\text{C}$  and HCs present)



water gas shift (WGS) reaction



Based on the effectiveness of  $\text{H}_2$  and complications involving  $\text{CO}$ , most of the experiments discussed in this dissertation were performed using  $\text{H}_2$  as the only reductant.

#### 2.2.4. Factors Influencing $\text{NO}_x$ Release.

Any reductant used to regenerate a LNT has to fulfill three functions:

1. Create a net reducing environment by consuming any oxygen present in the exhaust gas and adsorbed on the PGM, storage components, and catalyst support.
2. Facilitate the release of  $\text{NO}_x$ .
3. Reduce the  $\text{NO}_x$  to either  $\text{N}_2$  for LNT stand-alone applications or  $\text{NH}_3$  for LNT-SCR applications.

A reductant is passed over the catalyst to begin the regeneration of the catalyst. The Pt sites become saturated with excess oxygen present in the lean phase. The reductant reduces the Pt sites by scavenging the oxygen from the Pt-O species. The reductant is one or a combination of CO, H<sub>2</sub>, and a HC. For the conditions to be considered rich, a net reducing environment must exist in the exhaust stream. This condition is qualified by a lambda value of less than 1. The lambda value represents the ratio of the air to fuel ratio to the ratio of the stoichiometric air to fuel ratio. The air to fuel ratio is the ratio between the mass of air in the exhaust to the mass of fuel at any given moment. A stoichiometric exhaust stream would have a lambda value equal to 1. The reductants react with barium nitrites and nitrates present on the surface. The Ba sites are now returned to their original form and ready for storage. NO<sub>x</sub> is converted to N<sub>2</sub> on the platinum sites freed by the reaction of surface oxygen and reductants present in the exhaust stream [51].

Three factors, occurring independently or in combination, can cause NO<sub>x</sub> to be released from the surface of the catalyst: temperature increase, change in the gas composition in contact with the surface, and/or the creation of a net reducing environment. The increase in temperature is a result of exothermic reactions, such as the oxidation of the reductant by the oxygen present both in the gas stream and stored on the surface [119]. The releases of NO<sub>x</sub> can be particularly pronounced when the amount of NO<sub>x</sub> stored on the catalyst is close to the equilibrium coverage at a given temperature, and the temperature increase is large. The reducing environment is due to a lack of oxygen present in the gas stream [114,121]. The equilibrium stability of nitrate species is dramatically reduced. This instability creates a driving force for nitrate decomposition and NO<sub>x</sub> release from nitrites, which are substantially less stable than nitrates.

#### *2.2.5. Rich phase product selectivity.*

##### *2.2.5.1. Mechanisms of NO<sub>x</sub> reduction.*

Having established the reason as to why NO<sub>x</sub> release occurs, the focus is shifted to the reduction of NO<sub>x</sub> to various N-species. The principle of reduction of stored NO<sub>x</sub> either involves the spillover of NO<sub>x</sub> from the Ba storage sites to the Pt particles

[30,76,89,110,121,122] or the spillover of adsorbed hydrogen from Pt to Ba [113]. For Pt particles in close proximity to Ba sites, H<sub>2</sub> oxidation, nitrate decomposition, and formation of N-species occur during the regeneration [59]. For Pt sites located away from Ba, H<sub>2</sub> scavenges oxygen adsorbed on the Pt sites, and provides a clean surface for the decomposition of NO to N<sub>2</sub> and N hydrogenation to NH<sub>3</sub> [59].

Many authors [24,68,89,125-129] have reported the possibility of NO<sub>x</sub>, N<sub>2</sub>, N<sub>2</sub>O, and NH<sub>3</sub> as possible products formed during LNT regeneration. The “richness”, temperature, and relative coverages of NO, N, and H adspecies on the Pt particles during the rich phase dictate the product distribution [130]. The “richness” of the regeneration of the LNT determines the identity and quantity of products evolved. Shorter purges or purges with limited amount of reductants lead to partial release of NO<sub>x</sub> and product mixes with NO, NO<sub>2</sub> and N<sub>2</sub>. Longer and deeper purges lead to the presence of N<sub>2</sub>O and NH<sub>3</sub> in the product mix [131,132]. During shorter purges any NH<sub>3</sub> that is produced is consumed by NO and NO<sub>2</sub> to form N<sub>2</sub>. The effects of the length of purge should be viewed in terms of the diffusion of NO<sub>x</sub> from the storage sites back to the PGMs. If the rate of surface diffusion of NO<sub>x</sub> is less than the rate of NO<sub>x</sub> reduction, the storage sites are only partially regenerated [131,133].

Pihl et al. [123], and subsequently others, have suggested that the ratio of H<sub>2</sub> to NO, along with the reaction temperature, determine the product selectivity. Xu et al. presented a summary of these relationships [130]:

For H<sub>2</sub>:NO ratios < 0.5 (feeds containing excess NO and temperatures below 150 °C):



For 0.5 < H<sub>2</sub>:NO < 2 (about stoichiometric amounts of H<sub>2</sub> and NO, and temperatures above 150 °C):



For H<sub>2</sub>:NO ratios > 2 (feeds containing excess H<sub>2</sub> and temperatures above 150 °C):

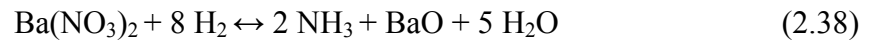


At temperatures above 350 °C, NH<sub>3</sub> decomposes to:

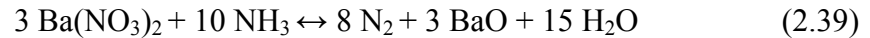


Many pathways have been proposed in the literature to describe the reactions between CO and HC with stored NO<sub>x</sub> [22,45]. For H<sub>2</sub> as the reducing agent, Nova [135] presented the following:

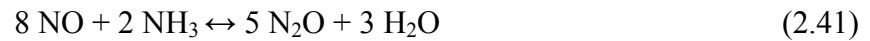
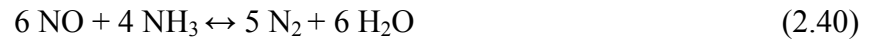
Fast formation of NH<sub>3</sub>:



Slower selective formation of N<sub>2</sub>:



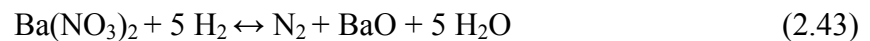
NH<sub>3</sub> produced can also reduce NO:



Again, at temperatures above 350 °C, NH<sub>3</sub> decomposition occurs:

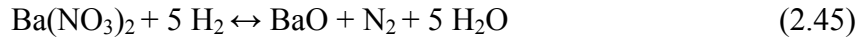
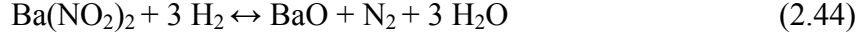


Overall, adding reactions (2.38) and (2.39):



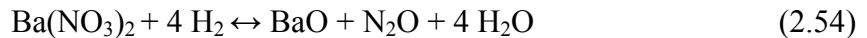
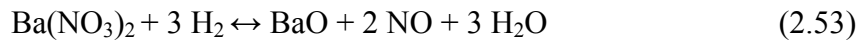
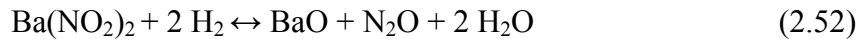
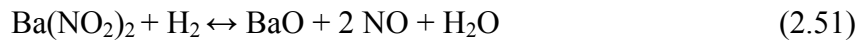
Lietti [14] provides a more comprehensive picture of the chemistry involved, taking into account the presence of different components in the gas stream (where O\*’ represents poorly active oxygen species and H\* represents a hydrogen species associated with Pt):

Reduction of the nitrate at the Ba sites:



O\* represents oxygen species associated with Pt sites, H\* represents a hydrogen species associated with Pt, and O\*’ represents “poorly reactive oxygen species” from the catalyst [14].

Formation of NO and N<sub>2</sub>O:

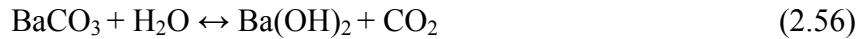


In the presence of Ba, N<sub>2</sub>O is not favored because Ba increases the rate of NO dissociation that reduces the probability of N<sub>2</sub>O formation by [14]:





Desorption of CO<sub>2</sub>:



Again, the water gas shift (WGS) reaction:



As previously stated, the WGS reaction is desired because the reaction enables the CO present to be converted into H<sub>2</sub> which has been shown to be a better reductant of NO<sub>x</sub> and SO<sub>2</sub> (to be discussed shortly) [112-116].

#### 2.2.5.2. NH<sub>3</sub> as an Intermediate.

The formation of NH<sub>3</sub> as a product during LNT regeneration can be an unwanted or wanted effect. In a standalone LNT application, NH<sub>3</sub> is an undesirable product from the reduction of NO<sub>x</sub> due to the fact that the NH<sub>3</sub> is toxic, corrosive, and is capable of being oxidized back to NO<sub>x</sub> (e.g. if NH<sub>3</sub> adsorbs to the surface during rich periods and then reacts with oxygen after the switch back to lean conditions). Conversely, NH<sub>3</sub> can be a desired product in a LNT-SCR application. The balance between the amounts of NH<sub>3</sub> and N<sub>2</sub> produced from the LNT depends on the application of the system. In a situation where NO<sub>x</sub> is emitted from the LNT during lean conditions, the selectivity of NH<sub>3</sub> should be optimized based on the amount of unreacted NO<sub>x</sub> from the LNT in a LNT-SCR application. This coupling is described at the end of this chapter.

As a means to minimize or maximize NH<sub>3</sub> selectivity, it is important that the sequence of events present during rich conditions is considered using the idea of a reductant front propagating along the length of the catalyst surface [123,125,130,134-136]. The beginning of this front is created when the conditions of the engine exhaust are adjusted from net oxidizing to net reducing. At this transition, a plug-like flow of the leading edge of the reductant front encounters stored NO<sub>x</sub> and chemisorbed oxygen on the Pt sites and catalyst surface. These oxidizing species consume hydrogen upon contact with the leading edge of the front. As more reductant passes these sites in the entrance to the

LNT, the ratio of  $H_2:NO$  at the Pt sites gradually increases. How this ratio influences the product selectivity was explained in the previous section.

Considering the reductant front in spatial and temporal terms, different zones are present on the catalyst surface. Pihl et al. [123] envisioned three zones: upstream of the front, at the front, and downstream of the front. Clayton et al. [14,59] and Cumaranatunge et al. [126] also describe  $NO_x$  reduction using this idea of a front traveling the length of the catalyst. Using Pihl's description of the reduction front,  $NH_3$  formation and consumption is readily understood.

Upstream of the front: The leading edge of the front has already passed this region of the LNT, and most of the Pt and Ba storage sites in close proximity are regenerated. While the hydrogen coverage of the Pt sites is increasing,  $NO_x$  that is stored on Ba sites located far from the Pt sites is transported back to the sites. By the time this  $NO_x$  reaches the Pt sites, the  $H_2:NO$  ratio is high enough to favor  $NH_3$  formation. The resulting  $NH_3$  is released into the gas stream where it is either oxidized by  $NO_x$  to  $N_2$  or emitted from the catalyst. Given that  $N_2$  is formed from the reaction of  $NH_3$  and  $NO_x$ , Cumaranatunge [127] likened  $NH_3$  to a  $H_2$  carrier.  $NH_3$  is just effective as a reductant as  $H_2$  to reduce  $NO_x$  to  $N_2$ .

At the leading edge of the front (located further downstream in the catalyst): There is an intermediate level of reductant and stored oxidants. The PGM sites in this region have a mixture of adsorbed oxygen, NO, and reductant species. Initially, an unreacted  $NO_x$  "puff" is seen, and thereafter, a mixture of  $N_2O$  and  $N_2$  is released from the PGM sites. The selectivities of  $N_2O$  and  $N_2$  are dependent on the temperature on the catalyst surface during this period and on the ratio of  $H_2:NO$ . At low temperatures ( $T < 150-200$  °C) and low  $H_2:NO$  ( $\sim 0.5$ )  $N_2O$  selectivity is favored [59,123,126-129,136]. Cumaranatunge et al. [125] believed  $N_2O$  was produced from the reaction between adsorbed NO from the gas phase and reduced Pt in the absence of adsorbed hydrogen as is the case at the leading edge of the front as the hydrogen concentration is depleted. The hydrogen on the surface of Pt reduces NO and  $N_2O$  before spilling over and releasing more NO. As

Cumaranatunge et al. reports [125], the production of  $N_2O$  continues until the Pt surface is oxidized from Pt to Pt-O at which point the reaction ceases. The Pt surface is eventually reduced back to Pt as the hydrogen concentration in the gas phase increases as the reduction front continues along the catalyst. As the coverage of adsorbed hydrogen on the Pt sites increases, so selectivity to  $N_2$  and then  $NH_3$  is increasingly favored [125].

Downstream of the front: The catalyst Pt and Ba species have yet to be regenerated. Here exists an oxidized state with most of the stored oxygen and  $NO_x$  still present on the surface. Any of the  $NH_3$  produced upstream of the front that slips past the leading edge of the reductant front reacts with oxygen and  $NO_x$  adsorbed on the catalyst sites. The products from the oxidation of  $NH_3$  by oxygen adatoms and/or  $NO_x$  depend on their relative coverages on the PGM and include a mixture of NO,  $N_2$ , and  $N_2O$ .

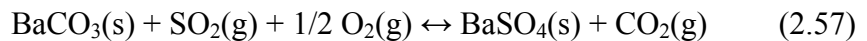
Based on this model, the temporal sequence of  $H_2$  and  $NH_3$  leaving the reactor is readily explained. Most authors [58,89,137] have reported that  $NH_3$  is detected only after  $H_2$  breakthrough from the LNT. The concentration of  $H_2$  in the gas stream over the catalyst increases with time as the reductant front travels from the front to the rear of the catalyst. By the time  $H_2$  reaches the catalyst outlet, all of the Pt sites are at least at a stoichiometric ratio of  $H_2:NO$ . The presence of  $H_2$  at the outlet of the LNT implies all of the oxidizing species adsorbed on Pt are reduced or  $H_2$  would have been consumed and would not have reached the end of the catalyst. For  $NH_3$  to be detected at the exit of the catalyst, almost all of the  $NO_x$  adsorbed at the proximal Pt/Ba sites has been released and reduced. Any of the remaining  $NO_x$  stored at the other Ba sites reaches the Pt sites with conditions that favor additional  $NH_3$  formation. For  $NH_3$  to reach the end of the catalyst, all of the oxygen adatoms and  $NO_x$  at the proximal Pt/Ba sites has to be reduced, given that these species are capable of oxidizing  $NH_3$  to  $N_2$  and  $H_2$ .

The ability of  $NH_3$  to reduce  $NO_x$  is presented in the literature in terms of its ability to act as a hydrogen carrier or hydrogen intermediate as shown by equations (2.38) and (2.39).

### 2.3. Drawbacks to LNT Utilization.

#### 2.3.1. Sulfur.

Based on the foregoing discussion, the effectiveness of the LNT to oxidize, store, release, and reduce NO<sub>x</sub> to N<sub>2</sub> is easily appreciated. However, there are some difficulties in its operation due to other components in the exhaust stream. The main concern is sulfur. Sulfur present in diesel fuel and engine oil, after conversion to sulfur dioxide (SO<sub>2</sub>) through the combustion cycle of engine operation, leads to poisoning of the NO<sub>x</sub> storage sites. In the presence of O<sub>2</sub>, the precious metals, such as Pt and Rh, are able to convert SO<sub>2</sub> to sulfur trioxide (SO<sub>3</sub>). Based on thermodynamic calculations, BaSO<sub>4</sub> is more stable than Ba(NO<sub>3</sub>)<sub>2</sub>; also the sulfate is more basic than the nitrate (stability increases with basicity) [14-18]. If the sulfates are not removed periodically, eventually the NO<sub>x</sub> conversion of the LNT to N<sub>2</sub> will approach zero as all of the available sites will be filled with sulfur-species. To remove the sulfates, prolonged rich conditions at elevated temperatures are required. Breen et al. performed thermodynamic calculations to evaluate the effects of gas composition and temperature on the various reactions of BaSO<sub>4</sub> and BaCO<sub>3</sub> under oxidizing and reducing conditions [138]. Breen found that BaSO<sub>4</sub> is very stable under oxidizing conditions. For rich conditions, Breen looked at various possible reactions in which BaSO<sub>4</sub> is reduced by calculating the Gibbs reaction energy, ΔG<sub>r</sub>. The ΔG<sub>r</sub> is used to establish the conditions under which a reaction should proceed spontaneously. For example, for the following reaction:



$$\Delta G_r = \Delta G^\theta + RT \left[ \ln \left( \frac{P_{\text{CO}_2}}{P_{\text{O}_2}^{0.5} P_{\text{SO}_2}} \right) \right] \quad (2.58)$$

The following partial pressures were used to calculate  $\Delta G_r$  [140]:

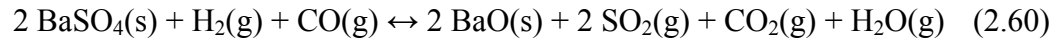
CO <sub>2</sub>	1 x 10 <sup>-1</sup> bar
H <sub>2</sub> O	1 x 10 <sup>-1</sup> bar
O <sub>2</sub>	5 x 10 <sup>-2</sup> bar
CO	5 x 10 <sup>-2</sup> bar
H <sub>2</sub>	5 x 10 <sup>-2</sup> bar
SO <sub>2</sub> or H <sub>2</sub> S	5 x 10 <sup>-5</sup> bar

If the temperature is greater than the temperature at which  $\Delta G_r = 0$ , then the forward reaction will occur spontaneously. Considering the composition of the exhaust stream with Ba as the storage material, the following reactions are possible [138]:

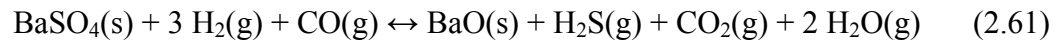
$$T(\Delta G_r = 0) = 617 \text{ }^\circ\text{C}$$



$$T(\Delta G_r = 0) = 984 \text{ }^\circ\text{C}$$



$$T(\Delta G_r = 0) = 622 \text{ }^\circ\text{C}$$



These results confirm that high temperatures are required to decompose BaSO<sub>4</sub>.

Kim et al. [139] also described the sulfation of the Al<sub>2</sub>O<sub>3</sub> sites on the support material of a LNT. As with NO oxidation, the Pt sites are oxidized by the dissociative adsorption of oxygen over Pt. The activated oxygen species then reacts with SO<sub>2</sub> to form SO<sub>3</sub> which then spills over to the Al<sub>2</sub>O<sub>3</sub> support to form Al<sub>2</sub>(SO<sub>4</sub>)<sub>3</sub>:

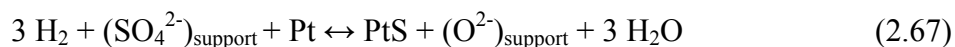


Kim went on to state that due to the greater basicity of the BaO molecule compared to Al<sub>2</sub>O<sub>3</sub>, BaO should be more reactive with the acidic SO<sub>2</sub> molecule [139].

The sulfates formed on the surface are classified according to their proximity to Pt sites. Sulfates located near Pt sites are typically considered to be surface sulfates, and on locations far from Pt, they are considered to be bulk sulfates. Additionally, the BaSO<sub>4</sub> can continue to react under rich conditions to form BaS [140]. The formation of BaS begins at 550 °C and the particles continue to grow up to 800 °C. If water is present, BaS can be hydrolyzed at 550 °C to form BaO and hydrogen sulfide, H<sub>2</sub>S. This reaction sequence is shown below:



In addition to the sulfation of the storage materials, the precious metals are also vulnerable to blockage by sulfur. Apesteguia et al. [141] stated that sulfate in close proximity to Pt sites can be reduced by H<sub>2</sub> at 500°C, resulting in the formation of platinum sulfide:



Sedlmair et al. stated that this reaction begins at 350 °C and an increase of temperature to 500 °C results in an increase of PtS in the bulk phase of the catalyst [73]. In both cases, the Pt sites could be recovered by exposing them to oxidizing conditions at 450 °C. More evidence for the formation of PtS is the increased N<sub>2</sub>O formation seen during the rich phase under increasing sulfation [140]. As discussed earlier, Ba reduces the likelihood of N<sub>2</sub>O formation. Another consequence of the sulfation of the Pt sites is that after the Pt

sites are oxidized by exposure to lean conditions, the SO<sub>2</sub> released from the sites spills over to the surrounding Ba sites where BaSO<sub>4</sub> is formed [40,139].

The decomposition of BaSO<sub>4</sub> requires the LNT to be exposed to rich conditions and high temperatures (650 to 800 °C) for several minutes. This need results in a fuel penalty that reduces the gains in fuel efficiency of lean-burn engines and gives rise to sintering of the precious metals and NO<sub>x</sub> storage components. Sintering occurs when particles such as Pt agglomerate and form less dispersed, large clusters. As discussed above, the platinum particle size affects the NO oxidation rate [40]. Larger particles can lead to sites becoming blocked due to steric hindrances or by the component species [6]. The growth of Pt particles due to sintering decreases the NO<sub>x</sub> storage efficiency [141-143]. Although, under normal operating temperatures (150 °C - 400 °C), the growth of Pt particles has been shown to increase NO oxidation rates [40,41], at elevated temperatures the loss in the surface area of Pt results in reduced NO oxidation rates [6]. This decrease in efficiency is caused by the reduced spillover rate of NO<sub>2</sub>, formed from the oxidation of NO over Pt, to the storage material, i.e. Ba [8,42,91].

High temperatures can also result in the migration of the storage components (i.e., sintering of Pt, redistribution of the Ba phase), which is problematic based on the above discussion of the requirement of the Pt and Ba sites to be in close proximity. Another problem is the occurrence of side reactions of components in the washcoat. Barium cerate, BaCeO<sub>3</sub>, and barium aluminate, BaAl<sub>2</sub>O<sub>4</sub>, are formed at 800 and 850 °C, respectively [91,144-147]. These compounds are not able to store NO<sub>x</sub> and therefore decrease the activity of the LNT.

The aforementioned problems (sintering of the precious metals, migration of the storage components on the surface, and unwanted side reactions between the storage components and the support) can be avoided if desulfation temperatures can be reduced. A potential solution that would enable lower desulfation temperatures is the addition of ceria, CeO<sub>2</sub>, as a storage material. Recent studies have shown that ceria can store some of the sulfur in the exhaust with the consequence that fewer barium sites are poisoned [3,17,18,146-

164]. The use of ceria as a component of three-way catalysts has been well-established because of its oxygen storage capacity that acts as a damper in maintaining stoichiometric conditions during various engine operating ranges, and also because of its ability to maintain high precious metal dispersions in the washcoat [165]. The main function of ceria in a LNT is to store and release oxygen when the LNT is functioning as a TWC. Moreover, under rich conditions, platinum-promoted ceria is known to promote the WGS reaction that produces H<sub>2</sub> and CO<sub>2</sub> from CO and water [155,166].



The additional hydrogen produced is available to regenerate and desulfate the trap. Additionally, ceria has demonstrated NO<sub>x</sub> storage capacity at low to moderate temperatures (< 400 °C) which is significant since diesel exhaust temperatures are usually lower than exhaust from gasoline engines [159].

Different research groups have reported additional benefits from the addition of ceria to LNTs. Theis et al. reported that the addition of ceria improved the sulfur tolerance of the LNT [3]. Peralta et al. reported that sulfur can be stored as Ce(SO<sub>4</sub>)<sub>2</sub> instead of BaSO<sub>4</sub>, thereby freeing up the Ba component for NO<sub>x</sub> storage [167]. In addition to improved sulfur tolerance, Kwak et al. reported that ceria-containing catalysts provide excellent resistance against Pt sintering as compared to alumina-based catalysts [18]. Using DRIFTS, Ji et al. showed that the addition of ceria improved sulfur resistance by reducing sulfur accumulation on BaO sites due to the presence of CeO<sub>2</sub> sites [164]. Ji also proposed that the addition of ceria would lower the fuel penalty and precious metal sintering associated with catalyst desulfation because sulfur stored at Ce sites can be removed under rich conditions at temperatures below 500 °C, which is lower than the > 650 °C required for Ba sites. Furthermore, as stated in the previous paragraph, under rich conditions, Pt-promoted ceria is known to catalyze the water-gas shift reaction that produces hydrogen and CO<sub>2</sub> from CO and water [155,166]. The additional hydrogen produced is available to regenerate the trap, which is highly beneficial because H<sub>2</sub> has



been shown to be a better NO<sub>x</sub> reductant than CO [113,114,116]. Likewise, H<sub>2</sub> is a more efficient reductant for LNT desulfation than CO [32,112,115,117].

### *2.3.2. Additional Concerns of LNT Utilization.*

In addition to the problems present when an LNT is exposed to an exhaust stream containing sulfur species, the costs inherent to the use of PGMs and undesired product formation have limited the penetration of LNT use into the automobile marketplace. Pt and Rh are two of the most expensive precious metals traded on the open market today. The one year averages for Pt and Rh are \$1538.18/oz. and \$1409.21/oz, respectively [168], thus making these metals as precious as gold. It is these high prices that are driving research efforts to reduce or replace their use in LNT catalysts.

As discussed previously, depending on the NO<sub>x</sub> loading and reaction conditions present during the rich phase, products such as NO<sub>x</sub>, N<sub>2</sub>O, and NH<sub>3</sub> can be released from an automobile's exhaust. NO<sub>x</sub> is a key component in photochemical smog and acid rain, N<sub>2</sub>O is a powerful greenhouse gas (7 times as powerful as CO<sub>2</sub>), and NH<sub>3</sub> is toxic and corrosive. What if there existed a means of not only reducing the use and therefore the costs of PGMs while eliminating the release of unwanted compounds?

### *2.4. LNT-SCR.*

As methods of reducing NO<sub>x</sub> emissions, both LNT and SCR catalysts have drawbacks associated with their usage. The high cost of PGMs and susceptibility to sulfur deactivation limit application of LNT catalysts. Thermal durability and the need for an on-board reductant such as NH<sub>3</sub> and its required injection system limit SCR catalyst use. In the past 4 to 6 years, significant efforts have been made to investigate the effects of using LNT and SCR catalysts together [169-189]. One of the first commercial applications of this technology was demonstrated on the 2007 Mercedes E320 Bluetec automobile. The catalyst system on the E320 was a LNT with a high-loading of PGM and a Fe-based zeolite SCR catalyst [189].

SCR catalysts were originally developed by Engelhard Corporation (now BASF Corporation) in 1957 for reducing NO<sub>x</sub> emissions from coal-powered installations such as

boilers and power plants. SCR catalysts are either base metal catalysts such as  $V_2O_5/WO_3/TiO_2$  or ion-exchanged zeolites [190]. These zeolites have higher thermal durability than the base metal SCR catalysts [191]. Two of the most common ion-exchanged zeolites, and the most active for the urea/ $NH_3$ -SCR process are Fe- and Cu-ZSM-5 [6,193,194]. ZSM-5 is aluminosilicate zeolite composed of five membered rings named pentasils that form its structure.

As stated before, a LNT possesses the ability to produce  $NH_3$  during the rich phase as  $NO_x$  is released and reduced by  $H_2$  depending on the temperature and composition of the exhaust emitted from the engine. When a SCR catalyst is positioned downstream of the LNT, the  $NH_3$  that manages to “slip” from the LNT is trapped and stored on the SCR.  $NH_3$  storage continues for the remaining duration of the rich phase until the exhaust gas is switched back to lean conditions. As mentioned during the description of  $NO_x$  storage during lean conditions, when the storage capacity of the LNT is reached,  $NO_x$  will also slip from the catalyst. The  $NO_x$  from the LNT reacts with stored  $NH_3$  on the SCR catalyst. This reaction can occur according to several different pathways, i.e., via the standard and so-called “fast” SCR reactions.

Standard SCR reaction:



Here the advantage of the SCR is realized as  $NO_x$  is now reduced to  $N_2$  in the presence of oxygen. The efficiency of the ion-exchanged zeolite is increased as the concentration of  $NO_2$  from the LNT increases, since this facilitates the occurrence of the so called “fast” SCR reaction [194,195].

Fast SCR reaction



This is also facilitated by the fact that Fe- and Cu-ZSM-5 SCR catalysts have the capability to oxidize  $NO$  to  $NO_2$  in the presence of oxygen. Wang et al., Xu et al., and

Corbos et al. have reported that  $\text{NO}_x$  can additionally be reduced by a non- $\text{NH}_3$  mechanism if hydrocarbons are present in the exhaust [175,191,196].

Examples of the improved performance afforded by the LNT-SCR synergy are provided by Forzatti et al., Lindholm et al., and Xu et al. [176,183,193]. Forzatti reported reduced amounts of  $\text{NH}_3$  from a LNT-SCR system at 150 °C as compared to a LNT-only system. As the temperature was increased to the 200 °C to 300 °C range, complete  $\text{N}_2$  selectivity was seen with the fast SCR reaction more likely to occur due to more  $\text{NO}_2$  being produced by the LNT at these temperatures [176]. Lindholm reported an improvement in  $\text{NO}_x$  removal efficiency from 86% to 99.5% at 300 °C and a decrease in  $\text{NH}_3$  yield from 34% to 21% [183]. Lastly, Xu reported that their LNT-SCR configuration (a low PGM-loaded LNT paired with a Cu-ZSM-5 catalyst) had a  $\text{NO}_x$  conversion of > 90% at 175 °C after aging for the equivalent of 70,000 miles. Xu summarized the benefits of the placement of a SCR downstream of a LNT [191]:

1. Reduced levels of  $\text{NH}_3$  emitted from the catalyst system with neither the fuel consumption penalty nor the need to operate the LNT as a  $\text{NH}_3$  generator.
2. Enhanced  $\text{NO}_x$  conversion
3. Potential PGM reduction as seen by the performance of LNTs with 30% less PGMs
4.  $\text{H}_2\text{S}$  emissions mitigated.

As will be discussed in the Chapter 3 concerning LNT sulfation, the majority of the sulfur is emitted as  $\text{H}_2\text{S}$  as the LNT undergoes desulfation. The placement of the SCR after the LNT enables the  $\text{H}_2\text{S}$  and COS present to be converted back to  $\text{SO}_2$ . This conversion allows the system to operate with quicker desulfation events without exceeding the odor threshold of  $\text{H}_2\text{S}$  [197].

The arrangement of the LNT-SCR system has been studied by Theis et al. and Morita et al. [186,198]. Theis investigated the effect of the arrangement of the catalysts on system

performance as measured by  $\text{NO}_x$  and  $\text{NH}_3$  concentrations. In this study, 4 and 8 alternating catalysts were compared to LNT-and SCR-only systems before and after hydrothermal aging and sulfur deactivation. The LNT-SCR systems with the alternating configurations demonstrated higher conversions of  $\text{NO}_x$  to  $\text{N}_2$ , along with lower  $\text{NH}_3$  and  $\text{N}_2\text{O}$  yields. The improved  $\text{NO}_x$  to  $\text{N}_2$  conversion was due to an improved balance of  $\text{NO}_x$  and  $\text{NH}_3$  in the SCR segments. The lower amount of  $\text{N}_2\text{O}$  generated was a result of more  $\text{NO}_x$  conversion in the SCR segments, since SCR catalysts are less prone to produce  $\text{N}_2\text{O}$  than a Pt-containing LNT [186]. The findings reported by Corbos et al. support this idea of alternating the catalysts based on similar studies with powder catalysts [175]. The selectivity to  $\text{N}_2$  was increased with less  $\text{NO}_x$  and  $\text{NH}_3$  slip for a physical mixture than for a configuration with a bed of LNT catalyst powder followed by a SCR bed. Morita et al. deposited the SCR catalyst on top of the LNT in a dual layer application to a support. This arrangement was reported to ensure sufficient  $\text{NO}_x$  and  $\text{NH}_3$  adsorption even at low temperatures while offering high  $\text{NO}_x$  reduction efficiency [198].

## 2.5. References.

- [1] N. Miyoshi, S. Matsumoto, K. Katoh, T. Tanaka, J. Hardara, N. Takashi, K. Yokota, M. Sugiura, K. Kasahara, Development of New Concept Three-Way Catalyst for Automotive Lean-Burn Engines. SAE Technical Paper Series 950809 (1995).
- [2] N. Takahashi, H. Shinjoh, T. Iijima, T. Suzuki, K. Yamazaki, K. Yokota, H. Suzuki, N. Miyoshi, S. Matsumoto, T. Tanizawa, T. Tanaka, S. Tateishi, K. Kasahara, The New Concept 3-Way Catalyst for Automotive Lean-Burn Engine: NO<sub>x</sub> Storage and Reduction Catalyst. Catalysis Today 27 (1996) 63-69.
- [3] J. Theis, J. Ura, C. Goralski, H. Jen, E. Thanasiu, Y. Graves, A. Takami, H. Yamada, S. Miyoshi, The Effect of Ceria Content on the Performance of a NO<sub>x</sub> Trap. SAE Technical Paper Series 2003-01-1160.
- [4] R.M. Heck, R.J. Farrauto. Catalytic Air Pollution Control: Commercial Technology, 2<sup>nd</sup> ed., John Wiley and Sons, Inc., New York, 2002.
- [5] V.I. Parvulescu, G. Grange, B. Delom, Catalytic Removal of NO. Catalysis Today 46 (1998) 233-317.
- [6] W.S. Epling, L.E. Campbell, A. Yezerets, N.W. Currier, J.E. Parks II, Overview of the Fundamental Reactions and Degradation Mechanisms of NO<sub>x</sub> Storage/Reduction Catalysts. Catalysis Reviews 46 (2004) 163-246.
- [7] M.F.L. Johnson, Surface Area Stability of Aluminas. Journal of Catalysis 123 (1990) 245-259.
- [8] N. Fekete, R. Kemmler, D. Voigtländer, B. Krutzsch, E. Zimmer, G. Wenninger, W. Strehlau, J. van den Tilaart, J. Leyrer, E. Lox, W. Müller, Evaluation of NO<sub>x</sub> Storage Catalysts for Lean Burn Gasoline Fueled Passenger Cars. SAE Technical Paper Series 970746 (1997).

- [9] H. Schaper, E.B.M. Doesburg, P.H.M. De Korte, L.L. Van Reijen, Thermal Stabilization of High Surface Area Alumina. *Solid State Ionics* 16 (1985) 261.
- [10] M. Pijolat, M. Dauzat, M. Soustelle, Influence of Water Vapor and Additives on the Surface Area Stability of  $\gamma$ -alumina. *Solid State Ionics* 50 (1992) 31-39.
- [11] H. Schaper, E.B.M. Doesburg, L.L. Van Reijen, The Influence of Lanthanum Oxide on the Thermal Stability of Gamma Alumina Catalyst Supports. *Applied Catalysis* 7 (1983) 211-220.
- [12] B. Béguin, E. Garbowski, M. Primet, Stabilization of Alumina by Addition of Lanthanum. *Applied Catalysis* 75 (1991) 119-132.
- [13] F. Oudet, P. Courtine, A. Vejux, Thermal Stabilization of Transition Alumina by Structural Coherence with  $\text{LnAlO}_3$  (Ln = La, Pr, Nd). *Journal of Catalysis* 114 (1988) 112-120.
- [14] L. Lietti, P. Forzatti, I. Nova, E. Tronconi,  $\text{NO}_x$  Storage Reduction Over Pt-Ba/ $\gamma$ - $\text{Al}_2\text{O}_3$  Catalyst. *Journal of Catalysis* 204 (2001) 175-191.
- [15] T. Yang, T. Chang, C. Yeh, Acidities of Sulfate Species Formed on a Superacid of Sulfated Alumina. *Journal of Molecular Catalysis A: Chemical* 115 (1997) 339-346.
- [16] D. Martin, D. Duprez, Evaluation of the Acid-Base Surface Properties of Several Oxides and Supported Metal Catalysis by Means of Model Reactions. *Journal of Molecular Catalysis A: Chemical* 118 (1997) 113-128.
- [17] E. Rohart, V. Bellière-Baca, K. Yokota, Harlé, C. Pitois, Rare Earth Based Oxides as Alternative Materials to Ba in  $\text{NO}_x$ -trap catalysts. *Topics in Catalysis* 42-43 (2007) 71-75.

- [18] E. Corbos, S. Elbouazzaoui, X. Courtois, N. Bion, P. Marecot, D. Duprez, NO<sub>x</sub> Storage Capacity, SO<sub>2</sub> Resistance, and Regeneration of Pt/(Ba)/CeZr Model Catalysts for NO<sub>x</sub>-Trap System. *Topics in Catalysis* 42-43 (2007) 9-13.
- [19] M. Takeuchi, S. Matsumoto, NO<sub>x</sub> Storage-Reduction Catalysis for Gasoline Engines. *Topics in Catalysis* 28 (2004) 151-156.
- [20] T. Kobayashi, T. Yamada, K. Kayano, Study of NO<sub>x</sub> Trap Reaction by Thermodynamic Calculation. SAE Technical Paper Series 970745 (1997).
- [21] P.-H. Han, Y.-K. Lee, S.-M. Han, H.-K. Rhee, NO<sub>x</sub> Storage and Reduction Catalysts for Automotive Lean-Burn Engines: Effect of Parameters and Storage Materials on NO<sub>x</sub> Conversion. *Topics in Catalysis* 16/17 (2001) 165-170.
- [22] L.J. Gill, P.G. Blakeman, M.V. Twigg, A.P. Walker, The Use of NO<sub>x</sub> Absorber Catalysts on Diesel Engines. *Topics in Catalysis* 28 (2004) 157-164.
- [23] L. Castoldi, L. Lietti, R. Matarrese, P. Forzatti, The NO<sub>x</sub> Reduction Mechanism by H<sub>2</sub> Under Near Isothermal Conditions over Pt–K/Al<sub>2</sub>O<sub>3</sub> Lean NO<sub>x</sub> Trap Systems. *Topics in Catalysis* 52 (2009) 1713-1718.
- [24] T. Lesage, C. Verrier, P. Bazin, J. Saussey, S. Malo, C. Hedouin, G. Blanchard, M. Daturi, Comparison between a Pt–Rh/Ba/Al<sub>2</sub>O<sub>3</sub> and a newly formulated NO<sub>x</sub>-Trap Catalysts Under Alternate Lean–Rich Flows. *Topics in Catalysis* 30/31 (2004) 31-36.
- [25] H. Ohtsuka, T. Tabata, Roles of Palladium and Platinum in the Selective Catalytic Reduction of Nitrogen Oxides by Methane on Palladium-Platinum-Loaded Sulfated Zirconia. *Applied Catalysis B: Environmental* 29 (2001) 177-183.

- [26] H. Ohtsuka, The Selective Catalytic Reduction of Nitrogen Oxides by Methane on Noble Metal-Loaded Sulfated Zirconia. *Applied Catalysis B: Environmental* 33 (2001) 325-333.
- [27] A. Amberntsson, E. Fridell, M. Skoglundh, Influence of Platinum and Rhodium Composition on the NO<sub>x</sub> Storage and Sulphur Tolerance of a Barium Based NO<sub>x</sub> Storage Catalyst. *Applied Catalysis B: Environmental* 46 (2003) 429-439.
- [28] H. Abdulhamid, E. Fridell, M. Skoglundh, The reduction phase in NO<sub>x</sub> Storage Catalysis: Effect of Type of Precious Metal and Reducing Agent. *Applied Catalysis B: Environmental* 62 (2006) 319-328.
- [29] J.R. Theis, J.A. Ura, R.W. McCabe, The Effects of Platinum and Rhodium on the Functional Properties of a Lean NO<sub>x</sub> Trap. *SAE Technical Paper Series 2007-01-1055* (2007).
- [30] L. Olsson, H. Persson, E. Fridell, M. Skoglundh, B. Andersson, A Kinetic Study of NO Oxidation and Storage on Pt/Al<sub>2</sub>O<sub>3</sub> and Pt/BaO/Al<sub>2</sub>O<sub>3</sub>. *Journal of Physical Chemistry B: Environmental* 105 (2001) 6895-6906.
- [31] W.S. Epling, J.E. Parks, G.C. Campbell, A. Yezerets, N.W. Currier, L.E. Campbell, Further Evidence of Multiple NO<sub>x</sub> Sorption Sites on NO<sub>x</sub> Storage/Reduction Catalysts. *Catalysis Today* 96 (2004) 21-30.
- [32] H. Mahzoul, J.F. Brillhac, P. Gilot, Experimental and mechanistic study of NO<sub>x</sub> adsorption over NO<sub>x</sub> trap catalysts. *Applied Catalysis B: Environmental* 20 (1999) 47-55.
- [33] S. Erkfeldt, E. Jobson, M. Larrson, The Effect of Carbon Monoxide and Hydrocarbons on NO<sub>x</sub> Storage at Low Temperature. *Topics in Catalysis* 16/17 (2001) 127-131.



- [34] K.S. Kabin, R.L. Muncrief, M.P. Harold, Y. Li, Dynamics of Storage and Reaction in a Monolith Reactor: Lean NO<sub>x</sub> Reduction. *Chemical Engineering Science* 59 (2004) 5319-5327.
- [35] S. Salasc, M. Skoglundh, E. Fridell, A Comparison Between Pt and Pd in NO<sub>x</sub> Storage Catalysts. *Applied Catalysis B: Environmental* 36 (2002) 145-160.
- [36] F. Prinetto, G. Ghiotti, I. Nova, L. Lietti, E. Tronconi, P. Forzatti, FT-IR and TPD Investigation of the NO<sub>x</sub> Storage Properties of BaO/Al<sub>2</sub>O<sub>3</sub> and Pt-BaO/Al<sub>2</sub>O<sub>3</sub> Catalysts. *Journal of Physical Chemistry B* 105 (2001) 12732-12745.
- [37] S. Kikuyama, I. Matsukuma, R. Kikuchi, K. Sasaki, K. Eguchi, A Role of Components in Pt-ZrO<sub>2</sub>/Al<sub>2</sub>O<sub>3</sub> as a Sorbent for Removal of NO and NO<sub>2</sub>. *Applied Catalysis A: General* 226 (2002) 23-30.
- [38] P.J. Schmitz, R.J. Baird, NO and NO<sub>2</sub> Adsorption on Barium Oxide: Model Study of the Trapping Stage of NO<sub>x</sub> Conversion via Lean NO<sub>x</sub> Traps. *Journal of Physical Chemistry B* 106 (2002) 4172-4180.
- [39] L. Olsson, B. Westerberg, H. Persson, E. Fridell, M. Skoglundh, B. Andersson, A Kinetic Study of Oxygen Adsorption/Desorption and NO Oxidation over Pt/Al<sub>2</sub>O<sub>3</sub> Catalysts. *Journal of Physical Chemistry B* 103 (1999) 10433-10439.
- [40] J.-H. Lee, H.H. Kung, Effect of Pt Dispersion on the Reduction of NO by Propene over Alumina-Supported Pt Catalysts Under Lean-Burn Conditions. *Catalysis Letters* 51 (1998) 1-4.
- [41] L. Olsson, E. Fridell, The Influence of Pt Oxide Formation and Pt Dispersion on the Reactions NO<sub>2</sub> ⇌ NO + ½ O<sub>2</sub> over Pt/Al<sub>2</sub>O<sub>3</sub> and Pt/BaO/Al<sub>2</sub>O<sub>3</sub>. *Journal of Catalysis* 210 (2002) 340-353.

- [42] D. Kim, Y. Chin, G. Muntean, A. Yereretz, N. Currier, W. Epling, H. Chen, H. Hess, C.H.F Peden, Relationship of Pt Particle Size to the NO<sub>x</sub> Storage Performance of Thermally Aged Pt/BaO/Al<sub>2</sub>O<sub>3</sub> Lean NO<sub>x</sub> Trap Catalysts. *Industrial & Engineering Chemistry Research* 45 (2006) 8815-8821.
- [43] C.G. Granqvist, R.A. Buhrman, Size Distributions For Supported Metal-Catalysts Coalescence Growth Versus Ostwald Ripening. *Journal of Catalysis* 42 (1976) 477-479.
- [44] T.K.N. Hoang, L. Derimaeker, V.B. La, R. Finsy, R. Monitoring the Simultaneous Ostwald Ripening and Solubilization of Emulsions. *Langmuir* 20 (2004) 8966-8969.
- [45] D. Bhatia, R.W. McCabe, M.P. Harold, V. Balakotaiah, Experimental and Kinetic Study of NO Oxidation on Model Pt Catalysts. *Journal of Catalysis* 266 (2009) 106-119.
- [46] R.L. Muncrief, R. Khanna, K.S. Kabin, M.P. Harold, Mechanistic and Kinetic Studies of NO<sub>x</sub> Storage and Reduction on Pt/BaO/Al<sub>2</sub>O<sub>3</sub>. *Catalysis Today* 98 (2004) 393-402.
- [47] H. Yoshida, Y. Yazawa, N. Takagi, A. Satsuma, T. Tanka, S. Yoshida, T. Hattori, XANES Study of the Support Effect on the State of Platinum Catalysts. *Journal of Synchrotron Radiation* 6 (1999) 471-473.
- [48] E. Fridell, M. Skoglundh, S. Johansson, H. Persson, B. Westergerg, A. Törnecrona, G. Smedler, Investigations of NO<sub>x</sub> Storage Catalysts. *Studies in Surface Science and Catalysis* 116 (1998) 537-547.

- [49] E. Fridell, A. Amberntsson, L. Olsson, A.W. Grant, M. Skoglundh, Platinum Oxidation and Sulphur Deactivation in  $\text{NO}_x$  Storage Catalysts. *Topics in Catalysis* 30/31 (2004) 143-146.
- [50] S.S. Mulla, N. Chen, L. Cumaranatunge, G.E. Blau, D.Y. Zemlyanov, W.N. Delgass, W.S. Epling, F.H. Ribeiro, Reaction of NO and  $\text{O}_2$  to  $\text{NO}_2$  on Pt: Kinetics and Catalyst Deactivation. *Journal of Catalysis* 241 (2006) 389-399.
- [51] E. Xue, K. Seshan, J.R.H. Ross, Roles of Supports, Pt Loading and Pt Dispersion in the Oxidation of NO to  $\text{NO}_2$  and of  $\text{SO}_2$  to  $\text{SO}_3$ . *Applied Catalysis B: Environmental* 11 (1996) 65-79.
- [52] P. Denton, A. Giroir-Fendler, H. Praliaud, M. Primet, Role of the Nature of the Support (Alumina or Silica), of the Support Porosity, and of the Pt Dispersion in the Selective Reduction of NO by  $\text{C}_3\text{H}_6$  under Lean-Burn Conditions. *Journal of Catalysis*. 189 (2000) 410-420.
- [53] S. Benard, L. Retailleau, F. Gaillard, P. Vernoux, A. Giroir-Fendler, Supported Platinum Catalysts for Nitrogen Oxide Sensors. *Applied Catalysis B: Environmental* 55 (2005) 11-21.
- [54] J. Segner, W. Vielhaber, G. Ertl, Interaction of  $\text{NO}_2$  with a Pt (111) Surface. *Israel Journal of Chemistry* 22 (1982) 375-379.
- [55] D.H. Parker, B.E. Koel, Chemisorption of High Coverages of Atomic Oxygen on the Pt (111), Pd (111), and Au (111) Surfaces. *Journal of Vacuum Science and Technology A: Vacuum, Surfaces, and Films* 8 (1990) 2585-2590.
- [56] R. Burch, T. Watling, The Effect of Promoters on Pt/ $\text{Al}_2\text{O}_3$  Catalysts for the Reduction of NO by  $\text{C}_3\text{H}_6$  Under Lean-Burn Conditions. *Applied Catalysis B: Environmental* 11 (1997) 207-216.

- [57] M. E. Bartram, R. G. Windham, B. E. Koel, Coadsorption of Nitrogen Dioxide and Oxygen on Pt(111). *Langmuir* 4 (1988) 240-246.
- [58] I. Nova, L. Lietti, L. Castoldi, E. Tronconi, P. Forzatti, New Insights in the NO<sub>x</sub> Reduction Mechanism with H<sub>2</sub> Over Pt-Ba/γ-Al<sub>2</sub>O<sub>3</sub> Lean NO<sub>x</sub> Trap Catalysis Under Near-Isothermal Conditions. *Journal of Catalysis* 239 (2006) 244-254.
- [59] R.D. Clayton, M.P. Harold, V. Balakotaiah, Performance Features of Pt/BaO Lean NO<sub>x</sub> Trap with Hydrogen as Reductant. *AIChE Journal* 55 (2009) 687-700.
- [60] A. Lindholm, N.W. Currier, E. Fridell, A. Yezerets, L. Olsson, NO<sub>x</sub> Storage and Reduction over Pt Based Catalysts with Hydrogen as the Reducing Agent. *Applied Catalysis B: Environmental* 75 (2007) 78-87.
- [61] A.J. Paterson, D.J. Rosenberg, J.A. Anderson, Possible Role of Spillover Processes in the Operation of NO<sub>x</sub> Storage and Reduction Catalysts. *Studies in Surface Science and Catalysis* 138 (2001) 429-436.
- [62] B. Westerberg, E. Fridell, A Transient FTIR Study of Species Formed During NO<sub>x</sub> Storage in the Pt/BaO/Al<sub>2</sub>O<sub>3</sub> System. *Journal of Molecular Catalysis A: Chemical* 165 (2001) 249-263.
- [63] C.K. Narula, S.R. Nakouzi, R. Wu, C.T. Goralski Jr., L.F. Allard Jr., Evaluation of Sol-Gel Processed BaO·nAl<sub>2</sub>O<sub>3</sub> Materials as NO<sub>x</sub> Traps. *AIChE Journal* 47 (2001) 744-753.
- [64] T.J. Toops, D.B. Smith, W.S. Epling, J.E. Parks, W.P. Partridge, Quantified NO<sub>x</sub> adsorption on Pt/K/gamma-Al<sub>2</sub>O<sub>3</sub> and the effects of CO<sub>2</sub> and H<sub>2</sub>O. *Applied Catalysis B: Environmental* 58 (2005) 255-264.

- [65] I. Nova, L. Castoldi, L. Lietti, E. Tronconi, P. Forzatti, On the Dynamic Behavior of  $\text{NO}_x$ -Storage/Reduction Pt–Ba/ $\text{Al}_2\text{O}_3$  Catalyst. *Catalysis Today* 75 (2002) 431-437.
- [66] F. Rodrigues, L. Juste, C. Potvin, J.F. Tempère, G. Blanchard, G. Djéga-Mariadassou,  $\text{NO}_x$  Storage on Barium-Containing Three-Way Catalyst in the Presence of  $\text{CO}_2$ . *Catalysis Letters* 72 (2001) 59-64.
- [67] W.S. Epling, G.C. Campbell, J.E. Parks, The Effects of  $\text{CO}_2$  and  $\text{H}_2\text{O}$  on the  $\text{NO}_x$  Destruction Performance of a Model  $\text{NO}_x$  Storage/Reduction Catalyst. *Catalysis Letters* 90, (2003) 45-56.
- [68] L. Castoldi, I. Nova, L. Lietti and P. Forzatti, Study of the Effect of Ba Loading for Catalytic Activity of Pt-Ba/ $\text{Al}_2\text{O}_3$  Model Catalysts. *Catalysis Today* 96 (2004) 43-52.
- [69] X. Li, M. Meng, P. Lin, Y. Fu, T. Hu, Y. Xie, J. Zhang, A Study on the Properties and Mechanisms for  $\text{NO}_x$  Storage Over Pt/Ba $\text{Al}_2\text{O}_4$ – $\text{Al}_2\text{O}_3$  Catalyst. *Topics in Catalysis* 22 (2003) 111-115.
- [70] L.F. Liotta, A. Macaluso, G.E. Arena, M. Livi, G. Centi, G. Deganello, A Study of the Behaviour of Pt Supported on  $\text{CeO}_2$ - $\text{ZrO}_2$ / $\text{Al}_2\text{O}_3$ -BaO as  $\text{NO}_x$  Storage-Reduction Catalyst for the Treatment of Lean Burn Engine Emissions. *Catalysis Today* 75 (2002) 439-449.
- [71] E. Fridell, H. Persson, B. Westerberg, L. Olsson, M. Skoglundh, The Mechanism of  $\text{NO}_x$  Storage. *Catalysis Letters* 66 (2000) 71-74.
- [72] C. Sedlmair, K. Seshan, A. Jentys, J.A. Lercher, Elementary Steps of  $\text{NO}_x$  Adsorption and Surface Reaction on a Commercial Storage-Reduction Catalyst. *Journal of Catalysis* 214 (2003) 308-316.

- [73] C. Sedlmair, K. Seshan, A. Jentys, J.A. Lercher, Studies on the Deactivation of NO<sub>x</sub> Storage-Reduction Catalysts by Sulfur Dioxide. *Catalysis Today* 75 (2002) 413-419.
- [74] I. Nova, L. Castaldi, L. Lietti, E. Tronconi, P. Forzatti, F. Prinetto, G. Ghiotti, NO<sub>x</sub> Adsorption Study Over Pt-Ba/Alumina Catalysts: FT-IR and Pulse Experiments. *Journal of Catalysis* 222 (2004). 377-388.
- [75] K.S. Kabin, P. Khanna, R.L. Muncrief, V. Medhekar, M.P. Harold, Monolith and TAP Reactor Studies of NO<sub>x</sub> Storage on Pt/BaO/Al<sub>2</sub>O<sub>3</sub>: Elucidating the Mechanistic Pathways and Roles of Pt. *Catalysis Today* 114 (2006) 72-85.
- [76] A. Scotti, I. Nova, E. Tronconi, L. Castaldi, L. Lietti, P. Forzatti, Kinetic Study of Lean NO<sub>x</sub> Storage over the Pt-Ba/Al<sub>2</sub>O<sub>3</sub> System. *Industrial & Engineering Chemistry Research* 43 (2004) 4522-4354.
- [77] E. Fridell, H. Persson, L. Olsson, B. Westerberg, A. Amberntsson, M. Skoglundh, Model Studies of NO<sub>x</sub> Storage and Sulphur Deactivation of NO<sub>x</sub> Storage Catalysts. *Topics in Catalysis* 16/17 (2001) 133-137.
- [78] L. Olsson, E. Fridell, M. Skoglundh, B. Andersson, Mean Field Modeling of NO<sub>x</sub> Storage on Pt/BaO/Al<sub>2</sub>O<sub>3</sub> *Catalysis Today* 73 (2002) 263-270.
- [79] N.W. Cant, M. Patterson, The Storage of Nitrogen Oxides on Alumina-Supported Barium Oxide. *Catalysis Today* 73 (2002) 271-278.
- [80] S. Xie, G. Mestl, M.P. Rosynek, J. H. Lunsford, Decomposition of Nitric Oxide over Barium Oxide Supported on Magnesium Oxide. 1. Catalytic Results and *in Situ* Raman Spectroscopic Evidence for a Barium-Nitro Intermediate. *Journal of the American Chemistry Society* 119 (1997) 10186-10191.

- [81] C.W. Yi, J.H. Kwak, J. Szanyi, Interaction of NO<sub>2</sub> with BaO: From Cooperative Adsorption to Ba(NO<sub>3</sub>)<sub>2</sub> Formation. *Journal of Physical Chemistry C*. 111 (2007) 15299-15305.
- [82] B.R. Kromer, L. Cao, L. Cumararatunge, S.S. Mulla, J.L. Ratts, A. Yezerets, N.W. Currier, F.H. Ribeiro, W.N. Delgass and J.M. Caruthers, Modeling of NO Oxidation and NO<sub>x</sub> Storage on Pt/BaO/Al<sub>2</sub>O<sub>3</sub> NO<sub>x</sub> traps. *Catalysis Today* 136 (2008) 93-103.
- [83] D. Bhatia, R.D. Clayton, M.P. Harold, V. Balakotaiah, A Global Kinetic Model for NO<sub>x</sub> Storage and Reduction on Pt/BaO/Al<sub>2</sub>O<sub>3</sub> Monolithic Catalysts. *Catalysis Today* 147 (2009) S250-S256.
- [84] J.H. Kwak, D.H. Kim, T. Szailer, C.H.F. Peden, J. Szanyi, Excellent NO<sub>x</sub> Uptake Mechanism on Pt/BaO/Al<sub>2</sub>O<sub>3</sub> Catalysts. *Catalysis Letters* 111 (2006) 119-126.
- [85] P. Forzatti, L. Castoldi, I. Nova, L. Lietti, E. Tronconi, NO<sub>x</sub> Removal Catalysis under Lean Conditions. *Catalysis Today* 117 (2006) 316-320.
- [86] I. Nova, L. Castoldi, F. Prinetto, V. Dal Santo, L. Lietti, E. Tronconi, P. Forzatti, G. Ghiotti, R. Psaro, S. Recchia, NO<sub>x</sub> adsorption study over Pt–Ba/alumina catalysts: FT-IR and reactivity study. *Topics in Catalysis* 30-31 (2004) 181-186.
- [87] P. Forzatti, L. Castoldi, L. Lietti, I. Nova, E. Tronconi, Identification of the Reaction Networks of the NO<sub>x</sub> Storage/Reduction in Lean NO<sub>x</sub> Trap Systems. *Studies in Surface Science and Catalysis* 171 (2007) 175-208.
- [88] A. Kumar, M.P. Harold, V. Balakotaiah, Isotopic Studies of NO<sub>x</sub> Storage and Reduction on Pt/BaO/Al<sub>2</sub>O<sub>3</sub> Catalyst Using Temporal Analysis of Products. *Journal of Catalysis* 270 (2010) 214-223.

- [89] N.W. Cant, I.O.Y. Liu, M.J. Patterson, The Effect of Proximity Between Pt and BaO on Uptake, Release, and Reduction of NO<sub>x</sub> on Storage Catalysts. *Journal of Catalysis* 243 (2006) 309-317.
- [90] R. Büchel, R. Ströbel, A. Baiker, S.E. Pratsinis, Effect of the Proximity of Pt to Ce or Ba in Pt/Ba/CeO<sub>2</sub> Catalysts on NO<sub>x</sub> Storage–Reduction Performance. *Topics in Catalysis* 52 (2009) 1709-1712.
- [91] A.K. Datye, Q. Xu, K.C. Kharas, J.M. McCarty, Particle Size Distributions in Heterogeneous Catalysts: What Do They Tell Us About the Sintering Mechanism? *Catalysis Today* 111 (2006) 59-67.
- [92] B.-H. Jang, T.-H. Yeon, H.-S. Han, Y.-K. Park, J.-E. Yie, Deterioration Mode of Barium-Containing NO<sub>x</sub> Storage Catalyst. *Catalysis Letters* 77 (2001) 21-28.
- [93] C.-W. Yi, J.H. Kwak, C.H.F. Peden, C. Wang, J. Szanyi, Understanding Practical Catalysts Using a Surface Science Approach: The Importance of Strong Interaction between BaO and Al<sub>2</sub>O<sub>3</sub> in NO<sub>x</sub> Storage Materials. *Journal of Physical Chemistry C: Letters* 111 (2007) 14942-14944.
- [94] E.C. Corbos, X. Courtois, F. Can, P. Marécot, D. Duprez, NO<sub>x</sub> Storage Properties of Pt/Ba/Al Model Catalysts Prepared by Different Methods: Beneficial effects of a N<sub>2</sub> Pre-Treatment Before Hydrothermal Aging. *Applied Catalysis B: Environmental* 84 (2008) 514-523.
- [95] J. Dawody, L. Eurenus, H. Abdulhamid, M. Skoglundh, E. Olsson, E. Fridell, Platinum Dispersion Measurements for Pt/BaO/Al<sub>2</sub>O<sub>3</sub>, NO<sub>x</sub> Storage Catalysts. *Applied Catalysis A: General* 296 (2005) 157-168.
- [96] J. Hepburn, E Thanasiu, D. Dobson, W. Watkins, Experimental and Modeling Investigations of NO<sub>x</sub> Trap Performance. SAE Technical Paper 962051 (1996).



- [97] J. Wang, Y. Ji, V. Easterling, M. Crocker, M. Dearth, R.W. McCabe, The Effect of Regeneration Conditions on the Selectivity of NO<sub>x</sub> Reduction in a Fully Formulated Lean NO<sub>x</sub> Trap Catalyst. *Catalysis Today* 175 (2011) 83-92.
- [98] M. Vaarkamp, J.T. Miller, F.S. Modica, G.S. Lane, D.C. Koningsberger, Sulfur Poisoning of a Pt/BaK-LTL Catalyst: A Catalytic and Structural Study Using Hydrogen Chemisorption and X-ray Absorption Spectroscopy. *Journal of Catalysis* 138 (1992) 675-685.
- [99] M. Vaarkamp, J.T. Miller, F.S. Modica, D.C. Koningsberger, On the Relation between Particle Morphology, Structure of the Metal-Support Interface, and Catalytic Properties of Pt/γ-Al<sub>2</sub>O<sub>3</sub>. *Journal of Catalysis* 163 (1996) 294-305.
- [100] N.A. Ottinger, T.J. Toops, K. Nguyen, B.G. Bunting, J. Howe, Effect of Lean/Rich High Temperature Aging on NO Oxidation and NO<sub>x</sub> Storage/Release of a Fully Formulated Lean NO<sub>x</sub> Trap. *Applied Catalysis B: Environmental* 101 (2011) 486-494.
- [101] R. Büchel, R. Strobel, F. Krumeich, A. Baiker, S.E. Pratsinis, Influence of Pt Location on BaCO<sub>3</sub> or Al<sub>2</sub>O<sub>3</sub> During NO<sub>x</sub> Storage Reduction. *Journal of Catalysis* 261 (2009) 201-207.
- [102] R.D. Clayton, M.P. Harold, V. Balakotaiah, NO<sub>x</sub> Storage and Reduction with H<sub>2</sub> on Pt/BaO/Al<sub>2</sub>O<sub>3</sub> Monolith: Spatio-Temporal Resolution of Product Distribution. *Applied Catalysis B: Environmental* 84 (2008) 616-630.
- [103] S.S. Chaugule, V.F. Kispersky, J.L. Ratts, A. Yezerets, N.W. Currier, F.H. Ribeiro, W.N. Delgass, Formation and Removal of Ba-Carbonates or Carboxylates on Pt/BaO/γ-Al<sub>2</sub>O<sub>3</sub> Lean NO<sub>x</sub> Traps. *Applied Catalysis B: Environmental* 107 (2011) 26-33.

- [104] S.S. Chaugule, A. Yezerets, N.W. Currier, F.H. Ribeiro, W.N. Delgass, 'Fast' NO<sub>x</sub> Storage on Pt/BaO/ $\gamma$ -Al<sub>2</sub>O<sub>3</sub> Lean NO<sub>x</sub> Traps with NO<sub>2</sub> + O<sub>2</sub> and NO + O<sub>2</sub>: Effects of Pt, Ba Loading. *Catalysis Today* 151 (2010) 291-303.
- [105] U. Elizundia, R. López-Fonseca, I. Landa, M.A. Gutiérrez-Ortiz, J.R. González-Velasco, FT-IR study of NO<sub>x</sub> Storage Mechanism over Pt/BaO/Al<sub>2</sub>O<sub>3</sub> Catalysts. Effect of the Pt-BaO Interaction. *Topics in Catalysis* 42–43 (2007) 37-41.
- [106] V. Easterling, Y. Ji, M. Crocker, M. Dearth, R.W. McCabe, Application of SpaciMS to the Study of Ammonia Formation in Lean NO<sub>x</sub> Trap Catalysts. *Applied Catalysis B: Environmental* 123-124 (2012) 339-350.
- [107] X. Chen, J. Schwank, J. Li, W.F. Schneider, C.T. Goralski Jr., P.J. Schmitz, Thermal Decomposition of Dispersed and Bulk-Like NO<sub>x</sub> Species in Model NO<sub>x</sub> Trap Materials. *Applied Catalysis B: Environmental* 61 (2005) 164-175.
- [108] X. Wei, X. Liu, M. Deeba, Characterization of Sulfated BaO-Based NO<sub>x</sub> Trap. *Applied Catalysis B: Environmental* 58 (2005) 41-49.
- [109] S. Hodjati, C. petit, V. Pitchon, A. Kienneman, NO<sub>x</sub> Sorption-Desorption Study: Application to Diesel and Lean-Burn Exhaust Gas (Selective NO<sub>x</sub> Recirculation Technique). *Catalysis Today* 59 (2000) 323-334.
- [110] D. James, E. Fourré, M. Ishii, M. Bowker, Catalytic Decomposition/Regeneration of Pt/Ba(NO<sub>3</sub>)<sub>2</sub> Catalysts: NO<sub>x</sub> Storage and Reduction. *Applied Catalysis B: Environmental* 45 (2) (2003) 147-159.
- [111] H. Abdulhamid, E. Fridell, M. Skoglundh, Influence of the Type of Reducing Agent (H<sub>2</sub>, CO, C<sub>3</sub>H<sub>6</sub> and C<sub>3</sub>H<sub>8</sub>) on the Reduction of Stored NO<sub>x</sub> in a Pt/BaO/Al<sub>2</sub>O<sub>3</sub> Model Catalyst. *Topics in Catalysis* 30-31 (2004) 161-168.

- [112] L. Limousy, H. Mahzoul, J. Brillhac, F. Garin, G. Maire, P. Gilot, A Study of the Regeneration of Fresh and Aged SO<sub>x</sub> Adsorbers Under Reducing Conditions. *Applied Catalysis B: Environmental* 45 (2003) 169-179.
- [113] Z. Liu, J. Anderson, Influence of Reductant on the Thermal Stability of Stored NO<sub>x</sub> in Pt/BaO/Al<sub>2</sub>O<sub>3</sub> NO<sub>x</sub> Storage and Reduction Traps. *Journal of Catalysis* 224 (2004) 18-27.
- [114] P. Jozsa, E. Jobson, M. Larsson, Reduction of NO<sub>x</sub> Stored at Low Temperatures on a NO<sub>x</sub> Adsorbing Catalyst. *Topics in Catalysis*. 30-31 (2004) 177-180.
- [115] Z. Liu, J. Anderson, Influence of Reductant on the Regeneration of SO<sub>2</sub>-Poisoned Pt/BaO/Al<sub>2</sub>O<sub>3</sub> NO<sub>x</sub> Storage and Reduction Catalyst. *Journal of Catalysis* 228 (2004) 243-253.
- [116] T. Szailer, J. Kwak, D. Kim, J. Hanson, C. Peden, J. Szanyi, Reduction of Stored NO<sub>x</sub> on Pt/Al<sub>2</sub>O<sub>3</sub> and Pt/BaO/Al<sub>2</sub>O<sub>3</sub> Catalysts with H<sub>2</sub> and CO. *Journal of Catalysis* 239 (2006) 51-64.
- [117] S. Poulston, R. Rajaram, Regeneration of NO<sub>x</sub> Trap Catalysts. *Catalysis Today* 81 (2003) 603-610.
- [118] M. Skoglundh, H. Johansson, L. Löwendahl, K. Jansson, L. Dahl, B. Hirschauser, Cobalt-Promoted Palladium as a Three-Way Catalyst. *Applied Catalysis B: Environmental* 7 (1996) 299-319.
- [119] K.S. Kabin, R.L. Muncrief, M.P. Harold, NO<sub>x</sub> Storage and Reduction on a Pt/BaO/alumina Monolithic Storage Catalyst. *Catalysis Today* 96 (2004) 79-89.

- [120] A. Amberntsson, H. Persson, P. Engstrom, B. Kasemo, NO<sub>x</sub> Release from a Noble Metal/BaO Catalyst: Dependence on Gas Composition. *Applied Catalysis B: Environmental* 31 (2001) 27-38.
- [121] J.A. Anderson, B. Bachiller-Baeza, M. Fernández-García, Role of Pt in Pt/Ba/Al<sub>2</sub>O<sub>3</sub> NO<sub>x</sub> Storage and Reduction Traps. *Physical Chemistry Chemical Physics* 5 (2003) 4418-4427.
- [122] G. Zhou, T. Luo, R.J. Gorte, An Investigation of NO<sub>x</sub> Storage on Pt-BaO-Al<sub>2</sub>O<sub>3</sub> *Applied Catalysis B: Environmental* 64 (2006) 88-95.
- [123] J. Pihl, J. Parks, C. Daw, T. Root, Product Selectivity During Regeneration of Lean NO<sub>x</sub> Trap Catalysts. *SAE Technical Paper Series* 2006-01-3441 (2006).
- [124] T. Lesage, C. Verrier, P. Bazin, J. Saussey, M. Daturi, Studying the NO<sub>x</sub>-trap Mechanism over a Pt-Rh/Ba/Al<sub>2</sub>O<sub>3</sub> Catalyst by *Operando* FT-IR Spectroscopy. *Physical Chemistry Chemical Physics* 5 (2003) 4435-4440.
- [125] L. Cumaranatunge, S.S. Mulla, A. Yezerets, N.W. Currier, W.N. Delgass, F.H. Ribeiro, Ammonia is a Hydrogen Carrier in the Regeneration of Pt/BaO/Al<sub>2</sub>O<sub>3</sub> NO<sub>x</sub> Traps with H<sub>2</sub>. *Journal of Catalysis* 246 (2007) 29-34.
- [126] H.G. Stenger Jr., J.S. Hepburn, Nitric Oxide Reduction by Alumina-supported Rhodium, Palladium, and Platinum, 1. Intrinsic Activities and Selectivities. *Energy Fuels* 1 (1987) 412-416.
- [127] H. Hirano, T. Yamada, K.I. Tanaka, J. Siera, P. Cobden, B.E. Nieuwenhuys, Mechanisms of the Various Nitric Oxide Reduction Reactions on a Platinum-Rhodium (100) Alloy Single Crystal Surface, *Surface Science*. 262 (1992) 97-112.

- [128] H. Hirano, T. Yamada, K.I. Tanaka, J. Siera, B.E. Nieuwenhuys, The Reduction of Nitric Oxide by Hydrogen over Platinum, Rhodium and Pt-Rh Single Crystal Surfaces. *Studies in Science Catalysis (New Frontiers in Catalysis, Part A)* 75 (1993) 345–357.
- [129] T.P. Kobylinski, B.W. Taylor, Catalytic Chemistry of Nitric Oxide. II. Reduction of Nitric Oxide over Noble Metal Catalysts, *Journal of Catalysis*. 33 (1974) 376-384.
- [130] J. Xu, R. Clayton, V. Balakotaiah, M.P. Harold, Experimental and Microkinetic Modeling of Steady-State NO Reduction by H<sub>2</sub> on Pt/BaO/Al<sub>2</sub>O<sub>3</sub> Monolith Catalysts. *Applied Catalysis B: Environmental* 77 (2008) 395-408.
- [131] W.S. Epling, A. Yezerets, N.W. Currier, The Effects of Regeneration Conditions on NO<sub>x</sub> and NH<sub>3</sub> Release from NO<sub>x</sub> Storage/Reduction Catalysts *Applied Catalysis B: Environmental* 74 (2007) 117-129.
- [132] R.G. Tonkyn, R.S. Disselkamp, C.H.F. Peden, Nitrogen Release from a NO<sub>x</sub> Storage and Reduction Catalyst. *Catalysis Today* 114 (2006) 94-101.
- [133] R.D. Clayton, M.P. Harold, V. Balakotaiah, C.Z. Wan, Pt Dispersion Effects During NO<sub>x</sub> Storage and Reduction on Pt/BaO/Al<sub>2</sub>O<sub>3</sub> Catalysts. *Applied Catalysis B: Environmental* 90 (2009) 662-676.
- [134] I. Nova, L. Lietti, P. Forzatti, Mechanistic Aspects of the Reduction of Stored NO<sub>x</sub> over Pt-Ba/Al<sub>2</sub>O<sub>3</sub> Lean NO<sub>x</sub> Trap Systems. *Catalysis Today* 136 (2008) 128-135.
- [135] W.P. Partridge, J.-S. Choi, NH<sub>3</sub> Formation and Utilization in Regeneration of Pt/Ba/Al<sub>2</sub>O<sub>3</sub> NO<sub>x</sub> Storage-Reduction Catalyst with H<sub>2</sub>. *Applied Catalysis B: Environmental* 91 (2009) 144-151.

- [136] R.D. Clayton, M.P. Harold, V. Balakotaiah, Selective Catalytic Reduction of NO by H<sub>2</sub> in O<sub>2</sub> on Pt/BaO/Al<sub>2</sub>O<sub>3</sub> Monolith NO<sub>x</sub> Storage Catalysts. *Applied Catalysis B: Environmental* 81 (2008) 161-181.
- [137] I. Nova, L. Castoldi, L. Lietti, E. Tronconi, P. Forzatti, A Low Temperature Pathway Operating the Reduction of Stored Nitrates in Pt-Ba/Al<sub>2</sub>O<sub>3</sub> lean NO<sub>x</sub> Trap Systems. *SAE Technical Paper Series 2006-01-1368* (2006).
- [138] J. Breen, M. Marella, C. Pistarino, J. Ross, Sulfur-Tolerant NO<sub>x</sub> Storage Traps: an Infrared and Thermodynamic Study of the Reactions of Alkali and Alkaline-Earth Metal Sulfates. *Catalysis Letter* 80 (2002) 123-128.
- [139] D. Kim, J. Kwak, J. Szanyi, S. Cho, C.H.F. Peden. Roles of Pt and BaO in the Sulfation of Pt/BaO/Al<sub>2</sub>O<sub>3</sub> Lean Trap Materials: Sulfur K-Edge XANES and Pt L<sub>III</sub> XAFS Studies. *Journal of Physical Chemistry* 112 (2008) 2981-2987.
- [140] D. Kim, J. Kwak, X. Wang, J. Szanyi, C.H.F. Peden. Sequential High Temperature Reduction, Low Temperature Hydrolysis for the Regeneration of Sulfated NO<sub>x</sub> Trap Catalysts. *Catalysis Today* 136 (2008) 183-197.
- [141] C. Apesteguia, T. Garetto, A. Borgna, On the Sulfur-Aided Metal-Support Interaction in Pt/Al<sub>2</sub>O<sub>3</sub>-Cl Catalysts. *Journal of Catalysis* 106 (1987) 73-84.
- [142] A. Ambertsson, M. Skoglundh, S. Ljungström, E. Fridell, Sulfur Deactivation of NO<sub>x</sub> Storage Catalysts: Influence of Exposure Conditions and Noble Metal. *Journal of Catalysis*. 217 (2003) 253-263.
- [143] S. Matsumoto, Catalytic Reduction of Nitrogen Oxides In Automotive Exhaust Containing Excess Oxygen and NO<sub>x</sub> Storage-Reduction Catalyst. *CATTECH* 4 (2000) 102-109.

- [144] G. Graham, H. Jen, W. Chun, H. Sun, X. Pan, R. McCabe, Coarsening of Pt Particles in a Model NO<sub>x</sub> Trap. *Catalysis Letters*. 93 (2004) 129-134.
- [145] S. Elbouazzaoui, X. Courtois, P. Marecot, D. Duprez, Characterization by TPR, XRD, and NO<sub>x</sub> Storage Capacity Measurements of the Aging by Thermal Treatment and SO<sub>2</sub> Poisoning of a Pt/Ba/Al NO<sub>x</sub>-trap Model Catalyst. *Topics in Catalysis*. 30/31 (2004) 493-496.
- [146] M. Casapu, J. Grunwaldt, M. Maciejewski, M. Wittrock, U. Göbel, A. Baiker, Formation and Stability of Barium Aluminate and Cerate in NO<sub>x</sub> Storage-Reduction Catalysts. *Applied Catalysis B: Environmental* 63 (2006) 232-242.
- [147] D. Kim, Y. Chin, J. Kwak, J. Szanyi, C.H.F. Peden. Changes in Ba Phases in BaO/Al<sub>2</sub>O<sub>3</sub> Upon Thermal Aging and H<sub>2</sub>O Treatment. *Catalysis Letters* 105 (2005) 259-268.
- [148] S. Elbouazzaoui, E.C. Corbos, X. Courtois, P. Marecot, D. Duprez, A Study of the Deactivation by Sulfur and Regeneration of a Model NSR Pt/Ba/Al<sub>2</sub>O<sub>3</sub> Catalyst. *Applied Catalysis B: Environmental* 61 (2005) 236-243.
- [149] M. Casapu, J. Grunwaldt, M. Maciejewski, A. Baiker, M. Wittrock, U. Göbel, S. Eckhoff, Thermal Aging Phenomena and Strategies Towards Reactivation of NO<sub>x</sub>-Storage Catalysts. *Topics in Catalysis* 42-43 (2007) 3-7.
- [150] P. Bazin, O. Saur, J. Lavalley, G. Blanchard, V. Visciglio, O. Touret, Influence of Platinum on Ceria. *Applied Catalysis B: Environmental* 13 (1997) 265-274.
- [151] T. Truex, Interaction of Sulfur with Automotive Catalysis and the Impact on Vehicle Emissions-A Review. *SAE Technical Paper Series* 1999-01-1543 (1999).

- [152] C. Courson, A. Khalfi, M. Mahzoul, S. Hodjati, N. Moral, A. Kiennemann, P. Gilot, Experimental Study of the SO<sub>2</sub> Removal Over a NO<sub>x</sub> Trap Catalyst. *Catalysis Communications* 3 (2002) 471-477.
- [153] S. Phillip, A. Drochner, J. Kunert, H. Vogel, J. Theis, E. Lox, Investigation of NO Adsorption and NO/O<sub>2</sub> Co-Adsorption on NO<sub>x</sub>-Storage-Components by DRIFT-Spectroscopy. *Topics in Catalysis* 30/31 (2004) 235-238.
- [154] F. Rohr, S. Peter, E. Lox, M. Kögel, A. Sassi, L. Juste, C. Rigau, G. Belot, P. Gélina, M. Primet, On the Mechanism of Sulphur Poisoning and Regeneration of a Commercial Gasoline NO<sub>x</sub> Storage Catalysts. *Applied Catalysis B: Environmental* 56 (2007) 201-212.
- [155] A. Phatak, N. Koryabkina, S. Rai, J.L. Ratts, W. Ruettinger, R.J. Farrauto, G.E. Blau, W.N. Deglass, F.H. Ribeiro, Kinetics of the Water-Gas Shift Reaction on Pt Catalysts Supported on Alumina and Ceria. *Catalysis Today* 123 (2007) 224-234.
- [156] M. Piacentini, M. Maciejewski, A. Baiker, Role and Distribution of Different Ba-Containing Phases in Supported Pt-Ba NSR Catalysts. *Topics in Catalysis* 42-43 (2007) 55-59.
- [157] M. Symalla, A. Drochner, H. Vogel, S. Phillip, U. Göbel, W. Müller, IR-Study of Formation of Nitrite and Nitrate During NO<sub>x</sub>-Adsorption on NSR-Catalysts-Compounds CeO<sub>2</sub> and BaO/CeO<sub>2</sub>. *Topics in Catalysis* 42-43 (2007) 199-202.
- [158] Y. Ji, T.J. Toops, M. Crocker, Effect of Ceria on the Storage and Regeneration Behavior of a Model Lean NO<sub>x</sub> Trap Catalyst. *Catalysis Letters* 119 (2007) 257-264.
- [159] Y. Ji, J.S. Choi, T.J. Toops, M. Crocker, M. Naseri, Influence of Ceria on the NO<sub>x</sub> Storage/Reduction Behavior of Lean NO<sub>x</sub> Trap Catalysts. *Catalysis Today* 136 (2008) 146-155.



- [160] E. Corbos, X. Courtois, N. Bion, P. Marecot, D. Duprez, Impact of the Support Oxide and Ba Loading on the Sulfur Resistance and Regeneration of Pt/Ba/Support Catalysts. *Applied Catalysis B: Environmental* 80 (2008) 62–71.
- [161] K. Adams, G. Graham, Impact of Redox Conditions on Thermal Deactivation of NO<sub>x</sub> Traps for Diesel. *Applied Catalysis B: Environmental* 80 (2008) 343-352.
- [162] L. Kylhammar, R. Carlsson, H. Ingelsten, H. Grönbeck, M. Skoglundh, Regenerable Ceria-Based SO<sub>x</sub> Traps for Sulfur Removal in Lean Exhausts. *Applied Catalysis B: Environmental* 84 (2008) 268-276.
- [163] J. Kwak, D. Kim, J. Szanyi, C.H.F. Peden, Excellent Sulfur Resistance of Pt/BaO/CeO<sub>2</sub> Lean NO<sub>x</sub> Trap Catalysts. *Applied Catalysis B: Environmental* 84 (2008) 545-551.
- [164] Y. Ji, T.J. Topps, M. Crocker, Effect of Ceria on the Sulfation and Desulfation Characteristics of a Model Lean NO<sub>x</sub> Catalyst. *Catalysis Letters*. 127 (2009) 55-62.
- [165] P. Eastwood. *Critical Topics in Exhaust Gas Aftertreatment Research Studies* Press, Ltd., Baldock, Hertfordshire, England, 2000.
- [166] G. Jacobs, L. Williams, U. Graham, D. Sparks, B. Davis, Low Temperature Water-Gas Shift: In Situ DRIFTS-Reaction Study of Ceria Surface Area on the Evolution of Formates on Pt/CeO<sub>2</sub> Processing Catalysts for Fuel Cell Applications. *Applied Catalysis, A: General* 252 (2003) 107-118.
- [167] M.A. Peralta, V.G. Milt, L.M. Cornaglia, C.A. Querini, Stability of Ba,K/CeO<sub>2</sub> Catalyst During Diesel Soot Combustion: Effect of Temperature, Water, and Sulfur Dioxide. *Journal of Catalysis* 242 (2006) 118-130.

- [168] <http://www.ebullionguide.com/>. Downloaded 10/24/12.
- [169] U.S. Patent Appl. US2004/0076565, and U.S. Patents 7332135, 7485273, 7640730, and 7674743.
- [170] J. Theis, E. Gulari, A LNT+SCR System for Treating the NO<sub>x</sub> Emissions from a Diesel Engine. SAE Technical Paper Series 2006-01-0210 (2006).
- [171] R. Snow, D. Dobson, R. Hammerle, S. Katare, Robustness of a LNT-SCR System to Aging Protocol. SAE Technical Paper Series 2007-01-0469 (2007).
- [172] R. Snow, G. Cavataio, D. Dobson, C. Montreuil, R. Hammerle, Calibration of a LNT-SCR Diesel Aftertreatment System. SAE Technical Paper Series 2007-01-1244 (2007).
- [173] H. Shinjoh, N. Takahashi, K. Yokota, Synergic Effect of Pd/ $\gamma$ -alumina and Cu/ZSM-5 on the Performance of NO<sub>x</sub> Storage Reduction Catalyst. Topics in Catalysis 42/43 (2007) 215-219.
- [174] T. Nakatsuji, M. Matsubara, J. Rouistenmaki, N. Sato, H. Ohno, A NO<sub>x</sub> Reduction System Using Ammonia-storage Selective Catalytic Reduction in Rich/Lean Excursions. Applied Catalysis B: Environmental 77 (2007) 190-201.
- [175] E.C. Corbos, M. Haneda, X. Courtois, P. Marecot, D. Duprez, H. Hamada, Cooperative Effect of Pt–Rh/Ba/Al and CuZSM-5 Catalysts for NO<sub>x</sub> Reduction During Periodic Lean-Rich Atmosphere. Catalysis Communications 10 (2008) 137-141.
- [176] P. Forzatti, L. Lietti, The Reduction of NO<sub>x</sub> Stored on LNT and Combined LNT–SCR Systems. Catalysis Today 155 (2010) 131-139.

- [177] L. Xu, R. McCabe, W. Ruona, G. Cavataio, Impact of a Cu-zeolite SCR Catalyst on the Performance of a Diesel LNT+SCR System. SAE Technical Paper Series 2009-01-0285 (2009).
- [178] E.C. Corbos, M. Haneda, X. Courtois, P. Marecot, D. Duprez, H. Hamada, NO<sub>x</sub> Abatement for Lean-Burn Engines under Lean–Rich Atmosphere over Mixed NSR-SCR Catalysts: Influences of the Addition of a SCR Catalyst and of the Operational Conditions. Applied Catalysis A: General. 365 (2009) 187-193.
- [179] J. Parks, V. Prikhodko, Ammonia Production and Utilization in a Hybrid LNT+SCR System. SAE Technical Paper Series 2009-01-2739 (2009).
- [180] J.R. Theis, J.A. Ura, R.W. McCabe, The Effects of Sulfur Poisoning and Desulfation Temperature on the NO<sub>x</sub> Conversion of LNT+SCR Systems for Diesel Applications. SAE Technical Paper Series 2010-01-0300 (2010).
- [181] J. McCarthy Jr., T. Korhumel Jr., A. Marougy, Performance of a Fuel Reformer, LNT and SCR Aftertreatment System Following 500 LNT Desulfation Events. SAE Technical Paper Series 2009-01-2835 (2009).
- [182] L. Xu, R. McCabe, M. Dearth, W. Ruona, Laboratory and Vehicle Demonstration of “2nd-Generation” LNT + in-situ SCR Diesel NO<sub>x</sub> Emission Control Systems. SAE Technical Paper Series 2010-01-0305 (2010).
- [183] A. Lindholm, A. Sjövall, L. Olsson, Reduction of NO<sub>x</sub> over a Combined NSR and SCR System. Applied Catalysis B: Environmental 98 (2010) 112-121.
- [184] R. Bonzi, L. Lietti, L. Castoldi, P. Forzatti, NO<sub>x</sub> Removal over a Double-Bed NSR-SCR Reactor Configuration. Catalysis Today 151 (2010) 376-385.

- [185] L. Xu, R. McCabe, P. Tennison, H-W. Jen, Laboratory and Vehicle Demonstration of “2nd-Generation” LNT + in-situ SCR Diesel Emission Control Systems. SAE Technical Paper Series 2011-01-0308 (2011).
- [186] J.R. Theis, M. Dearth, R. McCabe, LNT+SCR Catalyst Systems Optimized for NO<sub>x</sub> Conversion on Diesel Applications. SAE Technical Paper Series 2011-01-0305 (2011).
- [187] L. Castoldi, R. Bonzi, L. Lietti, P. Forzatti, S. Morandi, G. Ghiotti, S. Dzwigaj, Catalytic Behaviour of Hybrid LNT/SCR Systems: Reactivity and in situ FTIR study. *Journal of Catalysis* 282 (2011) 128-144.
- [188] L. Xu, R.W. McCabe, H.S. Gandhi, C.N. Montreuil, U.S. Patent allowed, July, 2011.
- [189] M. Weibel, N. Waldbüßer, R. Wunsch, D. Chatterjee, B. Bandl-Konrad, B.Krutzsch, A Novel Approach to Catalysis for NO<sub>x</sub> Reduction in Diesel Exhaust Gas. *Topics in Catalysis* 52 (2009) 1702-1708.
- [190] T. Johnson, Diesel Engine Emissions and Their Control. *Platinum Metals Review* 52 (2008) 23-37.
- [191] L. Xu, R.W. McCabe, LNT + *in situ* SCR Catalyst System for Diesel Emissions Control. *Catalysis Today* 184 (2012) 83-94.
- [192] R.Q. Long, R.T. Yang, Superior Fe-ZSM-5 Catalyst for Selective Catalytic Reduction of Nitric Oxide by Ammonia. *Journal of the American Chemistry Society* 121 (1999) 5595-5596.
- [193] A.Z. Ma, W. Grunert, Selective Catalytic Reduction of NO by Ammonia over Fe-ZSM-5 Catalysts. *Chemical Communications (Cambridge)* 1 (1999) 71-72.

- [194] A. Kato, S. Matsuda, T. Kamo, F. Nakajima, H. Kuroda, T. Narita, Reaction between NO, and NH<sub>3</sub>, on Iron Oxide-Titanium Oxide Catalyst. *Journal of Physical Chemistry* 85 (1981) 4099-4102.
- [195] M. Koebel, M. Elsener, G. Madia, Reaction Pathways in the Selective Catalytic Reduction Process with NO and NO<sub>2</sub> at Low Temperatures. *Industrial Engineering Chemical Research* 40 (2001) 52-59.
- [196] J. Wang, Y. Ji, Z. Hea, M. Crocker M. Dearth, R.W. McCabe, A Non-NH<sub>3</sub> Pathway for NO<sub>x</sub> Conversion in Coupled LNT-SCR Systems. *Applied Catalysis B: Environmental* 111– 112 (2012) 562– 570.
- [197] J.A. Ura, C.T. Goralski, Jr., G.W. Graham, R.W. McCabe, Laboratory Study of Lean NO<sub>x</sub> Trap Desulfation Strategies. *SAE Technical Paper Series* 2005-01-1114 (2005).
- [198] T. Morita, N. Suzuki, N. Satoh, K. Wada and H. Ohno, Study on Low NO<sub>x</sub> Emission Control Using Newly Developed Lean NO<sub>x</sub> Catalyst for Diesel Engines. *SAE Technical Paper Series* 2007-01-0239 (2007).

### **Chapter 3. Effect of Ceria on the Desulfation Characteristics of Model Lean NO<sub>x</sub> Trap Catalysts.**

**Note** - This chapter was published as an article in the following journal:

V. Easterling, Y. Ji, M. Crocker, J. Ura, J.R. Theis, R.W. McCabe, Effect of Ceria on the Desulfation Characteristics of Model Lean NO<sub>x</sub> Trap Catalysts. *Catalysis Today* 151 (2010) 338–346.

The article appears in this dissertation with permission from the publisher.

#### *3.1. Introduction.*

Lean-burn engines have the potential to provide better fuel economy than current stoichiometric engines through reduced pumping losses and enhanced combustion thermodynamics [1]. Although reduced CO<sub>2</sub> and hydrocarbon emissions are seen from lean-burn engines, NO<sub>x</sub> emissions do not meet current emission standards when these engines are coupled with three-way catalytic converters. This short-coming is caused by the inability of NO<sub>x</sub> to be reduced to nitrogen in atmospheres containing excess oxygen. To date, two main solutions have been proposed and implemented. One method is selective catalytic reduction (SCR) where ammonia is used as the reductant to convert NO<sub>x</sub> to nitrogen [2]. The other method is the use of lean NO<sub>x</sub> traps (LNTs). A LNT catalyst usually consists of a platinum group metal to oxidize the NO to NO<sub>2</sub>, an alkali or alkaline earth metal oxide to store NO<sub>x</sub>, and a high surface area support material (e.g.,  $\gamma$ -alumina) [3].

Although LNTs are starting to find commercial application, the issue of LNT durability remains problematic. Sulfur present in fuel and engine oil is converted to SO<sub>2</sub> through the combustion cycle of engine operation, and the SO<sub>2</sub> can subsequently undergo oxidation over platinum group metals (PGMs), such as Pt and Rh, to form SO<sub>3</sub>. Barium oxide has a greater affinity for SO<sub>3</sub> than NO<sub>2</sub> (the resulting BaSO<sub>4</sub> being

thermodynamically more stable than  $\text{Ba}(\text{NO}_3)_2$  [4]), resulting in poisoning of the  $\text{NO}_x$  storage sites. The decomposition of  $\text{BaSO}_4$  requires the LNT to be exposed to rich conditions and high temperatures (650 to 800 °C) for several minutes. This requirement results in a fuel penalty that reduces the gains in fuel efficiency of lean-burn engines and gives rise to sintering of the precious metals and  $\text{NO}_x$  storage components. The high temperatures also enable unwanted side reactions between the LNT washcoat components (e.g., resulting in formation of  $\text{BaAl}_2\text{O}_4$  and  $\text{BaCeO}_3$ ) [5-8]. The formation of  $\text{BaAl}_2\text{O}_4$  and  $\text{BaCeO}_3$  and growth of Pt particles due to sintering decreases LNT  $\text{NO}_x$  storage efficiency [9-11]. Some researchers have attributed this decrease in efficiency to the reduced spillover rate of  $\text{NO}_2$ , formed from the oxidation of NO over Pt, to the storage material [5,12,13].

Recent studies have shown that ceria in LNTs is able to store some of the sulfur in the exhaust with the consequence that fewer barium sites should be poisoned [1,14-17]. The use of ceria as a component of three-way catalysts is well established based on its ability to reversibly store oxygen (that acts as a damper in maintaining stoichiometric conditions during various engine operating ranges) and its ability to maintain high precious metal dispersions in the washcoat [18]. The main function of ceria in lean burn gasoline LNTs is similarly to act as an oxygen storage material, thereby enabling the LNT to function as a conventional three-way catalyst when the engine is operating under stoichiometric conditions. However, different research groups have reported additional benefits from the incorporation of ceria in LNTs. Theis et al. reported that the addition of ceria improved the sulfur tolerance of the LNT [1]. In addition to improved sulfur tolerance, Kwak et al. reported that ceria containing catalysts provide excellent resistance against Pt sintering as compared to alumina-based catalysts [16]. Using DRIFTS, Ji et al. showed the addition of ceria improved sulfur resistance by reducing sulfur accumulation on BaO sites [17]. In addition, Ji proposed that the addition of ceria would lower the fuel penalty and precious metal sintering associated with catalyst desulfation because the operating period between desulfation events could be extended. The presence of ceria has also been shown to improve the  $\text{NO}_x$  storage and reduction properties of LNTs, particularly at

low temperatures [19-21]. Furthermore, under rich conditions, Pt promoted ceria is known to catalyze the water-gas shift reaction that produces hydrogen and CO<sub>2</sub> from CO and water [22,23]. The additional hydrogen produced is available to regenerate the trap, which is very beneficial given that H<sub>2</sub> has been shown to be a better NO<sub>x</sub> reductant than CO [24-29]; likewise, H<sub>2</sub> is a more efficient reductant for LNT desulfation than CO [29,30].

Although ceria possesses these attractive characteristics when used in LNT catalysts, to date relatively few reports have dealt directly with its role in LNT sulfation and desulfation. In this study the effect of ceria on sulfation and desulfation behavior was investigated, using both model powder catalysts and fully formulated monolithic catalysts. The effect of precious metal loading and the importance of Pt location (relative to the Ba phase) on the ease of LNT desulfation were also examined.

### *3.2. Experimental.*

#### *3.2.1. Preparation of Powder Catalyst Samples.*

Powder samples were prepared by incipient wetness impregnation. Pt/Al<sub>2</sub>O<sub>3</sub> was made by impregnating  $\gamma$ -alumina (Sasol, surface area of 132 m<sup>2</sup>/g) with an aqueous solution of tetraamine platinum (II) nitrate. The sample was then dried under vacuum at 100 °C overnight and calcined in air at 500 °C for 3 h. Pt/CeO<sub>2</sub> was prepared by the same method using ceria (Rhodia, surface area of 119 m<sup>2</sup>/g). A stepwise method was used to make the Pt/BaO/Al<sub>2</sub>O<sub>3</sub> sample (denoted PBA).  $\gamma$ -alumina was impregnated with aqueous Ba(NO<sub>3</sub>)<sub>2</sub>, dried and calcined at 500 °C in air. The Ba-loaded Al<sub>2</sub>O<sub>3</sub> was then impregnated with aqueous tetraamine platinum (II) nitrate and again calcined at 500 °C. Finally, in order to investigate the effect of ceria addition on the Pt/BaO/Al<sub>2</sub>O<sub>3</sub> catalyst, a sample was prepared by physically mixing the Pt/BaO/Al<sub>2</sub>O<sub>3</sub> and Pt/CeO<sub>2</sub> powders in a 76:24 weight ratio (denoted PBAC). All of the powders were pressed into pellets using an IR pellet press and then crushed and screened to a size of ASTM 20 to 40 mesh.



### 3.2.2. Temperature Programmed Sulfation-Desulfation Experiments.

Each of the powder catalysts was subjected to a temperature-programmed reduction (TPR) procedure to determine the temperature required to decompose the sulfates stored on the different storage components. The microreactor used consisted of a ¼ inch o.d. quartz tube in which a section of ca. 3 inch length contained the 150 mg of powder catalyst. The tube was heated by a programmable Lindberg Blue furnace. A V&F Airsense 2000 chemical ionization mass spectrometer (CI-MS) analyzed the product gases from the reactor. A gas flow rate of 120 sccm was used, corresponding to a gas space velocity of ca. 30,000 h<sup>-1</sup>. Table 3.1 shows the lean and rich feed gas compositions for the powder reactor. All of the inlet and outlet lines for the reactor were heated using heat tape to above 100 °C to prevent water condensation prior to analysis in the CI-MS. Prior to the experiments, each sample was subjected to pretreatment at 450 °C. The sample was first oxidized in a mixture of 8% O<sub>2</sub>, 5% CO<sub>2</sub> and 5% H<sub>2</sub>O (with Ar as the balance) for 15 min, after which it was purged with 5% CO<sub>2</sub> and 5% H<sub>2</sub>O (with Ar as the balance) for 10 min. The sample was then reduced in 2% H<sub>2</sub>, 5% CO<sub>2</sub>, 5% H<sub>2</sub>O, and balance Ar. Finally, the sample was cooled to 350 °C while it was exposed to 5% CO<sub>2</sub> and 5% H<sub>2</sub>O (with Ar as the balance).

**Table 3.1. Feed composition for experiments utilizing powder catalysts.**

Component	Pre-Oxidation	Pre-Reduction	Sulfation	TPR
SO <sub>2</sub>	0	0	100 ppm	0
O <sub>2</sub>	8%	0	8%	0
H <sub>2</sub>	0	2%	0	2%
CO <sub>2</sub>	5%	5%	5%	5%
H <sub>2</sub> O	5%	5%	5%	5%
Ar	Balance	Balance	Balance	Balance
Total Gas Flow, sccm	120	120	120	120
GHSV, h <sup>-1</sup>	30,000	30,000	30,000	30,000

The powder samples were sulfated by exposure to a feed containing 100 ppm SO<sub>2</sub>, 8% O<sub>2</sub>, 5% CO<sub>2</sub>, 5% H<sub>2</sub>O, and balance Ar (feed rate of 120 sccm) for 34 minutes at 350 °C.

Assuming complete sulfur uptake, these conditions resulted in a loading equivalent to 1 g sulfur/L for a monolithic catalyst with a washcoat loading of 260 g/L. Higher loadings were achieved by extending the duration of the sulfation. The catalysts were then subjected to desulfation under reducing conditions for the TPR. The procedure consisted of exposing the sample to 2% H<sub>2</sub>, 5% CO<sub>2</sub> and 5% H<sub>2</sub>O (with Ar as the balance) as the temperature was increased from 350 to 800 °C at a rate of 5 °C /min. The product gas stream was analyzed using the CI-MS.

### *3.2.3. Preparation of Monolith Catalyst Samples.*

The samples, listed in Table 3.2, are categorized into three groups according to the variation in components. The preparation of the catalysts has been described in detail elsewhere [21]. In brief, the samples were prepared using the incipient wetness method. In a first step, Pt and Rh were co-impregnated in a 1:1 weight ratio (using Pt(NH<sub>3</sub>)<sub>4</sub>(OH)<sub>2</sub> and Rh(NO<sub>3</sub>)<sub>3</sub> as the precursors) onto  $\gamma$ -alumina stabilized with 3 wt% La<sub>2</sub>O<sub>3</sub>, after which the powder was calcined for 2 h at 500 °C. Separately, BaO/Al<sub>2</sub>O<sub>3</sub> was prepared by impregnating Ba(O<sub>2</sub>CCH<sub>3</sub>)<sub>2</sub> onto  $\gamma$ -alumina, followed by calcination (also at 500 °C for 2 h). To this the required amount of CeO<sub>2</sub> or CeO<sub>2</sub>-ZrO<sub>2</sub> was added. To achieve the total Pt loading, the balance of the Pt was then impregnated onto the mixture as (as Pt(NH<sub>3</sub>)<sub>4</sub>(OH)<sub>2</sub>), after which it was calcined at 500 °C for 2 h. The Pt and Rh containing powder (in an amount corresponding to 30 g/L) and the powder containing BaO/Al<sub>2</sub>O<sub>3</sub> and CeO<sub>2</sub> was added to a balance of  $\gamma$ -alumina powder to achieve the overall washcoat loading of 260 g/L. A small amount of boehmite sol was used as a binder. The resulting slurry was washcoated onto a 4" x 6" cordierite 400 cpsi/6.5 mil monolith by DCL International Inc. (Toronto, ON) using a proprietary vacuum coating process. The monoliths were calcined at 550 °C for 2 h.

**Table 3.2. Composition of monolith catalysts.**

Component	Catalyst Code/Component Loading <sup>a</sup>		
	Series 1	Series 2	Series 3
Pt, g/L (g/cuft)	3.53 (100)	3.53 (100)	3.53 (100), 1.77 (50)
Rh, g/L (g/cuft)	0.71 (20)	0.71 (20)	0.35 (10)
BaO, g/L	30	30	30
CeO <sub>2</sub> <sup>b</sup> , g/L	0, 50, 100	0	50
CeO <sub>2</sub> -ZrO <sub>2</sub> <sup>c</sup> , g/L	0	50, 100	0
Al <sub>2</sub> O <sub>3</sub> <sup>d</sup> , g/L	Balance	Balance	Balance

<sup>a</sup> Nominal loadings. Total washcoat loading = 260 g/L

<sup>b</sup> Stabilized with 5 wt.% La<sub>2</sub>O<sub>3</sub>

<sup>c</sup> Ce<sub>0.7</sub>Zr<sub>0.3</sub>O<sub>2</sub>

<sup>d</sup> Stabilized with 3 wt.% La<sub>2</sub>O<sub>3</sub>

In series 1, the sample codes reflect the amount of barium (held constant at 30 g/L) and the amount of CeO<sub>2</sub> present (0, 50, or 100 g/L). Series 2 is composed of two samples designated 30-50z and 30-100z. The “z” refers to amount of ceria-zirconia (Ce<sub>0.7</sub>Zr<sub>0.3</sub>O<sub>2</sub>) present in the sample instead of CeO<sub>2</sub>. Series 3 differs from the two other series in the amount of precious metal present in the washcoat. The Rh concentration was reduced from 0.71 to 0.35 g/L for the two samples, and the Pt concentration varied at 1.77 g/L (50 g/ft<sup>3</sup>) and 3.53 g/L (100 g/ft<sup>3</sup>). The two samples in series 3 are designated by the amount of platinum present: Pt-50 and Pt-100. The CeO<sub>2</sub> loading was held constant for both samples at 50 g/L. The total washcoat loading for all of the samples was 260 g/L and was held constant by adjusting the amount of balance Al<sub>2</sub>O<sub>3</sub> present.

#### 3.2.4. Monolith Catalyst Sulfation and Desulfation.

1.75 cm x 2.54 cm (d x l) sample cores were drilled from the monolith samples. A small hole was drilled in the center of each core so that a K-type thermocouple could be inserted to measure the temperature of the gas stream at the front face of the sample. The catalyst cores were contained in a vertical quartz tube reactor (1” outer diameter) heated by a Lindberg Blue electric furnace. Prior to sulfation/desulfation experiments, samples

were degreened (stabilized) by heating at 800 °C for 3 h in a slightly rich gas. The composition of the feed gas is listed in Table 4.3. The overall flow rate was 3 L/min, resulting in a GHSV of 30,000 h<sup>-1</sup>.

Monolith samples were sulfated at 350 °C for 16 h using the gas stream shown in Table 3.3. The gas stream alternated between one min lean periods to one min rich periods (1/1 cycles). The length of the rich period was chosen to ensure that the trap was completely purged of NO<sub>x</sub> before the next lean cycle. NO<sub>x</sub> concentrations were measured using a heated chemiluminescence detector (Beckman Industrial Model 951 NO/NO<sub>x</sub> analyzer). The data were used to calculate the NO<sub>x</sub> storage efficiency at every hour from the start of sulfation to the end of the 16 h period.

Sample desulfation was performed at one of the following temperatures: 650 °C, 675 °C, 700 °C, 725 °C, or 750 °C. To begin the desulfation, the sample was ramped to the desired desulfation temperature. During the ramp, 1 min lean /1 min rich alternating cycles were used until the temperature reached 580 °C, at which point the feed was switched to the lean gas mixture to prevent desorption of the sulfur stored on the monolith sample before the desulfation temperature was reached. Once the desulfation temperature was obtained, the conditions were switched to rich and the temperature was held constant for 5 min before cooling to 580 °C under lean conditions. At this point, the gas composition was switched from lean to alternating 5 min lean, 3 min rich cycles until the sample reached 350 °C. At 350 °C data were taken from three 5/3 cycles and then five 1/1 cycles, corresponding to “steady state” cycling conditions (i.e., reproducibly periodic). The schedule of heating to the desulfation temperature, cooling to 350 °C, and then evaluating the catalyst during the 5/3 and 1/1 cycles was repeated three times. After the third time the SO<sub>2</sub> was turned off and the sample was heated to 750 °C under rich conditions for 10 min using the method described above. This part of the cycle is referred to as the clean-off. After the clean-off, the sample was evaluated at 350°C as before using 5/3 and 1/1 cycles. At this point the sample was ready to be sulfated again so the catalyst could be studied at another desulfation temperature. It should be noted that the data from the 1/1 cycles are very similar to the 5/3 cycles in both the storage

efficiency values obtained and the resulting trends, and consequently, the 1/1 cycle data are not discussed in this paper.

Copyright © Vencon Glenn Easterling 2013

**Table 3.3. Feed gas composition during determination of NO<sub>x</sub> storage efficiency.**

Component	Lean	Rich
CO <sub>2</sub>	10%	10%
H <sub>2</sub> O	10%	10%
NO <sub>x</sub>	500 ppm	500 ppm
SO <sub>2</sub>	9 ppm	9 ppm
O <sub>2</sub>	5%	0
CO	0	1.20%
H <sub>2</sub>	0	0.40%
N <sub>2</sub>	Balance	Balance

### 3.2.5. Measurement of Total Sulfur Release During Desulfation.

In these experiments, the same lean and rich gas mixtures were used as for the sulfation-desulfation experiments described in section 3.2.4 with the exception that in order to expedite catalyst sulfation, the samples were sulfated with 90 ppm SO<sub>2</sub> at 350°C (for 1 h under lean conditions; see Table 3.4). After sulfation, the SO<sub>2</sub> was shut off, and the sample was heated to the desired desulfation temperature under lean conditions to avoid any loss of SO<sub>2</sub>. Once the desulfation temperature was reached, the feed was switched to the rich gas mixture containing CO and H<sub>2</sub> for 10 min. Each desulfation ended with heating the sample to 750 °C under lean conditions and then switching to rich conditions for 10 min. Again, the period at 750 °C is referred to a clean-off and was performed to remove as much sulfur as possible before the next sulfation experiment and to confirm the total amount of sulfur originally stored on the catalyst. This allowed the calculation of the fractional sulfur release as a function of temperature by comparing the amount of the total sulfur released at the desulfation temperature to the amount of sulfur released during the clean-off period. The gas composition at the catalyst outlet was continuously monitored during desulfation using a V&F Systems, Inc. chemical ionization mass spectrometer (CI-MS) equipped with three ion sources of different energies. Mercury is

the low energy source and is used to detect H<sub>2</sub>S. Xenon is the medium source and is used to detect SO<sub>2</sub> and COS. Krypton is the high energy source and was not used in this study. From the concentrations of the sulfur species evolved, the data were integrated to calculate how much of each species was released during desulfation and during the clean-off. The fraction of total sulfur released was used to compare and evaluate the performance of the monolith catalysts.

**Table 3.4. Feed gas composition during determination of fraction of sulfur released/stored.**

Component	Lean	Rich
CO <sub>2</sub>	10%	10%
H <sub>2</sub> O	10%	10%
NO <sub>x</sub>	500 ppm	500 ppm
SO <sub>2</sub>	90 ppm	90 ppm
O <sub>2</sub>	5%	0
CO	0	1.20%
H <sub>2</sub>	0	0.40%
N <sub>2</sub>	Balance	Balance

### 3.3. Results and Discussion.

#### 3.3.1. Powder Model Catalysts.

##### 3.3.1.1. Temperature Programmed Reduction.

Four model catalysts were examined in this study, comprising Pt/Al<sub>2</sub>O<sub>3</sub>, Pt/CeO<sub>2</sub>, PBA, and PBAC. The Pt/Al<sub>2</sub>O<sub>3</sub> and Pt/CeO<sub>2</sub> samples were used as references to distinguish between release events from alumina, ceria, and barium sites. Prior to TPR, the samples were sulfated to loadings of 1, 2.5, and 7.5 g sulfur adsorbed per L equivalent of monolithic catalyst (assuming a typical monolith washcoat loading of 260 g/L). A typical release of the sulfur species observed during TPR is shown in Figure 3.1 for Pt/Al<sub>2</sub>O<sub>3</sub>. The first species seen is SO<sub>2</sub> which is then followed by H<sub>2</sub>S. COS is also seen when SO<sub>2</sub> release begins, but unlike the concentration of SO<sub>2</sub>, which decreases for the remainder of the TPR, the concentration of COS continues to increase until about 750 °C. Given that

H<sub>2</sub>S is the main product during the TPR experiment, in the following TPR plots only the H<sub>2</sub>S release events are shown. Table 3.5 and Figure 3.2 summarize the results of the TPR experiments performed using Pt/Al<sub>2</sub>O<sub>3</sub>. At a loading equivalent to 1 g S/L, the H<sub>2</sub>S release began at 369 °C, peaked at 399 °C, and ended at 627 °C. As the sulfur loading was increased to 2.5 g S/L equivalent and then 7.5 g S/L, also shown in Figure 3.2, the release of H<sub>2</sub>S began at temperatures slightly lower than at the 1 g S/L loading (358 and 356 °C, respectively). The reason for the lowering of the first release temperature as the sulfur loading was increased is not totally clear; however, it is probably due to the fact that at low loadings sulfur is stored at the strongest adsorption sites (e.g., the most basic).

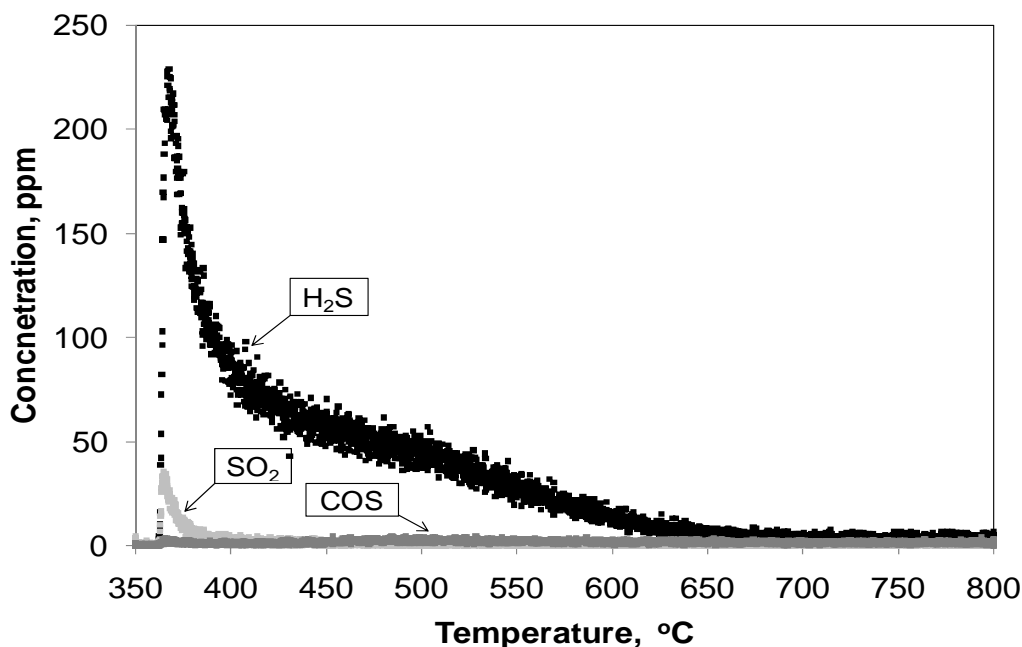


**Figure 3.1. Sulfur species released from Pt/Al<sub>2</sub>O<sub>3</sub> sulfated to 2.5 g sulfur/L of catalyst equivalent during TPR. Gas composition: 2% H<sub>2</sub>, 5% CO<sub>2</sub> and 5% H<sub>2</sub>O, balance Ar, GHSV=30,000 h<sup>-1</sup>.**

As the loading is increased, these sites are filled and sulfur is increasingly stored at sites where it is more weakly adsorbed. The maximum for this release event occurred at 368 °C for the 2.5 g S/L loading and 381 °C for the 7.5 g S/L sample. As the sulfur loadings increased so did the amount of sulfur released during TPR. In all three samples, the majority of the sulfur released was seen as H<sub>2</sub>S, its release peaking below 400 °C. This

result is broadly comparable with results reported in the literature. Wei et al. reported that peak H<sub>2</sub>S evolution from Pt/Al<sub>2</sub>O<sub>3</sub> occurred at 410 °C [31], while Elbouazzaoui et al. reported H<sub>2</sub>S release from Pt/Al<sub>2</sub>O<sub>3</sub> starting at 300°C and peaking at 450 °C [11].

**Table 3.5. Relative amounts of H<sub>2</sub>S released from different storage components during temperature-programmed reduction<sup>a</sup>**

Equivalent S loading, g/L			1		2.5		7.5	
Sample	Storage Component	Type	% H <sub>2</sub> S	Peak Temperature, °C	% H <sub>2</sub> S	Peak Temperature, °C	% H <sub>2</sub> S	Peak Temperature, °C
Pt/Al <sub>2</sub> O <sub>3</sub>	Al <sub>2</sub> O <sub>3</sub>	Surface	80	399	100	368	100	381
		Bulk	20	797	N/D <sup>b</sup>	--	N/D	--
Pt/CeO <sub>2</sub>	CeO <sub>2</sub>	Surface	100	518	100	463	100	451
PBA	Al <sub>2</sub> O <sub>3</sub>	Surface	9	477	11	433	35	384
		BaO	91	729	89	706	48	682
PBAC	Al <sub>2</sub> O <sub>3</sub>	Bulk	N/D	--	N/D	--	17	773
		Surface	N/D	--	N/D	--	1	382
	CeO <sub>2</sub>	Bulk	N/D	--	N/D	--	--	--
		Surface	35	465	43	462	62	451
	BaO	Bulk	--	--	--	--	--	--
		Surface	65	737	57	748	27	682
Pt/Al <sub>2</sub> O <sub>3</sub> : BaO/Al <sub>2</sub> O <sub>3</sub>	Al <sub>2</sub> O <sub>3</sub>	Bulk	N/D	--	N/D	--	10	781
		Surface	46	378	54	367	--	--
	BaO	Bulk	N/D	--	N/D	--	--	--
		Surface	19	748	21	735	--	--
		Bulk	34	791	25	766	--	--

<sup>a</sup> Rich phase for TPR: 2% H<sub>2</sub>, 5% CO<sub>2</sub>, 5% H<sub>2</sub>O, Ar balance, GHSV = 30,000 h<sup>-1</sup>

<sup>b</sup> N/D: Not detectable by CI-MS during the experiment



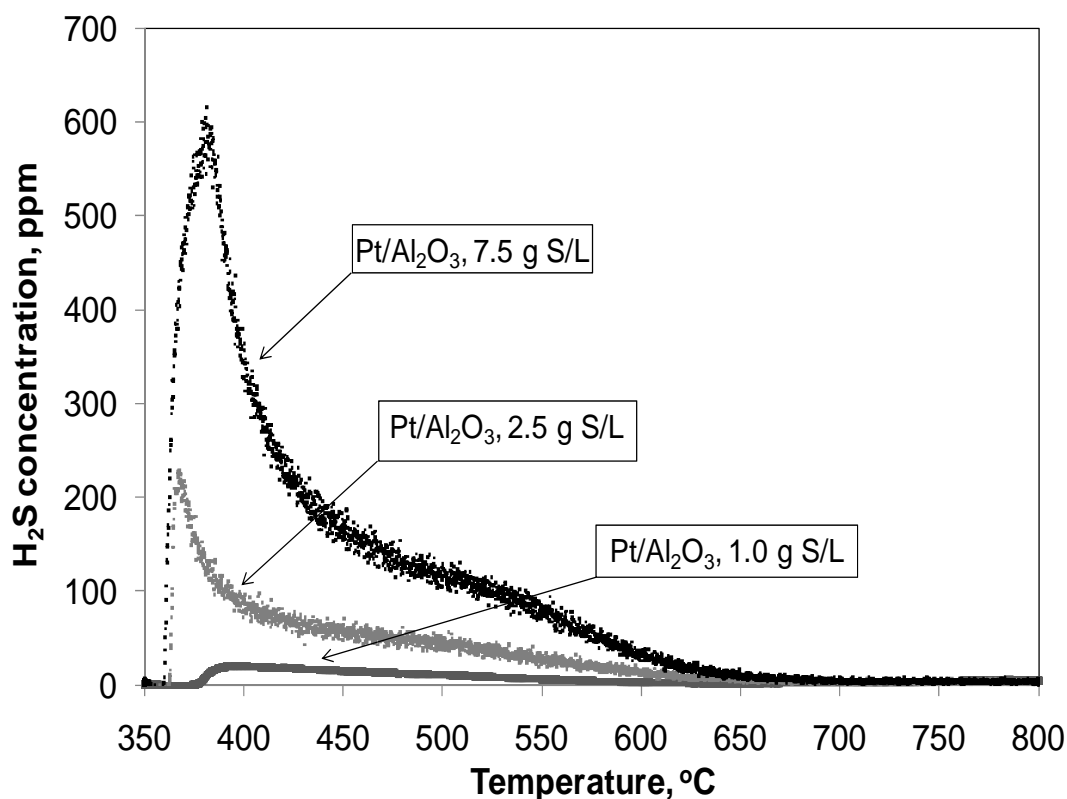


**Figure 3.2. Comparison of H<sub>2</sub>S released from Pt/Al<sub>2</sub>O<sub>3</sub> sulfated to 1.0, 2.5, and 7.5 g sulfur/L of catalyst during TPR. Gas composition as for Figure 3.1.**

TPR results for Pt/CeO<sub>2</sub> are shown in Table 3.5 and Figure 3.3. For the sulfur loadings of g S/L, 2.5 g S/L and 7.5 g S/L, H<sub>2</sub>S evolution commenced at 459, 415, and 423 °C, respectively, with the corresponding peak H<sub>2</sub>S releases at 518, 463, and 451 °C. These values compare well with the temperatures reported by Ji et al. (450 °C) [17], Bazin et al. (400-500 °C) [32,33], and Waqif et al. (480-550 °C) [34] for sulfate reduction and concomitant sulfur release from sulfated ceria. Similar to the Pt/Al<sub>2</sub>O<sub>3</sub> samples, the total amount of sulfur released from Pt/CeO<sub>2</sub> during TPR increased with increasing sample exposure to SO<sub>2</sub>, while for all three sulfur loadings H<sub>2</sub>S was the main species released by mass. In addition, there were indications of a possible minor secondary H<sub>2</sub>S release event centered at approximately 750 °C (see inset, Fig. 3.3). However, the magnitude of this event was such that it is hard to distinguish it from analytical noise, and consequently we have chosen not to include it in Table 3.5.

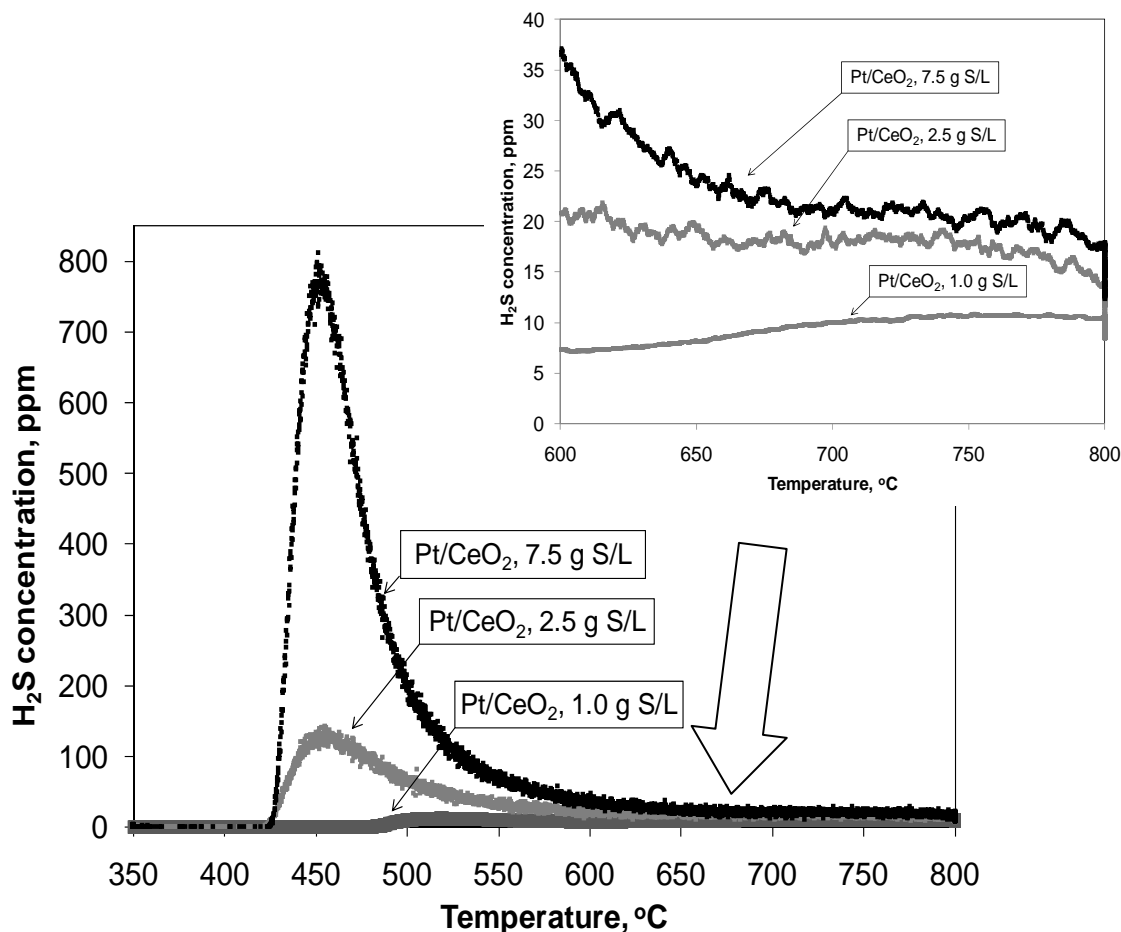


**Figure 3.3. Comparison of H<sub>2</sub>S released from Pt/CeO<sub>2</sub> sulfated to 1.0, 2.5, and 7.5 g sulfur/L of catalyst during TPR. Gas composition as for Figure 3.1.**

Turning to catalyst PBA, for the 1 g S/L loading (Table 3.5 and Figure 3.4), SO<sub>2</sub> release was observed at 400 °C, followed by the release of H<sub>2</sub>S that peaked at 477 °C. The evolution of these sulfur species can be assigned to sulfur release from alumina as seen for the Pt/Al<sub>2</sub>O<sub>3</sub> reference sample. A second release event started at about 573 °C and continued until 800 °C with the peak H<sub>2</sub>S concentration occurring at 729 °C. This is second release event for both loadings took place at 550 °C and in the case of the 2.5 g S/L sample reached a maximum concentration at 706 °C, a slightly lower value than for the sample sulfated to 1 g S/L. This result is consistent with the increase in sulfur loading and shift to a lower release temperature observed for the other samples. In the case of the

7.5 g S/L sample, a double peak was observed at high temperature. The first maximum of this double peak occurred at 682 °C, and the second occurred at 773 °C. The first of the maxima can be assigned to the release of sulfur stored as surface BaSO<sub>4</sub>, while the second can be attributed to sulfur stored as bulk BaSO<sub>4</sub>.

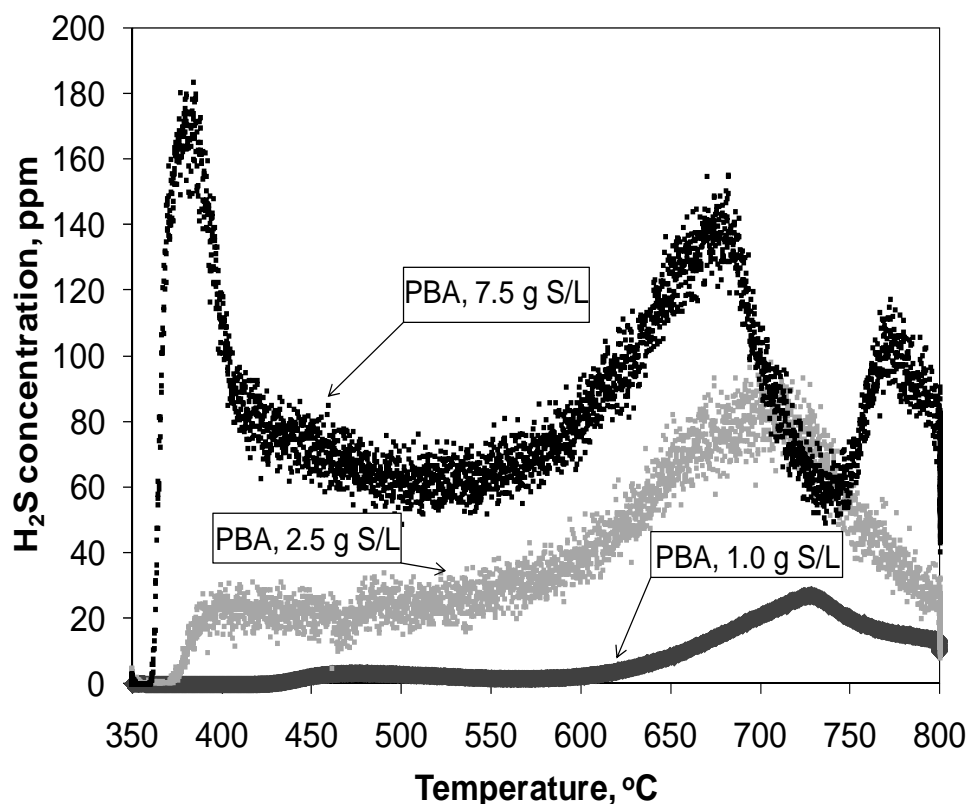


**Figure 3.4. Comparison of H<sub>2</sub>S released from PBA sulfated to 1.0, 2.5, 6.0, and 7.5 g sulfur/L of catalyst during TPR. Gas composition as for Figure 3.1.**

Several authors have made similar observations that temperatures above 700 °C are required for the decomposition of bulk BaSO<sub>4</sub> [4,11,35]. Sedlmair et al. reported that during sulfation surface sulfates can undergo migration into the support material to become bulk sulfates [36]. Elbouazzaoui et al. concluded that peaks corresponding to surface and bulk BaSO<sub>4</sub> were present in the TPR profile of a sulfated Pt/BaO/Al<sub>2</sub>O<sub>3</sub> catalyst [4,11]. These workers postulated that Pt promotes the reduction of surface BaSO<sub>4</sub> deposited in the vicinity of Pt but has no effect on BaSO<sub>4</sub> located far from the

metal sites. Using Raman spectroscopy, Wei et al. concluded that BaSO<sub>4</sub> close to Pt particles has a small crystallite size (< 3 nm) and is reduced at moderate temperatures (~650 °C). On the other hand, bulk sulfate has a larger crystallite size (> 10 nm) and is reducible only at high temperatures (~750 °C) [31]. Stakheev et al. also proposed that the presence of two peaks is due to surface and bulk barium sulfates or to BaSO<sub>4</sub> located close to and far away from Pt particles [35].

Based on the results from the two reference samples and catalyst PBA, the effects of ceria addition to PBA can be demonstrated. Looking at the TPR result for the PBAC sample loaded to 1 g S/L (Figure 3.5), two desorption maxima occur at 465 and 737 °C. The first release event can be assigned to release from ceria as seen with the Pt/CeO<sub>2</sub> sample, while the second corresponds to the release of sulfur from BaSO<sub>4</sub>, as seen with PBA. Comparing the PBAC and PBA samples at 1g S/L, Table 3.5, the amount of H<sub>2</sub>S released from Ba sites reflects the presence of ceria with a difference of 26% less H<sub>2</sub>S released from the Ba in PBAC compared to PBA. Comparing the release from the Al sites in PBA to the Ce sites in PBAC, a 26% difference is again seen in the amount of H<sub>2</sub>S evolved. The release of sulfur species from the Ce phases in PBAC demonstrates the additional storage provided by the Ce sites. As seen in Figure 3.5, when the loadings were increased from 1 to 2.5 to 7.5 g S/L, the height of the peak from the release of CeO<sub>2</sub> sites increased faster than the peak from the Ba sites. This increase is also reflected in Table 3.5, where the amount of H<sub>2</sub>S released from the Ce sites in PBAC increased from 35% of the total for 1 g S/L loading to 43% for 2.5 g S/L and 62% for 7.5 g S/L. This implies that sulfur was preferentially stored at the CeO<sub>2</sub> sites as opposed to the BaO sites as the loading increased.

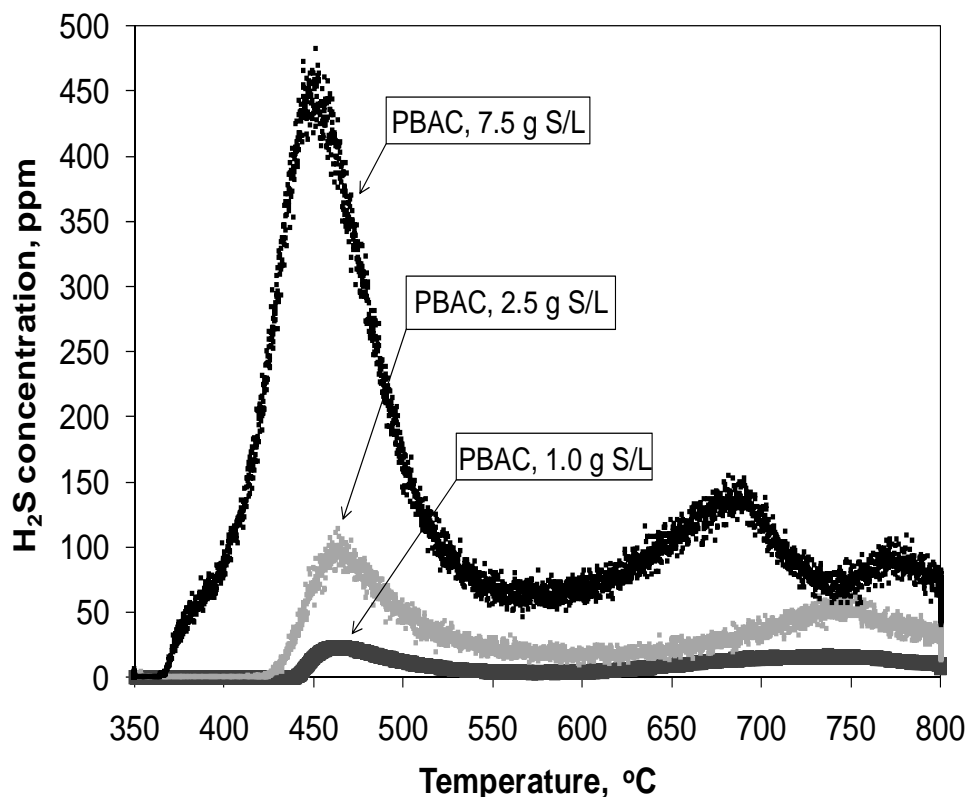


**Figure 3.5. Comparison of H<sub>2</sub>S released from PBAC sulfated to 1.0, 2.5, 6.0, and 7.5 g sulfur/L of catalyst during TPR. Gas composition as for Figure 3.1.**

### *3.3.1.2. Effect of Platinum Location on Desulfation Efficiency.*

In order to demonstrate the influence of Pt location (with respect to the Ba sites) on LNT desulfation, a sample was prepared in which the Pt and Ba phases were separated. This was done by physically mixing 1 wt% Pt/Al<sub>2</sub>O<sub>3</sub> and 20 wt% BaO/Al<sub>2</sub>O<sub>3</sub> powders in a 1:1 weight ratio. As shown in Table 3.5 and Figure 3.6, during TPR the physical mixture displays several H<sub>2</sub>S release events. For the sample loaded to 1 g S/L, the first release of H<sub>2</sub>S is seen at 356 °C and extends up to 580 °C, with a maximum at 378 °C. The second release begins at 580 °C, peaks at 748 °C and extends up to 752 °C, and the third begins at 752 °C and continues until the end of the TPR experiment at 800 °C, with a maximum at 791 °C. As the sulfur loading is increased to 2.5 g S/L, these maxima are slightly shifted towards lower temperature, as typically observed for the other catalyst samples discussed above.

Comparing the results for the physical mixture and sample PBA, although both samples release about the same amount of sulfur at the 1 g/L S loading (and correspondingly more at the 2.5 g/L loading), several significant differences are observed. First, sulfur release in the range 350-500 °C is observed to occur at lower temperatures and in relatively greater amounts for the physical mixture than for PBA. The release in this temperature range is consistent with the decomposition of sulfate on alumina [11,31], while the releases seen from both samples at the higher temperatures (>580 °C) can be assigned to the decomposition of BaSO<sub>4</sub> [4,11,35]. Second, whereas PBA shows a single H<sub>2</sub>S release event corresponding to the decomposition of surface BaSO<sub>4</sub>, the physical mixture shows a double peak corresponding to H<sub>2</sub>S release from both surface and bulk BaSO<sub>4</sub>. Third, the maxima for H<sub>2</sub>S release from surface BaSO<sub>4</sub> are shifted by between ~20 and 40 °C to higher temperature for the physical mixture as compared to PBA (the exact value being dependent on the sulfur loading). We note that a similar observation has been reported by Wei et al. during related TPR experiments [31]: for a physical mixture of Pt,Rh/Al<sub>2</sub>O<sub>3</sub> and BaO/Al<sub>2</sub>O<sub>3</sub>, the high temperature BaSO<sub>4</sub> release maximum occurred at a temperature that was 60 °C higher than for the corresponding peak observed for an impregnated sample containing BaO/Pt,Rh/Al<sub>2</sub>O<sub>3</sub>.

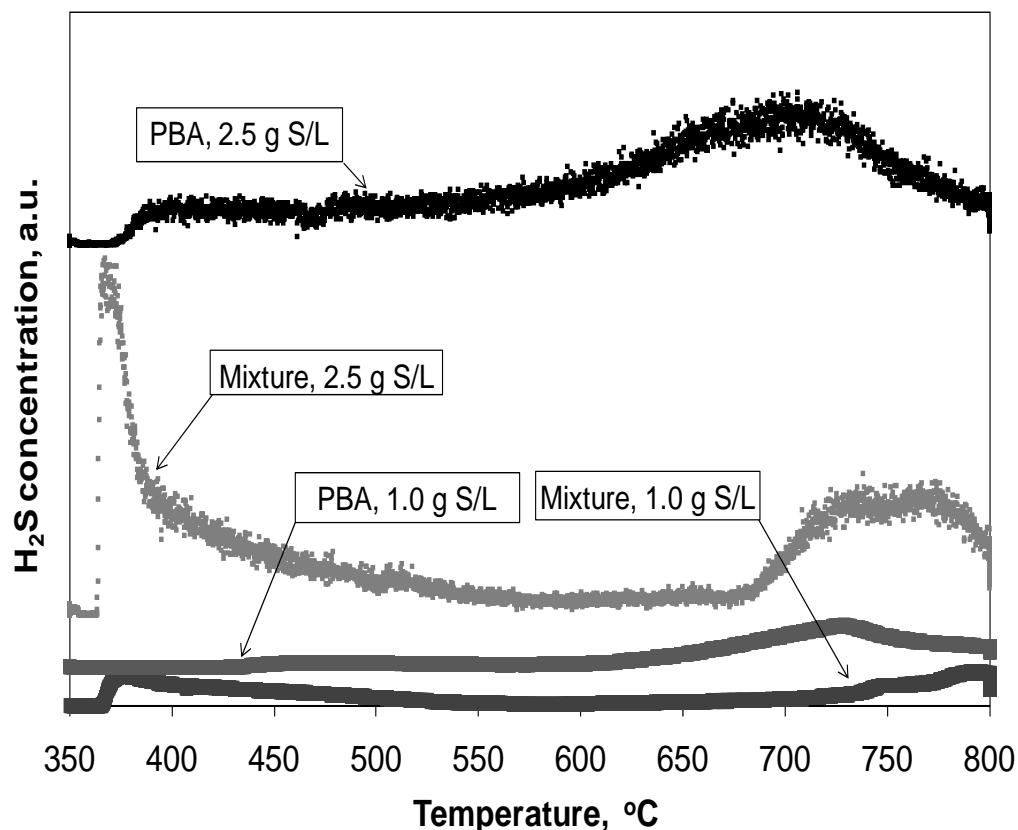


**Figure 3.6. Comparison of H<sub>2</sub>S released from PBA and 1:1 physical mixture of Pt/Al<sub>2</sub>O<sub>3</sub> and BaO/Al<sub>2</sub>O<sub>3</sub> sulfated to 1.0 and 2.5 g sulfur/L of catalyst during TPR. Gas composition as for Figure 3.1. Note that for clarity the plots have been stacked.**

From the foregoing it is apparent that in PBA most of the sulfur is stored on surface BaO sites, whereas in the physical mixture sulfur is stored on both Al<sub>2</sub>O<sub>3</sub> and BaO sites. Sulfur storage on the Al<sub>2</sub>O<sub>3</sub> sites can be attributed to spillover of SO<sub>3</sub> from Pt to the Al<sub>2</sub>O<sub>3</sub> support during sulfation. More significantly, the fact that the desulfation temperature of the Ba storage component is shifted towards higher temperature for the physical mixture relative to PBA is consistent with the idea that the decomposition of surface BaSO<sub>4</sub> is facilitated by adsorbed H atoms which spill over from the Pt sites onto the sulfated Ba phase. Physical separation of the Pt and Ba phases appears to inhibit this process, with the consequence that the surface BaSO<sub>4</sub> behaves more like bulk BaSO<sub>4</sub> with respect to its desulfation properties. We note that somewhat analogous findings have

been reported for nitrate decomposition on physical mixtures of Pt/Al<sub>2</sub>O<sub>3</sub> and BaO/Al<sub>2</sub>O<sub>3</sub> [37]: in the absence of hydrogen spillover from Pt to the Ba phase, considerably higher temperatures are required to achieve nitrate decomposition than is usual for Pt/BaO/Al<sub>2</sub>O<sub>3</sub> catalysts.

### *3.3.2. Monolith Catalysts.*

#### *3.3.2.1. Effects of Sulfur on NO<sub>x</sub> Storage Efficiency and Regeneration Temperature.*

In order to shed further light on washcoat component effects in LNT sulfation and desulfation, two experiments were performed using fully formulated monolithic catalysts in which the loadings of the various components (ceria, ceria-zirconia, and precious metals) were systematically varied. In the first experiment, the effect of desulfation at different temperatures on the lean phase NO<sub>x</sub> storage efficiency (NSE) during lean-rich cycling was examined. In the second experiment, the ability of the monolith sample to be desulfated under rich conditions was determined by calculating the amount of sulfur released during desulfation.

Considering the results of the first experiment (Figure 3.7), sample 30-0, containing no ceria, showed the largest decrease in the NSE during the lean period, corresponding to a loss of 60% after sulfation of the sample. Furthermore, the 30-0 sample was not able to achieve its pre-sulfation NSE value at any of the desulfation temperatures from 650 to 750 °C, as shown in Figure 3.8. The highest value was seen at 750 °C, corresponding to only 95% of the original NSE. Compared to the other catalysts, the NSE of 30-0 showed the greatest dependence on desulfation temperature (difference of greater than 20% over the temperature range). This finding can be explained on the basis of the TPR results presented above for catalyst PBA. Looking at Figure 3.8, it is evident that a temperature of less than 750 °C is insufficient to completely desulfate sample 30-0.



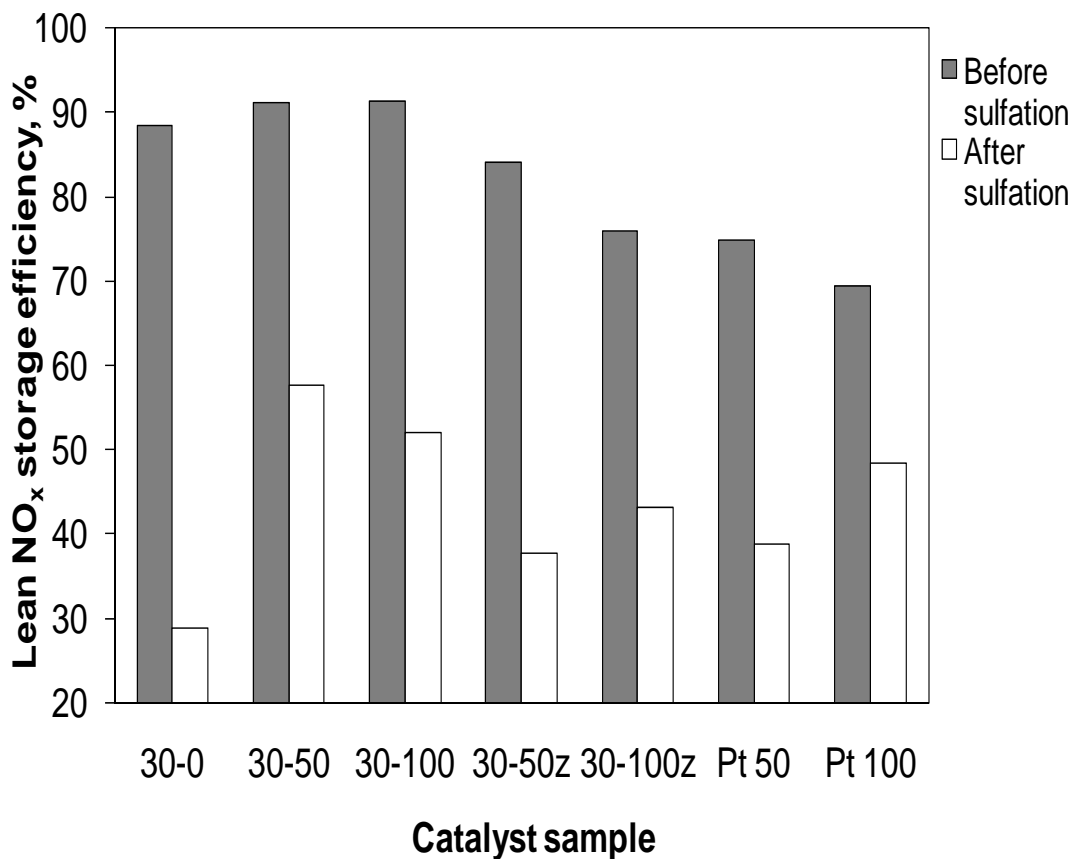


**Figure 3.7. Comparison of lean NO<sub>x</sub> storage efficiency values for fresh and sulfated monolith samples. Samples were sulfated with 9 ppm SO<sub>2</sub> for 16 h at 350 °C under 1 min lean/1 min rich conditions.**

Turning to the 30-50 and 30-100 samples containing 50 and 100 g/L of ceria, respectively, the presence of ceria in the monolith results in a higher NSE after sulfation (relative to 30-0) and a clear lowering of the desulfation temperatures required to approach the pre-sulfation NSE values of the catalysts. The NSE values after sulfation for 30-50 and 30-100 are roughly twice the value for 30-0 (Figure 3.7). As shown in Figure 3.8, sample 30-50 reached 94% of its clean-off NSE value at 675 °C and 97% at 700 °C. Sample 30-100 was even better than 30-50, reaching 95% of its clean-off value at 650 °C. Indeed, in general the NO<sub>x</sub> storage efficiency of 30-100 was higher over the entire temperature range used for desulfation than 30-0 or 30-50. The reason for the

superior performance of 30-50 and 30-100 over 30-0 can be assigned to the presence of  $\text{CeO}_2$  in the sample. As seen for PBAC,  $\text{CeO}_2$  can store sulfur, thereby decreasing the extent of bulk  $\text{BaSO}_4$  formation. Further, the  $\text{CeO}_2$  phase can be desulfated at relatively low temperature. An additional factor may be the high water-gas shift (WGS) activity of  $\text{Pt/CeO}_2$ . Indeed, in previous work we have demonstrated the superior WGS activity of 30-50 and 30-100 relative to 30-0 and the higher intra-catalyst  $\text{H}_2$  concentrations that result during rich operation [21].

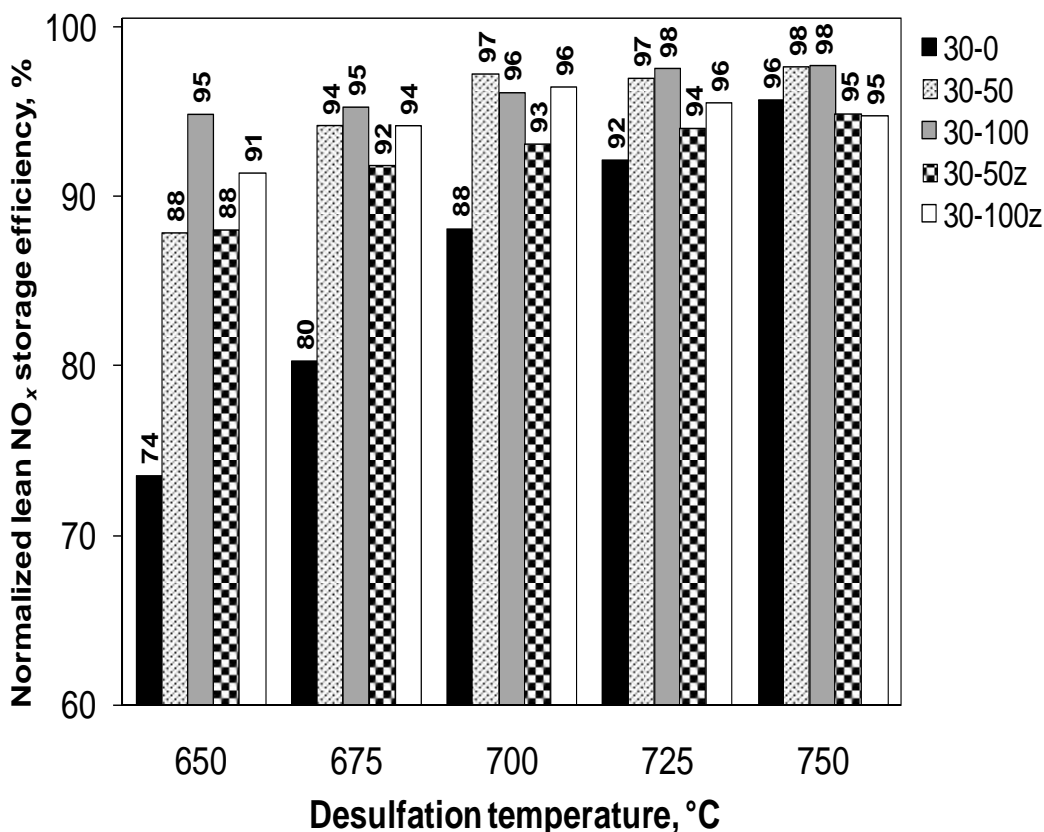


**Figure 3.8.** Comparison of normalized lean  $\text{NO}_x$  storage efficiency values ( $\text{NO}_x$  storage efficiency after desulfation divided by the  $\text{NO}_x$  storage efficiency after clean-off) for samples 30-0, 30-50, 30-100, 30-50z, and 30-100z. Desulfation conditions: 1.2%  $\text{CO}$ , 0.4%  $\text{H}_2$ , 10%  $\text{CO}_2$ , 10%  $\text{H}_2\text{O}$ , balance  $\text{N}_2$ ,  $\text{GHSV}=30000 \text{ h}^{-1}$ .

The effects of CeO<sub>2</sub> addition to the monolith catalysts are further supported by studying the fraction of sulfur released from the stored sulfur. Starting with series 1 (see Figure 3.9), the effect of CeO<sub>2</sub> is evidenced by the fact that larger fractions of the stored sulfur are released at lower temperatures (650 and 675 °C) as compared to catalyst 30-0. Indeed, sulfur release at these low temperatures increases with ceria loading. The amount of sulfur released during desulfation for the 30-0 sample is lower than 30-50 or 30-100 until 700 °C and higher. The increased fraction of sulfur released is attributed to the additional SO<sub>x</sub> storage sites provided by the ceria present in the sample, which as shown by the TPR results presented in section 3.3.1.1 above, releases H<sub>2</sub>S and SO<sub>2</sub> at significantly lower temperatures than the BaO phase.

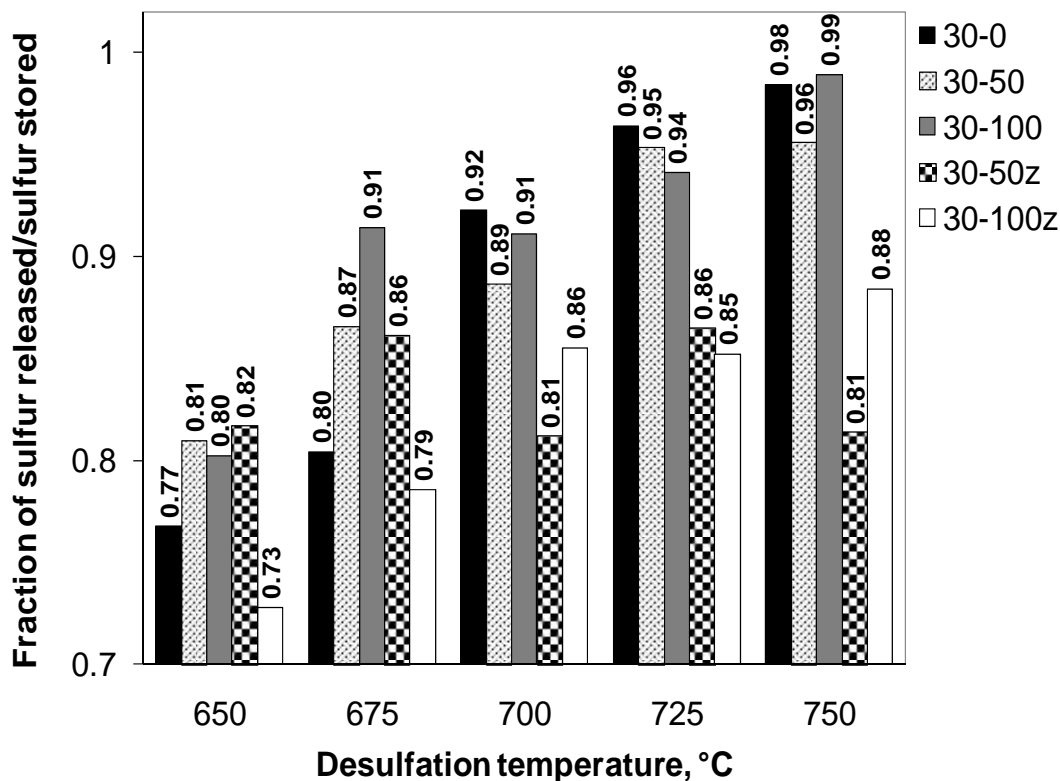


**Figure 3.9.** Comparison of fraction of sulfur released/stored after sulfation with 90 ppm SO<sub>2</sub> for 1 h for samples 30-0, 30-50, 30-100, 30-50z and 30-100z. Desulfation conditions as for Figure 3.8.

In addition to the ceria containing samples, two samples were examined that contained  $\text{CeO}_2\text{-ZrO}_2$  so that the effects of  $\text{CeO}_2$  and  $\text{CeO}_2\text{-ZrO}_2$  could be compared. Both samples contained 30 g/L of BaO, as for the series discussed above; the full compositions are given in Table 3.2 (series 2). The results obtained for this series are also shown in Figures 3.7 and 3.8. While the fresh  $\text{NO}_x$  storage efficiency value for 30-50z was only 7% lower than the value for 30-50 (84% vs. 91%), the measured value for 30-50z after sulfation was 20% lower: in absolute terms, the sample 30-50 lost 34% of its  $\text{NO}_x$  storage efficiency and the 30-50z lost 47%. Comparing samples 30-100 and 30-100z, the difference in the fresh NSE values was slightly larger (91% for 30-100 versus 76% for 30-100z). However, the difference in the NSE values after sulfation for 30-100 and 30-100z was only 9%. Looking at the NSE values after desulfation for these four samples (Figure 3.8), the differences were less than 7% at 650 °C and less than 4% over the remaining temperature range.

Data pertaining to the sulfur release during desulfation supports the observation that the catalysts containing  $\text{CeO}_2\text{-ZrO}_2$  display inferior desulfation characteristics as compared to their La-stabilized  $\text{CeO}_2$ -containing analogs (see Figure 3.9). This may be attributed to the less basic nature of the  $\text{CeO}_2\text{-ZrO}_2$  (relative to  $\text{CeO}_2$ ), which may lower the ability of  $\text{CeO}_2\text{-ZrO}_2$  to store sulfur and hence result in comparatively more severe sulfation of the Ba phase. Indeed, Rohart et al. have reported that the basicity of Ce-mixed oxides affects their  $\text{SO}_x$  storage capacity [38], sulfate adsorption being higher on ceria-rich oxides than on zirconia-rich oxides. Also relevant in this context are the results of a recent study by Bazin et al. [33], who found that the addition of zirconia into ceria limits sulfation in the bulk of the oxide, thereby limiting the total sulfur uptake. The same authors also report that zirconia addition raises the required desulfation temperature slightly; for example, weight loss maxima of 733 K and 753 K were observed during hydrogen reduction of sulfated  $\text{CeO}_2$  and  $\text{Ce}_{0.63}\text{Zr}_{0.37}\text{O}_2$ , respectively. Note that the surface areas of the La-stabilized  $\text{CeO}_2$  and  $\text{CeO}_2\text{-ZrO}_2$  used in the monolithic catalysts in the present study were very similar (119  $\text{m}^2/\text{g}$  and 114  $\text{m}^2/\text{g}$ , respectively), hence surface area should not be a factor with respect to their differing sulfation-desulfation behavior.

Finally, we note that ease of catalyst desulfation (as reflected in the fraction of sulfur released/sulfur stored) holds implications for long term catalyst use, given that the catalyst is subjected to repeated sulfation-desulfation cycles over the course of its useful life. For additives or specific compositions which negatively affect sulfur release from the catalyst, there is a greater tendency to accumulate residual sulfur during repeated sulfur/desulfation events, eventually leading to reduced  $\text{NO}_x$  storage efficiency. In an accompanying paper [39] we describe the results of accelerated aging experiments performed on catalysts 30-0, 30-50, 30-100 and 30-100z in which repetitive sulfation/desulfation cycles were performed, and we correlate the residual sulfur contents of the catalysts with their composition. The resulting data confirm that ceria-containing catalysts exhibit superior sulfation and desulfation characteristics as compared to their non-ceria analog; more particularly, the ability of ceria to trap sulfur results in decreased sulfur accumulation on the main Ba  $\text{NO}_x$  storage component. In addition, while the results presented above suggest that catalyst 30-100z should perform less well in this respect than 30-100, the  $\text{NO}_x$  conversion of 30-100z after aging is in fact slightly better than that of 30-100 [39]. The reason for this is not entirely clear, although it may be a consequence of the superior stability of the  $\text{Ce}_{0.7}\text{Zr}_{0.3}\text{O}_2$  mixed oxide with respect to thermally induced sintering as compared to La-stabilized  $\text{CeO}_2$ .

### *3.3.2.2. Effect of Precious Metal Loading on $\text{NO}_x$ Storage Efficiency and Regeneration Temperature.*

In the last group of catalysts (Series 3, Table 3.2), the amount of Pt was varied and the amount of Rh was halved. The two samples examined corresponded to Pt-50, containing  $50 \text{ g/ft}^3$  (1.77 g/L) Pt and  $10 \text{ g/ft}^3$  (0.35 g/L) Rh, and Pt-100, containing  $100 \text{ g/ft}^3$  (3.53 g/L) Pt and  $10 \text{ g/ft}^3$  (0.35 g/L) Rh. The BaO and  $\text{CeO}_2$  loadings were fixed at 30 g/L and 50 g/L, respectively (i.e., as for catalyst 30-50). Looking at the comparison of  $\text{NO}_x$  storage efficiency values for fresh and sulfated monolith samples (Figure 3.7), it is evident that the 30-50 sample, with double the amount of Rh, is less susceptible to poisoning than the Pt-50 or Pt-100 samples. Furthermore, as shown in Fig. 3.10, clear trends emerge when considering the NSE of the catalysts subjected to desulfation in the

range 700 - 750 °C. Specifically, the NSE of sample 30-50 is found to be slightly higher than that of Pt-100 after desulfation at temperatures of 700 °C and above, a finding which can be ascribed to the lower Rh loading in the latter sample. These results are consistent with the reports of Amberntsson et al. [40,41], who for Ba-based LNTs containing either Pt, Rh or Pt + Rh observed that the recovery of NO<sub>x</sub> storage capacity after desulfation in H<sub>2</sub> at 750 °C was complete only for the samples containing both Pt and Rh. This was attributed to the fact that Rh is more easily sulfur-regenerated than Pt [40]. Furthermore, it was found that Rh suffered from severe deactivation with respect to its NO oxidation function under SO<sub>2</sub> exposure but retained high NO<sub>x</sub> reduction activity under rich conditions; in contrast, the opposite behavior was observed for Pt. Consequently, it was concluded that a combination of Pt and Rh is preferable for minimizing the effects of sulfur deactivation [40,41]. In the case of Pt, it is known that under rich conditions Pt sulfides and/or elemental sulfur can form which block the Pt sites with respect to the adsorption of reductants [36,42]. From this it follows that desulfation should proceed most efficiently when a high concentration of Rh is present, since the Rh will be less susceptible to poisoning by the released sulfur and will enable the continuous adsorption and spillover of reductant molecules onto the sulfated oxides present.

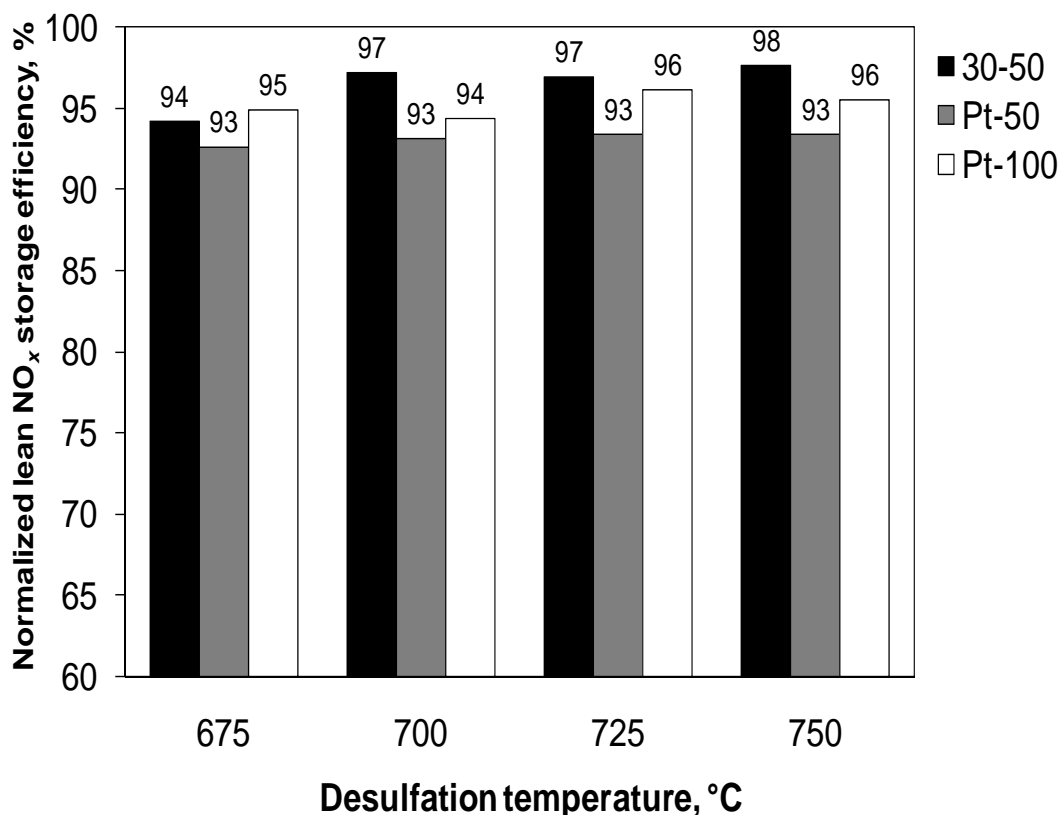


**Figure 3.10. Comparison of normalized lean NO<sub>x</sub> storage efficiency values (NO<sub>x</sub> storage efficiency after desulfation divided by the NO<sub>x</sub> storage efficiency after clean-off) for samples 30-50, Pt-50, Pt-100. Desulfation conditions as for Figure 3.8.**

Catalyst Pt-100, in turn, displays higher NSE at each of the desulfation temperatures when compared to catalyst Pt-50, a result which can be directly attributed to the extra Pt present. As a consequence of the additional platinum in Pt-100, the average distance between the Pt sites and the storage components should be decreased as compared to Pt-50 [43]. The effect of the increased proximity of the Pt to the sulfates stored at BaO was demonstrated in the PBA and Pt/Al<sub>2</sub>O<sub>3</sub> + BaO/Al<sub>2</sub>O<sub>3</sub> powders in section 3.1.2.

Specifically, decreasing the Pt-Ba distance can be anticipated to result in more efficient spillover of reductants from the Pt sites and hence, more extensive desulfation. Figure 3.11 shows the effects of precious metal loading on the fraction of sulfur released from

the samples by comparing the results for the series 3 catalysts to those obtained for 30-50. At almost every temperature, Pt-100 released a greater amount of stored sulfur than Pt-50, consistent with this reasoning.

Overall, in comparing all three of the series of monolith catalysts, the CeO<sub>2</sub> loading is observed to exert a greater influence on catalyst desulfation characteristics than the Pt loading (within the range studied), particularly at temperatures below 700 °C. Correspondingly, the results from the experiments in which sulfur evolution was monitored parallel the results gained from the NO<sub>x</sub> storage efficiency experiments. Comparing the three series of catalysts, the catalysts with the highest amounts of CeO<sub>2</sub> or CeO<sub>2</sub>-ZrO<sub>2</sub> have the best performance, as measured by the temperature required during desulfation to reach each individual catalyst's clean-off NSE value. A second measure of performance is the resistance to sulfur deactivation in the first place, where again the higher CeO<sub>2</sub> and CeO<sub>2</sub>-ZrO<sub>2</sub> containing samples have the best performance. Catalyst 30-100, the sample with the highest amount of CeO<sub>2</sub>, showed the best performance in NO<sub>x</sub> storage efficiency across all of the desulfation temperatures.



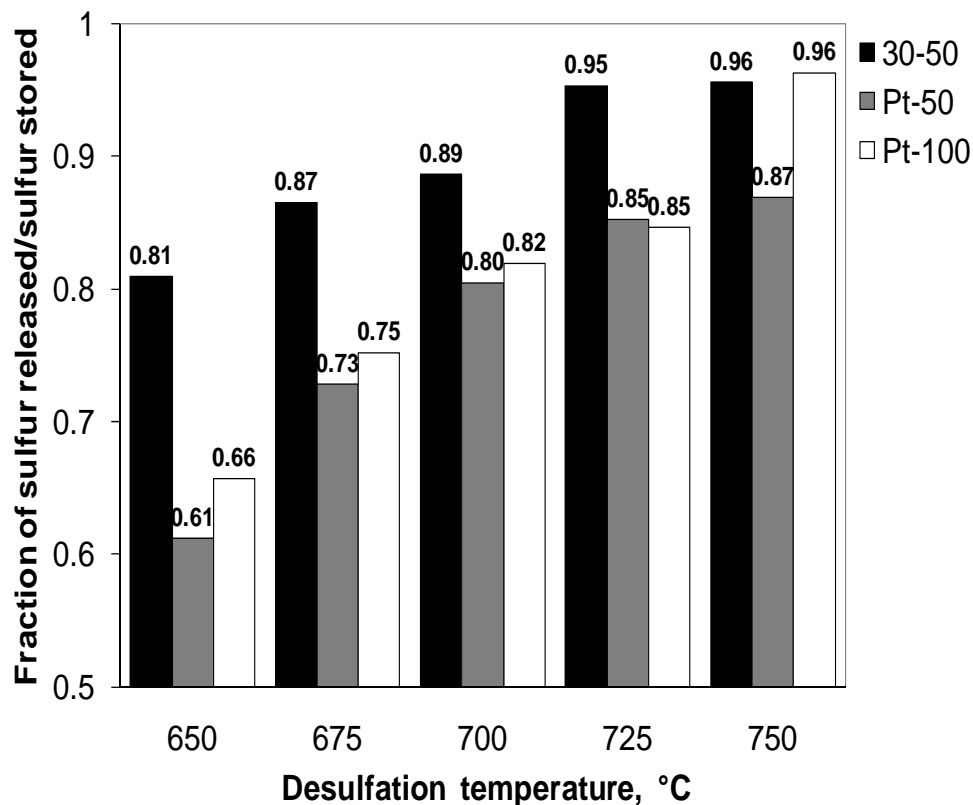


**Figure 3.11. Comparison of fraction of sulfur released/stored after sulfation with 90 ppm SO<sub>2</sub> for 1 h for samples 30-50, Pt-50 and Pt-100. Desulfation conditions as for Figure 3.8.**

#### *3.4. Conclusions.*

The effects of ceria on the sulfation and desulfation characteristics of Ba-based LNT catalysts have been demonstrated using both powder and fully formulated monolithic catalysts. TPR experiments performed on the powder catalysts showed that each of the oxide phases present (BaO, CeO<sub>2</sub>, and Al<sub>2</sub>O<sub>3</sub>) is able to store sulfur and that they possess distinct behavior in terms of the temperatures at which desulfation occurs. Overall, these findings confirm the idea that ceria can function as a sulfur sink in LNT catalysts, thereby helping to protect the main Ba NO<sub>x</sub> storage phase from sulfation.

In addition, the importance of maintaining the Pt and Ba phases in close proximity for efficient LNT desulfation has been demonstrated. It is evident that when Pt and Ba are

physically separated, the desulfation temperature of the surface BaSO<sub>4</sub> is shifted by 20-40 °C towards higher temperature, i.e., towards the position characteristic of bulk BaSO<sub>4</sub>. This observation is consistent with the idea that decomposition of surface BaSO<sub>4</sub> is facilitated by H ad-atoms which spill over from the Pt sites onto the sulfated Ba phase. Physical separation of the Pt and Ba phases appears to inhibit this process, with the consequence that the surface BaSO<sub>4</sub> behaves more like bulk BaSO<sub>4</sub> with respect to its desulfation properties. This finding is analogous to the results of nitrate decomposition studied on physical mixtures of Pt/Al<sub>2</sub>O<sub>3</sub> and BaO/Al<sub>2</sub>O<sub>3</sub> [37].

From the monolith studies, it was found that relative to a sample containing no ceria, samples containing La-stabilized CeO<sub>2</sub> or CeO<sub>2</sub>-ZrO<sub>2</sub> showed: 1) a greater resistance to deactivation during sulfation (as reflected by the NO<sub>x</sub> storage efficiency), and 2) required lower temperatures to restore the NO<sub>x</sub> storage efficiency to its pre-sulfation value. Additionally, the CeO<sub>2</sub> containing catalysts (series 1) released greater fractions of stored sulfur during desulfation. In addition to the ability of ceria to store sulfur and release it at relatively low temperatures under reducing conditions, these results can be attributed to the high water-gas shift activity displayed Pt/CeO<sub>2</sub>, which result in increased intra-catalysts concentrations of H<sub>2</sub> under rich conditions. The results also showed that precious metal loadings can significantly impact desulfation efficiency and that both high Rh and Pt loadings are beneficial for catalyst desulfation.

### 3.5. References.

- [1] J. Theis, J. Ura, C. Goralski, H. Jen, E. Thanasiu, Y. Graves, A. Takami, H. Yamada, S. Miyoshi, The Effect of Ceria Content on the Performance of a NO<sub>x</sub> Trap. SAE Technical Paper Series 2003-01-1160.
- [2] V.I. Parvulescu, G. Grange, B. Delom, Catalytic Removal of NO. *Catalysis Today* 46 (1998) 233-317.
- [3] L. Lietti, P. Forzatti, I. Nova, E. Tronconi, NO<sub>x</sub> Storage Reduction Over Pt-Ba/γ-Al<sub>2</sub>O<sub>3</sub> Catalyst. *Journal of Catalysis* 204 (2001) 175-191.
- [4] S. Elbouazzaoui, E.C. Corbos, X. Courtois, P. Marecot, D. Duprez, A Study of the Deactivation by Sulfur and Regeneration of a Model NSR Pt/Ba/Al<sub>2</sub>O<sub>3</sub> Catalyst. *Applied Catalysis B: Environmental* 61 (2005) 236-243.
- [5] B.-H. Jang, T.-H. Yeon, H.-S. Han, Y.-K. Park, J.-E. Yie, Deterioration Mode of Barium-Containing NO<sub>x</sub> Storage Catalyst. *Catalysis Letters* 77 (2001) 21-28.
- [6] D. Kim, Y. Chin, J. Kwak, J. Szanyi, C.H.F. Peden. Changes in Ba Phases in BaO/Al<sub>2</sub>O<sub>3</sub> Upon Thermal Aging and H<sub>2</sub>O Treatment. *105 Catalysis Letters* (2005) 259-268.
- [7] M. Casapu, J. Grunwaldt, M. Maciejewski, M. Wittrock, U. Göbel, A. Baiker, Formation and Stability of Barium Aluminate and Cerate in NO<sub>x</sub> Storage-Reduction Catalysts. *Applied Catalysis B: Environmental* 63 (2006) 232-242.
- [8] M. Casapu, J. Grunwaldt, M. Maciejewski, A. Baiker, M. Wittrock, U. Göbel, S. Eckhoff, Thermal Aging Phenomena and Strategies Towards Reactivation of NO<sub>x</sub>-Storage Catalysts. *Topics in Catalysis* 42-43 (2007) 3-7.

- [9] S. Matsumoto, Catalytic Reduction of Nitrogen Oxides In Automotive Exhaust Containing Excess Oxygen and NO<sub>x</sub> Storage-Reduction Catalyst. CATTECH 4 (2000) 102-109.
- [10] G. Graham, H. Jen, W. Chun, H. Sun, X. Pan, R. McCabe, Coarsening of Pt Particles in a Model NO<sub>x</sub> Trap. Catalysis Letters. 93 (2004) 129-134.
- [11] S. Elbouazzaoui, X. Courtois, P. Marecot, D. Duprez, Characterization by TPR, XRD, and NO<sub>x</sub> Storage Capacity Measurements of the Aging by Thermal Treatment and SO<sub>2</sub> Poisoning of a Pt/Ba/Al NO<sub>x</sub>-trap Model Catalyst. Topics in Catalysis. 30/31 (2004) 493-496.
- [12] N. Fekete, R. Kemmler, D. Voigtländer, B. Krutzsch, E. Zimmer, G. Wenninger, W. Strehlau, J. van den Tilaart, J. Leyrer, E. Lox, W. Müller, Evaluation of NO<sub>x</sub> Storage Catalysts for Lean Burn Gasoline Fueled Passenger Cars. SAE Technical Paper Series 970746 (1997).
- [13] D. Kim, Y. Chin, G. Muntean, A. Yereretz, N. Currier, W. Epling, H. Chen, H. Hess, C.H.F Peden, Relationship of Pt Particle Size to the NO<sub>x</sub> Storage Performance of Thermally Aged Pt/BaO/Al<sub>2</sub>O<sub>3</sub> Lean NO<sub>x</sub> Trap Catalysts. Industrial & Engineering Chemistry Research 45 (2006) 8815-8821.
- [14] M.A. Peralta, V.G. Milt, L.M. Cornaglia, C.A. Querini, Stability of Ba,K/CeO<sub>2</sub> Catalyst During Diesel Soot Combustion: Effect of Temperature, Water, and Sulfur Dioxide. Journal of Catalysis 242 (2006) 118-130.
- [15] E. Corbos, X. Courtois, N. Bion, P. Marecot, D. Duprez, Impact of the Support Oxide and Ba Loading on the Sulfur Resistance and Regeneration of Pt/Ba/Support Catalysts. Applied Catalysis B: Environmental 80 (2008) 62-71.

- [16] J. Kwak, D. Kim, J. Szanyi, C.H.F. Peden, , Excellent Sulfur Resistance of Pt/BaO/CeO<sub>2</sub> Lean NO<sub>x</sub> Trap Catalysts. *Applied Catalysis B: Environmental* 84 (2008) 545-551.
- [17] Y. Ji, T.J. Topps, M. Crocker, Effect of Ceria on the Sulfation and Desulfation Characteristics of a Model Lean NO<sub>x</sub> Catalyst. *Catalysis Letters*. 127 (2009) 55-62.
- [18] P. Eastwood. *Critical Topics in Exhaust Gas Aftertreatment*, Research Studies Press, Ltd., Baldock, Hertfordshire, England, 2000, p. 231.
- [19] Y. Ji, T.J. Toops, M. Crocker, Effect of Ceria on the Storage and Regeneration Behavior of a Model Lean NO<sub>x</sub> Trap Catalyst. *Catalysis Letters* 119 (2007) 257-264.
- [20] K. Adams, G. Graham, Impact of Redox Conditions on Thermal Deactivation of NO<sub>x</sub> Traps for Diesel. *Applied Catalysis B: Environmental* 80 (2008) 343-352.
- [21] Y. Ji, J.S. Choi, T.J. Toops, M. Crocker, M. Naseri, Influence of Ceria on the NO<sub>x</sub> Storage/Reduction Behavior of Lean NO<sub>x</sub> Trap Catalysts. *Catalysis Today* 136 (2008) 146-155.
- [22] G. Jacobs, L. Williams, U. Graham, D. Sparks, B. Davis, Low Temperature Water-Gas Shift: In Situ DRIFTS-Reaction Study of Ceria Surface Area on the Evolution of Formates on Pt/CeO<sub>2</sub> Processing Catalysts for Fuel Cell Applications. *Applied Catalysis, A: General* 252 (2003) 107-118.
- [23] A. Phatak, N. Koryabkina, S. Rai, J.L. Ratts, W. Ruettinger, R.J. Farrauto, G.E. Blau, W.N. Deglass, F.H. Ribeiro, Kinetics of the Water-Gas Shift Reaction on Pt Catalysts Supported on Alumina and Ceria. *Catalysis Today* 123 (2007) 224-234.

- [24] S. Poulston, R. Rajaram, Regeneration of NO<sub>x</sub> Trap Catalysts. *Catalysis Today* 81 (2003) 603-610.
- [25] Z. Liu, J. Anderson, Influence of Reductant on the Thermal Stability of Stored NO<sub>x</sub> in Pt/BaO/Al<sub>2</sub>O<sub>3</sub> NO<sub>x</sub> Storage and Reduction Traps. *Journal of Catalysis* 224 (2004) 18-27.
- [26] P. Jozsa, E. Jobson, M. Larsson, Reduction of NO<sub>x</sub> Stored at Low Temperatures on a NO<sub>x</sub> Adsorbing Catalyst. *Topics in Catalysis*. 30-31 (2004) 177-180.
- [27] T. Szailer, J. Kwak, D. Kim, J. Hanson, C. Peden, J. Szanyi, Reduction of Stored NO<sub>x</sub> on Pt/Al<sub>2</sub>O<sub>3</sub> and Pt/BaO/Al<sub>2</sub>O<sub>3</sub> Catalysts with H<sub>2</sub> and CO. *Journal of Catalysis* 239 (2006) 51-64.
- [28] Y. Ji, T.J. Toops, J.A. Pihl, M. Crocker, NO<sub>x</sub> Storage and Reduction in Model Lean NO<sub>x</sub> Trap Catalysts Studied by in situ DRIFTS. *Applied Catalysis B: Environmental* 91 (2009) 329-338.
- [29] H. Mahzoul, J. Brilhac, B. Stanmore, Reduction of NO<sub>x</sub> over a NO<sub>x</sub>-Trap Catalyst and the Regeneration Behaviour of Adsorbed SO<sub>2</sub>. *Topics in Catalysis*. 16/17 (2001) 293-298.
- [30] Z. Liu, J. Anderson, Influence of Reductant on the Regeneration of SO<sub>2</sub>-Poisoned Pt/BaO/Al<sub>2</sub>O<sub>3</sub> NO<sub>x</sub> Storage and Reduction Catalyst. *Journal of Catalysis* 228 (2004) 243-253.
- [31] X. Wei, X. Liu, M. Deeba, Characterization of Sulfated BaO-Based NO<sub>x</sub> Trap. *Applied Catalysis B: Environmental* 58 (2005) 41-49.

- [32] P. Bazin, O. Saur, J. Lavalley, G. Blanchard, V. Visciglio, O. Touret, Influence of Platinum on Ceria. *Applied Catalysis B: Environmental* 13 (1997) 265-274.
- [33] P. Bazin, O. Saur, F.C. Meunier, M. Daturi, J.C. Lavalley, A.M. Le Govic, V. Harlé, G. Blanchard, A Thermogravimetric and FT-IR Study of the Reduction by H<sub>2</sub> of sulfated Pt/Ce<sub>x</sub>Zr<sub>1-x</sub>O<sub>2</sub> Solids. *Applied Catalysis B* 90 (2009) 368-379.
- [34] M. Waqif, P. Bazin, O. Saur, J. Lavalley, G. Blanchard, O. Touret, Study of Ceria Sulfation. *Appl. Catal. B* 11 (1997) 193.
- [35] A. Stakheev, P. Gabrielsson, I. Gekas, N. Teleguina, G. Bragina, N. Tolkachev, G. Baeva, Combined XPS and TPR Study of Sulfur Removal from a Pt/BaO/Al<sub>2</sub>O<sub>3</sub> NO<sub>x</sub> Storage Reduction Catalyst. *Topics in Catalysis* 42-43 (2007) 143-147.
- [36] C. Sedlmair, K. Seshan, A. Jentys, J.A. Lercher, Studies on the Deactivation of NO<sub>x</sub> Storage-Reduction Catalysts by Sulfur Dioxide. *Catalysis Today* 75 (2002) 413-419.
- [37] I. Nova, L. Lietti, L. Castoldi, E. Tronconi, P. Forzatti, New Insights in the NO<sub>x</sub> Reduction Mechanism with H<sub>2</sub> over Pt–Ba/γ-Al<sub>2</sub>O<sub>3</sub> Lean NO<sub>x</sub> Trap Catalysts under Near-Isothermal Conditions. *Journal of Catalysis*. 239 (2006) 244-254.
- [38] E. Rohart, V. Bellière-Baca, K. Yokota, Harlé, C. Pitois, Rare Earth Based Oxides as Alternative Materials to Ba in NO<sub>x</sub>-trap catalysts. *Topics in Catalysis* 42-43 (2007) 71-75.
- [39] Y. Ji, C. Fisk, V. Easterling, U. Graham, A. Poole, M. Crocker, J.-S. Choi, W. Partridge, K. Wilson, NO<sub>x</sub> Storage-Reduction Characteristics of Ba-Based Lean NO<sub>x</sub> Trap Catalysts Subjected to Simulated Road Aging. *Catalysis Today* 151 (2010) 362-375.

- [40] A. Ambertsson, M. Skoglundh, S. Ljungström, E. Fridell, Sulfur Deactivation of NO<sub>x</sub> Storage Catalysts: Influence of Exposure Conditions and Noble Metal. *Journal of Catalysis*. 217 (2003) 253-263.
- [41] A. Ambertsson, E. Fridell, M. Skoglundh, Influence of Platinum and Rhodium Composition on the NO<sub>x</sub> Storage and Sulphur Tolerance of a Barium Based NO<sub>x</sub> Storage Catalyst. *Applied Catalysis B: Environmental* 46 (2003) 429-439.
- [42] C. Sedlmair, K. Seshan, A. Jentys, J.A. Lercher, Formation of Sulfur Surface Species on a Commercial NO<sub>x</sub>-Storage Reduction Catalyst. *Research on Chemical Intermediates* 29 (2003) 257-269.
- [43] H. Mahzoul, J.F. Brilhac, P. Gilot, Experimental and mechanistic study of NO<sub>x</sub> adsorption over NO<sub>x</sub> trap catalysts. *Applied Catalysis B: Environmental* 20 (1999) 47-55.



## **Chapter 4. Effect of Aging on the NO<sub>x</sub> Storage and Regeneration Characteristics of Fully Formulated Lean NO<sub>x</sub> Trap Catalysts.**

Disclaimer: The work provided in this chapter is the result of collaboration with Dr. Yaying Ji of the Center for Applied Energy Research at the University of Kentucky. Dr. Ji was responsible the material characterization of the catalysts used in this chapter. This information is described in sections 4.2.3. through 4.3.1.

**Note** - This chapter was published as an article in the following journal:

Y. Ji, V. Easterling, U. Graham, C. Fisk, M. Crocker, J.-S. Choi, Effect of Aging on the NO<sub>x</sub> Storage and Regeneration Characteristics of Fully Formulated Lean NO<sub>x</sub> Trap Catalysts. *Applied Catalysis B: Environmental* 103 (2011) 413-427.

The article appears in this dissertation with permission from the publisher.

### *4.1. Introduction.*

Lean NO<sub>x</sub> traps (LNTs), also known as NO<sub>x</sub> storage-reduction (NSR) catalysts, represent a promising technology for the abatement of NO<sub>x</sub> emissions from lean burn gasoline and diesel engines. LNT catalysts typically comprise precious metals (generally Pt and Rh) and an alkali or alkaline earth metal storage component (most commonly BaO) supported on a high surface area metal oxide such as  $\gamma$ -Al<sub>2</sub>O<sub>3</sub> [1]. LNT catalysts require cyclic operation between lean and rich conditions. Under lean conditions, NO is first oxidized to NO<sub>2</sub> over the precious metal, which is followed by NO<sub>x</sub> storage on the storage component as nitrates and nitrites. Stored NO<sub>x</sub> species are subsequently released and reduced to N<sub>2</sub> after switching to rich (i.e., net reducing) conditions. The trapping ability of the LNT catalysts is thus restored after a lean-rich cycle [2]. Although LNTs have been commercialized for some applications, the durability of LNT catalysts still remains problematic. Sulfur poisoning and thermal aging are recognized as two major causes of deactivation. The BaO NO<sub>x</sub> storage component of a LNT catalyst has a greater affinity for SO<sub>3</sub> than for NO<sub>2</sub>, and the resulting sulfate cannot be removed under typical rich

purging conditions as for nitrates; hence sulfur accumulates on the catalyst and blocks the Ba sites with respect to further NO<sub>x</sub> storage [3-9]. Desulfation requires high temperature treatment under rich conditions [10-14], and such treatments give rise to deactivation mechanisms such as precious metal sintering, total surface area loss, and solid state reactions between the various oxides present in the washcoat.

The presence of Pt in LNT catalysts is required not only to facilitate NO<sub>x</sub> storage through spillover of NO<sub>2</sub> from Pt to the Ba phase (subsequent to NO oxidation on Pt), but also to facilitate NO<sub>x</sub> reduction during rich purging. Both functions are related to the proximity between the Pt and Ba phases, and both can be significantly deteriorated by Pt sintering which results in decreased interaction between the two phases. An early study by Mahzoul et al. [15] showed that only the Pt sites close to BaO crystallites are responsible for nitrate formation (i.e., NO<sub>x</sub> storage), although other Pt sites can act as centers for the oxidation of NO. Nova et al. [16] studied the role of the Pt-Ba interaction in the regeneration behavior of LNTs. A comparison between Pt/BaO/Al<sub>2</sub>O<sub>3</sub> and a Pt/Al<sub>2</sub>O<sub>3</sub>-BaO/Al<sub>2</sub>O<sub>3</sub> physical mixture showed that the promoting effect of Pt on the rate of nitrate reduction required Pt and Ba dispersed on the same support, this being in line with the role of the Pt-Ba interface in nitrate decomposition suggested by Coronado et al. [17] and the involvement of NO<sub>x</sub> spillover from Ba to its nearest Pt sites suggested by Olsson et al. [18]. Similarly, Cant and co-workers [19] inferred the occurrence of forward and reverse spillover of NO<sub>x</sub> during exchange between gaseous <sup>15</sup>NO and stored NO<sub>x</sub>, these processes being five times faster when Pt and BaO were located on the same support.

In another study, Büchel et al. examined the influence of Pt location – on BaCO<sub>3</sub> or Al<sub>2</sub>O<sub>3</sub> – for Pt/Ba/Al<sub>2</sub>O<sub>3</sub> catalysts prepared by flame spray pyrolysis [20]. The benefit of a close interaction between Pt and Ba was confirmed for NO<sub>x</sub> storage, although Pt on Al<sub>2</sub>O<sub>3</sub> exhibited better NO oxidation activity which was limiting for NO<sub>x</sub> storage at low temperatures. During NO<sub>x</sub> reduction, Pt on Ba showed superior activity to Pt on Al<sub>2</sub>O<sub>3</sub>, which was attributed to the importance of reverse spillover and the promotional effect of Ba on the Pt reduction activity. A recent TAP reactor study by Kumar et al. has provided further evidence of the role of spillover processes and the importance of the Pt/Ba

interface during NO<sub>x</sub> storage and reduction [21]. Their data suggests that NO<sub>x</sub> storage proceeds radially outward from the Pt sites and that the stored NO<sub>x</sub> possesses some degree of mobility. In essence, Pt acts as a conduit for spillover to and from the Ba phase, in addition to playing a key role in catalyzing the NO oxidation and reduction reactions themselves. In another recent study [22] concerned with fast NO<sub>x</sub> storage on Pt/BaO/Al<sub>2</sub>O<sub>3</sub> (that is, the initial phase of storage when there is essentially no NO<sub>x</sub> slip from the LNT), it was concluded that the Pt-Ba interface plays a key role, associated with the spillover of dissociated oxygen atoms from Pt to Ba which participate in the adsorption of NO and NO<sub>2</sub> on the Ba sites via nitrite and nitrate formation. In summary, therefore, close proximity of Pt and Ba is required to achieve both efficient NO<sub>x</sub> storage and NO<sub>x</sub> reduction during lean-rich cycling.

Pt sintering mainly occurs under oxidizing conditions during thermal aging. Graham et al. compared the behavior of Pt under both reducing and oxidizing conditions [23], and found that the most significant Pt particle growth occurred under oxidizing conditions. A recent study by Datye and co-workers supports the notion that Pt sintering in air results from the formation of volatile Pt oxide, PtO<sub>x</sub>, leading to enhanced interparticle transport and sintering via Ostwald ripening [24]. However, sintering was significantly inhibited in reducing atmospheres, probably due to the low vapor pressure of metallic Pt; consequently, particle migration and coalescence was suggested to be the major mechanism of Pt sintering under reducing conditions. Pt sintering has a permanent impact on catalyst performance due to its irreversibility and consequently it has been recognized as a key issue associated with thermal deactivation. Indeed, a number of studies have provided evidence that Pt sintering can result in decreased interaction between the Pt and Ba phases (i.e., phase segregation) which in turn leads to degraded NO<sub>x</sub> storage and regeneration behavior [25-31]. Fekete et al. [25] attributed the observed decrease in NO<sub>x</sub> storage capacity after aging to loss of contact between the precious metals and the storage material, in addition to the formation of mixed metal oxides from unwanted side reactions between the storage material and the support. It was suggested that the diminished contact leads to a reduced spillover rate of NO<sub>2</sub> from the precious metal to the adsorbent, thereby decreasing NO<sub>x</sub> storage efficiency. Uy et al. [26]

characterized fresh and aged Pt/Ba/Al<sub>2</sub>O<sub>3</sub> catalysts using in situ UV and visible Raman spectroscopy and found evidence for Ba particles “separating from” or behaving independently from the Pt/Al<sub>2</sub>O<sub>3</sub> in aged Pt/Ba/Al<sub>2</sub>O<sub>3</sub>.

Unwanted side reactions between Ba and the support is another effect associated with thermal aging, resulting in the formation of Ba aluminate, zirconate, cerate, etc., as applicable [31-39]. From studies with Pt-Ba/Al<sub>2</sub>O<sub>3</sub> catalysts, Jang et al. [31] emphasized the importance of Ba-Al mixed oxide formation as a cause of degraded NO<sub>x</sub> storage capacity. Upon heating Pt-Ba/Al<sub>2</sub>O<sub>3</sub> from 550 to 850 °C, they observed the gradual conversion of Ba/Al<sub>2</sub>O<sub>3</sub> to BaAl<sub>2</sub>O<sub>4</sub>. Several other authors have similarly found that BaAl<sub>2</sub>O<sub>4</sub> forms at about 850 °C [33-35] and concluded that the formation of such mixed oxides is a significant factor in thermal deactivation. However, recent studies have shown that the formation of BaAl<sub>2</sub>O<sub>4</sub> and BaCeO<sub>3</sub> is largely reversible in nature [34-39]. For example, Casapu et al. [34] studied LNT catalysts that contain CeO<sub>2</sub> as a support material and observed the formation of BaCeO<sub>3</sub> at 800 °C. Decomposition of BaCeO<sub>3</sub> was found to occur at 300-500 °C in the presence of NO<sub>2</sub>/H<sub>2</sub>O or CO<sub>2</sub> [34,35], resulting in an improvement in NO<sub>x</sub> storage capacity. Another recent report indicates that BaCeO<sub>3</sub> formation is inhibited in the presence of CO<sub>2</sub> at a concentration as low as 5% [39]. In comparison, BaAl<sub>2</sub>O<sub>4</sub> is much more stable under typical operating conditions but can be converted to BaCO<sub>3</sub> and Al<sub>2</sub>O<sub>3</sub> at room temperature in the presence of liquid water [36,37].

In a previous paper [40], we reported the results of a study into the effect of catalyst ceria content and type (La-stabilized CeO<sub>2</sub> or CeO<sub>2</sub>-ZrO<sub>2</sub>) on LNT aging characteristics. Two main causes of LNT aging were discerned, corresponding to (i) sintering of the precious metals present and (ii) the accumulation of sulfur in the washcoat as BaSO<sub>4</sub>. In addition, spectacular improvement in LNT durability was observed for catalysts containing CeO<sub>2</sub> or CeO<sub>2</sub>-ZrO<sub>2</sub> relative to a non-ceria containing analog. This was attributed to the ability of ceria to participate in NO<sub>x</sub> storage/reduction as a supplement to the main Ba NO<sub>x</sub> storage component, the fact that Pt and the CeO<sub>2</sub>(-ZrO<sub>2</sub>) support remain in intimate contact, and the ability of ceria to trap sulfur, resulting in decreased sulfur accumulation

on the Ba component. In this chapter, we report the results of a study aimed at investigating the effects of precious metal (Pt, Rh) loading and BaO loading on catalyst durability.

## 4.2. Experimental.

### 4.2.1. Catalyst Preparation.

Four fully formulated Ba-based LNT catalysts were used in this study, the compositions of which are shown in Table 4.1. Details of the catalyst preparation have been described elsewhere [41]. Briefly, the powders for washcoating were prepared using the incipient wetness method. Three different powders were required to prepare the washcoat. First, Pt-Rh/Al<sub>2</sub>O<sub>3</sub> powder was prepared by co-impregnating 3 wt% La<sub>2</sub>O<sub>3</sub>-stabilized  $\gamma$ -alumina (Sasol Puralox SCFa-140 L3, BET surface area of 140 m<sup>2</sup>/g) with an aqueous solution of Pt(NH<sub>3</sub>)<sub>4</sub>(OH)<sub>2</sub> and Rh(NO<sub>3</sub>)<sub>3</sub>, followed by calcination at 500 °C for 2 h. Second, BaO/Al<sub>2</sub>O<sub>3</sub> powder was prepared by impregnating  $\gamma$ -alumina (Sasol Puralox SCFa-140 L3) with aqueous Ba(O<sub>2</sub>CCH<sub>3</sub>)<sub>2</sub>, followed by calcination at 500 °C for 2 h to give a powder containing either 21.5 wt% or 32 wt% BaO as appropriate (for a final BaO concentration in the catalyst of 30 or 45 g/L, respectively). Subsequently, the BaO/Al<sub>2</sub>O<sub>3</sub> material was ball milled with La-stabilized CeO<sub>2</sub> (Advanced Material Resources, BET surface area of 119 m<sup>2</sup>/g) in a weight ratio of 140:50, after which the physical mixture was impregnated with aqueous Pt(NH<sub>3</sub>)<sub>4</sub>(OH)<sub>2</sub> to achieve the total Pt loading required in the washcoat. To prepare the washcoat, 30 g/L of the Pt-Rh/Al<sub>2</sub>O<sub>3</sub> powder was slurried in deionized water with 190 g/L of the Pt/[BaO/Al<sub>2</sub>O<sub>3</sub> + CeO<sub>2</sub>] mixture to which  $\gamma$ -alumina powder (34 g/L) was added as balance to achieve a nominal washcoat loading of 260 g/L. Additionally, a small amount of boehmite sol (6 g/L) was added to the washcoat as a binder during preparation of the slurry. As shown in Table 4.1, these four catalysts have the same nominal loadings of CeO<sub>2</sub> (50 g/L) while the BaO, Pt and Rh loadings were varied as indicated. A detailed breakdown of the Pt loadings on the three different types of powder in the catalyst washcoats is given in Table 4.2, while Figure 4.1 provides a schematic representation of the composition and function of the different powders. As shown, Pt/CeO<sub>2</sub> functions as a supplement to the main Pt/BaO/Al<sub>2</sub>O<sub>3</sub> NO<sub>x</sub> storage-reduction component, while the function of the Pt-Rh/Al<sub>2</sub>O<sub>3</sub> component is mainly to

improve NO<sub>x</sub> reduction during rich purging. In all cases, the washcoat was applied to a 4” x 6” cordierite monolith substrate, possessing a cell density of 400 cpsi and a wall thickness of 6.5 mil.

**Table 4.1. Composition of catalysts subjected to simulated road aging.**

Component	Catalyst code / loading <sup>a</sup>			
	Pt-50	Pt-100	30-50	45-50
Pt, g/L (g/cuft)	1.77 (50)	3.53 (100)	3.53 (100)	3.53 (100)
Rh, g/L (g/cuft)	0.35 (10)	0.35 (10)	0.71 (20)	0.71 (20)
BaO, g/L	30	30	30	45
CeO <sub>2</sub> <sup>b</sup> , g/L	50	50	50	50
Al <sub>2</sub> O <sub>3</sub> <sup>c</sup> , g/L	Balance	Balance	Balance	Balance

<sup>a</sup> Nominal loadings. Total washcoat loading = 260 g/L.

<sup>b</sup> Stabilized with 5 wt% La<sub>2</sub>O<sub>3</sub>.

<sup>c</sup> Stabilized with 3 wt% La<sub>2</sub>O<sub>3</sub>.

**Table 4.2. Nominal Pt loading in the three different powders used for washcoat preparation.**

Catalyst	Nominal Pt loading in powder (g/L)			
	Total	Pt-Rh/Al <sub>2</sub> O <sub>3</sub> <sup>a</sup>	Pt/BaO/Al <sub>2</sub> O <sub>3</sub>	Pt/CeO <sub>2</sub>
Pt-50	1.77	0.35	1.05	0.37
Pt-100	3.53	0.35	2.34	0.84
30-50	3.53	0.71	2.08	0.74
45-50	3.53	0.71	2.08	0.74

<sup>a</sup> Rh loading same as for Pt loading.

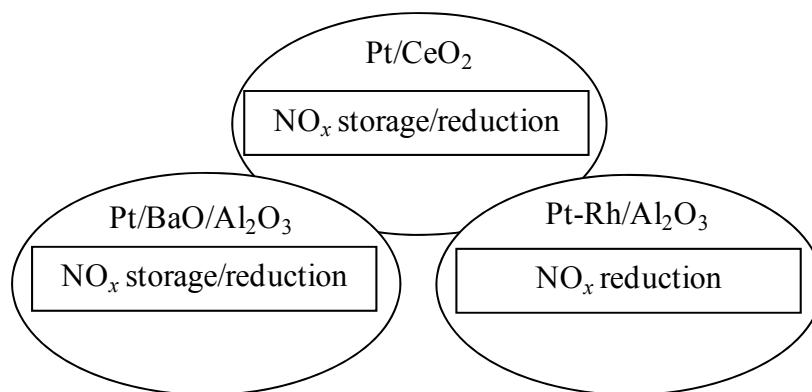


**Figure 4.1. Schematic showing the functions of the three different powders contained in the prepared catalysts. In addition, alumina powder was added to the washcoat as a balance.**

#### 4.2.2. Aging Protocol.

Catalyst aging was performed on a synthetic gas bench using cores (2.1 cm diameter x 7.4 cm long) drilled out from the LNT monoliths. The protocol used for the rapid aging has been detailed in earlier publications [40,42]. This method is designed to simulate the road aging of a LNT catalyst used in conjunction with a diesel particulate filter (DPF). Each aging cycle is composed of three modes: sulfation, desulfation, and simulated DPF regeneration, the corresponding gas compositions used being shown in Table 4.3.

Sulfation was carried out under cycling conditions (60s lean/5s rich) at 300 °C to give an equivalent sulfur loading of 1.0 g/L (assuming complete uptake of sulfur). Desulfation was performed under cycling conditions (5 s lean/15 s rich) at 700 °C for 10 min, after which the catalyst was held under lean conditions at 650 °C for 30 min (to simulate DPF regeneration). A maximum mid-bed catalyst temperature of 770 +/- 10 °C was observed during desulfation due to the exotherm resulting from the fast lean-rich cycling.

Depending on actual fuel sulfur levels, one aging cycle is estimated to be equivalent to 1,000-1,500 miles of road aging. 50 cycles were used for the aging runs, requiring a total aging time of ca. 100 h per sample. At the end of each aging run a final desulfation was performed under constant rich conditions, corresponding to 2% H<sub>2</sub> in the presence of 5% H<sub>2</sub>O and 5% CO<sub>2</sub> at 750 °C for 10 min, in order to remove as much residual sulfur as possible.

**Table 4.3. Gas compositions used for rapid aging, oxygen storage-reduction and NO<sub>x</sub> storage-reduction cycling experiments<sup>a</sup>.**

Parameter	Sulfation During Aging		Desulfation During Aging		Simulated DPF Regeneration During Aging	Oxygen Storage-Reduction Cycling		NO <sub>x</sub> Storage-Reduction Cycling	
	Lean	Rich	Lean	Rich		Lean	Rich	Lean	Rich
Duration, s	60	5	5	15	1800	60	5	60	5
Temperature (°C)	300	300	700	700	300	350	350	150-450	150-450
NO, ppm	300	300	300	300	0	0	0	300	0
SO <sub>2</sub> , ppm	45	45	0	0	0	0	0	0	0
O <sub>2</sub> , %	8	0	8	0	8	10	0	10	0
H <sub>2</sub> , %	0	1.3	0	1.3	0	0	4.2	0	1.575
CO, %	0	4	0	4	0	0	0	0	2.625
H <sub>2</sub> O, %	5	5	5	5	5	5	5	5	5
CO <sub>2</sub> , %	5	5	5	5	5	5	5	5	5
N <sub>2</sub> , %	Balance	Balance	Balance	Balance	Balance	Balance	Balance	Balance	Balance

<sup>a</sup> GHSV = 30,000 h<sup>-1</sup> for all conditions.

#### 4.2.3. Catalyst Evaluation.

Catalyst evaluation was performed on a synthetic gas bench reactor. Catalyst cores were wrapped in Zetex insulation tape and inserted into a horizontal quartz reactor tube (2.2 cm inner diameter). The reactor tube was heated by an electric furnace, and simulated exhaust gas mixtures were introduced from pressurized gas bottles (ultra high purity grade, Air Liquide). The gases were metered with mass flow controllers (Unit Instruments Series 7300, Kinetics Electronics) and pre-heated before entering the quartz reactor. Water was introduced by a peristaltic cartridge pump (Cole-Parmer) to a heated zone, vaporized and added to the simulated exhaust mixture. A rapid switching 4-way valve system was used to alternate between the lean and rich gas mixtures so that the lean/rich/lean transitions in these experiments were almost instantaneous (within 0.2 s). Three K-type thermocouples were placed just before the LNT, at the LNT mid-point and just after the LNT to monitor the temperature profiles. A multi-gas analyzer (MKS Model 2030) was used to monitor NO, NO<sub>2</sub>, N<sub>2</sub>O, NH<sub>3</sub>, CO, CO<sub>2</sub>, H<sub>2</sub>O at the reactor outlet. Determination of intra-catalyst hydrogen concentrations during oxygen storage capacity (OSC) measurements was performed using SpaciMS (Spatially Resolved



Capillary Inlet Mass Spectrometry) [43,44] with a removable capillary probe inserted into the channel of the core sample near the centerline. Activity evaluation and OSC measurements for the catalysts were performed under the conditions given in Table 4.3. During the cycling conditions described in Table 4.3, the observed catalyst breakthrough profiles stabilized to a fixed limit cycle in about 2 h, at which point it was possible to characterize the performance in terms of the ‘stationary’ concentration cycles. The selectivity to N<sub>2</sub> during the rich purge was determined by difference (i.e.,  $S_{N_2} = 100\% - S_{N_2O} - S_{NH_3}$ ). In the case of measurements performed on fresh catalysts, the samples were in all cases first de-greened by exposing them to lean-rich cycling conditions at 500 °C for 5 h.

#### *4.2.4. N<sub>2</sub> Physisorption.*

Surface area and pore volume measurements were performed according to the BET method by nitrogen adsorption at -196 °C using a Micromeritics Tri-Star system. Prior to the measurements catalyst samples (washcoat and monolith) were ground to a fine powder and outgassed overnight at 160 °C under vacuum.

#### *4.2.5. Pulsed H<sub>2</sub> Chemisorption.*

The dispersion of precious metal (Pt+Rh) was determined with a Micromeritics AutoChem II Analyzer by means of pulsed H<sub>2</sub> chemisorption at dry ice temperature (-78 °C). This temperature was chosen in an effort to minimize H spillover from the metal to the support material [45]. Unlike static volumetric methods, the total amount of chemisorbed hydrogen, as opposed to irreversibly chemisorbed hydrogen, was used to determine the metal dispersion in this study. 1 g of sample (as a fine powder), including both washcoat and substrate, was loaded into the reactor. After being oxidized at 400 °C in 10% O<sub>2</sub>/He for 15 min, followed by reduction at 300 °C in 10% H<sub>2</sub>/Ar for 15 min, the catalyst was heated up to 400 °C (hold time 10 min) in flowing Ar to remove adsorbed H. Pulsed H<sub>2</sub> chemisorption was initiated using a four-way valve after the catalyst had been cooled to -78 °C. During this measurement, 0.5 ml of 10 % H<sub>2</sub>/Ar was pulsed into the reactor every 2 min, the H<sub>2</sub> signal at the reactor outlet being monitored with a thermal conductivity detector (TCD). H<sub>2</sub> pulsing was terminated after the TCD signal had

reached a constant value, i.e., the total precious metal (Pt+Rh) sites were saturated with H<sub>2</sub>. Assuming a 1:1 ratio of atomic hydrogen to surface Pt or Rh, the metal dispersion was calculated based on the amount of H adsorbed.

#### *4.2.6. HRTEM-EELS.*

Electron microscopy studies (EM) were performed using a JEOL 2010F STEM outfitted with a URP pole piece, GATAN 2000 GIF, GATAN DigiScan II, Fischione HAADF STEM detector, and EmiSpec EsVision software. STEM images were acquired using the high resolution probe at 2 Å. EELS spectrum imaging was performed using the 1 nm probe, an alpha of 30 mrad, and a beta of 6 mrad. Materials for the EM analysis were powdered samples and minute amounts were supported on copper grids.

#### *4.2.7. Postmortem Sulfur Analysis.*

The amount of residual sulfur in the aged catalysts was measured by detecting the SO<sub>2</sub> evolved during heating of the ground catalyst sample to 1425 °C, using an ELTRA CS 500 Carbon Sulfur Determinator. Powder X-ray diffraction (XRD) measurements were performed on a Phillips X'Pert diffractometer using Cu K<sub>α</sub> radiation ( $\lambda = 1.5406 \text{ \AA}$ ) and a step size of 0.02°.

### *4.3. Results and Discussion.*

#### *4.3.1. Characterization.*

Physical data for the fresh and aged catalysts used in this study are listed in Table 4.4. From these data it is evident that aging resulted in a decrease in washcoat BET surface area. The decreased pore volumes and increased pore radii of the aged catalysts infer the collapse of some of the smaller pores after aging. This deterioration can be ascribed mainly to sintering of the CeO<sub>2</sub> component of the washcoat. Sintering of CeO<sub>2</sub> is unavoidable under the aging conditions used in this study, albeit that the CeO<sub>2</sub> used was stabilized by La<sub>2</sub>O<sub>3</sub>. Indeed, in our previous study [40] ceria-containing catalysts (including catalyst 30-50 used in the present study) were found to undergo a more pronounced decrease in BET surface area compared to a ceria-free analog. It is also worth noting that relative to the other three catalysts, catalyst 45-50 displayed lower BET surface area and pore volume in both the fresh and aged states relative to 30-50, which

can be ascribed to increased blockage of the pores in the alumina support at the higher BaO loading.

In principle, aggregation of the Ba phase might occur during aging as a consequence of its high mobility in the presence of water [39]. Unfortunately, the BaCO<sub>3</sub> peaks in the X-ray diffractograms of the fresh and aged catalyst were too weak (due to sample dilution by the cordierite substrate) to permit determination of the average BaCO<sub>3</sub> particle size. However, TEM data obtained for catalyst 45-50 (see below) support the idea that migration and aggregation of the Ba phase does indeed occur upon aging.

Consistent with our previous study [40], loss of platinum group metal (PGM) surface area represented the most significant impact of aging. As shown in Table 4.4, the overall PGM dispersion decreased by 62-82% (relative) after aging regardless of the Ba and PGM loading. In addition to precious metal sintering, the loss of PGM surface area after aging can be attributed to the sintering of the support materials, which can result in encapsulation of the PGM [46,47]. While sintering of the La-stabilized Al<sub>2</sub>O<sub>3</sub> support is negligible at the maximum temperature experienced by the catalysts during aging (770 °C) [48], sintering of the La-stabilized CeO<sub>2</sub> under these conditions is significant, as indicated in our earlier study [40].

**Table 4.4. Physical properties and oxygen storage capacity of fresh and aged catalysts.**

Catalyst	Estimated Washcoat BET		Total BET Surface		Pore Volume		Average Pore Radius		PM Dispersion		Oxygen Storage Capacity	
	SA (m <sup>2</sup> /g) <sup>a</sup>		Area (m <sup>2</sup> /g)		(cm <sup>3</sup> /g)		(nm)		(%)		(mmol/L)	
	Fresh	Aged	Fresh	Aged	Fresh	Aged	Fresh	Aged	Fresh	Aged	Fresh	Aged
Pt-50	119	95	44.8	35.7	0.146	0.132	6.51	7.43	30.1	11.5	19.2	n/a
Pt-100	126	96	51.1	38.9	0.167	0.143	6.52	7.37	48.2	11.2	49.4	31.7
30-50	126	88	47.5	32.7	0.156	0.12	6.56	7.35	51.2	9.2	38.1	26
45-50	120	82	43.7	30	0.134	0.109	6.13	7.28	43.1	12.4	30.1	24.3

<sup>a</sup> Estimate calculated from washcoat loading and surface area of 1 m<sup>2</sup>/g for cordierite substrate.

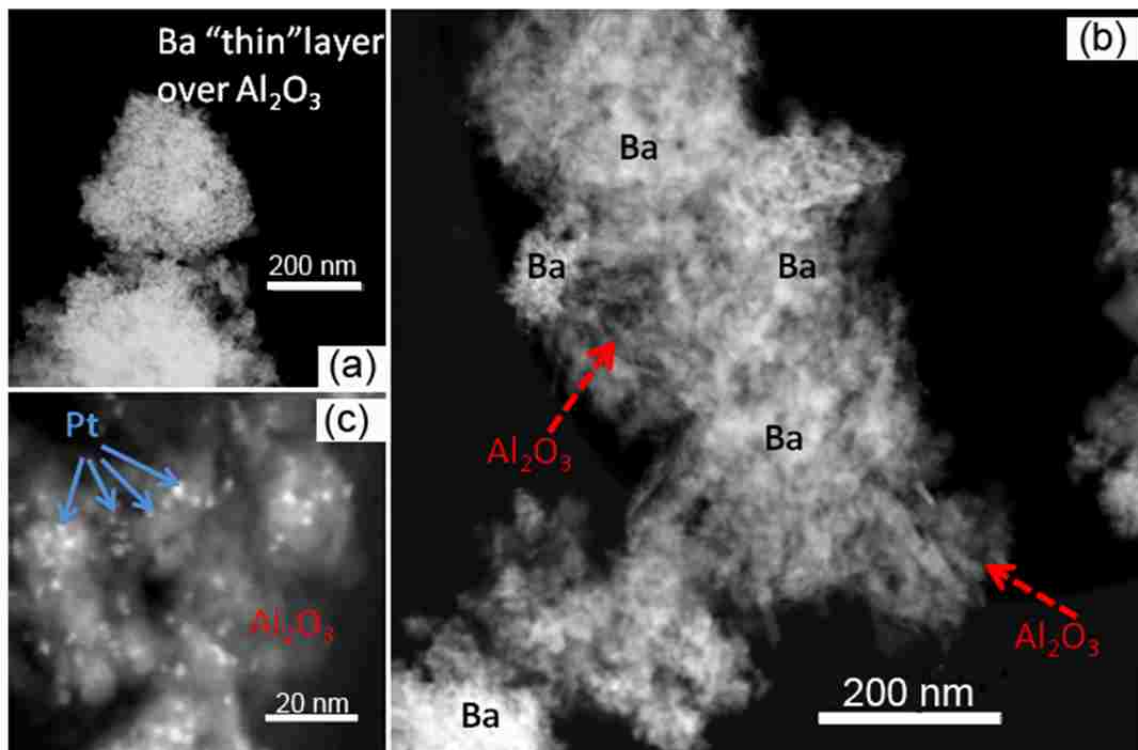
Another effect associated with catalyst aging under simulated road conditions is the accumulation of sulfur in the washcoat. Table 4.5 summarizes the results of sulfur analyses performed on the aged catalysts. Similar sulfur contents were found in the Pt-50, Pt-100 and 30-50 washcoats after aging (0.35 wt% – 0.38 wt%), whereas a sulfur content of 0.7 wt% was measured for 45-50. This result is expected, given that residual sulfur is associated with only the Ba phase in the catalysts (see discussion of TEM results below), i.e., the higher the BaO loading, the higher the residual sulfur concentration. In the case of Pt-50, Pt-100 and 30-50, if it is assumed that all of the sulfur to which the catalysts were exposed during aging was adsorbed during sulfation, then ~95% of the adsorbed sulfur was removed during desulfation (including the final desulfation step at 750 °C). This assumption is consistent with a recent characterization study on a commercial catalyst which also contained PM, Ba, Ce, Al as major washcoat components [49]. Table 4.5 also reports the residual sulfur levels in the catalysts normalized to the Ba loading determined by elemental analysis. From the resulting S:Ba mole ratios, it can be seen that between 28% and 33% of the Ba sites in the catalysts containing 30 g BaO/L were in the sulfated state and were thus unavailable for NO<sub>x</sub> storage (assuming sulfur is located only on the Ba phase after aging), while the same figure for catalyst 45-50 was 43%. In our previous study, residual sulfur in a series of related catalysts was found to be present exclusively as sulfate according to XPS data [40]. In the present work, the presence of crystalline BaSO<sub>4</sub> (JCPDS# 76-2133) was confirmed for aged 45-50 by powder XRD (not shown). No other sulfur species were observed, nor was BaAl<sub>2</sub>O<sub>4</sub>, the latter result being consistent with the fact that the maximum temperature experienced by the catalysts during aging did not exceed 780 °C.

**Table 4.5. Summary of elemental analysis data for aged catalysts.**

Catalyst	Measured Ba in Catalyst (wt%)	Residual Sulfur in Catalyst (wt%)	Residual Sulfur in Washcoat (wt%)	S:Ba Mole Ratio
Pt-50	5.79	0.38	1.02	0.28
Pt-100	4.61	0.35	0.86	0.33
30-50	4.98	0.38	1.02	0.33
45-50	7.75	0.78	2.12	0.43

It is also worth noting that the higher S:Ba ratio observed for catalyst 45-50 relative to the other catalysts is consistent with a previous report that as the BaO loading on an alumina support is increased, the BaO becomes increasingly more difficult to desulfate [50]. This is explained by the fact that as the BaO loading is increased, the amount of bulk BaO increases (as opposed to monolayer BaO) which in turn gives rise to bulk BaSO<sub>4</sub> upon sulfation. Several studies have shown that the decomposition of bulk BaSO<sub>4</sub> - corresponding to large BaSO<sub>4</sub> crystallites and/or Ba sulfate located far away from Pt sites - requires higher temperatures than surface BaSO<sub>4</sub> under typical reducing conditions [13]; indeed, we have previously found that complete decomposition of bulk BaSO<sub>4</sub> under conditions similar to those used in the present study requires temperatures slightly in excess of 750 °C [51]. Consequently, the high loading of BaO in catalyst 45-50 (32 wt% BaO/Al<sub>2</sub>O<sub>3</sub> versus 21.5 wt% BaO/Al<sub>2</sub>O<sub>3</sub> in the other catalysts) results in a higher concentration of bulk BaSO<sub>4</sub> relative to the other catalysts and hence a greater amount of residual sulfate after the final desulfation at 750 °C.

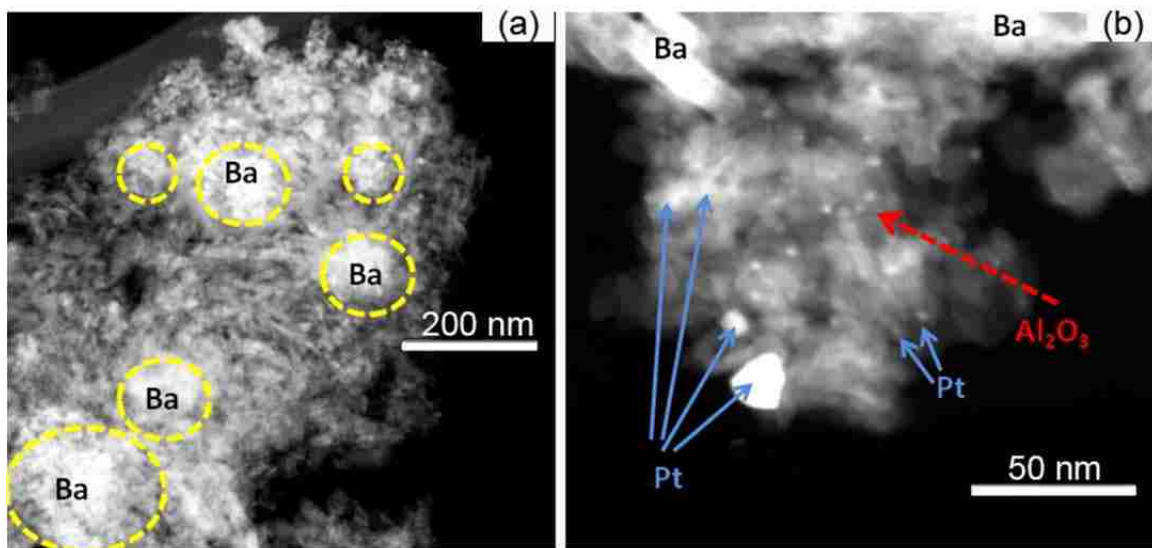
In addition to the foregoing analytical methods, detailed EM studies were performed on catalyst 45-50 in both the fresh and aged states in order to observe the impact of aging. The fresh catalyst is illustrated in Figure 4.2. At low magnification (Fig. 4.2a), the STEM image shows that the Al<sub>2</sub>O<sub>3</sub> support has been coated with a thin BaO layer. At higher magnification in Figure 4.2b, the rod-like morphology of the Al<sub>2</sub>O<sub>3</sub> support can be recognized even after addition of the thin BaO coating. It was also observed that the BaO coating is not covering all areas of the Al<sub>2</sub>O<sub>3</sub> support. No large BaO agglomerates or crystallites were observed in the fresh catalyst as those would otherwise be imaged in STEM mode as bright areas next to Al<sub>2</sub>O<sub>3</sub> due to the major difference in material density.



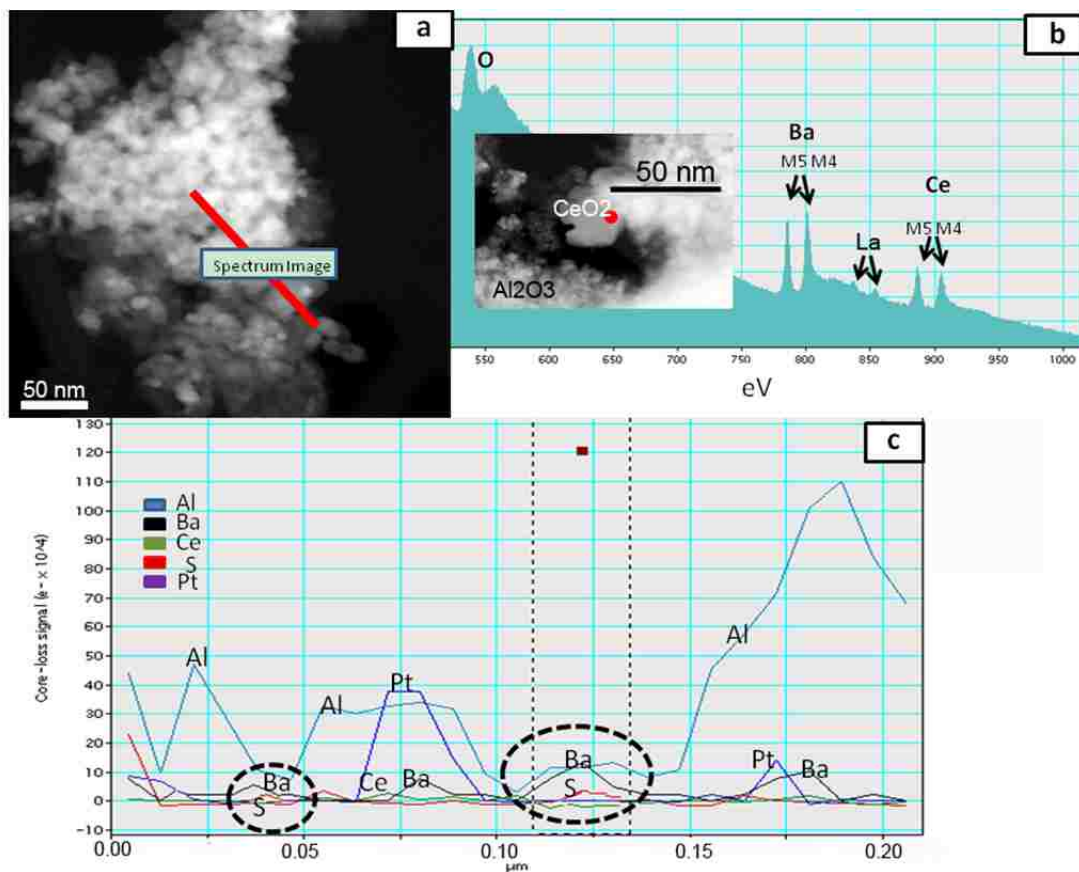
**Figure 4.2(a-c). Illustration of fresh catalyst sample 45-50 using STEM imaging.**

Figure 4.2c illustrates Al<sub>2</sub>O<sub>3</sub> with ultra small Pt nanoparticles on the surface that range in size from 2-8 nm and show excellent dispersion on the support surface. The aged 45-50 catalyst material is depicted in the STEM images in Figure 4.3. The Ba-rich areas now occur in clusters over the Al<sub>2</sub>O<sub>3</sub> support surface and in certain locations have formed coarse crystals. Note that the STEM image does not distinguish between BaO and BaSO<sub>4</sub>. From Figure 4.3a it appears that in the aged catalyst more of the Al<sub>2</sub>O<sub>3</sub> surfaces are exposed without a BaO layer, suggesting a possible migration and aggregation of the BaO phase during thermal treatment. Additionally, Figure 4.3b highlights a magnified area showing the rod-shaped Al<sub>2</sub>O<sub>3</sub> support with Pt nanoparticles on the surface. In comparison with the fresh material, the aged sample is characterized by a significant degree of Pt nanoparticle sintering; indeed, the image shows a Pt particle that is >20nm. Not all of the Pt nanoparticles participate in the sintering process, however, as there is evidence of residual Pt nanoparticles in the original size range of 2-8 nm. Figure 4.3b also illustrates the presence of a dense Ba phase. In the Al<sub>2</sub>O<sub>3</sub>-rich areas the EM study did not reveal any encapsulation of Pt nanoparticles by the support media. Figure 4.4

shows the presence of  $\text{Al}_2\text{O}_3$  and  $\text{CeO}_2$  particles side-by-side in the aged catalyst material. Figure 4.4b has a STEM insert that shows a dense  $\text{CeO}_2$  particle with Pt nanoparticles that do not appear to have undergone such significant sintering as those on the  $\text{Al}_2\text{O}_3$  support. The presence of a Ba-rich phase was also noticed in the vicinity of the  $\text{CeO}_2$  grains using EELS measurements, which is illustrated in Figure 4.4b; this shows the typical M4 M5 peaks for Ba and Ce, as well as a small contribution for the La peaks which are associated with the La-stabilized  $\text{CeO}_2$ . A line-scan spectrum image was collected across the aged catalyst material to observe any special relationship of sulfur in the vicinity of Ba-rich phase that segregated over the catalyst support material. The spectrum image is a compilation of EELS measurements along a particular area or line which is depicted in Figure 4.4a as the red line that spans approximately 250 nm in length across the catalyst. Along this line EELS measurements were performed and the results are plotted in 4.4c, showing the presence and relative concentration of Al, Ba, Ce, S and Pt. It is important to note that sulfur (red line) is typically associated with the Ba-rich phase, suggesting the presence of  $\text{BaSO}_4$ , and also that the line representing Pt indicates that the Pt nanoparticles are in a size-range that suggests Pt sintering took place during aging.



**Figure 4.3. Rod-shaped  $\text{Al}_2\text{O}_3$  crystals in aged 45-50 with local agglomeration of dense Ba-rich phase. (b)  $\text{Al}_2\text{O}_3$  support with large, sintered Pt nanoparticles.**



**Figure 4.4. STEM imaging of aged 45-50 and EELS spectrum imaging. (a) Aged catalyst with area of EELS line scan (red line). (b) STEM insert showing area of (sintered) La-stabilized CeO<sub>2</sub> after aging process. The red spot indicates the area of the EELS measurement shown in (b). (c) Relative elemental concentration obtained during EELS spectrum imaging for the line-scan shown in (a).**

#### 4.3.2. Oxygen Storage Capacity.

Oxygen storage capacity (OSC) was determined under lean-rich cycling conditions at 350 °C. From Table 4.4, catalyst Pt-100 showed the highest OSC among the four catalysts in both the fresh and aged states, while catalyst Pt-50 had the lowest. This finding is evidently related to the Pt loading on the CeO<sub>2</sub> washcoat component. It is well known that CeO<sub>2</sub> is the main oxygen storage component in LNT catalysts and that dynamic oxygen storage under lean-rich cycling conditions is dependent on oxygen mobility [52]. This mobility is promoted by Pt which facilitates O<sub>2</sub> dissociation followed by spillover to CeO<sub>2</sub> during oxygen storage and H<sub>2</sub> dissociation followed by spillover to CeO<sub>2</sub> during



reduction. One means of increasing oxygen mobility is to increase the Pt loading and hence the degree of Pt-CeO<sub>2</sub> contact. From this it follows that catalyst Pt-100, with the highest Pt loading on the CeO<sub>2</sub> washcoat component (Table 4.2), shows the greatest ability to store and reduce oxygen relative to the other catalysts (the actual CeO<sub>2</sub> loading of the catalysts being the same in all cases). All of the catalysts showed a significant decrease in OSC after aging, as evidenced by a drop of 35.8% for aged Pt-100 as compared to the fresh catalyst, which can be explained by the decreased surface area of the CeO<sub>2</sub> phase and by the decreased contact between the Pt and CeO<sub>2</sub> as a result of Pt sintering.

#### *4.3.3. NO<sub>x</sub> Storage.*

NO<sub>x</sub> concentration profiles for both fresh and aged catalysts under “stationary” cycling conditions are shown in Figures 4.5 and 4.6, respectively. Comparatively high lean-phase NO<sub>x</sub> slip was observed at 150 °C and 450 °C relative to the results obtained at 250 °C and 350 °C, regardless of the state of the catalysts. It should be noted that the observation of lean phase NO<sub>2</sub> slip for all of the catalysts at 150 °C implies that NO<sub>x</sub> storage capacity at this temperature was not limited by the kinetics of NO oxidation. While we cannot completely exclude the possibility that the kinetics of nitrate/nitrite formation may be a limiting factor at 150 °C, our previous studies [53] suggest that it is mainly the inability to remove nitrates and nitrites at low temperature during the rich phase regeneration that limits the lean phase NO<sub>x</sub> storage efficiency. At 250 °C and 350 °C fresh Pt-50 showed higher lean-phase NO<sub>x</sub> slip than the other catalysts, indicative of an inferior NO<sub>x</sub> storage function, while almost no lean-phase NO<sub>x</sub> breakthrough was observed for fresh 30-50 and 45-50. Relative to the fresh catalysts, aging in all cases resulted in increased lean-phase NO<sub>x</sub> slip, with earlier breakthrough times in the range 250-450 °C. Evidently, NO<sub>x</sub> storage efficiency (NSE) was deteriorated by aging.

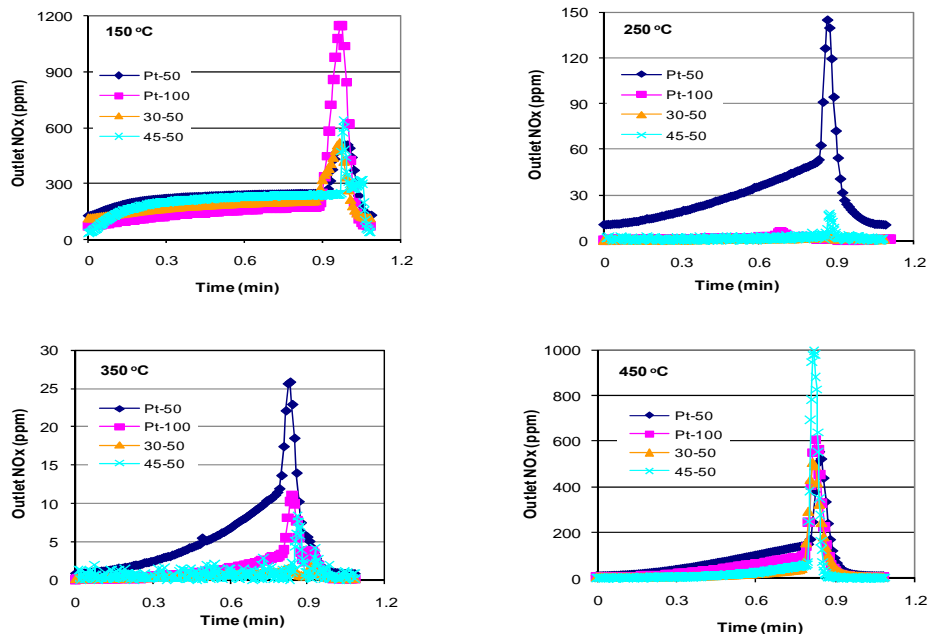


Figure 4.5. NO<sub>x</sub> storage and release during lean-rich cycling for fresh catalysts.

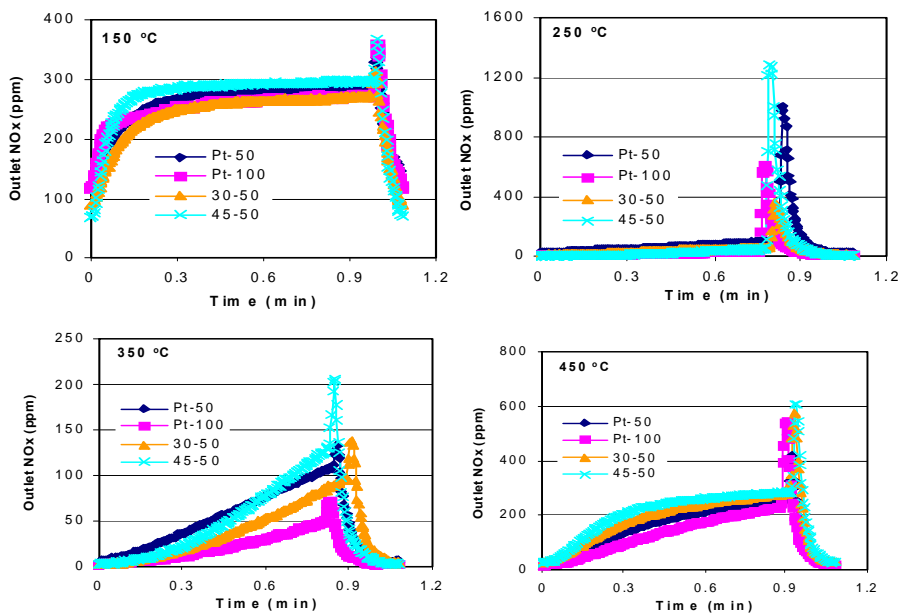


Figure 4.6. NO<sub>x</sub> storage and release during lean-rich cycling for aged catalysts.

From Table 4.6 it is apparent that increased lean-phase NO<sub>2</sub> slip was observed for the aged catalysts relative to the fresh ones, indicating that the deteriorated NO<sub>x</sub> storage function after aging was not due to a limitation in the kinetics of NO oxidation.

Examination of the lean-phase NSE calculated from the lean-rich cycling data reveals that aging caused a decrease in NSE for all the catalysts in the range 150 to 450 °C. As shown in Table 4.6, with the exception of Pt-50, the catalysts showed only small differences in NSE in the range 250-350 °C before aging, while aging enlarged the differences between the catalysts. Pt-100 showed a less pronounced decrease in NSE than 30-50 and 45-50 after aging, as evidenced by a NSE drop of only ~5%. Consequently, Pt-100 was still able to achieve a NSE of 94% at 250 °C and 350 °C after aging.

**Table 4.6. Comparison of NO<sub>x</sub> storage and release during lean-rich cycling.**

Catalyst	Temperature (°C)	Lean-phase NO <sub>2</sub> Slip (μmol) <sup>a</sup>		Lean-phase NO <sub>x</sub> Storage Efficiency (%)		Rich-phase NO <sub>x</sub> Release (%) <sup>b</sup>		Cycle-averaged NO <sub>x</sub> Conversion (%)	
		Fresh	Aged	Fresh	Aged	Fresh	Aged	Fresh	Aged
Pt-50	150	45.3	48.6	22.6	14.3	50.9	44.2	11.1	8
	250	9.7	25.1	91.4	80.9	3	15.1	88.7	68.7
	350	1.5	17.7	98.7	84.6	0.5	2.4	98.1	82.5
	450	13.8	30.6	80	50.7	12.6	11.4	69.9	45
Pt-100	150	24.5	69.1	42.8	17.4	41.7	37.6	25	10.8
	250	0.5	7.4	99.6	94.3	0.1	7.9	99.5	86.9
	350	0.4	7.2	99.7	94.3	0.2	1.1	99.5	93.2
	450	5.6	22.9	88.9	61.9	11.8	12.6	78.4	54.1
30-50	150	52.5	47.6	35.2	21.2	27.7	28.3	25.5	15.2
	250	0.4	14.3	99.7	89.1	0.1	6.3	99.6	83.5
	350	0.1	14.2	99.8	88.7	0	2.3	99.8	86.7
	450	4.5	35.3	94.2	44.3	9.2	17.6	85.5	36.5
45-50	150	24.1	57.1	33.3	15.6	31.9	35.6	22.6	10.1
	250	0.3	9.1	99.7	92.7	0.2	16.1	99.5	77.7
	350	0	17.4	99.9	86.7	0.1	3.3	99.8	83.9
	450	2.3	40.6	95.8	39.3	11.7	19.7	84.6	31.6

<sup>a</sup> The total amount of input NO per lean-rich cycle was 171.5 μmol.

<sup>b</sup> (NO<sub>x</sub> released in rich purge/NO<sub>x</sub> stored in lean phase) x 100%.

As discussed in our previous study [40], the NSE under “stationary” cycling conditions is different from the initial NSE measured under continuous lean conditions, the NSE under stationary cycling conditions being dependent on both the initial NSE (i.e., the NSE for a catalyst initially totally free of NO<sub>x</sub>) and the extent to which the NO<sub>x</sub> storage sites are regenerated by rich purging during lean-rich cycling. To identify the NSE-limiting step

under lean-rich cycling, a comparison between the initial and the cycle-averaged NSE was made, as shown in Figure 4.7. Herein, the NSE obtained in the first lean cycle after complete catalyst regeneration at 500 °C is regarded as the initial (or “first-cycle”) NSE whereas the NSE obtained in the lean cycle under stationary cycling conditions is regarded as the “cycle-averaged” NSE. All of the fresh catalysts showed a very high initial NSE at the four temperatures tested, and only slight differences were observed between them. The drop in NSE under subsequent cycling was observed to be small in the range 250-450 °C, showing that the fresh catalysts were able to retain a good balance between NO<sub>x</sub> storage and regeneration under cycling conditions. After aging only small decreases in initial NSE were observed in the range 150-350 °C, which can be attributed to the contribution of ceria to NO<sub>x</sub> storage, as a supplement to the main BaO NO<sub>x</sub> storage phase. Given the inability of ceria to store NO<sub>x</sub> at 450 °C [54], a significant drop in initial NSE at 450 °C after aging indicates that the NO<sub>x</sub> storage function of the Pt/BaO/Al<sub>2</sub>O<sub>3</sub> component was severely degraded. A further drop in NSE during lean-rich cycling in the range 250-450 °C can be ascribed to the degradation of the regeneration function after aging, i.e., incomplete release of NO<sub>x</sub> from the storage sites during rich purging resulted in cycle-averaged NSE well below that of the initial NSE.

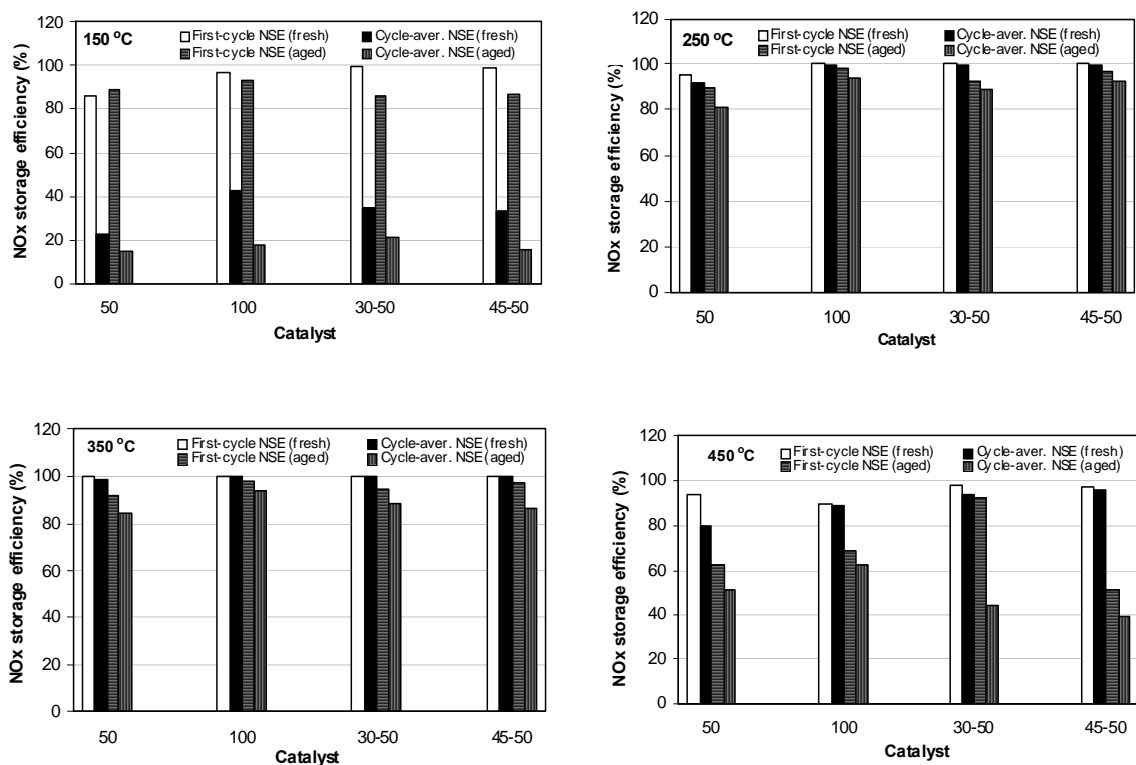


**Figure 4.7. Comparison of NO<sub>x</sub> storage efficiency during the first cycle and during subsequent lean-rich cycling for fresh and aged catalysts.**

Considering the data collected at 450 °C in Figure 4.7, it is interesting to note that the small difference in the first-cycle and cycle-average NSE for the fresh and aged catalysts, this being especially pronounced for catalyst Pt-50. In contrast, virtually no difference was observed at 350 °C for the fresh catalysts, indicating complete catalyst regeneration at this temperature (and by implication at higher temperatures). This discrepancy between the first-cycle and cycle-average NSE values at 450 °C is plausibly due to the creation of an exotherm from the combustion of reductants on the catalyst during the rich to lean transition, resulting in higher effective storage temperatures during the beginning of the lean phase and hence lower NSE. This effect has previously been reported by Epling et al. [55]. In this work, measured exotherms during cycling at 450 °C spanned the range 16-22 °C for the fresh catalysts and 8-12 °C after aging. Given that dispersed Ba nitrates are reported to decompose close to 450 °C [56], even a relatively modest temperature rise could be expected to exert a destabilizing effect on NO<sub>x</sub> storage. Furthermore, surface temperature swings at the precious metal sites (adjacent to the stored

NO<sub>x</sub>) could be much larger, as shown in a recent paper [57]. Scrutiny of the NO<sub>x</sub> concentration profiles at 450 °C failed to show clear indications of a link between the exotherms and decreased NO<sub>x</sub> storage as reported by Epling et al. [55]; however, given the relatively small magnitude of the discrepancy between the first-cycle and cycle-average NSE values, this is unsurprising.

Turning to the role of Pt in NO<sub>x</sub> storage and reduction, in the fresh state a slight improvement in the initial NSE was observed in the range 150-250 °C with increase of the Pt loading from 1.77 g/L (Pt-50) to 3.53 g/L (Pt-100) (Figure 4.7). Aging magnified the impact of Pt loading on both the initial and cycle-averaged NSE, the decreases in both the initial and cycle-based NSE observed for Pt-50 at 250 °C and 350 °C after aging being of a greater magnitude than for Pt-100. As confirmed by our TEM analysis, Pt is highly dispersed in the fresh catalysts and consequently the Pt particles and the NO<sub>x</sub> storage components (BaO/Al<sub>2</sub>O<sub>3</sub> and CeO<sub>2</sub>) are in close proximity, i.e., there is a large interfacial perimeter between the Pt and NO<sub>x</sub> storage phases. As discussed above, aging resulted in significant sintering of the Pt and as a consequence the interfacial perimeter between the Pt and Ba decreased, as did that between the Pt and CeO<sub>2</sub> (although to a lesser extent). Based on the mechanism of NO<sub>x</sub> storage and reduction, as proposed in the literature [18], the limiting step during cycling is believed to be transfer of NO<sub>x</sub> between Pt and Ba, and the distance between the Pt and Ba phases can significantly impact the NO<sub>x</sub> spillover from Pt to Ba during NO<sub>x</sub> storage and reverse NO<sub>x</sub> spillover from Ba to Pt during NO<sub>x</sub> reduction. As a result, both NO<sub>x</sub> storage and reduction capability are degraded after aging due to segregation of the Pt and Ba; however, our results indicate that increasing Pt loading can, to a certain extent, alleviate the effect of aging. A further comparison between Pt-100 and 30-50 infers that a higher Pt loading on NO<sub>x</sub> storage components (BaO and CeO<sub>2</sub>, see Table 4.2), as for Pt-100, can benefit the LNT performance of aged catalysts albeit the total Pt loading is the same in both of them. Consistent with these findings, Clayton et al. [58] observed that during lean-rich cycling, the amount of stored NO<sub>x</sub> increased with increasing Pt dispersion in the temperature range studied (125-340 °C) for Ba-based model catalysts; this was similarly attributed to the enhanced NO<sub>x</sub> spillover from Pt to the Ba phase that should result from the larger Pt surface area and

Pt/Ba interfacial perimeter. Likewise, a tendency for slower catalyst regeneration with increasing Pt particle size was also noted, suggesting that a kinetic process, such as reverse spillover of stored NO<sub>x</sub> or the spillover of reductant from Pt to the NO<sub>x</sub> storage phase, may limit the overall rate.

The effect of Ba loading on initial NSE also became more evident after aging. Whereas in the fresh state catalysts 30-50 and 45-50 showed little difference in initial or cycle-averaged NSE, after aging 45-50 displayed superior initial NSE at 250 °C and 350 °C. At 450 °C this trend was reversed for reasons that are not clear. However, there was little difference in the NSE values of the two catalysts under cycling conditions, implying that cycling performance was limited by catalyst regeneration rather than initial NO<sub>x</sub> storage efficiency. In other words, degradation of the NO<sub>x</sub> regeneration function is the critical issue for these catalysts with respect to their NSE after aging.

#### *4.3.4. NO<sub>x</sub> Release and Reduction.*

NO<sub>x</sub> release under rich purging is shown in Figures 4.5 and 4.6. The fresh catalysts showed much higher NO<sub>x</sub> release at 150 °C than the aged catalysts. The kinetics of NO<sub>x</sub> reduction are slow at low temperature [59], a fact which is exacerbated by the presence CO in the rich phase gas feed; at low temperatures CO coverage on the PM sites is high, thereby effectively poisoning the sites for NO<sub>x</sub> adsorption and reduction [43]. Consequently, the fresh catalysts, possessing high initial NSE, showed considerable rich phase NO<sub>x</sub> slip due to their limited NO<sub>x</sub> reduction ability. In contrast to the low temperature behavior, the rich phase slip in the range 250-350 °C increased after aging, reflecting deterioration in NO<sub>x</sub> reduction activity, and a resulting imbalance in the rates of NO<sub>x</sub> release and reduction. This is most clearly illustrated by catalyst 45-50, peak NO<sub>x</sub> concentrations of 1300 ppm being observed at 250 °C after aging, corresponding to release – without reduction – of 16% of the stored NO<sub>x</sub>. At 450 °C this effect is reversed, i.e., rich phase NO<sub>x</sub> slip is lower for the aged catalysts relative to their fresh counterparts, a finding which can be attributed to the significantly lower NSE after aging. However, even at 450 °C the amount of rich phase NO<sub>x</sub> slip expressed as a percentage of the total amount of NO<sub>x</sub> stored is generally higher for the aged catalysts compared to their fresh

analogues, e.g., 19.7% versus 11.7% for 45-50 (Table 4.6). This again reflects deterioration in the NO<sub>x</sub> reduction function of the catalysts caused by aging.

The overall impact of aging under lean-rich cycling is reflected in the cycle-averaged NO<sub>x</sub> conversions reported in Table 4.6. Overall, NO<sub>x</sub> conversion is observed to decrease after aging as a consequence of decreased NSE and increased rich phase NO<sub>x</sub> slip. Whereas cycle-averaged NO<sub>x</sub> conversion in the range 250-350 °C is similar for the four catalysts in the fresh state (being close to 100% for Pt-100, 30-50 and 45-50, and only slightly lower for Pt-50), after aging a clear ordering is observed, namely: Pt-100 > 30-50 > 45-50 > Pt-50. Given the importance of the Pt-Ba interface, it follows that high Pt loadings are beneficial for catalyst performance since they provide one means of ensuring a high degree of Pt-Ba contact. On this basis, and bearing in mind that the Pt dispersions in the aged catalysts were very similar, the inferior performance of Pt-50 is readily explained. As discussed in section 4.3.3, the superior performance of Pt-100 relative to 30-50 and 45-50 is ascribed to the higher Pt loading on the BaO and CeO<sub>2</sub> NO<sub>x</sub> storage components, albeit the total Pt loading is the same in the three catalysts.

Interestingly, after aging catalyst Pt-100 was able to outperform 30-50 and 45-50 despite the fact that the Rh loading in Pt-100 was only half that of the other two catalysts. From Table 4.6, it is apparent that Pt-100 displayed superior NSE than 30-50 in both the fresh and aged states. This is not surprising, given that Rh is not considered to contribute significantly to NO oxidation, being less active than Pt. Comparing rich phase NO<sub>x</sub> release, it is found that 30-50 generally outperformed Pt-100, particularly at low temperatures when the kinetics of NO<sub>x</sub> reduction are slow. This is consistent with the superior activity of Rh, as compared to Pt, in anaerobic NO<sub>x</sub> reduction [60]. However, in general the superior NSE of Pt-100 is seen to outweigh the lower rich phase NO<sub>x</sub> release displayed by 30-50, with the consequence that aged Pt-100 showed slightly better cycle-averaged NO<sub>x</sub> conversion than aged 30-50 in the temperature range 250-450 °C.



#### 4.3.5. Selectivity of NO<sub>x</sub> Reduction.

The selectivity to NO<sub>x</sub> reduction products during rich purging is summarized in Figure 4.8. For the fresh catalysts, N<sub>2</sub>O was the dominant product at 150 °C, while N<sub>2</sub> was the main product in the range 250-450 °C. Compared to the other three catalysts, in the fresh state Pt-50 exhibited higher N<sub>2</sub>O and lower N<sub>2</sub> selectivity, with only small differences in product selectivity being observed among Pt-100, 30-50 and 45-50. After aging, all of the catalysts exhibited decreased selectivity to N<sub>2</sub>O at 150 °C and significantly increased NH<sub>3</sub> production in the range 250-450 °C, although N<sub>2</sub> remained the dominant product at 350 °C and 450 °C.

Due to the slow response time of the FT-IR analyzer, the inherent time resolution of the data collected in this study is significantly longer than the 5 s duration of the rich phase. Consequently, it proved impossible to establish reliably the time dependence of N<sub>2</sub>O release relative to the other N-containing species evolved (NO, NO<sub>2</sub> and NH<sub>3</sub>). However, a number of previous studies have indicated that N<sub>2</sub>O is formed immediately after the lean to rich transition, and that NH<sub>3</sub> is observed after a slight delay [61-63]. This implies that N<sub>2</sub>O is formed in the reaction front, in a reaction which must proceed in close association with removal of oxygen from the surface of the Pt particles via reaction with H<sub>2</sub>. Under these conditions, the local H<sub>2</sub>/NO stoichiometry at Pt will be low, due to the simultaneous release of NO<sub>x</sub> and consumption of H<sub>2</sub> in the reaction front by stored oxygen, including that on the oxidized Pt particles (in addition to oxygen stored on the ceria washcoat component). At low temperature (75-150 °C) low H<sub>2</sub>/NO ratios are known to favor the formation of N<sub>2</sub>O [64]. This can be understood in terms of the formation of N<sub>2</sub>O via the reactions of molecularly adsorbed NO according to equations (4.1) and/or (4.2) [65,66]:



Based on energy barriers determined from DFT calculations, Burch et al. [66] reasoned that equation (4.1), which proceeds via an adsorbed (NO)<sub>2</sub> intermediate, should be

avored at low temperatures (ca. 100 °C), whereas equation (4.2) is likely to be responsible for N<sub>2</sub>O formation at higher temperatures (> 200 °C).

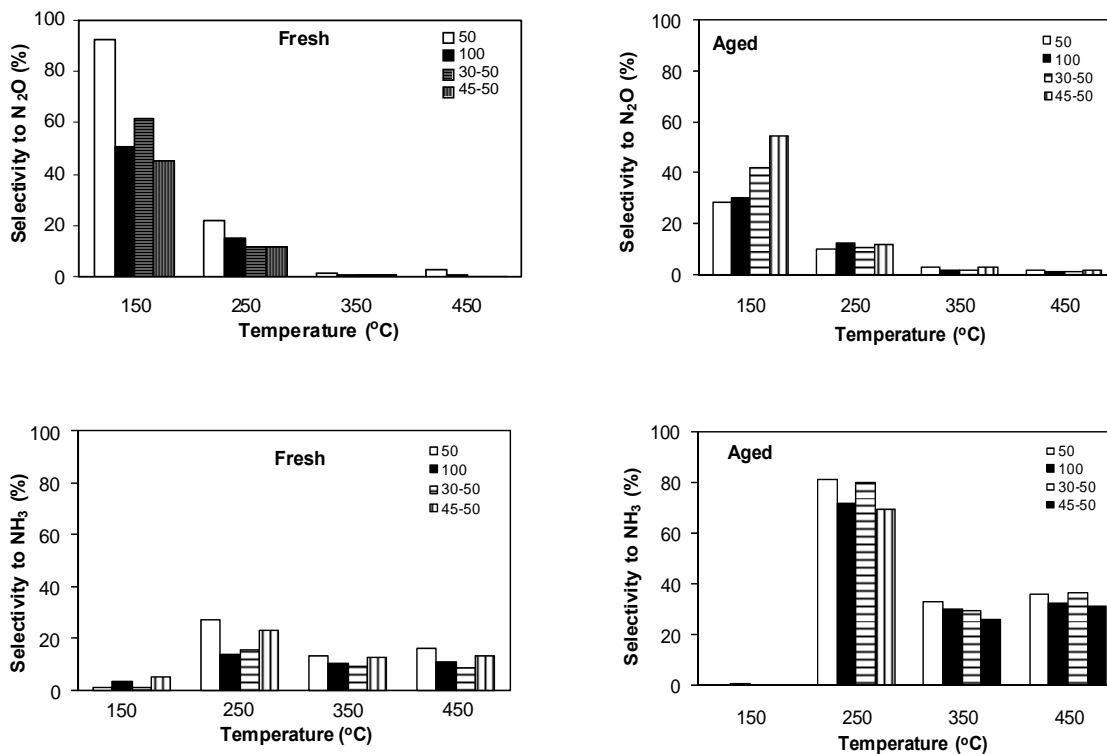


**Figure 4.8. Selectivity to N<sub>2</sub>O (top), NH<sub>3</sub> (middle) and N<sub>2</sub> (bottom) for NO<sub>x</sub> reduction during lean-rich cycling.**

Molecular adsorption of NO on Pt, as opposed to dissociative adsorption, will be favored (i) at low temperatures, when the rate of NO bond scission is low, (ii) when Pt is partially covered by O, such that the paired surface sites required for NO dissociation are scarce, and (iii) when the concentration of adsorbed hydrogen is relatively low. The latter consideration stems from reports suggesting that the presence of adsorbed hydrogen promotes NO dissociation on metal surfaces [67-69]. Hecker and Bell [67] proposed that NO dissociation results from the abstraction of molecularly adsorbed NO by adsorbed H:



Indeed, calculations show that the activation energy is lower for the assisted decomposition of NO (equation 4.3) than for simple dissociation [70]:



In addition, it has been suggested that enhanced electron donation from the metal to the NO antibonding orbital when adsorbed hydrogen is present may promote NO bond scission [68].

Temporal analysis of products (TAP) experiments by Harold and co-workers [69] support the occurrence of equation (4.3), the adsorbed N reacting with NO to form N<sub>2</sub>O (equation 4.2). From this it follows that N<sub>2</sub>O formation can only be avoided when NO adsorbed on the catalyst is fully dissociated, a conclusion reached by Burch and Watling in their study of the C<sub>3</sub>H<sub>6</sub>-NO-O<sub>2</sub> reaction over Pt catalysts [71].

In terms of lean-rich switching, it is evident that at low temperatures and at short rich times, as H<sub>2</sub> removes adsorbed O from Pt, molecularly adsorbed NO will form N<sub>2</sub>O via equations (4.1) and/or (4.2), the latter being preceded by equation (4.3). At longer rich times, when the reaction front has passed, the local concentration of H<sub>2</sub> will be higher (since it is not being consumed via reduction of the initially oxidized Pt particles or other forms of stored oxygen), while the NO<sub>x</sub> concentration will be lower. Hence, H and N adatoms will dominate and N<sub>2</sub> and NH<sub>3</sub> will be the main NO<sub>x</sub> reduction products formed [62]. Higher temperatures should also favor N<sub>2</sub> and NH<sub>3</sub> production due to more extensive NO dissociation. Finally, it should be noted that other formation routes for N<sub>2</sub>O are conceivable, such as the reaction of NH<sub>3</sub> with NO<sub>x</sub> or the reaction of NH<sub>3</sub> with stored oxygen. However, the formation of N<sub>2</sub>O from these processes is typically observed at temperatures in excess of 150 °C [64].

Turning to the factors influencing NH<sub>3</sub> production, as mentioned above, recent studies have shown that the product distribution during NO<sub>x</sub> reduction is a function of the relative NO<sub>x</sub> and reductant concentrations, high H<sub>2</sub>:NO<sub>x</sub> ratios favoring the formation of NH<sub>3</sub> [65]. Since the same amount of reductant was available during rich purging for the

fresh and aged catalysts, a higher ratio of reductant to stored  $\text{NO}_x$  for the aged catalysts (due to the lowered NSE) should result in increased selectivity to  $\text{NH}_3$  over  $\text{N}_2$ . Indeed, several recent studies have shown that selectivity to  $\text{NH}_3$  increases with decreasing amount of  $\text{NO}_x$  stored [72,73]. Another important factor that can influence the  $\text{NO}_x$  reduction selectivity of the aged catalysts is their OSC. Previously we have shown that selectivity to  $\text{N}_2$  tends to increase with increasing OSC [41]. However, in this case there is no simple correlation between product selectivity and OSC. Although the catalysts with the lowest OSC at 350 °C showed the highest selectivity to  $\text{NH}_3$  in the fresh state (Pt-50 and 45-50), after aging catalysts Pt-100, 30-50 and 45-50 showed the opposite trend. However, all of the catalysts displayed a remarkable increase in selectivity to  $\text{NH}_3$  after aging. In addition to the effective increase in local  $\text{H}_2:\text{NO}_x$  ratio mentioned above, there are several other possible reasons for this. First, a decrease in OSC brought on by aging should result in an increased reductant concentration in the gas front during rich purging (as compared to the fresh catalyst), due to reduced consumption of the reductant by reaction with the stored oxygen, thereby favoring the formation of  $\text{NH}_3$ . Second,  $\text{NH}_3$  formed at the front of the catalyst can be converted to  $\text{N}_2$  via reaction with the oxygen stored in the rear of the catalyst. As catalyst OSC is decreased, so less  $\text{NH}_3$  tends to be converted to  $\text{N}_2$  at the rear of the catalyst. From Table 4.4 it is apparent that after aging, all of the catalysts showed decreased OSC. In this context, it is instructive to examine the outlet CO profile during cycling (Figure 4.9). As shown, CO slip was observed in all cases during rich purging, indicative of complete consumption of the stored oxygen. As for the  $\text{NH}_3$  measured in the effluent, the amount of CO in the effluent increased after aging. This is consistent with the role of stored oxygen in consuming reducing species present in the catalyst, although in the case of CO it is possible that decreased water-gas shift activity after aging may have contributed to the higher outlet CO concentration.

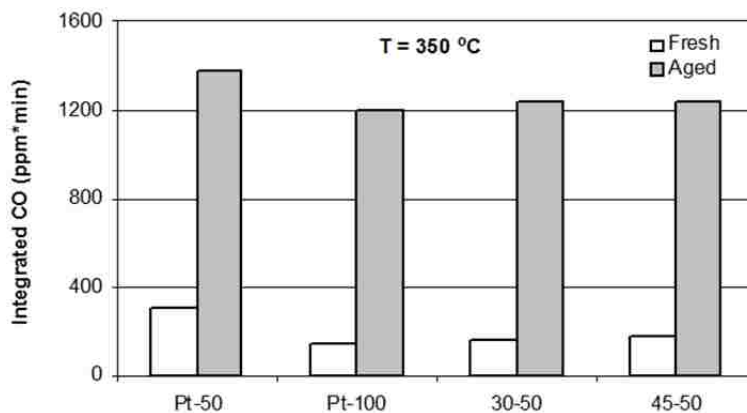


**Figure 4.9. Comparison of integrated outlet CO concentration before and after aging (T = 350 °C).**

In addition to OSC, other factors play a role in determining the selectivity of  $\text{NO}_x$  reduction. The dispersion of precious metal has recently been shown to be important on this regard, lower Pt dispersions favoring the production of  $\text{NH}_3$  [58]. This can be rationalized on the basis that as the Pt/Ba interfacial perimeter decreases (with decreasing Pt dispersion), the rate of transport of stored  $\text{NO}_x$  to Pt (i.e., reverse spillover) is decreased. If this rate is slower than the  $\text{H}_2$  feed rate, then  $\text{H}_2$  will break through with substantially more  $\text{NO}_x$  remaining on the catalyst after  $\text{H}_2$  breakthrough. Consequently, the Pt surface will be predominantly covered by hydrogen, and as the stored  $\text{NO}_x$  transports to the Pt particles,  $\text{NH}_3$  will be preferentially formed. Indeed, a recent modeling study confirms the idea that  $\text{NH}_3$  generation is favored under conditions when  $\text{NO}_x$  transport to the Pt/Ba interface is the rate determining process [74].

Lengthening of the  $\text{NO}_x$  storage-reduction (NSR) zone can also be expected to contribute to the observed increase in selectivity to  $\text{NH}_3$  after aging. A recent study employing SpaciMS suggests that the longer the NSR zone (i.e., the axial portion of the catalyst where  $\text{NO}_x$  is stored and reduced), the shorter the downstream OSC-only zone (i.e., the axial portion free of stored  $\text{NO}_x$ ) [75]. This leads to decreased oxidation of  $\text{NH}_3$ , slipping from the upstream NSR-zone, by oxygen stored in the OSC-only zone [75,76]. This effect is particularly noticeable for sulfated catalysts, since as sulfation proceeds there are fewer active sites available per unit of catalyst volume, causing the NSR zone to be

stretched towards the rear of the catalyst. Similarly, this effect is expected to be significant for the catalysts in this work based on the observed decreases in both initial and cycle averaged NSE after aging; these findings are consistent with an effective decrease in the concentration of NO<sub>x</sub> storage sites, which in turn implies that the NSR zone in the aged catalysts must be greatly expanded relative to their fresh analogues.

Finally, it should be mentioned that since overall catalyst selectivity to NH<sub>3</sub> is governed by the relative rates of NH<sub>3</sub> generation and consumption, if catalyst aging were to result in a decrease in the rate of the NO<sub>x</sub>-NH<sub>3</sub> reaction occurring in the reductant front [77], then selectivity to NH<sub>3</sub> would also be expected to increase. However, in separate work [78], we have found that the SCR reaction rate for model catalysts similar to the ones used in this study is not greatly affected by aging (under the same conditions used in this work). Consequently, we conclude that this is not a major factor in the observed increase in catalyst selectivity to NH<sub>3</sub> after aging.

#### *4.3.6. Effects of Aging on Specific Catalyst Functions.*

It is generally accepted that the functioning of LNT catalysts involves four sequential steps [18]: (i) NO oxidation to NO<sub>2</sub>, (ii) NO<sub>x</sub> storage, (iii) NO<sub>x</sub> release (i.e., nitrate decomposition) and (iv) NO<sub>x</sub> reduction. As for our previous study [40], in this work it was found that simulated road aging resulted in significant deterioration of catalyst performance in steps (ii), (iii) and (iv). Considering step (ii), besides the effect of Pt-Ba phase segregation, the other important factor responsible for decrease of the initial and cycle-averaged NSE after aging is residual sulfur. Sulfation of the Ba phase is reflected in the initial (“first cycle”) NSE values measured at 450 °C. At this temperature ceria does not contribute to NO<sub>x</sub> storage [54], hence the significant deterioration in initial NSE at 450 °C observed after catalyst aging reflects the deterioration of the ability of the Ba phase to trap NO<sub>x</sub>. In addition, we cannot rule out the effect of the likely decreased Ba dispersion caused by aging due to its high mobility.

The effect of Pt sintering is reflected in the performance of the aged catalysts with respect to steps (ii), (iii) and (iv). In the case of step (iv), rich phase NO<sub>x</sub> slip in the range 250-

350 °C increased after aging (as shown in Table 4.6), indicative of an imbalance in the rates of NO<sub>x</sub> release and reduction arising from deterioration of the NO<sub>x</sub> reduction activity. This observation is consistent with the literature for three-way catalysts, which indicates that decreased NO<sub>x</sub> reduction activity is associated with precious metal sintering [79].

In the case of steps (ii) and (iii) it is difficult to decouple the effects of Pt sintering, since under cycling conditions NO<sub>x</sub> storage efficiency is dependent on the extent to which stored NO<sub>x</sub> is released during rich purging (as discussed in section 4.3.3). However, it is instructive to consider the NSE data measured at 150 °C (Figure 4.7). Comparison of the high initial NSE with the low cycle-averaged NSE values observed for the different catalysts suggests that during cycling a kinetic process, such as reverse spillover of stored NO<sub>x</sub> or the spillover of hydrogen from Pt to the BaO and CeO<sub>2</sub> storage components, limits the nitrate decomposition rate both for the fresh and aged catalysts. This, in turn, limits the cycled-averaged NSE. As shown, the initial NSE at 150 °C does not drop significantly after aging, indicating that NO<sub>x</sub> storage (step (ii)) on the BaO and/or CeO<sub>2</sub> phases is not markedly impacted. Given that ceria plays a significant role in NO<sub>x</sub> storage at such low temperatures, this relatively small decline in initial NSE can be attributed to the retention of a reasonably high Pt dispersion on the ceria phase, as indicated by the HRTEM measurements presented above, as well as the fact that the ceria phase is not contaminated with residual sulfur (unlike the Ba phase). A more significant impact of aging is observed on the cycle-averaged NSE at 150 °C, indicating that NO<sub>x</sub> release (step (iii)) is more deteriorated by aging than the NO<sub>x</sub> storage step. However, at higher temperatures these trends become less clear. This is because the Ba storage phase plays an increasingly greater role in NO<sub>x</sub> storage as the temperature increases, and the deterioration of the initial NSE – due to sulfation of the Ba phase – becomes a more significant contributor to the overall decrease in cycled averaged NSE. However, it is clear that after aging the kinetics of nitrate release are at least partially limiting with respect to cycle-averaged NSE since the deterioration in cycle-averaged NSE in all cases exceeds the drop in initial NSE, i.e., the degradation of cycle-averaged NSE at higher temperatures cannot be explained solely by the deterioration in initial NSE.

As shown in Table 4.6, the cycled-averaged storage efficiency for all of the catalysts dropped significantly after aging at all temperatures. Comparison of the changes in cycle-averaged NO<sub>x</sub> conversion for the fresh and aged catalysts with the corresponding changes in the lean phase (cycled-averaged) NSE and with the changes in rich phase NO<sub>x</sub> release reveals a strong correlation between NO<sub>x</sub> conversion and NSE. This is shown by the correlation plot depicted in Figure 4.10. As shown, when the values for the different catalyst are plotted and grouped by temperature, strong correlations are observed for the data collected at 350 and 450 °C. In principle, a strong correlation between cycle averaged NO<sub>x</sub> conversion and storage efficiency is to be expected if there is no limitation with respect to NO<sub>x</sub> reduction. Given that the kinetics of NO<sub>x</sub> reduction are limiting at low temperatures, as evidenced by the considerable rich phase NO<sub>x</sub> slip observed at 150 °C and 250 °C in Figure 4.6, the weak correlations observed at these lower temperatures are not surprising. This is particularly evident for the 250 °C data points. As shown in Table 4.6, after aging a large increase in rich phase NO<sub>x</sub> slip is observed at 250 °C for all of the catalysts, indicative of a deterioration in the NO<sub>x</sub> reduction function. At higher temperatures, the kinetics of NO<sub>x</sub> reduction are presumably sufficiently fast that, even allowing for the deterioration, NO<sub>x</sub> reduction is not limiting.

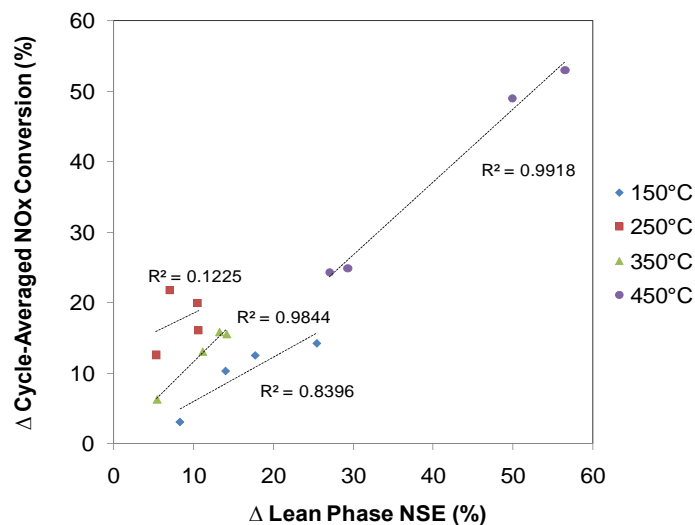


**Figure 4.10. Correlation of the change in cycle-averaged NO<sub>x</sub> conversion after aging with the change in cycle-averaged lean phase NSE.**



Overall, these results show that the deterioration in catalyst performance at 350 and 450 °C after aging is largely the result of the deterioration in cycle-averaged NSE. This in turn, can be ascribed to (i) a decrease in NO<sub>x</sub> storage capacity resulting from sulfation of the Ba phase and (ii) sintering of the Pt, resulting in less efficient NO<sub>x</sub> storage and nitrate decomposition. At the lower temperatures, the deterioration in NO<sub>x</sub> reduction activity represents a significant additional factor.

#### 4.3.7. Interfacial Pt-Support Perimeter.

As indicated in the Introduction, previous studies [15-21] have demonstrated the importance of the proximity of the Pt and Ba phases for efficient LNT functioning. Given that Pt is believed to act as a conduit for NO<sub>x</sub> spillover to and from the Ba phase, it follows that close proximity of Pt and Ba are required to achieve efficient NO<sub>x</sub> storage and reduction. The effect of Pt sintering on the Pt-Ba interface can be illustrated by consideration of the interfacial perimeter between Pt and its support (in this case BaO) at different levels of Pt dispersion. Assuming a hemispherical morphology for Pt particles, the relationship between the number of atoms in a Pt particle (N<sub>Pt</sub>) and the particle diameter (d) is given by:

$$N_{Pt} = \frac{\frac{2}{3}\pi\left(\frac{d}{2}\right)^3 \sigma N_a}{W_a} \quad (4.5)$$

where  $N_a$  is Avogadro's number, and  $W_a$  is the atomic weight. Based on face-centered cubic (FCC) packing for Pt, the number of surface atoms (N<sub>Pt<sub>s</sub></sub>) as a function of particle diameter is given by:

$$N_{Pt_s} = 2\pi(d/2)^2\omega \quad (4.6)$$

where  $\omega$  is the average atom density of Pt particle surface [80]. Dispersion is defined as the percentage of surface atoms in the particle, i.e.:

$$\text{Dispersion} = \frac{N_{Pt_s}}{N_{Pt}} \quad (4.7)$$

From eqn. (4.5), it follows that the number of particles per gram of Pt ( $\Sigma_p$ ) is given by:

$$\Sigma_p = \frac{3/2}{\pi(d/2)^3\sigma} \quad (4.8)$$

Assuming that the interfacial perimeter of a Pt particle corresponds directly to its circumference, the total interfacial perimeter per gram of Pt ( $\lambda_{Pt}$ ) is obtained as follows:

$$\lambda_{Pt} = \pi * d * \Sigma_p \quad (4.9)$$

As shown in Table 4.7, for a Pt dispersion of 38%, which is close to the values observed prior to aging for the catalysts in this study (see Table 4.4), the total perimeter of the Pt particles amounts to  $6.22 \times 10^{19}$  nm/g Pt. However, for a dispersion of 11%, which is close to the values observed after aging, the total perimeter is only  $5.6 \times 10^{18}$  nm/g Pt, i.e., a factor of eleven lower. These simple calculations are illustrative of the critical role that Pt particle size plays in determining the extent of Pt-Ba contact and, by implication, in governing LNT functioning. From this it follows that future attempts to predictively model the deactivation of LNT catalysts will have to incorporate the extent of Pt sintering as a key parameter.

**Table 4.7. Total Pt-support interfacial perimeter as a function of Pt particle size, assuming hemispherical particle morphology.**

Average Pt Particle Size (nm)	Dispersion	Number of Atoms in Particle	Number of Particles/g Pt	Total Interfacial Perimeter (nm/g Pt)
1	100	18	1.78E+20	5.6E+20
2	57	139	2.22E+19	1.40E+20
3	38	468	6.60E+18	6.22E+19
4	29	1110	2.78E+18	3.50E+19
5	23	2167	1.42E+18	2.24E+19
8	14	8876	3.48E+17	8.76E+18
10	11	17336	1.78E+17	5.60E+18
20	6	138684	2.22E+16	1.40E+18

#### 4.4. Conclusions.

According to physico-chemical data for the fresh and aged catalysts in this work, aging resulted in two main changes which can explain the accompanying degradation in catalyst activity for NO<sub>x</sub> storage and reduction. First, according to H<sub>2</sub> chemisorption and TEM data, sintering of the precious metals in the washcoat occurred, being most evident for Pt located on the BaO/Al<sub>2</sub>O<sub>3</sub> washcoat component. The resulting decrease in contact between the Pt and Ba phases contributed to decreased first cycle NSE due to less efficient NO<sub>x</sub> spillover from Pt to Ba during NO<sub>x</sub> adsorption. An even larger decrease in cycle-averaged NO<sub>x</sub> storage points to the fact that the ability to regenerate the NO<sub>x</sub> storage sites was also adversely affected, i.e., Pt-Ba phase segregation adversely affected the rate of reductant spillover from Pt to Ba and hence NO<sub>x</sub> release. In addition, at low temperatures (250 °C) an increase in rich phase NO<sub>x</sub> slip was observed after aging, consistent with a decrease in the rate of the reverse NO<sub>x</sub> spillover process and/or the intrinsic rate of PM-catalyzed NO<sub>x</sub> reduction.

Second, elemental analysis, TEM and XRD data indicate the accumulation of sulfur in the washcoat, present as BaSO<sub>4</sub>. At the measured concentrations, approximately 30% of the Ba present was typically present in the sulfated form, providing an additional

explanation for the loss in initial and cycle-averaged NSE after catalyst aging.

For the four catalysts used in this study, cycle-averaged NO<sub>x</sub> conversions in the range 250-350 °C were similar in the fresh state, while after aging a clear ordering was observed: Pt-100 > 30-50 > 45-50 > Pt-50. Given the importance of the Pt-Ba interface, it follows that high Pt loadings are beneficial for catalyst performance since they provide one means of ensuring a high degree of Pt-Ba contact. On this basis, and bearing in mind that the Pt dispersions in the aged catalysts were very similar, the inferior performance of Pt-50 is explained. The superior performance of Pt-100 relative to 30-50 and 45-50 is ascribed to the higher Pt loading on the BaO and CeO<sub>2</sub> NO<sub>x</sub> storage components in Pt-100, albeit the total Pt loading is the same in the three catalysts. The effect of Rh loading was after aging found to be marginal within the range studied; although the higher Rh loaded catalyst 30-50 showed slightly better low temperature NO<sub>x</sub> reduction activity than Pt-100 (containing half as much Rh), the superior NSE of Pt-100 outweighed this effect. Finally, it was found that increasing the BaO loading in washcoat from 30 to 45 g/L produced no measurable benefit.

#### 4.5. References.

- [1] N. Miyoshi, S. Matsumoto, K. Katoh, T. Tanaka, J. Hardara, N. Takashi, K. Yokota, M. Sugiura, K. Kasahara, Development of New Concept Three-Way Catalyst for Automotive Lean-Burn Engines. SAE Technical Paper Series 950809 (1995).
- [2] N. Takahashi, H. Shinjoh, T. Iijima, T. Suzuki, K. Yamazaki, K. Yokota, H. Suzuki, N. Miyoshi, S. Matsumoto, T. Tanizawa, T. Tanaka, S. Tateishi, K. Kasahara, The New Concept 3-Way Catalyst for Automotive Lean-Burn Engine: NO<sub>x</sub> Storage and Reduction Catalyst. *Catalysis Today* 27 (1996) 63-69.
- [3] J. Breen, M. Marella, C. Pistarino, J. Ross, Sulfur-Tolerant NO<sub>x</sub> Storage Traps: an Infrared and Thermodynamic Study of the Reactions of Alkali and Alkaline-Earth Metal Sulfates. *Catalysis Letter* 80 (2002) 123-128.
- [4] K. Yamamoto, R. Kikuchi, T. Takeguchi, K. Eguchi, Development of NO sorbents tolerant to sulfur oxides. *Journal Catalysis* 238 (2006) 449-457.
- [5] N. Takahashi, A. Suda, I. Hachisuka, M. Sugiura, H. Sobukawa, H. Shinjoh, Sulfur Durability of NO<sub>x</sub> Storage and Reduction Catalyst with Supports of TiO<sub>2</sub>, ZrO<sub>2</sub> and ZrO<sub>2</sub>-TiO<sub>2</sub> Mixed Oxides. *Applied Catalysis B: Environmental* 72 (2007) 187-195.
- [6] W.S. Epling, L.E. Campbell, A. Yezerets, N.W. Currier, J.E. Parks II, Overview of the Fundamental Reactions and Degradation Mechanisms of NO<sub>x</sub> Storage/Reduction Catalysts. *Catalysis Reviews* 46 (2004) 163-246.
- [7] S. Elbouazzaoui, E.C. Corbos, X. Courtois, P. Marecot, D. Duprez, A Study of the Deactivation by Sulfur and Regeneration of a Model NSR Pt/Ba/Al<sub>2</sub>O<sub>3</sub> Catalyst. *Applied Catalysis B: Environmental* 61 (2005) 236-243.

- [8] H. Abdulhamid, E. Fridell, J. Dawody, M. Skoglundh, In situ FTIR Study of SO<sub>2</sub> Interaction with Pt/BaCO<sub>3</sub>/Al<sub>2</sub>O<sub>3</sub> NO<sub>x</sub> Storage Catalysts under Lean and Rich Conditions. *Journal of Catalysis* 241 (2006) 200-210.
- [9] L. Lietti, P. Forzatti, I. Nova, E. Tronconi, NO<sub>x</sub> Storage Reduction over Pt–Ba/γ-Al<sub>2</sub>O<sub>3</sub> Catalyst. *Journal of Catalysis* 204 (2001) 175-191.
- [10] F. Rohr, U. Gobel, P. Kattwinkel, S. Philipp, P. Gelin, New Insight into the Interaction of Sulfur with Diesel NO<sub>x</sub> Storage Catalysts. *Applied Catalysis B: Environmental* 70 (2007) 189-197.
- [11] C. Courson, A. Khalfi, M. Mahzoul, S. Hodjati, N. Moral, A. Kiennemann, P. Gilot, Experimental Study of the SO<sub>2</sub> Removal Over a NO<sub>x</sub> Trap Catalyst. *Catalysis Communications* 3 (2002) 471-477.
- [12] S. Poulston, R. Rajaram, Regeneration of NO<sub>x</sub> Trap Catalysts. *Catalysis Today* 81 (2003) 603-610.
- [13] X. Wei, X. Liu, M. Deeba, Characterization of Sulfated BaO-Based NO<sub>x</sub> Trap. *Applied Catalysis B: Environmental* 58 (2005) 41-49.
- [14] Z. Liu, J. Anderson, Influence of Reductant on the Regeneration of SO<sub>2</sub>-Poisoned Pt/BaO/Al<sub>2</sub>O<sub>3</sub> NO<sub>x</sub> Storage and Reduction Catalyst. *Journal of Catalysis* 228 (2004) 243-253.
- [15] H. Mahzoul, J.F. Brilhac, P. Gilot, Experimental and Mechanistic Study of NO<sub>x</sub> Adsorption over NO<sub>x</sub> Trap Catalysts. *Applied Catalysis B: Environmental* 20 (1999) 47-55.

- [16] I. Nova, L. Lietti, L. Castoldi, E. Tronconi, P. Forzatti, New Insights in the NO<sub>x</sub> Reduction Mechanism with H<sub>2</sub> over Pt–Ba/γ -Al<sub>2</sub>O<sub>3</sub> Lean NO<sub>x</sub> Trap Catalysts under Near-Isothermal Conditions. *Journal of Catalysis* 239 (2006) 244-254.
- [17] J.M. Coronado, J.A. Anderson, FTIR Study of the Interaction of NO<sub>2</sub> and Propene with Pt/BaCl<sub>2</sub>/SiO<sub>2</sub>. *Journal of Molecular Catalysis A: Chemical* 138 (1998) 83-96.
- [18] L. Olsson, H. Persson, E. Fridell, M. Skoglundh, B. Andersson, A Kinetic Study of NO Oxidation and NO<sub>x</sub> Storage on Pt/Al<sub>2</sub>O<sub>3</sub> and Pt/BaO/Al<sub>2</sub>O<sub>3</sub> *Journal of Physical Chemistry B* 105 (2001) 6895-6906.
- [19] N.W. Cant, I.O.Y. Liu, M.J. Patterson, The Effect of Proximity Between Pt and BaO on Uptake, Release, and Reduction of NO<sub>x</sub> on Storage Catalysts. *Journal of Catalysis* 243 (2006) 309-317.
- [20] R. Büchel, R. Ströbel, F. Krumeich, A. Baiker, S.E. Pratsinis, Influence of Pt Location on BaCO<sub>3</sub> or Al<sub>2</sub>O<sub>3</sub> During NO<sub>x</sub> Storage Reduction. *Journal of Catalysis* 261 (2009) 201-207.
- [21] A. Kumar, M.P. Harold, V. Balakotaiah, Isotopic Studies of NO<sub>x</sub> Storage and Reduction on Pt/BaO/Al<sub>2</sub>O<sub>3</sub> Catalyst Using Temporal Analysis of Products. *Journal of Catalysis* 270 (2010) 214-223.
- [22] S.S. Chaugule, A. Yezerets, N.W. Currier, F.H. Ribeiro, W.N. Delgass, 'Fast' NO<sub>x</sub> Storage on Pt/BaO/γ-Al<sub>2</sub>O<sub>3</sub> Lean NO<sub>x</sub> Traps with NO<sub>2</sub> + O<sub>2</sub> and NO + O<sub>2</sub>: Effects of Pt, Ba Loading. *Catalysis Today* 151 (2010) 291-303.
- [23] G. Graham, H. Jen, W. Chun, H. Sun, X. Pan, R. McCabe, Coarsening of Pt Particles in a Model NO<sub>x</sub> Trap. *Catalysis Letters*. 93 (2004) 129-134.

- [24] A.K. Datye, Q. Xu, K.C. Kharas, J.M. McCarty, Particle Size Distributions in Heterogeneous Catalysts: What Do They Tell Us About the Sintering Mechanism? *Catalysis Today* 111 (2006) 59-67.
- [25] N. Fekete, R. Kemmler, D. Voigtländer, B. Krutzsch, E. Zimmer, G. Wenninger, W. Strehlau, J. van den Tilaart, J. Leyrer, E. Lox, W. Müller, Evaluation of NO<sub>x</sub> Storage Catalysts for Lean Burn Gasoline Fueled Passenger Cars. SAE Technical Paper Series 970746 (1997).
- [26] D. Uy, A.E. O'Neill, J. Li, W.L.H Watkins, UV and Visible Raman Study of Thermal Deactivation in a NO<sub>x</sub> Storage Catalyst. *Catalysis Letters* 95 (2004) 191-201.
- [27] D. Kim, Y. Chin, G. Muntean, A. Yereretz, N. Currier, W. Epling, H. Chen, H. Hess, C.H.F Peden, Relationship of Pt Particle Size to the NO<sub>x</sub> Storage Performance of Thermally Aged Pt/BaO/Al<sub>2</sub>O<sub>3</sub> Lean NO<sub>x</sub> Trap Catalysts. *Industrial & Engineering Chemistry Research* 45 (2006) 8815-8821.
- [28] T.J. Toops, B.G. Bunting, K. Nguyen, A. Gopinath, Effect of engine-based thermal aging on surface morphology and performance of Lean NO<sub>x</sub> Traps. *Catalysis Today* 123 (2007) 285-293.
- [29] K. Nguyen, H. Kim, B.G. Bunting, T.J. Toops, C.S. Yoon, Rapid Aging of Diesel Lean NO<sub>x</sub> Traps by High-Temperature Thermal Cycling. SAE Technical Paper Series 2007-01-0470 (2007).
- [30] M. Casapu, J.-D. Grunwaldt, M. Maciejewski, A. Baiker, S. Eckhoff, U. Göbel, M. Wittrock, The fate of platinum in Pt/Ba/CeO<sub>2</sub> and Pt/Ba/Al<sub>2</sub>O<sub>3</sub> catalysts during thermal aging. *Journal of Catalysis* 251 (2007) 28-38.



- [31] D.H. Kim, Y.-H. Chin, J.H. Kwak, C.H.F. Peden, Promotional Effects of H<sub>2</sub>O Treatment on NO<sub>x</sub> Storage Over Fresh and Thermally Aged Pt–BaO/Al<sub>2</sub>O<sub>3</sub> Lean NO<sub>x</sub> Trap Catalysts. *Catalysis Letters* 124 (2008) 39-45.
- [32] B.H. Jang, T.H. Yeon, H.S Han, Y.K. Park, J.E. Yie, Deterioration Mode of Barium-Containing NO<sub>x</sub> Storage Catalyst. *Catalysis Letters* 77 (2001) 21-28.
- [33] S. Elbouazzaoui, X. Courtois, P. Marecot, D. Duprez, Characterization by TPR, XRD, and NO<sub>x</sub> Storage Capacity Measurements of the Aging by Thermal Treatment and SO<sub>2</sub> Poisoning of a Pt/Ba/Al NO<sub>x</sub>-trap Model Catalyst. *Topics in Catalysis*. 30/31 (2004) 493-496.
- [34] M. Casapu, J. Grunwaldt, M. Maciejewski, M. Wittrock, U. Göbel, A. Baiker, Formation and Stability of Barium Aluminate and Cerate in NO<sub>x</sub> Storage-Reduction Catalysts. *Applied Catalysis B: Environmental* 63 (2006) 232-242.
- [35] M. Casapu, J. Grunwaldt, M. Maciejewski, A. Baiker, M. Wittrock, U. Göbel, S. Eckhoff, Thermal Aging Phenomena and Strategies Towards Reactivation of NO<sub>x</sub>-Storage Catalysts. *Topics in Catalysis* 42-43 (2007) 3-7.
- [36] D.H. Kim, Y.-H. Chin, J.H. Kwak, J. Szanyi, C.H.F. Peden, Changes in Ba Phases in BaO/Al<sub>2</sub>O<sub>3</sub> upon Thermal Aging and H<sub>2</sub>O Treatment. *Catalysis Letters* 105 (2005) 259-268.
- [37] D.H. Kim, J.H. Kwak, J. Szanyi, S.D. Burton, C.H.F. Peden, Water-Induced Bulk Ba(NO<sub>3</sub>)<sub>2</sub> Formation from NO<sub>2</sub> Exposed Thermally Aged BaO/Al<sub>2</sub>O<sub>3</sub>. *Applied Catalysis B: Environmental* 72 (2007) 233-239.
- [38] R. Strobel, F. Krumeich, S.E. Pratsinis, A. Baiker, Flame-derived Pt/Ba/Ce<sub>x</sub>Zr<sub>1-x</sub>O<sub>2</sub>: Influence of Support on Thermal Deterioration and Behavior as NO<sub>x</sub> Storage-Reduction Catalysts. *Journal of Catalysis* 243 (2006) 229-238.

- [39] M. Yang, Y. Li, J. Wang, M. Shen, Effects of CO<sub>2</sub> and Steam on Ba/Ce-Based NO<sub>x</sub> Storage Reduction Catalysts during Lean Aging. *Journal of Catalysis* 271 (2010) 228-238.
- [40] Y. Ji, C. Fisk, V. Easterling, U. Graham, A. Poole, M. Crocker, J.-S. Choi, W.P. Partridge, K. Wilson, *Catal. Today* 151 (2010) 362.
- [41] Y. Ji, J.S. Choi, T.J. Toops, M. Crocker, M. Naseri, Influence of Ceria on the NO<sub>x</sub> Storage/Reduction Behavior of Lean NO<sub>x</sub> Trap Catalysts. *Catalysis Today* 136 (2008) 146-155.
- [42] L. Xu, R. McCabe, W. Ruona, G. Cavataio, Impact of a Cu-zeolite SCR Catalyst on the Performance of a Diesel LNT+SCR System. *SAE Technical Paper Series* 2009-01-0285 (2009).
- [43] J.-S. Choi, W.P. Partridge, C.S. Daw, Spatially Resolved *in situ* Measurements of Transient Species Breakthrough during Cyclic, Low-Temperature Regeneration of a Monolithic Pt/K/Al<sub>2</sub>O<sub>3</sub> NO<sub>x</sub> Storage-Reduction Catalyst. *Applied Catalysis A: General* 293 (2005) 24-40.
- [44] J.-S. Choi, W.P. Partridge, W.S. Epling, N.W. Currier, T. M. Yonushonis, Intra-Channel Evolution of Carbon Monoxide and its Implication on the Regeneration of a Monolithic Pt/K/Al<sub>2</sub>O<sub>3</sub> NO<sub>x</sub> Storage-Reduction Catalyst. *Catalysis Today* 114 (2006) 102-111.
- [45] V. Perrichon, L. Retailleau, P. Bazin, M. Daturi, J.C. Lavalley, Metal Dispersion of CeO<sub>2</sub>-ZrO<sub>2</sub> Supported Platinum Catalysts Measured by H<sub>2</sub> or CO Chemisorption. *Applied Catalysis* 260 (2004) 1-8.

- [46] F. Fajardie, J.-F. Tempere, J.-M. Manoli, O. Touret, G. Djéga-Mariadassou, Thermal stability of (0.15–0.35 wt%) rhodium on low-loaded ceria-supported rhodium catalysts. *Catalysis Letters* 54 (1998) 187-193.
- [47] G.W. Graham, H.-W. Jen, W. Chun, R.W. McCabe, High-Temperature-Aging-Induced Encapsulation of Metal Particles by Support Materials: Comparative Results for Pt, Pd, and Rh on Cerium–Zirconium Mixed Oxides *Journal of Catalysis* 182 (1999) 228-233.
- [48] H. Schaper, E.B.M. Doesburg, L.L. van Reijen, The Influence of Lanthanum Oxide on the Thermal Stability of Gamma Alumina Catalyst Supports. *Applied Catalysis* 7 (1983) 211-220.
- [49] J.-S. Choi, W.P. Partridge, M.J. Lance, L.R. Walker, J.A. Pihl, T.J. Toops, C.E.A. Finney, C.S. Daw, Nature and Spatial Distribution of Sulfur Species in a Sulfated Barium-Based Commercial Lean NO<sub>x</sub> Trap Catalyst. *Catalysis Today* 151 (2010) 354-361.
- [50] D.H. Kim, J. Szanyi, J.H. Kwak, T. Szailer, J. Hanson, C.M. Wang, C.H.F. Peden, Effect of Barium Loading on the Desulfation of Pt-BaO/Al<sub>2</sub>O<sub>3</sub> Studied by H<sub>2</sub> TPRX, TEM, Sulfur K-edge XANES, and in Situ TR-XRD. *Journal of Physical Chemistry B* 110 (2006) 10441-10448.
- [51] V. Easterling, Y. Ji, M. Crocker, J. Ura, J.R. Theis, R.W. McCabe, Effect of Ceria on the Desulfation Characteristics of Model Lean NO<sub>x</sub> Trap Catalysts. *Catalysis Today* 151 (2010) 338–346.
- [52] J. Kašpar, P. Fornasiero, M. Graziani, Use of CeO<sub>2</sub>-Based Oxides in the Three-Way Catalysis. *Catalysis Today* 50 (1999) 285-298.

- [53] Y. Ji, T.J. Toops, M. Crocker, Effect of Ceria on the Storage and Regeneration Behavior of a Model Lean NO<sub>x</sub> Trap Catalyst. *Catalysis Letters* 119 (2007) 257-264.
- [54] Y. Ji, T.J. Toops, U.M. Graham, G. Jacobs, M. Crocker, A Kinetic and DRIFTS Study of Supported Pt Catalysts for NO Oxidation. *Catalysis Letters* 110 (2006) 29-37.
- [55] W.S. Epling, A. Yezerets, N.W. Currier, The Effect of Exothermic Reactions during Regeneration on the NO<sub>x</sub> Trapping Efficiency of a NO<sub>x</sub> Storage/Reduction Catalyst. *Catalysis Letters* 110 (2006) 143-148.
- [56] X. Chen, J. Schwank, J. Li, WF. Schneider, C.T. Goralski Jr., P.J. Schmitz, Thermal Decomposition of Dispersed and Bulk-Like NO<sub>x</sub> Species in Model NO<sub>x</sub> Trap Materials. *Applied Catalysis B: Environmental* 61 (2005) 164-175.
- [57] J.R. Theis, E. Gulari, Estimating the Temperatures of the Precious Metal Sites on a Lean NO<sub>x</sub> Trap during Oxidation Reactions. *Applied Catalysis B: Environmental* 75 (2007) 39-51.
- [58] R.D. Clayton, M.P. Harold, V. Balakotaiah, C.Z. Wan, Pt Dispersion Effects During NO<sub>x</sub> Storage and Reduction on Pt/BaO/Al<sub>2</sub>O<sub>3</sub> Catalysts. *Applied Catalysis B: Environmental* 90 (2009) 662-676.
- [59] J. Sjöblom, K. Papadakis, D. Creaser, C.U. I. Odenbrand, Use of Experimental Design in Development of a Catalyst System. *Catalysis Today* 100 (2005) 243-248.
- [60] H. Abdulhamid, E. Fridell, M. Skoglundh, The reduction phase in NO<sub>x</sub> Storage Catalysis: Effect of Type of Precious Metal and Reducing Agent. *Applied Catalysis B: Environmental* 62 (2006) 319-328.

- [61] R.G. Tonkyn, R.S. Disselkamp, C.H.F. Peden, Nitrogen Release from a NO<sub>x</sub> Storage and Reduction Catalyst. *Catalysis Today* 114 (2006) 94-101.
- [62] L. Cumaranatunge, S.S. Mulla, A. Yezerets, N.W. Currier, W.N. Delgass, F.H. Ribeiro, Ammonia is a Hydrogen Carrier in the Regeneration of Pt/BaO/Al<sub>2</sub>O<sub>3</sub> NO<sub>x</sub> Traps with H<sub>2</sub>. *Journal of Catalysis* 246 (2007) 29-34.
- [63] L. Castoldi, I. Nova, L. Lietti, P. Forzatti, Study of the Effect of Ba Loading for Catalytic Activity of Pt–Ba/Al<sub>2</sub>O<sub>3</sub> Model Catalysts. *Catalysis Today* 96 (2004) 43-52.
- [64] J.A. Pihl, J.E. Parks, C. Stuart Daw, T.W. Root, Product Selectivity During Regeneration of Lean NO<sub>x</sub> Trap Catalyst. SAE Tech. Paper 2006-01-3441, 2006.
- [65] R. Burch, The Investigation of Mechanisms in Environmental Catalysis Using Time-Resolved Methods. *Topics in Catalysis* 24 (2003) 97-102.
- [66] R. Burch, S.T. Daniells, P. Hu, The Mechanism of N<sub>2</sub>O Formation via the (NO)<sub>2</sub> Dimer: A Density Functional Theory Study. *Journal Chemical Physics* 121 (2004) 2737-2745.
- [67] W.C. Hecker, A.T. Bell, Reduction of NO by H<sub>2</sub> over Silica-Supported Rhodium: Infrared and Kinetic Studies. *Journal of Catalysis* 92 (1985) 247-259.
- [68] N. Macleod, R.M. Lambert, An in situ DRIFTS Study of Efficient Lean NO<sub>x</sub> Reduction with H<sub>2</sub> + CO over Pd/Al<sub>2</sub>O<sub>3</sub>: the Key Role of Transient NCO Formation in the Subsequent Generation of Ammonia. *Applied Catalysis B: Environmental* 46 (2003) 483-495.

- [69] R.D. Clayton, M.P. Harold, V. Balakotaiah, Selective Catalytic Reduction of NO by H<sub>2</sub> in O<sub>2</sub> on Pt/BaO/Al<sub>2</sub>O<sub>3</sub> Monolith NO<sub>x</sub> Storage Catalysts. *Applied Catalysis. B* 81 (2008) 161-181.
- [70] E. Shustorovich and A.T. Bell, Decomposition and Reduction of NO on Transition Metal Surfaces: Bbond Order Conservation Morse Potential Analysis. *Surface Science* 289 (1993) 127-138.
- [71] R. Burch, T. Watling, Adsorbate-Assisted NO Decomposition in NO Reduction by C<sub>3</sub>H<sub>6</sub> over Pt/Al<sub>2</sub>O<sub>3</sub> Catalysts under Lean-Burn Conditions. *Catalysis Letters* 37 (1996) 51-55.
- [72] I. Nova, L. Castoldi, L. Lietti, E. Tronconi, and P. Forzatti, How to Control the Selectivity in the Reduction of NO<sub>x</sub> with H<sub>2</sub> over Pt-Ba/Al<sub>2</sub>O<sub>3</sub> Lean NO<sub>x</sub> Trap Catalysts. *Topics in Catalysis* 42–43, (2007) 21-25.
- [73] M. Abul-Milh, H. Westberg, Reduction of NO<sub>2</sub> Stored in a Commercial Lean NO<sub>x</sub> Trap at Low Temperatures. *Topics in Catalysis* 42-43 (2007) 209-214.
- [74] D. Bhatia, M.P. Harold, V. Balakotaiah, A Global Kinetic Model for NO<sub>x</sub> Storage and Reduction on Pt/BaO/Al<sub>2</sub>O<sub>3</sub> Monolithic Catalysts. *Catalysis Today* 151 (2010) 314-329.
- [75] J.-S. Choi, W.P. Partridge, J.A. Pihl, C.S. Daw, Sulfur and Temperature Effects on the Spatial Distribution of Reactions Inside a Lean NO<sub>x</sub> Trap and Resulting Changes in Global Performance. *Catalysis Today* 136 (2008) 173-182.
- [76] J. Wang, Y. Ji, V. Easterling, M. Crocker, M. Dearth, R.W. McCabe, The Effect of Regeneration Conditions on the Selectivity of NO<sub>x</sub> Reduction in a Fully Formulated Lean NO<sub>x</sub> Trap Catalyst. *Catalysis Today* 175 (2011) 83-92

- [77] S.S. Mulla, S.S. Chaugule, A. Yezerets, N.W. Currier, W.N. Delgass, F.H. Ribeiro, Regeneration Mechanism of Pt/BaO/Al<sub>2</sub>O<sub>3</sub> Lean NO<sub>x</sub> Trap Catalyst with H<sub>2</sub>. *Catalysis Today* 136 (2008) 136-145.
- [78] J. Wang, M. Crocker, unpublished data.
- [79] A. Martínez-Arias, M. Fernández-García, A. Iglesias-Juez, A.B. Hungria, J.A. Anderson, J.C. Conesa, J. Soria, Influence of Thermal Sintering on the Activity for CO–O<sub>2</sub> and CO–O<sub>2</sub>–NO Stoichiometric Reactions over Pd/(Ce, Zr)O<sub>x</sub>/Al<sub>2</sub>O<sub>3</sub> Catalysts. *Applied Catalysis B: Environmental* 38 (2002) 151-158.
- [80] H. Kubicka, The Specific Activity of Technetium, Rhenium, Ruthenium, Platinum, and Palladium in Catalytic Reactions of Benzene with Hydrogen. *Journal of Catalysis* 12 (1968) 223-227.

## **Chapter 5. Application of SpaciMS to the Study of Ammonia Formation in Lean NO<sub>x</sub> Trap Catalysts.**

**Note** - This chapter was published as an article in the following journal:

V. Easterling, Y. Ji, M. Crocker, M. Dearth, R.W. McCabe, Application of SpaciMS to the Study of Ammonia Formation in lean NO<sub>x</sub> Trap Catalysts. *Catalysis Today* 151 (2010) 338–346.

The article appears in this dissertation with permission from the publisher.

### *5.1. Introduction.*

Recent years have witnessed concerted efforts to reduce NO<sub>x</sub> emissions from mobile sources of lean exhaust gas using lean NO<sub>x</sub> trap (LNT) or selective catalytic reduction (SCR) catalysts. Although both technologies have many positive features, each approach has drawbacks which have slowed their application to the automotive marketplace. For LNT catalysts, one of the main disadvantages is the cost associated with the use of platinum group metals (PGMs), while for SCR, the cost of the injection system and refilling of the NH<sub>3</sub> source adds to the consumer's costs. However, recent studies have shown that by combining LNT and SCR catalysts in series, these drawbacks can be lessened [1-5]. In this configuration the SCR catalyst functions in a passive or in situ mode, i.e., with the storage and utilization of NH<sub>3</sub> generated by the LNT during rich purge events. Given that the presence of the SCR catalyst relaxes the NO<sub>x</sub> conversion requirements of the LNT catalyst, the volume of the LNT in the LNT-SCR system can, in principle, be lower than for an LNT-only system, thereby reducing the precious metal costs. Furthermore, the need for a urea injection system is eliminated.

To realize a LNT-SCR system capable of achieving these aims, an understanding is required of the interplay between system operating parameters and the underlying chemistry of NO<sub>x</sub> reduction. Probably the most important aspects to be considered are the generation of NH<sub>3</sub> over the LNT, and its subsequent reaction with NO<sub>x</sub> over the SCR catalyst. A potential problem in studying these processes in a LNT-SCR system is the



integral nature of the catalysts. Reactants and products can react, adsorb, and desorb multiple times before exiting the system. This makes the study of LNT-SCR systems difficult using traditional laboratory techniques based on analysis of the reactor effluent.

To overcome these problems, spatially resolved capillary inlet mass spectrometry (SpaciMS), developed at Oak Ridge National Laboratory, has been applied to monitor the composition of simulated exhaust gas as it passes through LNT catalysts [6-14]. The key feature of a SpaciMS system is the use of a capillary connected to the sample cell of a mass spectrometer. The capillary allows the internal gas stream to be analyzed at different points along the length of the LNT or SCR catalyst under study. Consequently, the gaseous components present can be monitored on both a spatial and temporal scale. Partridge et al. employed SpaciMS to study  $\text{NH}_3$  formation and utilization over a Pt/Ba/ $\text{Al}_2\text{O}_3$  catalyst during regeneration with  $\text{H}_2$  [10]. It was found that  $\text{NH}_3$  was formed at the same time as the  $\text{N}_2$  product inside the catalyst during regeneration, and was consumed as aggressively as the  $\text{H}_2$  reductant along the catalyst. From this it was concluded that the intermediate  $\text{NH}_3$  regeneration pathway plays an important role in LNT catalyst regeneration. The same research group also utilized this technique to study the effect of sulfur on the spatiotemporal distribution of  $\text{NO}_x$  storage and reduction [11]. Prior to sulfation,  $\text{NO}_x$  storage/reduction was found to be localized in the front portion of catalyst, whereas sulfation resulted in a shift of the  $\text{NO}_x$  storage/reduction (NSR) zone downstream, thereby decreasing the length of the downstream zone in which only oxygen was stored. These workers also reported an increase in selectivity to  $\text{NH}_3$  after sulfation, and ascribed it to decreased oxidation of  $\text{NH}_3$  slipping from the NSR zone by the oxygen stored downstream [11,12]. A more recent study by this group further demonstrated that  $\text{NH}_3$  slip at the catalyst exit increased with sulfur loading due to its formation closer to the catalyst outlet and decreased  $\text{NH}_3$  conversion by stored oxygen downstream of the NSR zone [13]. Moreover, during catalyst regeneration the extent of  $\text{NO}_x$  readsorption downstream of the NSR zone was found to diminish after sulfation, resulting in earlier and broader  $\text{NO}_x$  peaks at the catalyst outlet. The SpaciMS technique was also applied in another recent LNT study by Luo et al. [14] in which catalyst desulfation was examined. For a partially sulfated commercial catalyst, the plug-like sulfur profile was redistributed

after desulfation at 600 °C as a result of re-adsorption. The extent of re-adsorption was found to be determined by the catalyst formulation and sulfation degree.

We have previously investigated the effect of regeneration conditions on NH<sub>3</sub> formation in LNT catalysts [15]. One of the findings from these studies was that NH<sub>3</sub> selectivity is dependent on the local H<sub>2</sub>:NO<sub>x</sub> ratio at the precious metal sites. Increasing the regeneration time or reductant concentration fed to the catalyst increases this ratio and thereby increases the amount of NH<sub>3</sub> formed, as opposed to N<sub>2</sub>. Conversely, increasing the amount of NO<sub>x</sub> stored decreases the selectivity to NH<sub>3</sub>. It was also observed that the addition of a ceria-based oxygen storage material to a Pt/Rh/BaO/Al<sub>2</sub>O<sub>3</sub> catalyst caused a decrease in NH<sub>3</sub> selectivity [15-18], which was explained on the basis that consumption of reductant by stored oxygen results in decreased H<sub>2</sub>:NO<sub>x</sub> ratios during regeneration, which favors the formation of N<sub>2</sub> over NH<sub>3</sub>. In addition, oxygen stored in the rear of the catalyst can consume NH<sub>3</sub> formed upstream via oxidation to produce N<sub>2</sub>, NO, or N<sub>2</sub>O. After aging, increased selectivity to NH<sub>3</sub> was observed, for both the ceria-containing and ceria-free catalyst. In principle, this increase in selectivity to NH<sub>3</sub> can be accounted for by any one of a number of factors [15]:

- (i) Aging-induced Pt sintering, resulting in Pt-Ba phase segregation. Consequently, the rate of NO<sub>x</sub> transport to the Pt sites during regeneration is decreased. As Harold and co-workers have pointed out [19], if this rate is slower than the H<sub>2</sub> feed rate, then H<sub>2</sub> will break through with substantially more NO<sub>x</sub> remaining on the catalyst. Consequently, the Pt surface will be predominantly covered by hydrogen, and as the stored NO<sub>x</sub> diffuses to the Pt particles, NH<sub>3</sub> will be formed with high selectivity. Modeling studies confirm this idea, i.e., that NH<sub>3</sub> formation is favored when solid-phase diffusion of NO<sub>x</sub> to the Pt/Ba interface is the rate determining process, which becomes increasingly likely as the Pt dispersion decreases [20].
- (ii) For a fixed concentration of reductant, the decreased oxygen storage capacity (OSC) of the aged catalysts should result in higher effective H<sub>2</sub>:NO<sub>x</sub> ratios in the reduction front due to decreased reductant consumption by stored oxygen, thereby

favoring  $\text{NH}_3$  formation. Furthermore, there is less oxygen available downstream of the reductant front to react with formed  $\text{NH}_3$ .

- (iii) After aging, there are fewer  $\text{NO}_x$  storage sites available per unit of catalyst length. This should result in higher effective  $\text{H}_2:\text{NO}_x$  ratios in the reductant front, again favoring  $\text{NH}_3$  formation [15].
- (iv) The length of the  $\text{NO}_x$  storage-reduction zone increases due to the decrease in  $\text{NO}_x$  storage capacity (NSC) as the catalyst ages [11,12,15]. More  $\text{NH}_3$  slips from the LNT without being oxidized because the increased length of the NSR zone decreases the length of the downstream OSC-only zone.
- (v) After aging, higher  $\text{NH}_3$  emissions may result from decreases in the rates of  $\text{NH}_3$  consumption via reaction with  $\text{NO}_x$  or  $\text{O}_2$  stored downstream of the reaction front.

From the foregoing, it is evident that  $\text{NH}_3$  selectivity after aging is likely to be dependent – at least in part – on the residual OSC of the catalyst, as well as the amount of  $\text{NO}_x$  stored. In an effort to distinguish between the factors that can account for increased LNT selectivity to  $\text{NH}_3$  after aging, in this study we adjusted the amount of reductant used to regenerate each catalyst (degreened and thermally aged) based on the OSC of the catalyst and the  $\text{NO}_x$  storage capacity (NSC). In this way we attempted to correct for the change in catalyst OSC and NSC after aging, thereby eliminating these as factors. SpaciMS was used to monitor the  $\text{NO}_x$  storage and reduction processes for degreened and aged catalysts in order to investigate the contribution of other factors to  $\text{NO}_x$  reduction selectivity.

## 5.2. Experimental.

### 5.2.1. Catalyst Preparation.

Two fully formulated Ba-based LNT catalysts were used in this study, the compositions of which are shown in Table 5.1. For simplicity, the BaO-only formulation is denoted as B-225 (where 225 refers to the washcoat loading in g/L), while the catalyst containing both BaO and  $\text{CeO}_2$  is denoted as BC-175 (containing a washcoat loading of 175 g/L). Details of the catalyst preparation have been described elsewhere [16,17]. In both cases, the washcoat was applied to a 4” x 6” cordierite monolith substrate, possessing a cell density of 400 cpsi and a wall thickness of 6.5 mil. The BaO component (21.5 wt %) was

supported on  $\gamma$ -alumina, while bare alumina was also used as a balance to bring the total washcoat loadings to the values indicated in Table 5.1.

**Table 5.1. Composition of catalysts used in this study.**

Component	Catalyst code / nominal loading	
	B-225	BC-175
Pt, g/L	3.05	2.38
Rh, g/L	0.61	0.48
BaO <sup>a</sup> , g/L	26	20
CeO <sub>2</sub> <sup>b</sup> , g/L	0	67
$\gamma$ -Al <sub>2</sub> O <sub>3</sub> <sup>c</sup> , g/L	Balance	Balance
Total washcoat, g/L	225	175

<sup>a</sup> 21.5 wt% supported on  $\gamma$ -Al<sub>2</sub>O<sub>3</sub>.

<sup>b</sup> Stabilized with 5 wt% La<sub>2</sub>O<sub>3</sub>.

<sup>c</sup> Stabilized with 3 wt% La<sub>2</sub>O<sub>3</sub>.

### 5.2.2 Catalyst Aging.

A 1.75 cm x 2.54 cm (d x l) core was drilled out from the LNT monolith and was wrapped with ceramic fiber and positioned in a quartz tube. Degreening the catalyst consisted of exposing the catalyst to neutral conditions (5% CO<sub>2</sub>, 5% H<sub>2</sub>O, balance N<sub>2</sub>) at 800 °C for 2 h. Aging the catalyst involved subjecting the catalyst to continuous lean conditions (8% O<sub>2</sub>, 5% CO<sub>2</sub>, 5% H<sub>2</sub>O, and balance N<sub>2</sub>) at 800 °C for 24 h. In both cases, the gas flow was adjusted to give a GHSV of 30,000 h<sup>-1</sup>.

### *5.2.3. Catalyst Characterization.*

#### *5.2.3.1. N<sub>2</sub> Physisorption.*

Surface area and pore volume analysis was performed according to the BET method by nitrogen adsorption at -196 °C using a Micromeritics Tri-Star system. Prior to the measurements catalyst samples (washcoat and monolith) were ground to a fine powder and outgassed overnight at 160 °C under vacuum.

#### *5.2.3.2. Pulsed H<sub>2</sub> Chemisorption.*

The dispersion of precious metal (Pt + Rh) was determined with a Micromeritics AutoChem II Analyzer by means of pulsed H<sub>2</sub> chemisorption at dry ice temperature (-78 °C). This temperature was chosen in an effort to minimize H spillover from the metal to the support material [21]. 1 g of sample (as a fine powder), including both washcoat and substrate, was loaded into the reactor. After being oxidized at 400 °C in 10% O<sub>2</sub>/He for 15 min, followed by reduction at 300 °C in 10% H<sub>2</sub>/Ar for 15 min, the catalyst was heated to 400°C (hold time 10 min) in flowing Ar to remove adsorbed H. Pulsed H<sub>2</sub> chemisorption was initiated using a four-way valve after the catalyst had been cooled to -78 °C. During this measurement, 0.5 mL of 10% H<sub>2</sub>/Ar was pulsed into the reactor every 2 min, the H<sub>2</sub> signal at the reactor outlet being monitored with a thermal conductivity detector (TCD). H<sub>2</sub> pulsing was terminated after the TCD signal had reached a constant value, i.e., the total precious metal (Pt + Rh) sites were saturated with H<sub>2</sub>. Assuming a 1:1 ratio of atomic hydrogen to surface Pt or Rh, the metal dispersion was calculated based on the amount of H adsorbed.

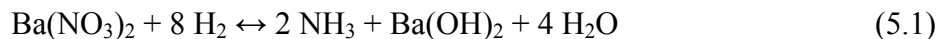
### *5.2.4. SpaciMS Measurements.*

#### *5.2.4.1. Determination of the Amount of Reductant Required for Catalyst Regeneration.*

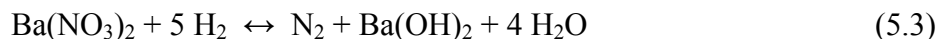
Determination of the amount of reductant required for catalyst regeneration was based on the catalyst oxygen storage capacity (OSC) and the amount of NO<sub>x</sub> stored during lean-rich cycling. Hydrogen was measured using a V & F Airsense H-sense mass spectrometer. All other species, i.e., NO, NO<sub>2</sub>, O<sub>2</sub>, H<sub>2</sub>O, and NH<sub>3</sub>, were measured using a V & F Airsense 2000 mass spectrometer using the low energy source, Hg, as the ion source; this enabled these species to be tracked individually, without interference from

other species present. The mass spectrometer had been modified for SpaciMS measurements by incorporating a 0.37 mm outer diameter (0.18 mm i.d.) stainless steel capillary connected to the sample chamber. The sampling rate was 14 sccm and data were collected at 3 Hz. After the SpaciMS was calibrated, the sample was purged by heating it to 450 °C under a 4.2% H<sub>2</sub> in N<sub>2</sub> flow until the NH<sub>3</sub> concentration measured by the SpaciMS fell to below 4 ppm at a position 1 mm from the rear of the catalyst. Once this level was achieved, the reactor temperature was dropped to the desired temperature (200 °C, 250 °C, or 300 °C) and the samples were exposed to 60 s lean/5 s rich cycles. The lean phase gas contained 8% O<sub>2</sub>, 5% CO<sub>2</sub>, 5% H<sub>2</sub>O, and balance N<sub>2</sub>, while the rich phase gas contained 4.2% H<sub>2</sub>, 5% CO<sub>2</sub>, 5% H<sub>2</sub>O, and balance N<sub>2</sub>. After 5 cycles the flow was switched from the outlet of the reactor to the reactor bypass so that the baseline hydrogen level could be measured. The OSC was determined by subtracting the cycle-averaged outlet H<sub>2</sub> concentration from the inlet H<sub>2</sub> concentration.

In separate experiments, the NO<sub>x</sub> storage capacity of the LNT was determined. The feed was switched to neutral conditions (5% CO<sub>2</sub>, 5% H<sub>2</sub>O, and balance N<sub>2</sub>), and once equilibrated, the catalyst was subjected to lean conditions for 60 s, using a feed consisting of 300 ppm NO, 8% O<sub>2</sub>, 5% CO<sub>2</sub>, 5% H<sub>2</sub>O, and balance N<sub>2</sub>. Simultaneously, the outlet NO<sub>x</sub> concentration was monitored by the SpaciMS probe at a position 1 mm from the rear catalyst face. At the end of the lean 60 s period, the SpaciMS probe was moved to a position 4 cm in front of the catalyst and the measurement was repeated. The difference between the two integrated NO<sub>x</sub> concentrations gave the amount of NO<sub>x</sub> stored. The amount of reductant required for LNT regeneration was then calculated from the sum of the measured OSC and 2.5 times the value of the NO<sub>x</sub> storage measurement. This factor of 2.5 represents the stoichiometry of NO<sub>x</sub> reduction by H<sub>2</sub> to give N<sub>2</sub> (assuming that NO<sub>x</sub> is stored as nitrate) as reported in the literature [22,23]:



The sum of reactions (5.1) and (5.2) leads to the overall stoichiometry for the reduction of Ba nitrate by H<sub>2</sub>:



#### 5.2.4.2. *NO<sub>x</sub> Storage and Reduction Measurements.*

With the required reductant amounts having been determined for each catalyst (both degreened and aged) at 200, 250, and 300 °C, NO<sub>x</sub> storage and reduction measurements were performed at these temperatures during 60 s lean/5 s rich cycles. The lean phase gas contained 300 ppm NO, 8% O<sub>2</sub>, 5% CO<sub>2</sub>, 5% H<sub>2</sub>O, and balance N<sub>2</sub>, while the rich phase gas contained the calculated amount of H<sub>2</sub> for each catalyst, 5% CO<sub>2</sub>, 5% H<sub>2</sub>O, and balance N<sub>2</sub>. Prior to the measurements, each sample was exposed to the cycling conditions until the component concentrations in the reactor effluent were constant from one cycle to the next. Once “stationary” cycles had been attained (~ 1 h), data pertaining to the concentrations of NO, NO<sub>2</sub>, O<sub>2</sub>, H<sub>2</sub>O and NH<sub>3</sub> were collected at different positions using SpaciMS. The first of these positions corresponded to the rear face of the catalyst (25.4 mm from the catalyst inlet), with successive sampling at, 16.4 mm, 8.4 mm, 4.4 mm, and the front face (0 mm from the inlet). By sampling in this manner (from rear to front), the chances of contaminating the capillary with particles from the washcoat of the catalyst were lessened. Note that the “0 mm” position actually corresponds to a position of 0.1 mm; this was done in order to ensure that the capillary was correctly aligned with the selected channel. Consequently, when feeding NO in the lean phase, some NO<sub>2</sub> (corresponding to ca. 15% NO conversion) was detected at the 0.1 mm position, arising from a combination of catalyzed NO oxidation in the first 0.1 mm of the catalyst and gas phase NO oxidation in the feed lines. For each position, the system was allowed to stabilize for two 60 s/5 s cycles before data were taken over five successive cycles. These cycles were then averaged to produce the spatio-temporal plots of species concentration versus time for each axial location.

NO<sub>x</sub> storage efficiency (NSE) is defined in this study as:

$$\frac{\text{Inlet concentration of } NO_x - \text{Concentration of } NO_x \text{ at measurement location}}{\text{Inlet concentration of } NO_x} * 100\% \quad (5.4)$$

Rich phase NO<sub>x</sub> release is defined as:

$$\frac{\text{Concentration of rich phase } NO_x \text{ release at measurement location}}{\text{Inlet lean concentration of } NO_x - \text{Outlet lean concentration of } NO_x} * 100\% \quad (5.5)$$

In both eqns. (5.4) and (5.5), all concentrations are cycle-averaged integrated values (ppm\*s).

### 5.3. Results and Discussion.

#### 5.3.1. Catalyst Characterization.

The results of N<sub>2</sub> physisorption and H<sub>2</sub> chemisorption measurements performed on the degreened and aged catalysts are collected in Table 5.2. Both catalysts displayed a small loss in surface area after aging, which for the B-225 sample was accompanied by a decrease in the pore volume. Sintering of the catalyst is evidenced by an increase in the average pore radius, which can be attributed to collapse of the smaller pores during aging. Comparing the PGM dispersions derived from H<sub>2</sub> chemisorption measurements, it is evident that exposure of the catalysts to high temperatures during aging resulted in significant PGM sintering. Indeed, for both catalysts, a decrease in PGM dispersion of ca. 75% was seen. These results are consistent with the degree of Pt sintering observed in a previous study in which model LNT catalysts were likewise subjected to continuous lean conditions at 800 °C for periods of up to 16 h [24].



**Table 5.2. Physical properties of degreened and aged catalysts.**

Catalyst	Total BET surface area (m <sup>2</sup> /g) <sup>a</sup>		Pore volume (cm <sup>3</sup> /g) <sup>a</sup>		Average pore radius (nm) <sup>a</sup>		PGM dispersion (%)	
	Degreened	Aged	Degreened	Aged	Degreened	Aged	Degreened	Aged
B-225	41.1	35.4	0.148	0.137	7.19	7.72	21.6	5.4
BC-175	26.3	25.4	0.105	0.109	7.96	8.56	9.8	2.5

<sup>a</sup> Includes cordierite monolith.

### 5.3.2. Amount of Reductant Required for Complete NO<sub>x</sub> Reduction during Rich Purging.

The minimum amount of reductant required to fully regenerate a LNT during lean-rich cycling can be determined from the oxygen storage capacity (OSC) and the NO<sub>x</sub> storage capacity (NSC). In this study, the H<sub>2</sub> concentration during lean-rich cycling was adjusted so that the degreened and aged catalysts would be exposed to a stoichiometric quantity of H<sub>2</sub> with respect to complete regeneration. This adjustment allows for a sounder basis when comparing fresh and aged catalysts in terms of the selectivity of NO<sub>x</sub> reduction, given that excess reductant would influence the selectivity towards NH<sub>3</sub> production. The results from these OSC and NSC measurements, performed on catalysts B-225 and BC-175, are shown in Fig. 5.1. The column chart is arranged such that the data for the non-ceria-containing catalyst B-225 are shown on the left half of the figure, while data for the ceria-containing catalyst are on the right. Each of the stacked columns shows the amount of H<sub>2</sub> required to consume the oxygen stored on the catalyst and to reduce the stored NO<sub>x</sub>. The fact that H<sub>2</sub> concentrations required for complete regeneration of BC-175 are greater than those for B-225 can be attributed to the presence of La-stabilized CeO<sub>2</sub> in BC-175. Comparing the OSC and NSC with temperature, it is apparent that for both the B-225 and BC-175 catalysts the measured values increase with temperature. This trend is expected for BC-175 since CeO<sub>2</sub> has increased OSC at higher temperatures due to the increased concentration of oxygen defect sites [25]. In addition, the NSC of Ba-based catalysts increases with temperature for the temperature range studied here [16,17].

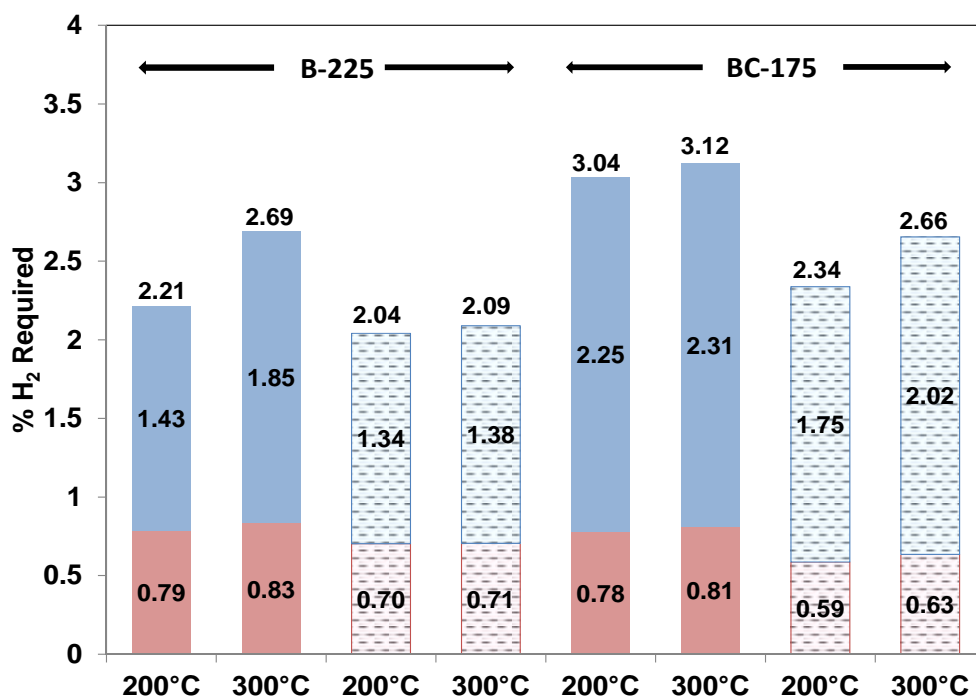


**Figure 5.1. Required amount of H<sub>2</sub> during 60 s lean – 5 s rich cycling for catalyst regeneration. Solid colors represent values for degreased catalysts and patterned colors represent values for aged catalysts. The blue or top values in the columns represent the oxygen storage capacities, and the red or bottom values represent the NO<sub>x</sub> storage capacities.**

Considering the aged catalysts, an obvious trend is that the amount of reductant required for catalyst regeneration decreases after aging due to decreases in OSC and NSC. During aging, Pt sintering occurs, leading to a decrease in the Pt-Ba interfacial perimeter [16,20], i.e., phase segregation occurs between the Pt and Ba storage sites [26-31]. Consequently, for a given length of catalyst, fewer storage sites are present and less reductant is needed. Additionally, agglomeration of the Pt during aging reduces the number of sites available for oxygen adsorption during lean conditions. Finally, in the case of BC-175, a significant portion of the decrease in OSC can be attributed to the loss of oxygen defect sites in the structure of the La-stabilized CeO<sub>2</sub> component after aging. Mamontov et al. [25] have shown that OSC correlates with defect site concentration rather than surface area, the latter being relatively unchanged after aging based on the negligible change in

total catalyst surface area (Table 5.2). Indeed, in their work Mamontov and co-workers found that significant decrease of OSC occurred upon aging a ceria sample at 800 °C. In addition, some contribution to the loss in OSC may come from the sintering of Pt supported on the CeO<sub>2</sub> component, given that Pt acts essentially as a conduit for oxygen storage and release.

### *5.3.3. Non-Ceria Containing Catalyst.*

#### *5.3.3.1. NO<sub>x</sub> Storage.*

Once the amounts of reductant required for catalyst regeneration were determined, the catalysts were subjected to NO<sub>x</sub> storage-reduction experiments. The non-ceria containing sample was subjected to 60/5 s cycles and evaluated at three temperatures: 200 °C, 250 °C, and 300 °C. Data pertaining to the measured lean NO<sub>x</sub> storage efficiencies (NSEs) are shown in Fig. 5.2. For degreened catalyst B-225 the NSE increases along the length of the catalyst (at all temperatures), while NSE also increases with temperature in the range studied. Maximum NSE values are reached around the midpoint of the catalyst, providing an indication of the length of the NO<sub>x</sub> storage zone under these experimental conditions. Additional detail is provided in Figs. 5.3a and 5.3b, in which the cycle-averaged NO and NO<sub>2</sub> concentrations are plotted at each measurement point along the length of the catalyst. For the degreened catalyst, a rapid decrease in the NO concentration begins at 4.4 mm, the NO concentration reaching zero by the 16.4 mm position. At this juncture, an explanation is required for the slight increase in NO and NO<sub>2</sub> concentrations observed in moving from the 16.4 to 25.4 mm positions in Fig. 5.3. As noted by Partridge and Choi [10], the SpaciMS system is capable of great sensitivity. This, combined with possible over-sampling at the rear of the catalyst (due to the high sampling rate and sampling position) can lead to the capillary sampling gas slightly beyond the rear of the catalyst. At this location the gas is comprised of the effluent from all of the channels in the catalyst. Bearing in mind that not all of the channels in the catalyst will have exactly the same amount of washcoat, the concentration of NO<sub>x</sub> just outside the rear of the catalyst can be different compared to the channel in which the capillary is located. Furthermore, the outer diameter of the capillary used in these experiments (0.37 mm) was significant compared to the channel width (1.1 mm). The

resulting restriction of the gas flow in the channel may result in a slightly different residence time, and hence gas composition, compared to the surrounding channels.

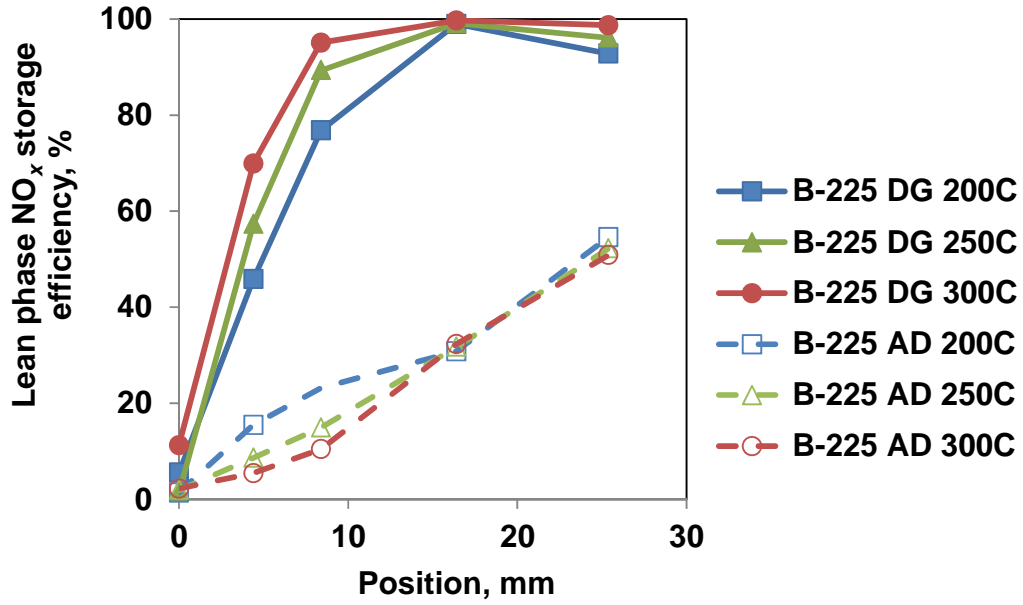


Figure 5.2. Lean NO<sub>x</sub> storage efficiency as a function of position for degreened (DG) and aged (AD) catalyst B-225.

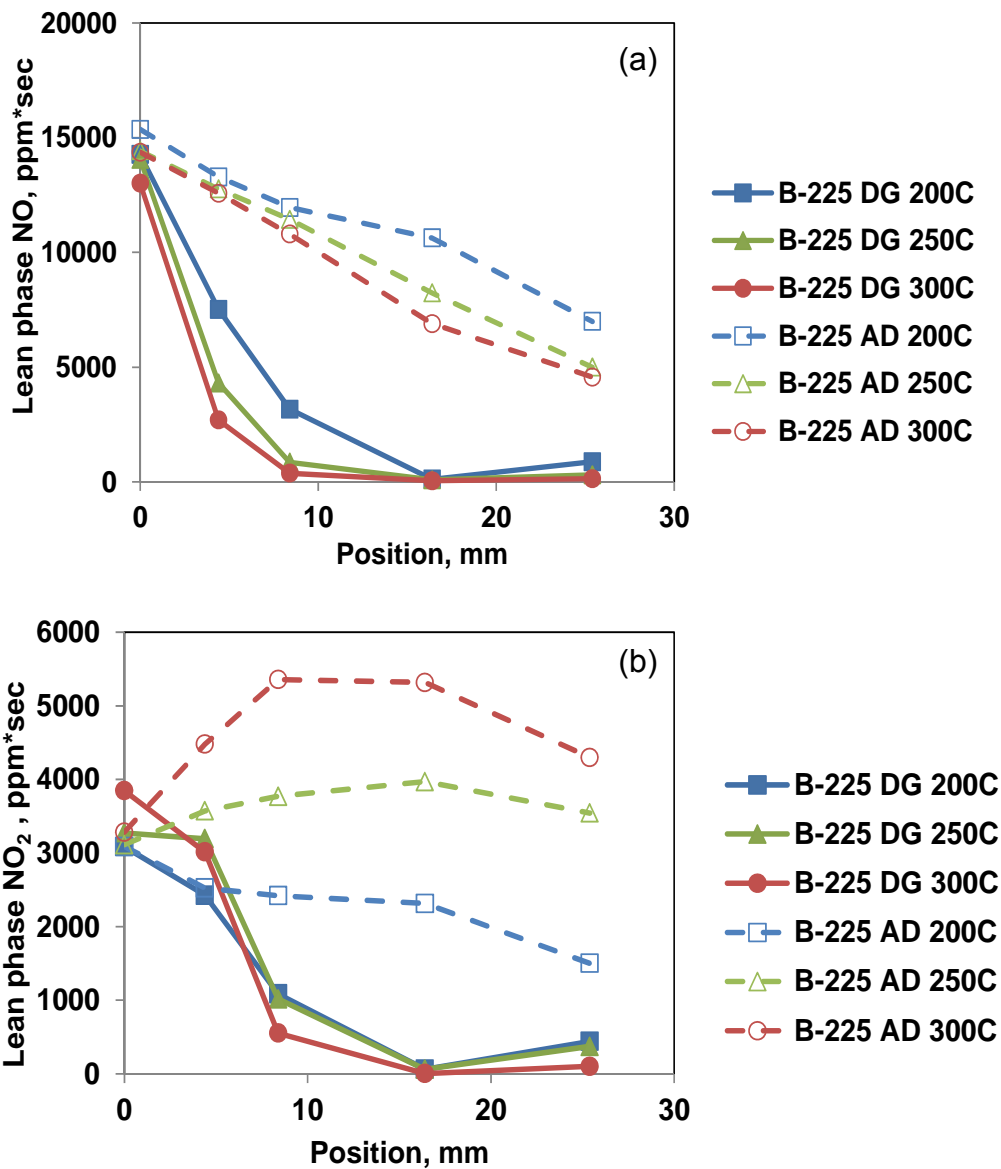
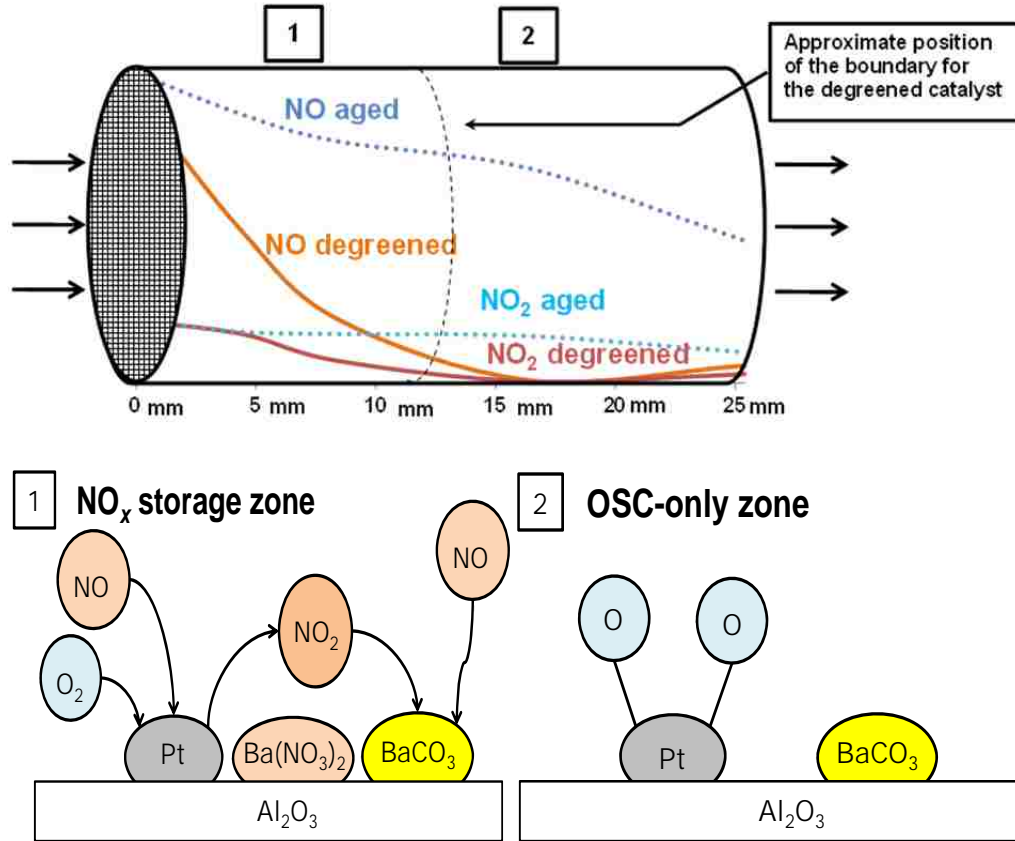


Figure 5.3. a) Lean phase NO concentration and b) lean phase NO<sub>2</sub> concentration as a function of position during NO<sub>x</sub> storage on degraded (DG) and aged (AD) catalyst B-225.

From Fig. 5.3a it is evident that the amount of NO present at each position increases with decreasing temperature. Conversely, the NO<sub>2</sub> concentrations increase with increasing temperature in the range 200-300 °C. These results are consistent with an increase in the

rate of oxidation of NO to NO<sub>2</sub> with increasing temperature. At 300 °C, the rate of NO<sub>2</sub> formation is fast relative to the linear gas velocity and NO<sub>2</sub> is stored in the front of the catalyst. At the lowest temperature, 200 °C, the slower rate of oxidation of NO results in the feed gas traveling further along the length of catalyst before NO<sub>2</sub> is generated and then stored. Consequently, more of the catalyst is used for NO<sub>x</sub> storage. This finding is consistent with a previous report that the length of the NSR zone decreases with increasing temperature [11]. In addition, at lower temperatures, a portion of the NO<sub>x</sub> can be stored as Ba(NO<sub>2</sub>)<sub>2</sub>, although the literature suggests that this pathway is fairly minor. For example, under their experimental conditions Forzatti and co-workers [4] found that at 200 °C ca. 20% of NO<sub>x</sub> was stored as Ba(NO<sub>2</sub>)<sub>2</sub> and 80% was stored as Ba(NO<sub>3</sub>)<sub>2</sub>. Fig. 5.4 provides a schematic of the NO<sub>x</sub> storage process and depicts the relative NO and NO<sub>2</sub> concentrations measured at 200 °C along the length of the catalyst.



**Figure 5.4. Schematic showing NO and NO<sub>2</sub> concentrations along the length of the catalyst and the mechanism of NO<sub>x</sub> storage under lean conditions. Note that the relative concentrations depicted correspond to actual data collected at 200 °C for catalyst B-225.**

Fig. 5.2 also contains the NSE results for the aged B-225 catalyst. In contrast to the data for the degreened catalyst, the NSE does not reach a maximum value within the length of the catalyst, indicating that the whole of the catalyst is used for NO<sub>x</sub> storage. Indeed, the maximum NSE after aging does not exceed 60% at any measurement temperature. Hence, the OSC-only zone in the schematic shown in Fig. 5.4 (which corresponds to zone 2) is effectively eliminated after aging. NSEs at the three temperatures are very similar, although because the data point at the 8.4 mm position in Fig. 5.2 is not available, the NSE at 200 °C appears to be greater than at 250 or 300 °C. This is largely a consequence of the missing point, given that at all of the other measurement points the values at each of the temperatures are very similar.

From Fig. 5.3a, it is evident that the NO concentrations measured for the aged sample decrease gradually compared to the degreened case, NO being present in significant concentrations throughout the entire length of the catalyst. As shown in Fig. 5.3b, the NO<sub>2</sub> concentrations increase along the catalyst before reaching a maximum and then decreasing. A comparison between the data collected for the degreened and aged catalyst at 200 °C is shown in Fig. 5.4. The increase in measured NO and NO<sub>2</sub> concentrations for the aged sample can be explained on the basis that the concentration of NO<sub>x</sub> storage sites is decreased after aging. Due to sintering of the Pt particles, the distance between Pt and Ba is increased, thereby necessitating that the NO<sub>2</sub> formed on Pt has to diffuse a greater distance to reach the Ba storage sites as compared to the degreened catalyst. This results in an effective decrease in the number of fast NO<sub>x</sub> storage sites with the consequence that NO<sub>2</sub> tends to travel downstream of the NO oxidation sites before eventually being stored. At the same time, it is evident that the NO oxidation function of the catalyst is degraded after aging. As noted above, the NO concentration decreases quite slowly along the length of the catalyst, whereas, a sharp drop-off in NO concentration is depicted in Fig. 5.3a for the degreened B-225 catalyst. This indicates that aging results in both a loss of NO oxidation sites and NO<sub>2</sub> storage sites relative to the degreened sample.

#### 5.3.3.2. NO<sub>x</sub> Reduction.

During NO<sub>x</sub> reduction experiments, the rich phase of the 60/5 s cycles contained a concentration of H<sub>2</sub> determined from the OSC/NSC study shown in Fig. 5.1, along with 5% CO<sub>2</sub>, 5% H<sub>2</sub>O, and balance N<sub>2</sub>. The resulting cycle-averaged NO<sub>x</sub> conversions are collected in Table 5.3. In general, cycle-averaged NO<sub>x</sub> conversion in lean-rich cycling experiments show a strong correlation with NO<sub>x</sub> storage efficiencies [16]. Comparing the cycle-averaged conversions in Table 5.3 with the lean NSE values shown in Fig. 5.2, a larger discrepancy is seen between the two values at 200 °C, as compared to 300 °C (Fig. 5.5). The source of this difference can be attributed to the 1 NO<sub>x</sub> “puff” that occurs at the beginning of the transition from lean to rich conditions. Data pertaining to the “puff” are depicted graphically in Fig. 5.6. For the degreened B-225 catalyst, the amount of rich NO<sub>x</sub> release decreases at 250 °C and 300 °C along the entire length of the catalyst, indicating that it is re-adsorbed and subsequently reduced. In contrast, at 200 °C the rich



NO<sub>x</sub> release increases along the length of the catalyst until 8.4 mm from the front of the catalyst and then decreases. This increased amount of NO<sub>x</sub> measured during the rich phase at 200 °C (and indeed emitted from the catalyst) can be explained on the basis that (i) NO<sub>x</sub> storage and release is moved further along the length of the catalyst at low temperatures [11,12], and (ii) the rich phase NO<sub>x</sub> release is greater at low temperatures due to the imbalance in the rates of NO<sub>x</sub> release and NO<sub>x</sub> reduction [16,17], i.e., a fraction of the NO<sub>x</sub> is rapidly released into the product stream but is not fully consumed by H<sub>2</sub>.

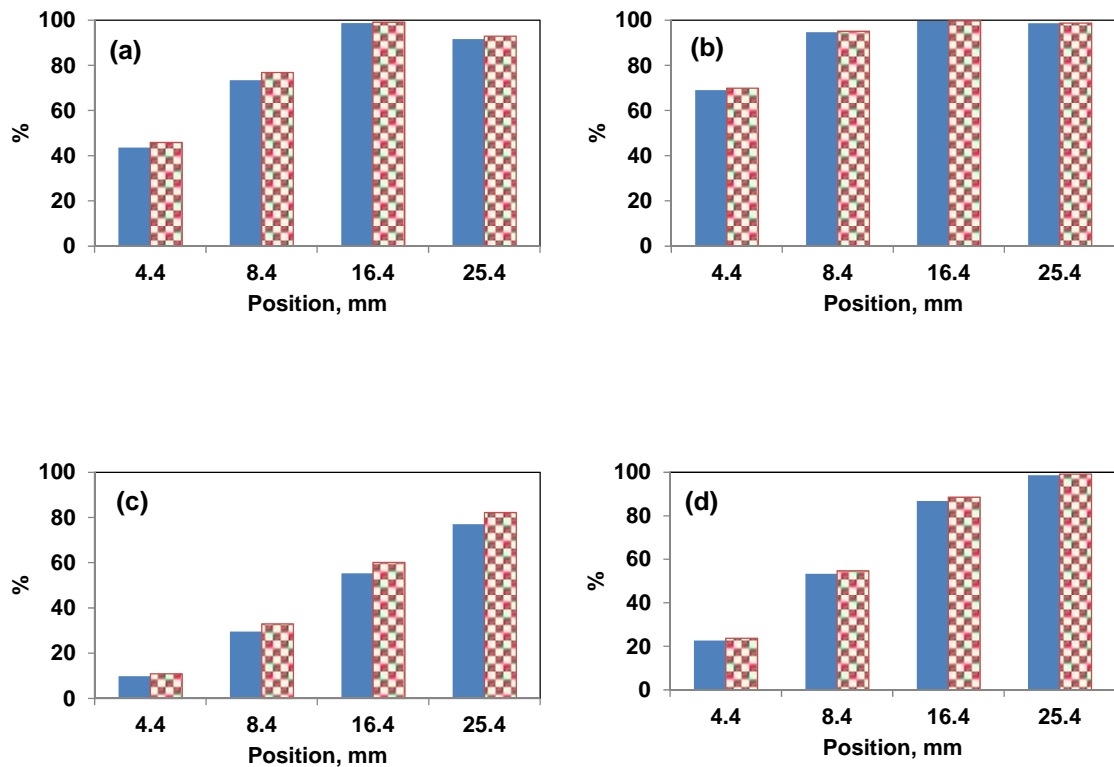


**Figure 5.5. Comparison of cycled-averaged NO<sub>x</sub> conversion (solid bars) and NO<sub>x</sub> storage efficiency (checkered bars) as a function of position for degreased catalysts: a) B-225 at 200 °C, b) B-225 at 300 °C, c) BC-175 at 200 °C, and d) BC-175 at 300 °C.**

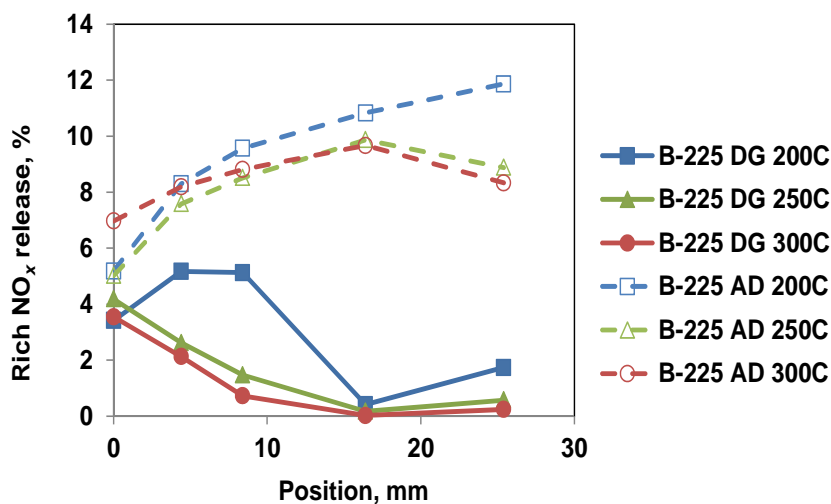


**Figure 5.6. Rich phase NO<sub>x</sub> release as a function of position during regeneration of degreened (DG) and aged (AD) catalyst B-225.**

Selectivity to NH<sub>3</sub> as a function of the sampling position in the catalyst is shown in Table 5.3 and Fig 5.7. Note that in this work N<sub>2</sub>O, the other possible NO<sub>x</sub> reduction product along with N<sub>2</sub> and NH<sub>3</sub>, was not monitored. For the degreened B-225 catalyst the NH<sub>3</sub> selectivity first increases from the front face of the catalyst, reaches a maximum close to the end of the NO<sub>x</sub> storage zone, and then decreases. In order to explain these findings, it is necessary to consider the reductant front as it moves along the axial length of the catalyst. According to the model proposed by Ribeiro and co-workers [32,33] and others [10,23,34,35], during LNT regeneration a H<sub>2</sub>-rich reaction front propagates along the length of the catalyst in which N<sub>2</sub> and NH<sub>3</sub> are formed from the reduction of the stored NO<sub>x</sub>. The formed NH<sub>3</sub> may then react further with nitrates stored downstream of the front, resulting in the formation of N<sub>2</sub>. This explains the temporal sequence of product formation, N<sub>2</sub> breakthrough occurring before NH<sub>3</sub>. Breakthrough of the NH<sub>3</sub> corresponds to the point at which the stored NO<sub>x</sub> and O<sub>2</sub> are sufficiently depleted for the NH<sub>3</sub> consumption to be incomplete.

**Table 5.3. Comparison of cycle-averaged NO<sub>x</sub> conversion and NH<sub>3</sub> selectivity during lean-rich cycling for degreened and aged catalysts.**

Catalyst	Temperature (°C)	Position (mm)	Cycle-averaged NO <sub>x</sub> conversion (%)		NH <sub>3</sub> selectivity (%)	
			Degreened	Aged	Degreened	Aged
B-225	200	4.4	43.6	13.6	6.4	2.4
		8.4	73.4	-- <sup>a</sup>	9.8	-- <sup>a</sup>
		16.4	98.7	27.2	4.3	7.5
		25.4	91.6	49.8	2.6	11.1
	300	4.4	69.0	4.7	9.3	0.8
		8.4	94.6	9.3	5.9	3.0
		16.4	99.7	30.0	0.4	11.9
		25.4	98.6	48.6	1.0	21.4
BC-175	200	4.4	9.8	7.6	6.1	1.0
		8.4	29.6	28.2	29.4	34.2
		16.4	55.4	54.4	56.2	60.4
		25.4	77.0	88.8	45.1	72.2
	300	4.4	22.7	8.1	3.7	1.6
		8.4	53.3	23.3	9.4	6.9
		16.4	86.8	56.0	8.6	15.2
		25.4	98.6	66.5	0.9	14.9

<sup>a</sup> Data not available for this position.

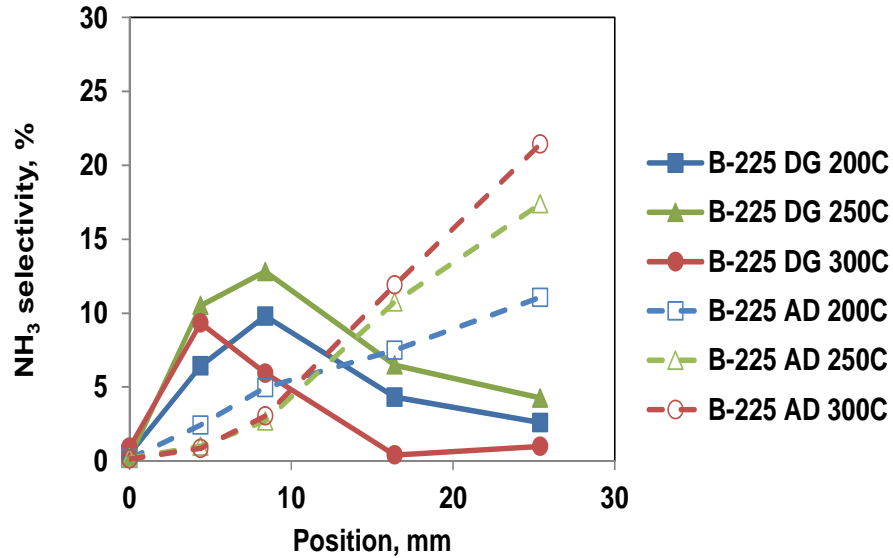


**Figure 5.7. Rich phase NH<sub>3</sub> selectivity as a function of position for degreened (DG) and aged (AD) catalyst B-225.**

During regeneration, a number of zones effectively exist in the catalyst (see Fig. 5.8) [11-13,34-36]. Upstream of the reductant front (zone 1), hydrogen has already consumed oxygen present on the Pt sites and depending on the temperature (vide infra), may or may not have reduced all of the stored NO<sub>x</sub>. The ratio of H<sub>2</sub> to residual NO<sub>x</sub> (if present) is high (given that the reduction front has already moved downstream), and hence NH<sub>3</sub> formation is favored. In the reductant front (zones 2 and 3), NH<sub>3</sub> is both generated and consumed. Downstream of the front (zone 4), NO<sub>x</sub> and adsorbed oxygen are present. The significance of this is that NH<sub>3</sub> produced in or behind the front can be consumed in the NO<sub>x</sub>-NH<sub>3</sub> SCR or NH<sub>3</sub>-O<sub>2</sub> reactions. Zone 5 corresponds to the OSC-only zone, i.e., the region downstream of the NSR zone.

Given that at moderate to high temperatures NO<sub>x</sub> reduction displays the characteristics of a feed-limited process [33,34,36], significant NO<sub>x</sub> reduction behind the reduction front is not expected in this temperature range, i.e., stored NO<sub>x</sub> should be fully consumed in the reduction front. However, Clayton et al. [35] have observed that at lower temperatures implication being that catalyst regeneration is limited by chemical processes at the Pt/Ba interface. This explains why catalyst selectivity to NH<sub>3</sub> increases significantly with

decreasing temperature, as illustrated by the data in Table 5.3. Modeling studies by the same group [20] have confirmed that  $\text{NH}_3$  generation is favored under conditions when  $\text{NO}_x$  transport to the Pt/Ba interface is the rate determining process. A contributing factor to the increased  $\text{NH}_3$  selectivity observed at low temperatures can be the slow kinetics of the  $\text{NO}_x$ - $\text{NH}_3$  SCR reaction [23]. However, several studies employing catalysts and conditions similar to those employed in the present work have shown that the SCR reaction typically lights off below 200 °C [23,35,37,38]; hence, this is not a factor in the case of degreened catalyst B-225.

Aging at 800 °C significantly affects the performance of the B-225 catalyst, as shown by the greatly decreased cycle-averaged  $\text{NO}_x$  conversions reported in Table 5.3. As shown, the  $\text{NO}_x$  conversions measured at 200 and 300 °C reach a maximum at the outlet of the catalyst (25.4 mm), reflecting the lengthening of the NSR zone after aging. This latter point is clearly apparent in Fig. 5.6, which shows that the rich phase  $\text{NO}_x$  release increases over the length of the catalyst rather than peaking within the first 8.4 mm (as seen for the degreened catalyst). The total amount of  $\text{NO}_x$  release is also greater than for the degreened sample. Higher  $\text{NO}_x$  release at 0.0 mm is explained by an increase in the imbalance of  $\text{NO}_x$  release and reduction rates. Aging results in sintering of the PGM sites and consequently the rate of reduction of  $\text{NO}_x$  by adsorbed hydrogen at these sites is slower [40]. Furthermore, for a given length of catalyst, there are now fewer sites located downstream for the  $\text{NO}_x$  in the gas phase to re-adsorb on the catalyst. This is due to the stretching of the  $\text{NO}_x$  storage zone, i.e., the storage sites downstream have already been filled.

As shown in Table 5.3 and Fig. 5.7, the selectivity to  $\text{NH}_3$  continues to increase to the end of the aged catalyst sample. For the degreened sample maximum  $\text{NH}_3$  release is seen towards the end of the  $\text{NO}_x$  storage zone; given that the NSR zone now encompasses the entire length of the sample, it follows that  $\text{NH}_3$  selectivity reaches a maximum towards the rear of the sample. Indeed, as shown in Fig. 5.8, for the degreened sample both the  $\text{NH}_3$  and  $\text{NO}$  concentrations reach a maximum within the first 10 mm of the catalyst, whereas these concentrations continue to increase along the length of the catalyst for the

aged sample. For the aged catalyst, two additional effects must be considered. First, stretching of the storage-reduction zone results in the elimination of the downstream OSC-only zone. Therefore, the  $\text{NH}_3$  that is formed is less likely to be consumed by adsorbed oxygen downstream of the reduction front. Second, as discussed in the Introduction, segregation of the Pt and Ba phases during aging results in a decrease in the rate of  $\text{NO}_x$  transport (reverse spillover) to the Pt sites. Consequently, the Pt surface will be predominantly covered by hydrogen, and as the stored  $\text{NO}_x$  diffuses to the Pt particles,  $\text{NH}_3$  will be preferentially formed.

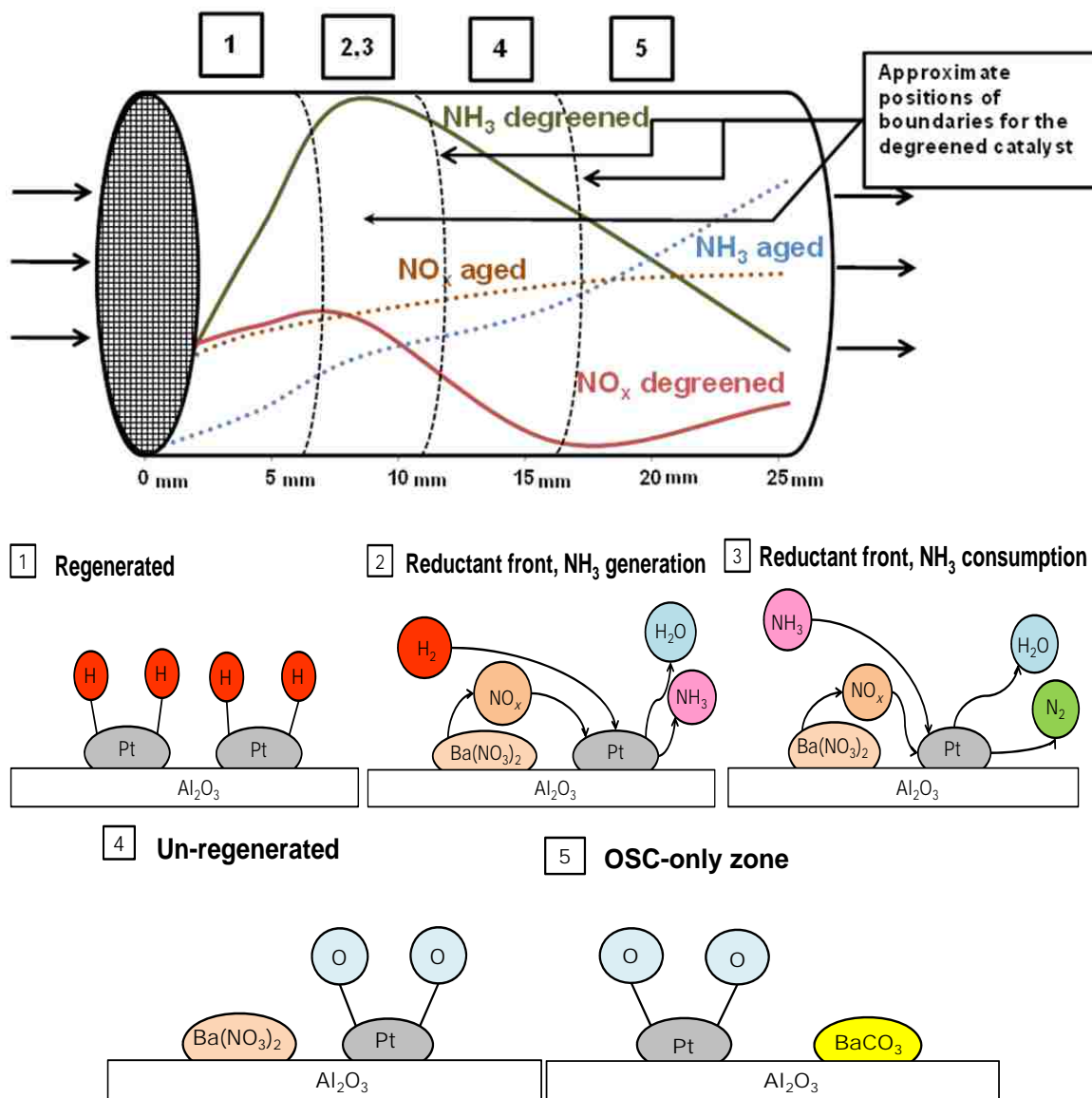


**Figure 5.8. Schematic showing  $\text{NO}_x$  and  $\text{NH}_3$  concentrations along the length of the catalyst and the mechanism of  $\text{NO}_x$  reduction under rich conditions (after Pihl et al. [38]). Note that the relative concentrations depicted correspond to actual data collected at 200 °C for catalyst B-225.**

Analysis of the temporal data provides additional insights. In Figs. 5.9a and 5.9b,  $\text{NH}_3$  concentrations are plotted versus time at each sampling position for the degreened and aged catalysts, respectively. Note that in the plots, the feed gas was switched from lean to rich at 31 s. Examining the data for the degreened catalyst in Fig. 5.8a, the  $\text{NH}_3$  concentration increases from the front of the catalyst until the midpoint of the catalyst

(between the 8.4 mm and 16.4 mm positions). Furthermore, a delay is present in the appearance of  $\text{NH}_3$  from one sampling position to the next over the length of the catalyst. For example, at the 4.4 mm position, a  $\sim 1$  s delay from the onset of rich conditions to the appearance of  $\text{NH}_3$  exists, with additional delays at each of the subsequent measurement points. This finding is consistent with previous reports [10,35] and is evidence that significant  $\text{H}_2$  consumption precedes  $\text{NH}_3$  formation, i.e., due to the reaction of  $\text{H}_2$  with stored oxygen and  $\text{NO}_x$  to generate  $\text{N}_2$ . The decrease in  $\text{NH}_3$  concentration that begins between the 8.4 mm and 16.4 mm positions and continues until the rear of catalyst demonstrates that some of the  $\text{NH}_3$  is being consumed before reaching the end of the catalyst.

Comparing these results with the data for the aged catalyst, a clear difference is the lack of delay between the appearance of  $\text{NH}_3$  at each measurement point in the aged catalyst. Indeed, as shown in Fig. 5.9b, the initiation of  $\text{NH}_3$  release at the different sampling locations occurs almost simultaneously for the aged sample. These observations clearly indicate that the reductant front propagates more rapidly along the length of the aged catalyst than the degreened sample. This increase in the velocity of the front can be attributed in part to the lower amounts of  $\text{NO}_x$  and  $\text{O}_2$  stored in the front of the catalyst. Similar reasoning has been used to explain the acceleration in the  $\text{H}_2$  front typically observed along the length of LNT catalysts during regeneration, i.e., since more  $\text{NO}_x$  is stored in the front of a given catalyst, more  $\text{H}_2$  is needed to reduce the stored  $\text{NO}_x$  and so the front propagates more slowly in this region than in the rear of the catalyst [36]. Additionally, if  $\text{NO}_x$  is released more slowly from storage sites (due to Pt-Ba phase segregation), such that the kinetics of  $\text{NO}_x$  reduction are controlled by the rate of  $\text{NO}_x$  diffusion to the Pt sites, then an acceleration in the velocity of the front edge of the reduction zone is to be expected. Taking these factors together, the increase in selectivity to  $\text{NH}_3$  can be readily understood.



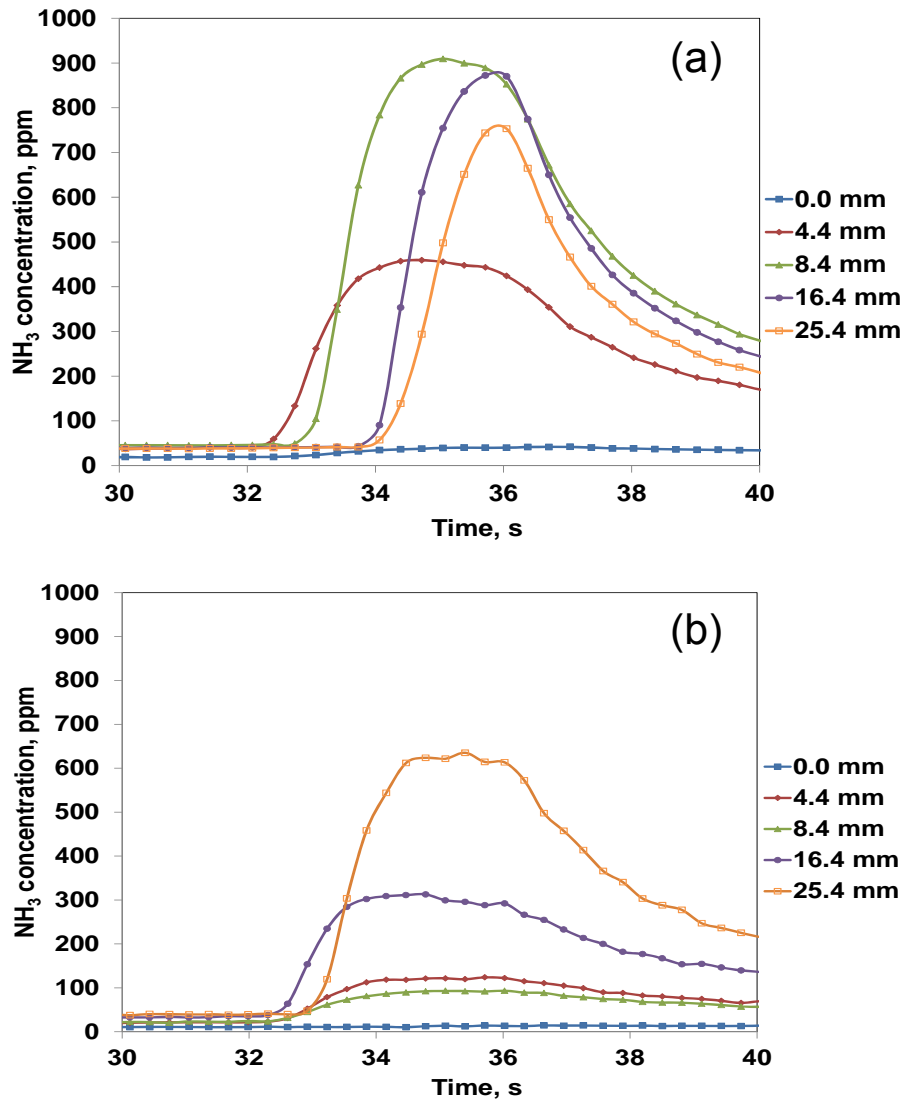


**Figure 5.9. NH<sub>3</sub> concentration vs. time at each sampling location at 200°C for a) degreened B-225 and b) aged B-225.**

Evidence for the fact that the kinetics of NO<sub>x</sub> reduction in aged catalyst B-225 are not limited by the reductant supply rate is provided by the observation that NO<sub>x</sub> release (and hence reduction) is still on-going when NH<sub>3</sub> breakthrough occurs at the catalyst outlet. This is illustrated for the degreened and aged B-225 in Fig. 5.10, which displays the NO<sub>x</sub> concentration measured at the 16.4 mm position as a function of time for regeneration events at 200 °C and at 300 °C. The start and end of the regeneration period are indicated, as is the moment when NH<sub>3</sub> breakthrough occurs at the 25.4 mm position for

the different experiments (note that the data have been time aligned, such that the rich phase starts at the same time for each experiment). For degreened B-225 at 200 °C it is evident that some NO<sub>x</sub> is still being released at the 16.4 mm position when NH<sub>3</sub> breaks through, indicating that at this temperature NO<sub>x</sub> reduction is limited by the kinetics of NO<sub>x</sub> release, rather than being feed limited. This is in agreement with the report of Clayton et al. [36] cited earlier. For aged B-225 tested at 200 °C, the decrease in the NH<sub>3</sub> breakthrough time relative to the degreened catalyst is apparent (corresponding to a shift of ~ 0.9 s), while it is evident that considerable NO<sub>x</sub> release continues after NH<sub>3</sub> breakthrough. In contrast, at 300 °C the degreened catalyst shows essentially no NO<sub>x</sub> release at the 16.4 mm position, consistent with fast NO<sub>x</sub> release and reduction in the front of the catalyst. However, for the aged catalyst significant NO<sub>x</sub> release is observed at 300 °C, while the NH<sub>3</sub> breakthrough time is decreased by ~1.2 s. Continued NO<sub>x</sub> release after NH<sub>3</sub> breakthrough indicates that NO<sub>x</sub> reduction, unlike the degreened catalyst, is limited by the kinetics of NO<sub>x</sub> release, i.e., even at 300 °C NO<sub>x</sub> reduction is not feed limited for the aged catalyst.

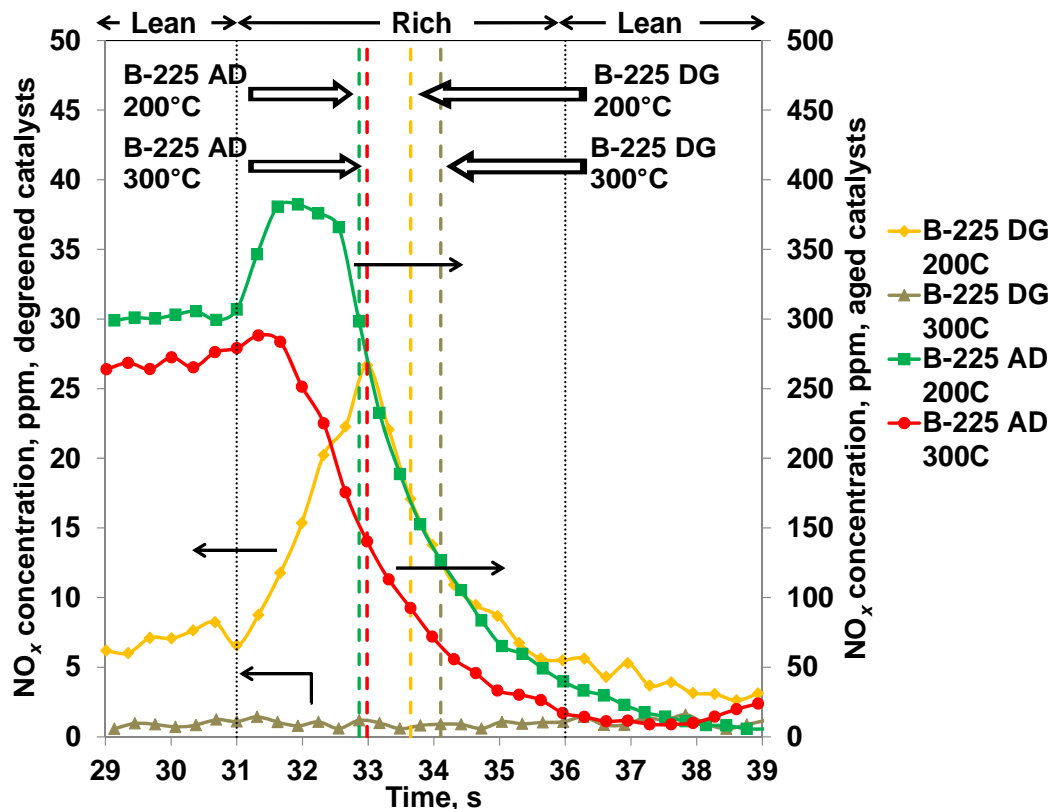


**Figure 5.10.**  $\text{NO}_x$  concentration profiles measured at the 16.4 mm position for degreened (DG) and aged (AD) B-225 as a function of time for regeneration events at 200°C and at 300°C. The dashed vertical lines indicate the time at which  $\text{NH}_3$  breaks through at the 25.4 mm position.

#### 5.3.4. Ceria-containing Catalyst.

##### 5.3.4.1. $\text{NO}_x$ Storage.

As for the experiments with catalyst B-225, cycling experiments using catalyst BC-175 employed a  $\text{H}_2$  concentration tailored to the OSC and  $\text{NO}_x$  storage capacity of the catalyst. Fig. 5.11 reports the measured lean  $\text{NO}_x$  storage efficiencies. For the degreened catalyst, the NSE increased at each point along the length of the catalyst with increasing temperature. Maximum NSE (<100% at 200 and 250 °C) was not reached until the 25.4 mm position, indicating that the whole length of the catalyst was used for storage under these experimental conditions. Additional information is provided in Figs. 5.12a and 5.12b, in which data pertaining to the cycle-averaged NO and  $\text{NO}_2$  concentrations are plotted at each measurement point along the length of the catalyst. A gradual decrease in

NO concentration along the length of the degreened sample occurs at each temperature with the minimum being attained at the 25.4 mm position.

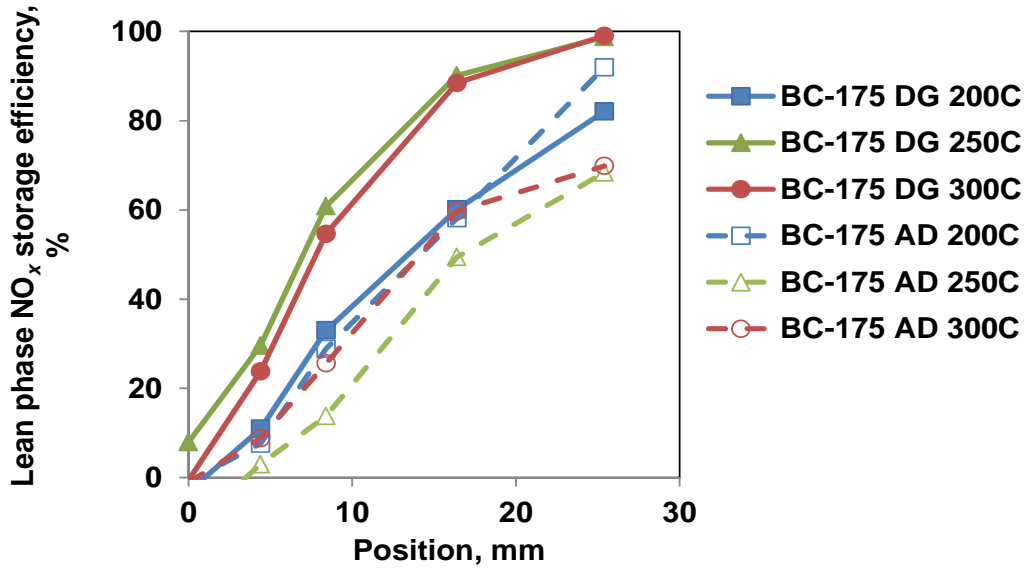


**Figure 5.11. Lean NO<sub>x</sub> storage efficiency as a function of position for degreened (DG) and aged (AD) catalyst BC-175.**

As with B-225, for BC-175 the NO<sub>2</sub> concentration increases along the length of the catalyst for the first third, before decreasing as the rear face of the catalyst is reached. However, it is apparent that NO<sub>x</sub> storage is less efficient on BC-175 relative to B-225, as indicated by the longer NO/NO<sub>2</sub> storage zone in the case of BC-175. This finding contrast with our previously reported results for similar catalyst compositions in which it was found that the degreened catalysts showed similar NSE at 250 °C under lean-rich cycling conditions [17]. However, in the present study the washcoat loading of BC-175 (175 g/L) was significantly lower than that of B-225 (225 g/L), in contrast to the previous study when the samples used had the same loading. Evidently, NSE under these conditions is sensitive to washcoat loading.

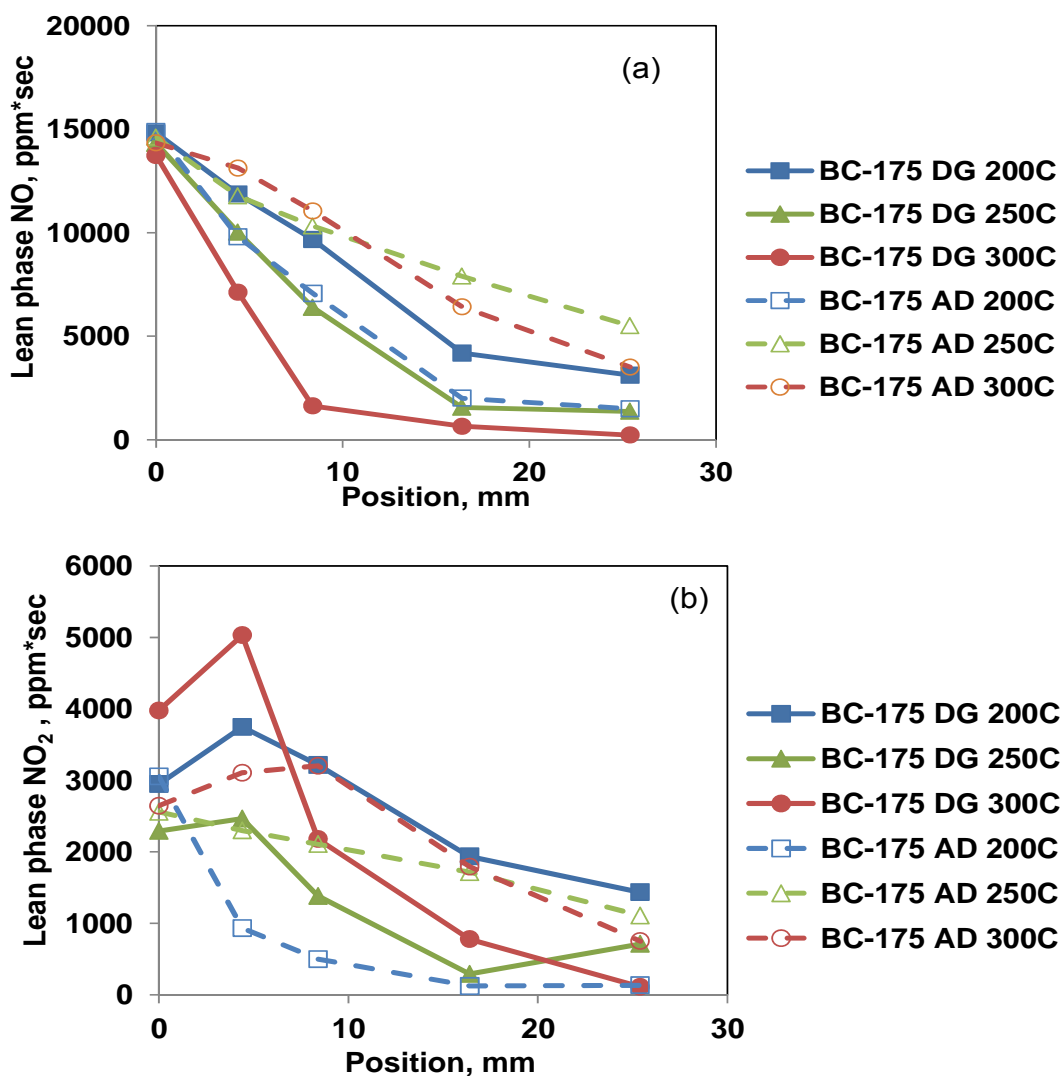


**Figure 5.12. a) Lean phase NO concentration and b) lean phase NO<sub>2</sub> concentration as a function of position during NO<sub>x</sub> storage on degreened (DG) and aged (AD) catalyst BC-175.**

As shown in Table 5.2, aging of catalyst BC-175 results in the same effects as seen with the non-ceria catalyst, i.e., PGM sintering and hence Pt/Ba and Pt/CeO<sub>2</sub> phase segregation. However, comparison of Figs. 5.2 and 5.11 indicate that whereas before aging the NSE of B-225 at 200 °C and 250 °C was superior to that of BC-175 (at every position in the catalyst), after aging the NSE of BC-175 is superior to that of B-225. This observation is consistent with our previous studies [16,17,39] indicating the beneficial

effects of ceria addition on catalyst performance after aging. Evidently, these benefits more than compensate for the lower washcoat loading of catalyst BC-175 after aging at 800 °C.

#### 5.3.4.2. $NO_x$ Reduction.

Cycled-averaged  $NO_x$  conversion data for the degreened and aged BC-175 samples (see Table 5.3) are consistent with the NSR zone extending the whole length of the catalyst, the  $NO_x$  conversion attaining its maximum value at the rear of the catalyst in each case. Considering the lean phase NSE, while aging results in a decrease in  $NO_x$  conversion levels (notably at 300 °C), the deterioration is significantly less than that observed for catalyst B-225 (see Figure 5.13). Again, this serves to illustrate the importance of ceria in aiding LNT durability.

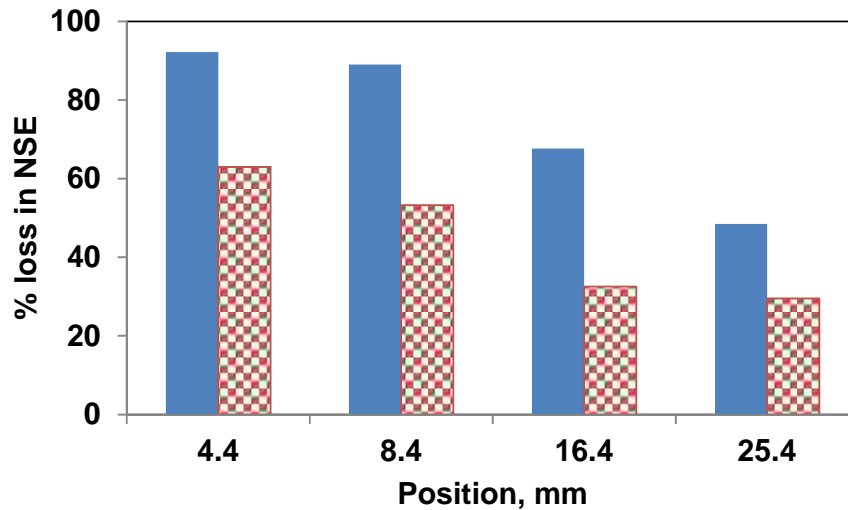


**Figure 5.13. Percent change in  $NO_x$  storage efficiency (NSE) after aging as a function of position for: B-225 at 300 °C (solid bars) and BC-175 at 300 °C (checkered bars). Percent change in NSE is defined as:  $100 \times (\text{degreened NSE} - \text{aged NSE})/\text{degreened NSE}$ .**

Fig. 5.14 depicts the cycle-averaged rich phase  $NO_x$  release as a function of measurement position. For the degreened catalyst, the trends in rich phase  $NO_x$  release are similar to catalyst B-225, i.e., at 250 and 300 °C  $NO_x$  release decreases over the length of the

catalyst, indicating that readsorption and reduction of the released  $\text{NO}_x$  occurs. At 200 °C the  $\text{NO}_x$  release is notably higher due to the imbalance in the rates of  $\text{NO}_x$  release and reduction. However, in contrast to B-225, the  $\text{NO}_x$  release at 200 °C does not decrease significantly in the rear of the BC-175 sample, which can be attributed to the longer  $\text{NO}_x$  storage-reduction zone in this catalyst.

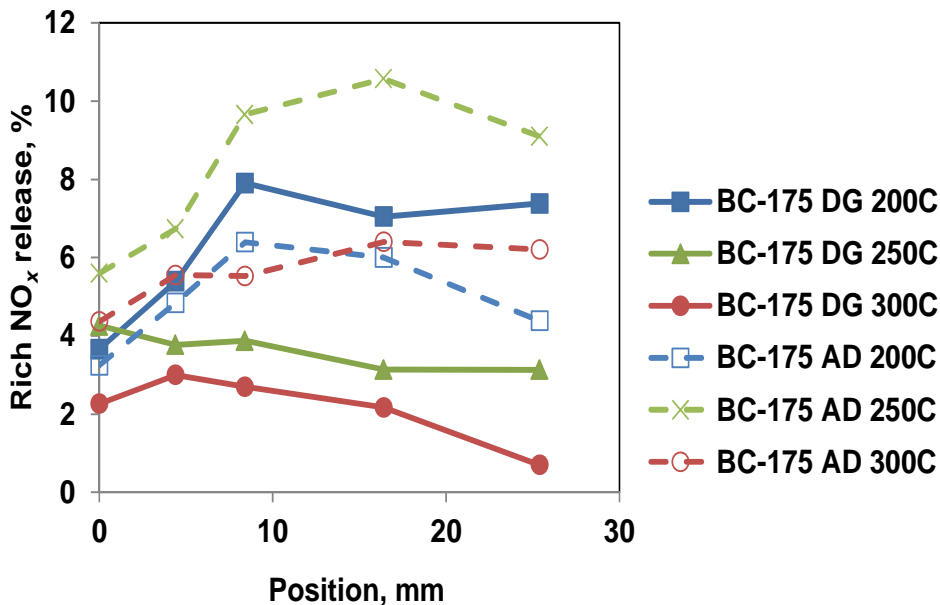


**Figure 5.14. Rich phase  $\text{NO}_x$  release as a function of position during regeneration of degreened (DG) and aged (AD) catalyst BC-175.**

As for the B-225 catalyst,  $\text{NH}_3$  formation over BC-175 tracks the  $\text{NO}_x$  storage zone. Consequently, as shown in Fig. 5.15, peak  $\text{NH}_3$  concentrations measured for degreened BC-175 tend to occur closer to the rear of the catalyst in comparison with B-225. As for B-225, the selectivity to  $\text{NH}_3$  exhibited by BC-175 increases after aging. Furthermore, the maxima in  $\text{NH}_3$  selectivity are located further down the length of the catalyst after aging, consistent with stretching of the NSR zone.

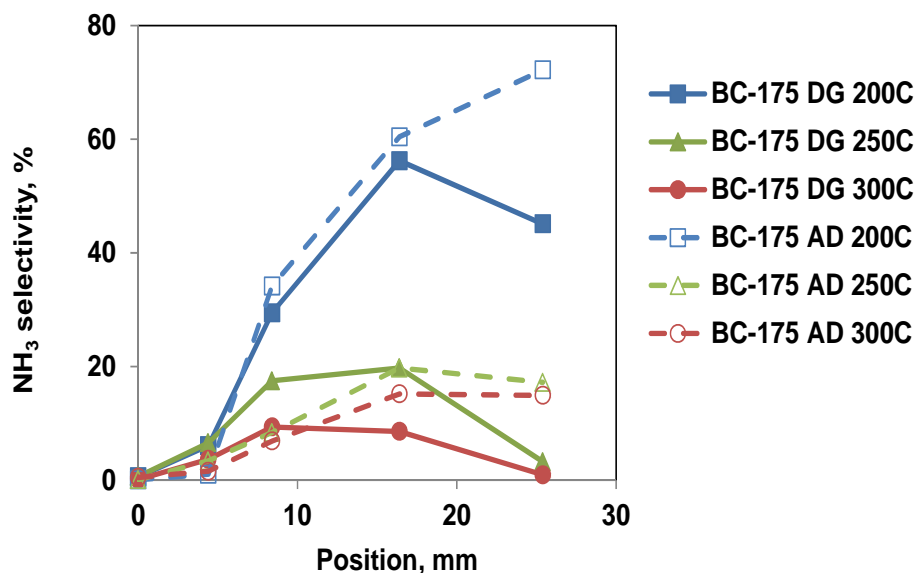


**Figure 5.15. Rich phase  $\text{NH}_3$  selectivity as a function of position for degreened (DG) and aged (AD) catalyst BC-175.**

Temporal data for the  $\text{NH}_3$  release from catalyst BC-175 are shown in Figs. 5.16a and 5.16b. Although not as apparent as with the B-225 catalyst, a delay between the appearance of  $\text{NH}_3$  for each sampling point is present for the degreened BC-175 catalyst. The fact that the delay is less pronounced than for B-225 can be attributed to the lower washcoat loading of BC-175, and hence the lower concentration of storage sites per unit catalyst length. In contrast to B-225, the  $\text{NH}_3$  concentration continues to increase down the length of the catalyst. Again, this can be attributed to the lower washcoat of the BC-175 catalyst compared to B-225, which, as discussed earlier, results in utilization of a significantly larger portion of the catalyst for  $\text{NO}_x$  storage. Since  $\text{NH}_3$  evolution tracks the  $\text{NO}_x$  storage-reduction zone, it follows that peak  $\text{NH}_3$  concentrations for BC-175 are attained further along the catalyst than for B-225. In the case of the aged BC-175 catalyst (Fig. 5.16b), the delay in  $\text{NH}_3$  evolution at the different measurement points is again minor, indicative of fast propagation of the reductant front. As for B-225, there is a notable increase in the amount of  $\text{NH}_3$  released from the aged BC-175 sample after aging. Moreover, similar to B-225, regeneration of BC-175 at 300 °C is limited by the kinetics of  $\text{NO}_x$  reduction after aging, rather than the rate of reductant supply, as indicated by the



observation that  $\text{NO}_x$  release and reduction is still on-going at the 16.4 mm position when  $\text{NH}_3$  breaks through the catalyst (Figure 5.17).

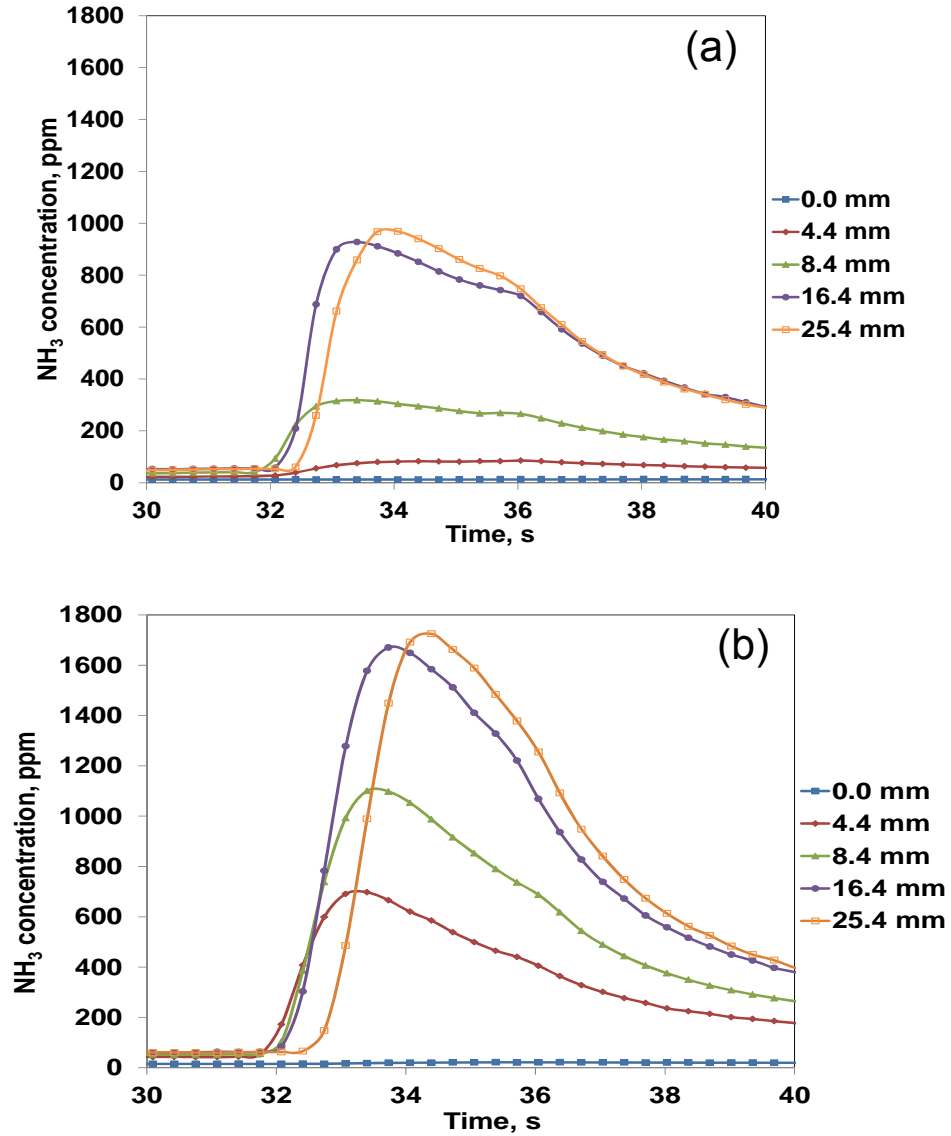
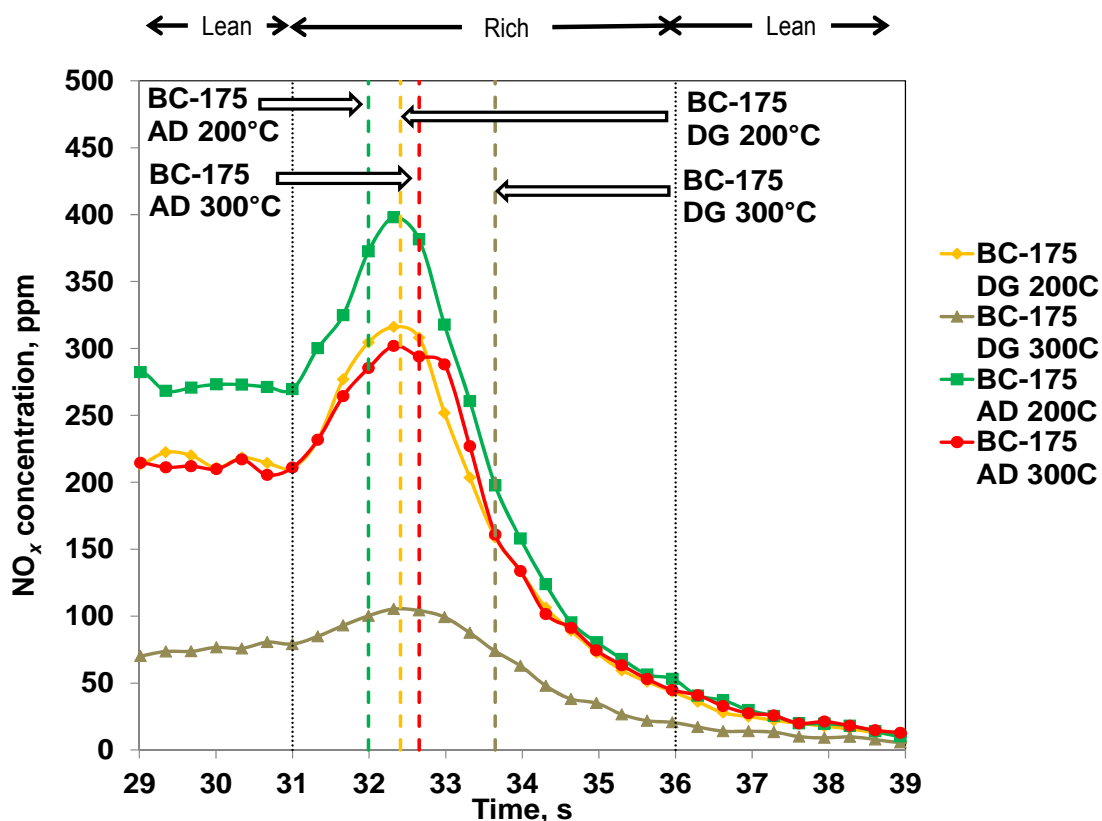


Figure 5.16.  $\text{NH}_3$  concentration vs. time at each sampling location at  $200^\circ\text{C}$  for a) degreased BC-175 and b) aged BC-175.



**Figure 5.17.  $\text{NO}_x$  concentration profiles measured at the 16.4 mm position for degreened (DG) and aged (AD) BC-175 as a function of time for regeneration events at 200 °C and at 300 °C. The dashed vertical lines indicate the time at which  $\text{NH}_3$  breaks through at the 25.4 mm position.**

As stated in the Introduction, there are at least five potential factors which can explain the increase in selectivity to  $\text{NH}_3$  observed for B-225 and BC-175 after aging. Factor (ii) in the list, pertaining to the decreased OSC of the aged catalysts, and factor (iii) concerning the decrease of the catalyst NSE after aging, were accounted for in this study by adjusting the  $\text{H}_2$  concentrations used. In this manner, excessively high  $\text{H}_2:\text{NO}_x$  ratios in the reductant front were avoided; instead, a stoichiometric amount of  $\text{H}_2$  (based on reaction 5.1) was used during regeneration. With these two factors largely excluded, one or all of the following explanations must be invoked to account for the increase in  $\text{NH}_3$  selectivity after aging:

(a) The imbalance in the rates of  $\text{NO}_x$  release and propagation of the reductant front, resulting from the Pt-Ba phase segregation that occurs upon aging. This imbalance results in increased  $\text{H}_2:\text{NO}_x$  ratios at the Pt sites, thereby favoring  $\text{NH}_3$  formation over  $\text{N}_2$ .

(b) Stretching of the NSR zone, resulting from a decrease in concentration of  $\text{NO}_x$  storage sites per unit length of catalyst. The stretching of this zone decreases the length of the OSC-only zone located in the rear of the catalyst, resulting in diminished  $\text{NH}_3$  oxidation and decreased  $\text{NH}_3$  consumption by  $\text{NO}_x$  that re-adsorbs downstream of the reduction front.

(c) Higher  $\text{NH}_3$  emissions may result from decreases in the rates of  $\text{NH}_3$  consumption via reaction with  $\text{NO}_x$  or  $\text{O}_2$  stored downstream of the reaction front (due to PGM sintering).

Of these explanations, (a) and (b) are supported by the data presented in this paper. Increased  $\text{NH}_3$  emissions are clearly associated with stretching of the NSR zone, a conclusion which has previously been reported by workers at Oak Ridge National Laboratory (ORNL) [10-12]. Indeed, as the data in Table 5.3 show, after aging selectivity to  $\text{NH}_3$  is most clearly increased at positions towards the end of the catalyst (e.g., at the 16.4 and 25.4 mm positions). At the same time, temporal data show that after aging the rate of reductant front propagation is increased. This, combined with the fact that Pt-Ba phase segregation results in slower transport of  $\text{NO}_x$  to PGM sites during catalyst regeneration [20], means that  $\text{H}_2:\text{NO}_x$  ratios at the PGM sites will increase after aging.

Turning to point (c) above, we have previously presented steady-state, continuous flow data for a catalyst containing the same washcoat composition as B-225 (but slightly higher washcoat loading) [39]. Results showed that after aging (during which the maximum temperature was  $770 \pm 10$  °C) the rate of the  $\text{NO}_x\text{-NH}_3$  SCR reaction was measurably decreased. On the other hand, for the same catalyst the kinetics of the  $\text{NH}_3\text{-O}_2$  reaction were essentially unchanged [40]. Therefore, in the present work we cannot

exclude the possibility that a decrease in the rate of the  $\text{NO}_x$ - $\text{NH}_3$  SCR reaction after aging also contributes to the observed increase in catalyst selectivity to  $\text{NH}_3$ .

#### *5.4. Conclusions.*

SpaciMS was employed in this study to understand the factors influencing the  $\text{NH}_3$  selectivity of fully formulated LNT catalysts, particularly after thermal aging. Physical characterization of the aged catalysts revealed that the surface area, pore volume and PGM dispersion decreased. This fact helps to explain the decreases in  $\text{NO}_x$  storage efficiency and increases in  $\text{NH}_3$  selectivity and rich phase  $\text{NO}_x$  release observed during lean-rich cycling experiments. Specifically, the losses in surface area, accompanied by segregation of the Pt/Rh sites and BaO storage sites, account for the decreased  $\text{NO}_x$  storage efficiency of the aged catalysts. During  $\text{NO}_x$  storage during the lean phase, NO and  $\text{NO}_2$  were required to travel further to reach storage sites due to the decreased storage site concentration. Consequently, after aging the  $\text{NO}_x$  storage-reduction zone was elongated.

Stretching of the NSR zone has significant implications for catalyst regeneration. The first effect is the increase of the  $\text{NO}_x$  “puff” that appears during the onset of the rich front as it travels along the length of the catalyst. Since  $\text{NO}_x$  release from the catalyst tracks the NSR zone, for an aged catalyst the  $\text{NO}_x$  concentration peaks closer to the rear of the catalyst. Hence the probability that  $\text{NO}_x$  can re-adsorb downstream of the reduction front and subsequently undergo reduction by  $\text{NH}_3$  is diminished, and consequently the  $\text{NO}_x$  emission is higher.

Second, the “stretching” of the NSR zone causes the  $\text{NH}_3$  selectivity of an aged catalyst to increase. For degreened (but not aged) catalysts,  $\text{NH}_3$  is generally observed in the effluent from the catalyst after the stored  $\text{NO}_x$  and adsorbed oxygen located downstream from its point of generation have been consumed; hence, a longer NSR zone for a given length of catalyst means that less catalyst (corresponding to the OSC-only zone) is available to consume  $\text{NH}_3$  produced upstream by either the  $\text{NH}_3$ - $\text{NO}_x$  SCR or  $\text{NH}_3$ - $\text{O}_2$  reaction.

Third, the loss of OSC and NO<sub>x</sub> storage sites leads to an increase in the rate of propagation of the reductant front in the aged catalyst compared to the degreened catalyst. Additionally, NO<sub>x</sub> is released more slowly from storage sites (due to Pt-Ba phase segregation), such that for the aged catalysts the kinetics of NO<sub>x</sub> reduction are controlled by the rate of NO<sub>x</sub> diffusion to the Pt sites (rather than being feed limited). Taken together, these factors give rise to increased H<sub>2</sub>:NO<sub>x</sub> ratios at the Pt/Rh sites and hence selectivity to NH<sub>3</sub> increases.

### 5.5. References.

- [1] L. Xu, R. McCabe, W. Ruona, G. Cavataio, Impact of a Cu-zeolite SCR Catalyst on the Performance of a Diesel LNT+SCR System. SAE Technical Paper Series 2009-01-0285 (2009).
- [2] R. Zukerman, L. Vradman, M. Herskowitz, E. Liverts, M. Liverts, A. Massner, M. Weibel, J.F. Brilhac, P.G. Blakeman, L.J. Peace, Modeling and Simulation of a Smart Catalytic Converter Combining NO<sub>x</sub> Storage, Ammonia Production and SCR. Chemical Engineering Journal 155 (2009) 419-426.
- [3] D. Chatterjee, P. Koči, V. Schmeißer, M. Marek, M. Weibel, B. Krutzsch, Modelling of a Combined NO<sub>x</sub> Storage and NH<sub>3</sub>-SCR Catalytic System for Diesel Exhaust Gas Aftertreatment. Catalysis Today 151 (2010) 395-409.
- [4] P. Forzatti, L. Lietti, The Reduction of NO<sub>x</sub> Stored on LNT and Combined LNT-SCR Systems. Catalysis Today 155 (2010) 131-139.
- [5] A. Lindholm, A. Sjövall, L. Olsson, Reduction of NO<sub>x</sub> over a Combined NSR and SCR System. Applied Catalysis B: Environmental 98 (2010) 112-121.
- [6] J.-S. Choi, W.P. Partridge, C.S. Daw, Spatially Resolved *in situ* Measurements of Transient Species Breakthrough during Cyclic, Low-Temperature Regeneration of a Monolithic Pt/K/Al<sub>2</sub>O<sub>3</sub> NO<sub>x</sub> Storage-Reduction Catalyst. Applied Catalysis A: General 293 (2005) 24-40.
- [7] J.-S. Choi, W.P. Partridge, W.S. Epling, N.W. Currier, T. M. Yonushonis, Intra-Channel Evolution of Carbon Monoxide and its Implication on the Regeneration of a Monolithic Pt/K/Al<sub>2</sub>O<sub>3</sub> NO<sub>x</sub> Storage-Reduction Catalyst. Catalysis Today 114 (2006) 102-111.

- [8] W.P. Partridge, T.J. Toops, J.B. Green, T.R. Armstrong, Intra-Fuel Cell Stack Measurements of Transient Concentration Distributions. *Journal of Power Sources* 160 (2006) 454-461.
- [9] V.Y. Prikhodko, K. Nguyen, J.-S. Choi, C.S. Daw, Axial Length Effects on Lean NO<sub>x</sub> Trap Performance. *Applied Catalysis B: Environmental* 92 (2009) 9-16.
- [10] W.P. Partridge, J.-S. Choi, NH<sub>3</sub> Formation and Utilization in Regeneration of Pt/Ba/Al<sub>2</sub>O<sub>3</sub> NO<sub>x</sub> Storage-Reduction Catalyst with H<sub>2</sub>. *Applied Catalysis B: Environmental* 91 (2009) 144-151.
- [11] J.-S. Choi, W.P. Partridge, J.A. Pihl, C.S. Daw, Sulfur and Temperature Effects on the Spatial Distribution of Reactions Inside a Lean NO<sub>x</sub> Trap and Resulting Changes in Global Performance. *Catalysis Today* 136 (2008) 173-182.
- [12] J.-S. Choi, W.P. Partridge, C.S. Daw, Sulfur Impact on NO<sub>x</sub> Storage, Oxygen Storage, and Ammonia Breakthrough During Cyclic Lean/Rich Operation of a Commercial Lean NO<sub>x</sub> Trap. *Applied Catalysis B* 77 (2007) 145-156.
- [13] J.-S. Choi, W.P. Partridge, J.A. Pihl, M.-Y. Kim, P. Kočí, C.S. Daw, Spatiotemporal Distribution of NO<sub>x</sub> Storage and Impact NH<sub>3</sub> and N<sub>2</sub>O Selectivities During Lean/Rich Cycling of a Ba-Based Lean NO<sub>x</sub> Trap Catalyst. *Catalysis Today*, 184 (2012) 20-26.
- [14] J.-Y. Luo, M. Al-Harbi, M. Pang, W.S. Epling, Spatially Resolving LNT Desulfation: Re-Adsorption Induced by Oxygen Storage Materials. *Applied Catalysis B: Environmental* 106 (2011) 664-671.
- [15] J. Wang, Y. Ji, V. Easterling, M. Crocker, M. Dearth, R.W. McCabe, The Effect of Regeneration Conditions on the Selectivity of NO<sub>x</sub> Reduction in a Fully Formulated Lean NO<sub>x</sub> Trap Catalyst. *Catalysis Today* 175 (2011) 83-92.

- [16] Y. Ji, V. Easterling, U. Graham, C. Fisk, M. Crocker, J.-S. Choi, Effect of Aging on the NO<sub>x</sub> Storage and Regeneration Characteristics of Fully Formulated Lean NO<sub>x</sub> Trap Catalysts. *Applied Catalysis B: Environmental* 103 (2011) 413-427.
- [17] Y. Ji, C. Fisk, V. Easterling, U. Graham, A. Poole, M. Crocker, J.-S. Choi, W. Partridge, K. Wilson, NO<sub>x</sub> Storage–Reduction Characteristics of Ba-Based Lean NO<sub>x</sub> Trap Catalysts Subjected to Simulated Road Aging. *Catalysis Today* 151 (2010) 362-375.
- [18] Y. Ji, J.-S. Choi, T.J. Toops, M. Crocker, M. Naseri, Influence of Ceria on the NO<sub>x</sub> Storage/Reduction Behavior of Lean NO<sub>x</sub> Trap Catalysts. *Catalysis Today* 136 (2008) 146-155.
- [19] R.D. Clayton, M.P. Harold, V. Balakotaiah, C.Z. Wan, Pt Dispersion Effects During NO<sub>x</sub> Storage and Reduction on Pt/BaO/Al<sub>2</sub>O<sub>3</sub> Catalysts. *Applied Catalysis B: Environmental* 90 (2009) 662-676.
- [20] D. Bhatia, M.P. Harold, V. Balakotaiah, A Global Kinetic Model for NO<sub>x</sub> Storage and Reduction on Pt/BaO/Al<sub>2</sub>O<sub>3</sub> Monolithic Catalysts. *Catalysis Today* 151 (2010) 314-329.
- [21] V. Perrichon, L. Retailleau, P. Bazin, M. Daturi, J.C. Lavalley, Metal Dispersion of CeO<sub>2</sub>–ZrO<sub>2</sub> Supported Platinum Catalysts Measured by H<sub>2</sub> or CO Chemisorption. *Applied Catalysis* 260 (2004) 1-8.
- [22] W.S. Epling, L.E. Campbell, A. Yezerets, N.W. Currier, J.E. Parks II, Overview of the Fundamental Reactions and Degradation Mechanisms of NO<sub>x</sub> Storage/Reduction Catalysts. *Catalysis Reviews* 46 (2004) 163-246.
- [23] I. Nova, L. Lietti, P. Forzatti, Mechanistic Aspects of the Reduction of Stored NO<sub>x</sub> over Pt–Ba/Al<sub>2</sub>O<sub>3</sub> Lean NO<sub>x</sub> Trap Systems. *Catalysis Today* 136 (2008) 128-135.



- [24] D.H. Kim, Y.-H. Chin, G.G. Muntean, A. Yezeretz, N.W. Currier, W.S. Epling, H.-Y. Chen, H. Hess, C.H.F. Peden, Relationship of Pt Particle Size to the NO<sub>x</sub> Storage Performance of Thermally Aged Pt/BaO/Al<sub>2</sub>O<sub>3</sub> Lean NO<sub>x</sub> Trap Catalysts. *Industrial Engineering Chemistry Research* 45 (2006) 8815-8821.
- [25] E. Mamontov, T. Egami, R. Brezny, M. Koranne, S. Tyagi, Lattice Defects and Oxygen Storage Capacity of Nanocrystalline Ceria and Ceria-Zirconia. *Journal Physical Chemistry B* 104 (2000) 11110-11116.
- [26] N. Fekete, R. Kemmler, D. Voigtländer, B. Krutzsch, E. Zimmer, G. Wenninger, W. Strehlau, J. van den Tilaart, J. Leyrer, E. Lox, W. Müller, Evaluation of NO<sub>x</sub> Storage Catalysts for Lean Burn Gasoline Fueled Passenger Cars. *SAE Technical Paper Series 970746* (1997).
- [27] D. Uy, A.E. O'Neill, J. Li, W.L.H. Watkins, UV and Visible Raman Study of Thermal Deactivation in a NO<sub>x</sub> Storage Catalyst. *Catalysis Letters* 95 (2004) 191-201.
- [28] T.J. Toops, B.G. Bunting, K. Nguyen, A. Gopinath, Effect of engine-based thermal aging on surface morphology and performance of Lean NO<sub>x</sub> Traps. *Catalysis Today* 123 (2007) 285-292.
- [29] K. Nguyen, H. Kim, B.G. Bunting, T.J. Toops, C.S. Yoon, Rapid Aging of Diesel Lean NO<sub>x</sub> Traps by High-Temperature Thermal Cycling. *SAE Technical Paper Series 2007-01-0470* (2007).
- [30] M. Casapu, J.-D. Grunwaldt, M. Maciejewski, A. Baiker, S. Eckhoff, U. Göbel, M. Wittrock, The fate of platinum in Pt/Ba/CeO<sub>2</sub> and Pt/Ba/Al<sub>2</sub>O<sub>3</sub> catalysts during thermal aging. *Journal of Catalysis* 251 (2007) 28-38.

- [31] D.H. Kim, Y.-H. Chin, J.H. Kwak, C.H.F. Peden, Promotional Effects of H<sub>2</sub>O Treatment on NO<sub>x</sub> Storage Over Fresh and Thermally Aged Pt–BaO/Al<sub>2</sub>O<sub>3</sub> Lean NO<sub>x</sub> Trap Catalysts. *Catalysis Letters* 124 (2008) 39-45.
- [32] L. Cumararatunge, S.S. Mulla, A. Yezerets, N.W. Currier, W.N. Delgass, F.H. Ribeiro, Ammonia is a Hydrogen Carrier in the Regeneration of Pt/BaO/Al<sub>2</sub>O<sub>3</sub> NO<sub>x</sub> traps with H<sub>2</sub>. *Journal of Catalysis* 246 (2007) 29–34.
- [33] S.S. Mulla, S.S. Chaugule, A. Yezerets, N.W. Currier, W.N. Delgass, F.H. Ribeiro, Regeneration Mechanism of Pt/BaO/Al<sub>2</sub>O<sub>3</sub> Lean NO<sub>x</sub> Trap Catalyst with H<sub>2</sub>. *Catalysis Today* 136 (2008) 136-145.
- [34] L. Letti, I. Nova, P. Forzatti, Role of Ammonia in the Reduction by Hydrogen of NO<sub>x</sub> Stored over Pt–Ba/Al<sub>2</sub>O<sub>3</sub> Lean NO<sub>x</sub> Trap Catalysts. *Journal of Catalysis* 257 (2008) 270-282.
- [35] R.D. Clayton, M.P. Harold, V. Balakotaiah, Selective Catalytic Reduction of NO by H<sub>2</sub> in O<sub>2</sub> on Pt/BaO/Al<sub>2</sub>O<sub>3</sub> Monolith NO<sub>x</sub> Storage Catalysts. *Applied Catalysis. B* 81 (2008) 161-181.
- [36] J.A. Pihl, J.E. Parks, C. Stuart Daw, T.W. Root, Product Selectivity During Regeneration of Lean NO<sub>x</sub> Trap Catalyst. SAE Tech. Paper 2006-01-3441, 2006.
- [37] R.D. Clayton, M.P. Harold, V. Balakotaiah, NO<sub>x</sub> Storage and Reduction with H<sub>2</sub> on Pt/BaO/Al<sub>2</sub>O<sub>3</sub> Monolith: Spatio-Temporal Resolution of Product Distribution. *Applied Catalysis B: Environmental* 84 (2008) 616-630.
- [38] J. Wang, Y. Ji, U. Graham, C. Cesar Spindola de Oliveira, M. Crocker, NO<sub>x</sub> Reduction on Fully Formulated Lean NO<sub>x</sub> Trap Catalysts Subjected to Simulated Road Aging: Insights from Steady-State Experiments. *Chinese Journal of Catalysis* 32 (2011) 736-745.

- [39] A. Martínez-Arias, M. Fernández-García, A. Iglesias-Juez, A.B. Hungria, J.A. Anderson, J.C. Conesa, J. Soria, Influence of Thermal Sintering on the Activity for CO–O<sub>2</sub> and CO–O<sub>2</sub>–NO Stoichiometric Reactions over Pd/(Ce, Zr)O<sub>x</sub>/Al<sub>2</sub>O<sub>3</sub> Catalysts. *Applied Catalysis B: Environmental* 38 (2002) 151-158.
- [40] J. Wang, M. Crocker, unpublished results.

## **Chapter 6. An Investigation into the Validity of a Crystallite-Scale Model to Predict the NH<sub>3</sub> Regeneration of a Pt/Rh/BaO/Al<sub>2</sub>O<sub>3</sub> Lean NO<sub>x</sub> Trap Catalyst.**

### *6.1. Introduction.*

Over the past two decades, intensive research has been focused on reducing NO<sub>x</sub> emissions (NO + NO<sub>2</sub>) from lean burn applications using Lean NO<sub>x</sub> Trap (LNT) Catalysts and Selective Catalytic Reduction (SCR) catalysts. The LNT operates by oxidizing NO<sub>x</sub> emitted during combustion over precious group metals (PGMs), such as Pt and Rh, and then storing the resulting nitrates and nitrites on a storage component such as Ba [1,2]. Before the storage capacity of the LNT is reached, engine operation is modified to rich conditions creating a net-reducing environment in which stored NO<sub>x</sub> is released and migrates back to the PGM component where it reacts with a reductant such as H<sub>2</sub> to form N-species such as N<sub>2</sub>, NH<sub>3</sub>, and N<sub>2</sub>O. The SCR catalyst achieves NO<sub>x</sub> reduction by catalyzing the reaction of NH<sub>3</sub> with NO<sub>x</sub> emitted from the engine to form N<sub>2</sub> [3].

While either of these approaches is capable of reducing NO<sub>x</sub> concentrations in engine exhaust, neither system is without shortcomings. The application of LNTs is limited by the cost of the PGMs. In addition, undesired products are formed during the rich phase, including unreacted NO<sub>x</sub> along with NH<sub>3</sub> and N<sub>2</sub>O. The SCR catalyst, on the other hand, requires an external source for the reductant. A common example of this application involves using urea as the NH<sub>3</sub> source [4-6], which requires an external storage tank and injection system for the urea to be injected into the exhaust system. Both of these requirements add additional weight and cost to the vehicle system.

In the past decade, to address the shortcomings of the LNT and SCR applications, researchers have developed LNT-SCR systems [7-34]. The aim of coupling these catalysts is to reduce the amount of LNT required thereby reducing the amount of PGM required to meet NO<sub>x</sub> emission targets. This coupling also eliminates the need for an external source of reductant by tuning the operation of the LNT such that it operates as an NH<sub>3</sub> generator.

To fully implement a LNT-SCR system, operation during the lean and rich phases needs to be tuned based on the amount of  $\text{NO}_x$  emitted from the engine and also based on the product selectivity that results from the LNT. Specifically, a balance must exist between the amount of  $\text{NO}_x$  and  $\text{NH}_3$  that is emitted from the LNT upstream of the SCR.

To achieve these aims, one must have a thorough understanding of the factors that control product selectivity during regeneration of the LNT. One factor that determines the selectivity of the products from regeneration is the ratio of hydrogen, nitrogen, and oxygen present on the PGM component [35-40]. The ratio of these species changes as the exhaust conditions are switched from lean to rich phase. If one considers the idea of a reductant front propagating along the length of the monolith, the change in the relative amount of these components is readily explained [35,36,41-47]. As the front moves along the catalyst, the adsorbed oxygen on the catalyst will be consumed by the reductants (e.g.  $\text{H}_2$ ,  $\text{CO}$ ,  $\text{HC}$ ). As the stored oxygen is consumed, a low reductant to  $\text{NO}_x$  ratio exists at the PGM sites. This ratio of reductant to  $\text{NO}_x$  increases after the leading edge of the front continues to travel down the length of the monolith. Eventually, a situation exists in which a large excess of reductant is present. The transition from low to equal to high ratios coincides with the shift in product selectivity from  $\text{N}_2\text{O}$  to  $\text{N}_2$  to  $\text{NH}_3$  during the regeneration of a LNT catalyst.

The proximity of the PGM to the storage component is another factor that determines the products formed during regeneration. The proximity between these components establishes the distance that  $\text{NO}_x$  must diffuse from the Ba to Pt sites. As this distance increases, the ratio of H:N species at the Pt crystallites also increases. The studies by Clayton et al. focused on this Pt/Ba proximity [45,46]. Nova et al. [48,49] stated that the Pt catalyzed reduction of stored  $\text{NO}_x$  only occurs efficiently when Pt and BaO are dispersed on the same support. Cant et al. [50] discussed the importance of the Pt/Ba proximity during storage and reduction of a Pt/BaO/ $\text{Al}_2\text{O}_3$  catalyst. Cant related the observed selectivity and relative breakthrough times of  $\text{H}_2$  and  $\text{NH}_3$  to the transport of  $\text{NO}_x$  from the storage site back to the PGM. Büchel et al. noted that the best storage and reduction performance was observed when Pt was in close proximity to Ba [51].

The preceding discussion highlights some of the experimental research that has been conducted. Equally important have been the modeling efforts that have been put forth by various research groups. Tuttlies et al. [52] proposed that a model based on the diffusion of  $\text{NO}_x$  into the storage particle is strongly affected by solid volume changes. Under regeneration conditions, the dense nitrate layer formed during storage breaks up into  $\text{BaCO}_3$ . Schmeißer et al. [53] described the regeneration process as one in which reductants diffuse through an increasingly thickening nitrate layer. Using experimental data from steady-state experiments focusing on the Pt-catalyzed  $\text{NO}/\text{H}_2$  reaction system, Xu et al. [38] formulated a micro-kinetic model that incorporated an integral short monolith reactor model [54] using available parameters from existing literature and the remaining parameters from experiments. Their model was able to predict the  $\text{NO}_x$  surface coverage during storage and the selectivities as a function of the  $\text{H}_2:\text{NO}_x$  ratio occurring during regeneration. Larson et al. [55] devised an elementary surface reaction model to describe the regeneration reactions occurring at the PGM sites of a LNT. Larson et al. were able to determine the parameters for their model for their extensive experimental database [35] and were able to validate some of the proposed kinetic mechanisms with data collected using DRIFTS using a commercial LNT catalyst [50]. Lindholm [57] et al. developed a model that utilized a multi-site mechanism for  $\text{NO}_x$  storage. During the regeneration phase, the mechanism includes  $\text{H}_2$  reacting with stored oxygen on Pt and  $\text{NH}_3$  acting as intermediate in  $\text{N}_2$  production from the reduction of stored  $\text{NO}_x$  with  $\text{H}_2$ . Kočí et al. [58] were able to compare the effect of different reductants ( $\text{CO}$ ,  $\text{H}_2$ ,  $\text{C}_3\text{H}_6$ ) on  $\text{NH}_3$  selectivity in the presence of  $\text{CO}_2$  and  $\text{H}_2\text{O}$  in a heterogeneous, 1-D model. Kočí described the propagation of the reductant as well as the production and consumption of  $\text{NH}_3$  as fronts travel down the axis of the monolith.

Short-comings of these modeling efforts include the lack of transparency of the parameters that constitute the model and the development of a model for a certain catalyst operating under a very specified set of conditions. In order to advance the understanding of these catalysts, models are needed that are capable of predicting the experimental data of LNTs under a wide set of conditions. Bhatia et al. proposed a crystallite-scale model to study the effect of Pt dispersion and temperature during the regeneration of a LNT

comprising a Pt/BaO catalyst [44]. The data provided by the model was compared with the data generated from fixed storage experiments performed by Clayton et al. [46]. Bhatia was able to achieve a good fit of the data obtained by Clayton et al. for NH<sub>3</sub> generation as the dispersion and temperature during storage and regeneration was varied.

Research concerning product selectivity has been conducted using both experimental and computer simulation approaches. The goal of the present study was to validate the model created by Bhatia et al. [44] for a catalyst slightly different than the ones used in their study. Bhatia used Pt/BaO/Al<sub>2</sub>O<sub>3</sub> LNT catalysts in which the dispersion (and hence Pt particle size) was varied by employing different Pt loadings. For this study, the LNT catalysts employed are also comprised of Pt/BaO/Al<sub>2</sub>O<sub>3</sub> but differ due to the inclusion of Rh. Pt is the primary choice for oxidation of NO, but Rh is more active for NO<sub>x</sub> reduction [59,60]. Moreover, Kobayashi et al. showed that a combination of Pt/Rh had a higher trapping activity than either Pd/Rh or Pd [61]. Additionally, Theis et al. reported that a combination of Pt and Rh had the best overall NO<sub>x</sub> conversion at low temperatures (250°C) for fresh and aged catalysts as compared to Pt-only samples [62]. Furthermore, comparing the vapor pressure of both the metal and the oxide, the vapor pressure for Pt is higher (3x for the metal, 2x for the oxide) than the vapor pressure for Rh [63]. The vapor pressure provides an indication of the sintering behavior of the PGM, i.e., the higher the vapor pressure, the more severe the sintering is expected to be. The dispersions of the PGM in the catalysts used in this study were varied by sintering the catalyst. Because the PGM will be exposed to a variety of conditions that may result in the loss of PGM dispersion, the ability of a model to predict the behavior of an aged catalyst would be beneficial in the design of an LNT.

## *6.2. Experimental.*

This study incorporated two elements: first, an experimental study of the effect of Pt dispersion and temperature on the NH<sub>3</sub> selectivity from a LNT regenerated with a fixed amount of NO<sub>x</sub>, and second, a modeling study to predict the data gathered from the experimental study. The experimental study used a Pt/Rh/BaO/Al<sub>2</sub>O<sub>3</sub> fully formulated catalyst whose preparation has been described elsewhere [64]. The washcoat was applied

by DCL International, Inc. (Toronto, ON) using a proprietary vacuum coating process. The washcoat was applied to a 4" x 6" cordierite monolith substrate, which had a cell density of 400 cpsi and a wall thickness of 6.5 mil. The BaO component (21.5 wt %) was supported on  $\gamma$ -alumina, while bare alumina was used as a balance to bring the total washcoat loading to the value indicated in Table 6.1.

**Table 6.1. Composition of catalysts used in this study.**

Component	Catalyst code / nominal loading
	B-225
Pt, g/L	3.05
Rh, g/L	0.61
BaO <sup>a</sup> , g/L	26
CeO <sub>2</sub> <sup>b</sup> , g/L	0
$\gamma$ -Al <sub>2</sub> O <sub>3</sub> <sup>c</sup> , g/L	Balance
Total washcoat, g/L	225

<sup>a</sup> 21.5 wt% supported on  $\gamma$ -Al<sub>2</sub>O<sub>3</sub>.

<sup>b</sup> Stabilized with 5 wt% La<sub>2</sub>O<sub>3</sub>.

<sup>c</sup> Stabilized with 3 wt% La<sub>2</sub>O<sub>3</sub>.

### 6.2.1. Catalyst Aging.

A 1.75 cm x 2.54 cm (d x l) core was drilled from the LNT monolith and was wrapped with ceramic fiber and positioned in a quartz tube. Degreening the catalyst consisted of exposing the catalyst to neutral conditions (5% CO<sub>2</sub>, 5% H<sub>2</sub>O, balance N<sub>2</sub>) at 800°C for 2 h. Aging the catalyst involved subjecting the catalyst to continuous lean conditions (8% O<sub>2</sub>, 5% CO<sub>2</sub>, 5% H<sub>2</sub>O, and balance N<sub>2</sub>) at 800°C for 24 h. In both cases, the gas flow was adjusted to give a GHSV of 30,000 h<sup>-1</sup>.

### 6.2.2 Pulsed H<sub>2</sub> Chemisorption.

The dispersion of precious metal (Pt + Rh) was determined using a Micromeritics AutoChem II Analyzer by means of pulsed H<sub>2</sub> chemisorption at dry ice temperature (-78°C). This temperature was chosen in an effort to minimize H spillover from the



metal to the support material [65]. 1 g of sample (as a fine powder), including both washcoat and substrate, was loaded into the reactor. After being oxidized at 400°C in 10% O<sub>2</sub>/He for 15 min, followed by reduction at 300°C in 10% H<sub>2</sub>/Ar for 15 min, the catalyst was heated to 400°C (hold time 10 min) in flowing Ar to remove adsorbed H. Pulsed H<sub>2</sub> chemisorption was initiated using a four-way valve after the catalyst had been cooled to -78°C. During this measurement, 0.5 mL of 10% H<sub>2</sub>/Ar was pulsed into the reactor every 2 min, while the H<sub>2</sub> signal at the reactor outlet was being monitored with a thermal conductivity detector (TCD). H<sub>2</sub> pulsing, i.e., the total precious metal (Pt + Rh) sites were saturated with H<sub>2</sub>, was terminated after the TCD signal had reached a constant value. Assuming a 1:1 ratio of atomic hydrogen to surface Pt or Rh, the metal dispersion was calculated based on the amount of H adsorbed.

### *6.2.3 SpaciMS and H-Sense Mass Spectrometers.*

All of the data in the experimental portion of this study were collected using either an Airsense High Speed Multi-component Gas Analyzer or an Airsense H-Sense Hydrogen Gas Analyzer. The Airsense analyzer is a chemical-ionization mass spectrometer that has been modified for SpaciMS (spatially-resolved capillary inlet chemical ionization mass spectrometry) applications by incorporating a 0.37 mm outer diameter (0.18 mm i.d.) stainless steel capillary connected to the sample chamber. The sampling rate was 14 sccm and data were collected at 3 Hz. Data pertaining to the concentrations of NO, NO<sub>2</sub>, O<sub>2</sub>, H<sub>2</sub>O, and NH<sub>3</sub> at different positions were collected using the spaciMS, and the measurement locations are shown in Fig. 6.1. The first of these positions corresponded to the rear face of the catalyst (25.4 mm from the catalyst inlet), with successive sampling at 16.4 mm, 8.4 mm, 4.4 mm, and the front face (0 mm from the inlet). By sampling in this manner (from rear to front), the chance of contaminating the capillary with particles from the washcoat of the catalyst was decreased. Note that the “0 mm” position actually corresponds to a position of 0.1 mm; this was done in order to ensure that the capillary was correctly aligned with the selected channel.

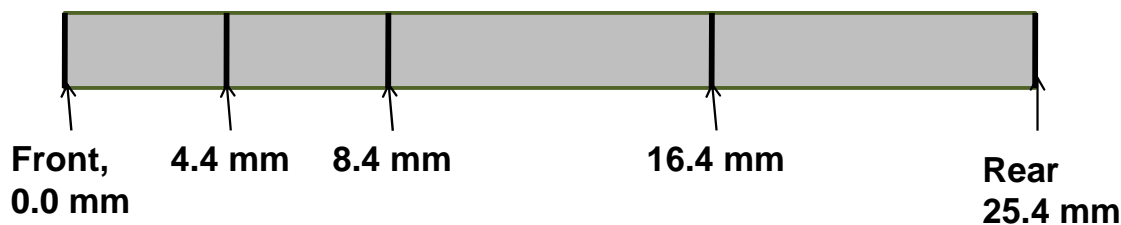


**Figure 6.1. Description of the Measurement Locations Along the Length of the Monolith Catalyst.**

The other mass spectrometer employed in this study was an Airsense H-Sense Hydrogen Gas Analyzer to measure  $H_2$  concentration only at the exit of the reactor. The H-Sense uses the principle of Electron Pulse Ionization (EIMS) mass spectrometer principle optimized for  $H_2$ -only analysis.

#### *6.2.4. Determination of the Amount of $NO_x$ Stored.*

Since the goal of this experiment was to study  $NH_3$  selectivity, a repeatable starting point at the end of the lean ( $NO_x$  storage) phase was required. To achieve this goal, both the degreened and aged catalysts were subjected to continuously lean conditions to determine the time required to reach a certain  $NO_x$  storage level. The catalysts were subjected to a pre-treatment step consisting of fifteen 60 s lean (500 ppm NO, 5%  $O_2$ , bal. Ar) / 10 s Rich (2%  $H_2$ , 0.5%  $O_2$ , bal. Ar) cycles at 450 °C followed by exposure to 2%  $H_2$  in Ar at 450 °C. The duration of the rich conditions at 450 °C lasted until the concentrations of  $NH_3$  and  $H_2O$  in the effluent approached 0 ppm as measured outside the rear of the catalyst by the SpaciMS. Upon reaching this temperature, the catalyst was cooled in Ar to the experimental temperature (200 or 300 °C). Once this temperature was reached, the catalyst was exposed to continuous lean conditions (500 ppm NO, 5%  $O_2$ , bal. Ar). After the desired  $NO_x$  storage level was attained, conditions in the reactor were switched to rich (2%  $H_2$  bal. Ar) in order to regenerate the storage sites. This procedure was repeated to ensure the accuracy of the storage level.

### 6.2.5. $\text{NH}_3$ Selectivity.

Once the time for a fixed level of  $\text{NO}_x$  storage had been determined, the catalyst was subjected to the same pretreatment as described previously and then subjected to continuous lean conditions followed by continuous rich conditions, during which the products formed by the reduction of stored  $\text{NO}_x$  were monitored using the spaciMS. Again, the lean conditions were 500 ppm  $\text{NO}$ , 5%  $\text{O}_2$ , and bal. Ar, but the rich phase was 1500 ppm  $\text{H}_2$  and bal. Ar. The temperature for the lean and rich phases was either 200 or 300 °C. As during the pretreatment step, once the  $\text{NH}_3$  and  $\text{H}_2\text{O}$  concentrations decreased to less than 4 ppm, the temperature of the reactor was increased to 450 °C to ensure that all of the Ba storage sites were regenerated. Once the catalyst was sufficiently regenerated, it was cooled to the next temperature to be studied. These processes were first performed at the 25.4 mm position (outlet of the catalyst) and progressively moved to other measurement positions towards the front of the catalyst as described above. Again, it is worth noting again that while the SpaciMS measurements for  $\text{NO}$ ,  $\text{NO}_2$ ,  $\text{O}_2$ ,  $\text{H}_2\text{O}$ , and  $\text{NH}_3$  were collected at each of the locations previously described along the axis of the catalyst, all of the  $\text{H}_2$  measurements were collected from the effluent of the catalyst.

The selectivity (6.1 and 6.2) and yield (6.3 and 6.4) are defined as:

Selectivity:

$$\frac{\text{Concentration of rich phase } \text{NH}_3 \text{ release at measurement location}}{\text{NO}_x \text{ converted on catalyst}} * 100\% \quad (6.1)$$

with:

$$\begin{aligned} \text{NO}_x \text{ converted on catalyst} = & \text{Inlet lean NO}_x - \text{Outlet lean NO}_x \\ & - \text{Concentration of rich NO}_x \text{ released at the measurement location} \end{aligned} \quad (6.2)$$

Yield:

Conversion =

$$\frac{\text{Feed NO}_x - \text{Lean NO}_x \text{ at measurement location} - \text{Rich NO}_x \text{ at measurement location}}{\text{Feed NO}_x - \text{Lean NO}_x \text{ at measurement location}}$$

$$* 100\% \tag{6.3}$$

$$\text{Yield} = \text{Selectivity} * \text{Conversion} \tag{6.4}$$

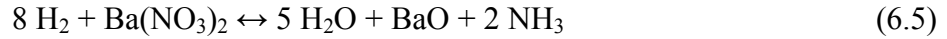
In eqns. (6.14), (6.15), and (6.16), all concentrations are cycle-averaged integrated values (ppm\*s).

### 6.3. Model Development.

The model employed in this study of NH<sub>3</sub> selectivity resulting from the regeneration of a LNT catalyst with fixed NO<sub>x</sub> loading was developed by Bhatia et al. [44] based on experimental work by Clayton et al. [46]. The current study is part of a collaboration between research groups at the University of Kentucky and the University of Houston. The crystallite-scale model was based on the effects that Pt dispersion and temperature have on the processes that occur at the Pt/Ba interface in LNT catalysts. During regeneration of LNT, NO<sub>x</sub> undergoes a reverse spillover from the Ba storage phase back to at the Pt particles and then reacts with H<sub>2</sub> that is chemisorbed onto the Pt particles. Additionally, the NO<sub>x</sub> can be reduced by the intermediate NH<sub>3</sub> produced as NO<sub>x</sub> is reduced by H<sub>2</sub>. The perimeter resulting from the interface that exists between the Pt and Ba phases is subjected to changes as different Pt dispersions and loadings are used on these catalysts. This interface is also changed during the aging of the catalyst as the Pt particles are sintered.

The computer model is comprised of a localized material balance for stored NO<sub>x</sub>, species balances for H<sub>2</sub>, NH<sub>3</sub>, and N<sub>2</sub>, and a balance for the vacant sites on Pt. Along with these balances the following overall catalytic reactions are proposed to occur at the Pt/Ba interface:

Reduction of  $\text{NO}_x$  by hydrogen to produce the reaction intermediate  $\text{NH}_3$ ,  $k_1$  ( $\text{m}^4/\text{mol s}$ ):



Reduction of  $\text{NO}_x$  by the intermediate  $\text{NH}_3$  to produce  $\text{N}_2$ ,  $k_2$  ( $\text{m}^4/\text{mol s}$ ):



Consumption of  $\text{H}_2$  by chemisorbed oxygen on the Pt crystallites,  $k_3$  ( $\text{m}^3/\text{mol s}$ ):



For the development of the governing material balances and other equations used by the model the reader is referred to Bhatia et al. [44] or Appendix A.2. The following is a list of the assumptions made in realizing the model:

1.  $\text{NO}_x$  undergoes reverse spillover from the Ba phase to Pt particles where the  $\text{NO}_x$  is reduced by  $\text{H}_2$  and the intermediate  $\text{NH}_3$ .
2. The Pt particles are hemispherical in shape. This assumption is used to develop the relations for the total number of Pt atoms in a crystallite and number of crystallites per monolith channel. These are used to calculate the exposed surface area and total Pt/Ba interfacial perimeter. Figure 6.2 shows the radius of Pt crystallite,  $R_C$ , and the effective storage radius of the  $\text{NO}_x$  stored in the Ba phase,  $R_{\text{eff}}$ , as supported on  $\text{Al}_2\text{O}_3$ .

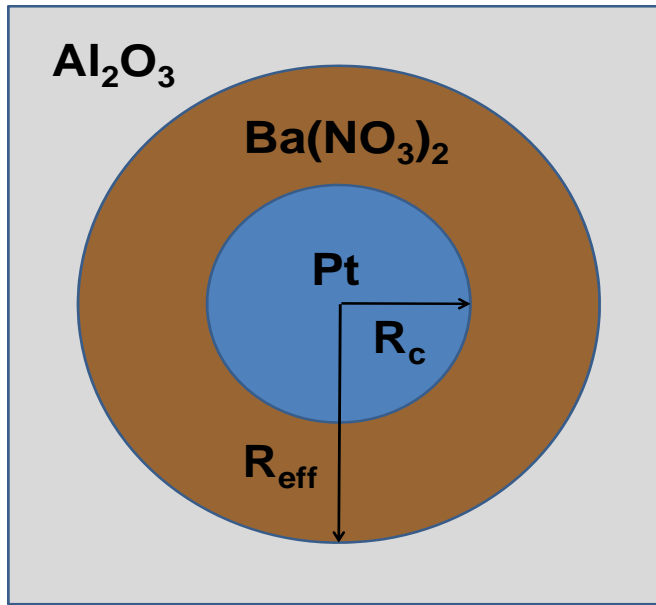


**Figure 6.2. Illustration of down-looking view of Pt on exposed BaO supported on  $\text{Al}_2\text{O}_3$ .**

3. Both Pt and Ba are assumed to have a FCC crystal structure. This gives the atomic packing factor,  $A_{PF}$ , 0.74 for Pt. For Ba, the assumption used to calculate the surface density of BaO (BaO molecules/exposed BaO area over which  $\text{NO}_x$  is stored) is from a study by Bowker et al [66].
4. All of the stored  $\text{NO}_x$  is assumed to be in the form of nitrates. While nitrites are also expected to be present, this assumption only affects the quantitative aspect of the data predicted by the model, not the spatiotemporal trend of  $\text{N}_2$  and  $\text{NH}_3$  concentrations with respect to Pt dispersion and temperature.
5. Ba is proposed to be present in the form of  $\text{Ba}(\text{OH})_2$  on account that CO and  $\text{CO}_2$  are not present in the gas phase at any time. This eliminates the need to configure the model to account for  $\text{NO}_x$  storage at different phases of Ba sites.
6. The diffusion of stored  $\text{NO}_x$  occurs in a radial direction only (1-dimensional). Although gradients exist due to contributions from the spillover of  $\text{NO}_x$  to Pt and the adsorption/desorption at the Ba sites away from Pt, the 1-D diffusion is assumed since a model depicting these gradients does not exist in the literature.

7. The process is considered to be isothermal. This assumption is supported by the minimal increase ( $< 5\text{ }^{\circ}\text{C}$ ) observed by Clayton et al. [46] during the switch from lean to rich conditions during the anaerobic regeneration of a LNT.

The assumptions listed in #5 through #7 above give the following relation for the localized material balance of stored  $\text{NO}_x$ :

$$\frac{\partial c_A}{\partial t} = \frac{D_A}{r} \frac{\partial}{\partial r} \left( r \frac{\partial c_A}{\partial r} \right); \quad R_C \leq r \leq R_{\text{eff}} \quad (6.8)$$

where  $c_A$  is the surface concentration of stored  $\text{NO}_x$  ( $\text{mol}/\text{m}^2$  exposed BaO),  $D_A$  is the diffusivity of stored  $\text{NO}_x$  in the Ba phase ( $\text{m}^2/\text{s}$ ),  $r$  is the radial coordinate (m), and  $t$  is time during regeneration (s). The initial and boundary conditions (I.C. and B.C. for (6.9) are:

$$\text{I.C. At } t = 0 \quad c_A = c_{\text{AO}}(r), \quad R_C \leq r \leq R_{\text{eff}} \quad (6.9a)$$

where  $c_A$  is the surface concentration of stored  $\text{NO}_x$  ( $\text{mol}/\text{m}^2$  exposed BaO),  $c_{\text{AO}}$  is the surface concentration of stored  $\text{NO}_x$  before the start of regeneration ( $\text{mol}/\text{m}^2$  exposed BaO).

$$\text{B.C.1. At } r = R_C \quad D_A \frac{\partial c_A}{\partial r} = k_1 c_A c_{\text{H}_2, \text{WC}} + k_2 c_A c_{\text{NH}_3, \text{WC}} \quad (6.9b)$$

$$\text{B.C.2. At } r = R_{\text{eff}} \quad \frac{\partial c_A}{\partial r} = 0 \quad (6.9c)$$

8. BaO is assumed to be present on the Al<sub>2</sub>O<sub>3</sub> surface as a monolayer. This is supported by Clayton et al., Castoldi et al., and Fanson et al. [46,67,68]. Although FT-IR studies by Dawody et al. [69] showed that all of the Al<sub>2</sub>O<sub>3</sub> sites might be covered by the BaO monolayer, the contribution of the Al<sub>2</sub>O<sub>3</sub> sites is not expected to change the predicted trends due to competitive adsorption of molecular H<sub>2</sub>O at the Al<sub>2</sub>O<sub>3</sub> sites.

The additional equations required to predict the trends of H<sub>2</sub>, NH<sub>3</sub>, and N<sub>2</sub> observed during regeneration are provided by a balance of each of these species in the gas and solid phases. The species balance for component  $j$  ( $j = \text{H}_2, \text{NH}_3, \text{or N}_2$ ) in the fluid phase is given by:

$$\frac{\partial c_{jm}}{\partial t} = -\bar{u} \frac{\partial c_{jm}}{\partial x} - \frac{k_{c,j}(x)}{R_\Omega} (c_{jm} - c_{j,W_C}) \quad (6.10)$$

where  $c_{jm}$  is the cup-mixing concentration of species  $j$  at the fluid-washcoat interface (mol/m<sup>3</sup>),  $k_{c,j}(x)$  is the mass transfer coefficient of species  $j$  (m/s),  $c_{j,W_C}$  is the concentration of species  $j$  at the fluid-washcoat interface (mol/m<sup>3</sup>),  $x$  is the axial coordinate (m), and  $R_\Omega$  effective transverse length scale (m).

H<sub>2</sub> balance:

$$\begin{aligned} \frac{\partial c_{H_2,W_C}}{\partial t} = & \frac{1}{\varepsilon_{W_C} \delta_C (a + \delta_C)} \left[ a k_{C,H_2}(x) (c_{H_2,m} - c_{H_2,W_C}) \right. \\ & \left. - \frac{c_{H_2,W_C} N_C 2\pi R_C}{4L} (4k_1 c_A|_{r=R_C} + k_3 c_{Pt} \theta_{O-Pt} R_C) \right] \quad (6.11) \end{aligned}$$

where  $\varepsilon_{W_C}$  is the porosity within the washcoat,  $\delta_C$  is the thickness of the washcoat (m),  $a$  is the width or hydraulic diameter of the channel (m),  $N_C$  is the number crystallites per channel,  $R_C$  is the radius of the crystallite (m),  $L$  is the length of the monolith (m), and  $\theta_{O-Pt}$  is the fractional surface coverage of chemisorbed oxygen on Pt



9. The  $4k_1c_A|_{r=R_C}$  term in equation (6.6) represents the consumption of  $H_2$  by stored  $NO_x$ , and  $k_3c_{Pt}\theta_{O-Pt}R_C$  represents the consumption of  $H_2$  by chemisorbed oxygen on the exposed Pt surface. These two terms are based on the assumption that the reaction rate between  $H_2$  and stored  $NO_x$  is proportional to the perimeter of the Pt/Ba interface and the reaction between  $H_2$  and chemisorbed oxygen is proportional to the surface area of the exposed Pt atoms, respectively.

$NH_3$  balance:

$$\frac{\partial NH_{3,WC}}{\partial t} = \frac{1}{\varepsilon_{WC}\delta_C(a+\delta_C)} \left[ ak_{C,NH_3}(x)(c_{NH_{3,m}} - c_{NH_{3,WC}}) + \frac{N_C 2\pi R_C c_A|_{r=R_C} (k_1 c_{H_2,WC} - (5/3) k_2 c_{NH_3,WC})}{4L} \right] \quad (6.12)$$

Finally, a species balance for  $N_2$  in the solid phase:

$$\frac{\partial N_{2,WC}}{\partial t} = \frac{1}{\varepsilon_{WC}\delta_C(a+\delta_C)} \left[ ak_{C,N_2}(x)(c_{N_{2,m}} - c_{N_{2,WC}}) + \frac{N_C 2\pi R_C k_2 c_A|_{r=R_C} c_{NH_3,WC}}{3L} \right] \quad (6.13)$$

To complete this series of equations, a balance for the vacant sites,  $\theta_V$ , on Pt is necessary:

$$\frac{\partial \theta_V}{\partial t} = k_3 c_{N_2,WC} \theta_{O-Pt} \quad (6.14)$$

The initial and boundary conditions for equations (6.10) through (6.14) are:

$$\text{I.C. At } t = 0, c_{j,m} = 0, \quad c_{j,WC} = 0, \quad \theta_V = 0, \quad 0 < x \leq L \quad (6.15a)$$

$$\text{B.C. At } x = 0, \quad c_{j,m} = c_j^{\text{in}} \quad (6.15b)$$

Equations (6.8) through (6.15) have been non-dimensionalized for use in the model and are found in Appendix A.2.

#### *6.4. Results and Discussion.*

##### *6.4.1. Determination of the Amount of NO<sub>x</sub> Stored on the Catalysts.*

One of the main features of the model employed to predict the NH<sub>3</sub> selectivity during regeneration of the LNT catalyst used in the experimental study was that regeneration commenced at the point of NO<sub>x</sub> storage at the Ba sites. This point in the lean storage phase not only needed to be repeatable but also comparable across different catalysts. As was shown by Easterling et al., the oxygen storage capacity (OSC) and NO<sub>x</sub> storage capacity (NSC) vary from one catalyst to another and these properties influence the selectivity of the N-species formed during the rich phase [47].

After several initial storage and regeneration experiments, a linear relationship became apparent between the time of the storage phase and the amount of NO<sub>x</sub> stored on the catalyst. All of the NO<sub>x</sub> stored was assumed to be in the form of nitrates for the purpose of the storage calculation and in the development of the model. As the length of the storage time and hence the amount of NO<sub>x</sub> storage increased, the relationship between time and storage gradually changed from linear to a curved resembling an exponential as shown in Fig. 6.3.

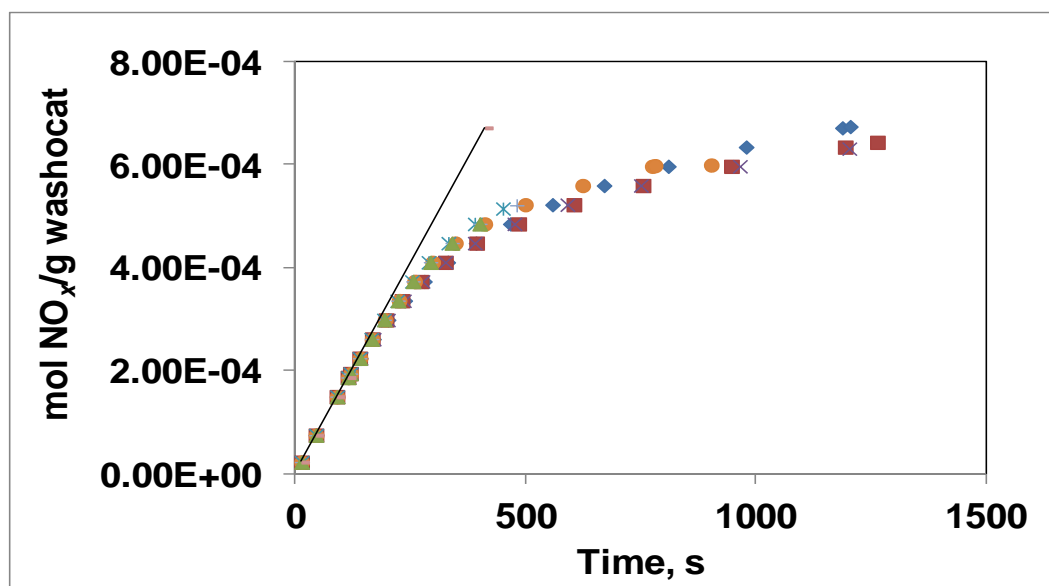


**Figure 6.3. Transition from a linear to exponential relationship occurring during NO<sub>x</sub> storage on the B-225 DG catalyst. Feed gas: 500 ppm NO, 5% O<sub>2</sub>, bal Ar at 200 °C.**

Additionally, it became apparent that the regeneration of the LNT with NO<sub>x</sub> storage up to this change from a linear to an exponential relationship was easily repeatable with regards to the time required to reach a subsequent specified level of NO<sub>x</sub> storage. After this transition point, the repeatability of using the same storage time across multiple experimental runs decreased. It was postulated that the change in the slope of these curves was due to NO<sub>x</sub> storage switching from easily accessible sites to bulk storage sites. The existence of multiple storage sites has been presented in the literature by several groups [46,49,70-75]. The consensus concerning the bulk storage sites is that these sites require longer and deeper purges to be regenerated. As observed in storage and regeneration trials, the level of regeneration would vary from one experiment to another, which would in turn affect the time required to reach a level of NO<sub>x</sub> storage. Based on the existence of this transition point, the amount of NO<sub>x</sub> storage for each sample was chosen to be the time required to reach the limit where the storage capacity of the easily accessible or surface sites was reached. This selection of the fixed storage amount was also in line with the assumption utilized in the model that the BaO sites exist as a monolayer on the Al<sub>2</sub>O<sub>3</sub> surface [66].

The amounts of NO<sub>x</sub> storage selected for the degreened and aged Pt/Rh/Ba/Al<sub>2</sub>O<sub>3</sub> catalysts are provided in Table 6.2. The difference in storage capacity between these two catalysts is reflected in the greater amount of NO<sub>x</sub> stored in the degreened catalyst as compared to the aged one. This result is expected since the NSC of a catalyst is reduced after aging due to phase separation between the Pt crystallites and Ba storage phase. As discussed previously and reported in the literature, a close proximity of Pt and Ba is required for efficient NO<sub>x</sub> storage in the form of the spillover mechanism [35,39,46,47,51,71,73,76-94]. As a LNT undergoes aging, sintering of the Pt particles occurs, resulting in the growth of the crystallites and decrease in dispersion. Larger crystallites and lower dispersion results in an increase in phase segregation and decrease in proximity of the Pt and Ba, the storage capacity is reduced. This effect can be illustrated using the concept of different zones existing along the length of the catalyst as reported in the literature [35,46,47,95-99]. As these researchers proposed, upon aging, the NO<sub>x</sub> storage zone in the catalyst extends further along the length of the catalyst due to fewer Pt sites existing per length of catalyst. In other words, a greater length of catalyst is now required to store an equal amount of NO<sub>x</sub> in an aged LNT as compared to a degreened one.

**Table 6.2. Amount of NO<sub>x</sub> for each of catalysts.**

Catalyst	Condition	Temperature, °C	Amount of NO <sub>x</sub> stored, mol NO <sub>x</sub> / g washcoat	Storage Time, s
B-225	DG	200	3.36 x 10 <sup>-4</sup>	229
	DG	300	3.36 x 10 <sup>-4</sup>	255
	AD	200	2.47 x 10 <sup>-4</sup>	130
	AD	300	2.47 x 10 <sup>-4</sup>	150

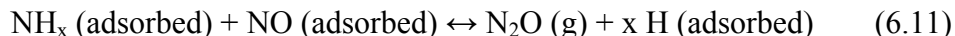
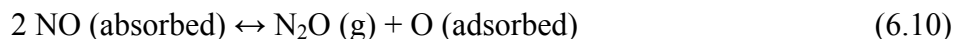
Another trend visible in Table 6.2 is the effect of temperature on storage time. For the two temperatures chosen, 200 and 300 °C, it took less time to reach the fixed level of storage at the lower temperature. At first this result seemed unexpected based on the reasoning that the time needed to reach a fixed amount at the higher temperature should be less than the time needed at the lower temperature due to the kinetics of NO<sub>x</sub> oxidation being faster at higher temperatures. While the kinetics at 300 °C were faster as evidenced

by the increased amount of NO<sub>2</sub> detected (data not shown), it is not meaningful to compare storage times because the storage capacities are different.

#### 6.4.2 Experimental Results: NH<sub>3</sub>, N<sub>2</sub>O, H<sub>2</sub>.

##### 6.4.2.1 B-225 DG.

As mentioned in the Introduction, the ratio of H:N:O species at the Pt sites affects the products formed during regeneration of the LNT catalyst. As a reminder, low H<sub>2</sub>:NO<sub>x</sub> ratios favor N<sub>2</sub>O formation, and high H<sub>2</sub>:NO<sub>x</sub> ratios favor NH<sub>3</sub> formation [35-40]. An idea of the value of this ratio at any time during regeneration is provided by comparing the time required for the products (e.g., NH<sub>3</sub> and N<sub>2</sub>O) and the reductants (e.g., H<sub>2</sub>) to emerge from the catalyst outlet. Looking at Fig. 6.4, these trends are presented. The time originates at the transition from lean to rich conditions. In Fig. 6.4a, N<sub>2</sub>O is present almost immediately in the reactor effluent. This almost instantaneous formation of N<sub>2</sub>O is explained by examining the conditions that must be present on the catalyst surface for N<sub>2</sub>O production. According to Lietti [100], N<sub>2</sub>O is produced either by:



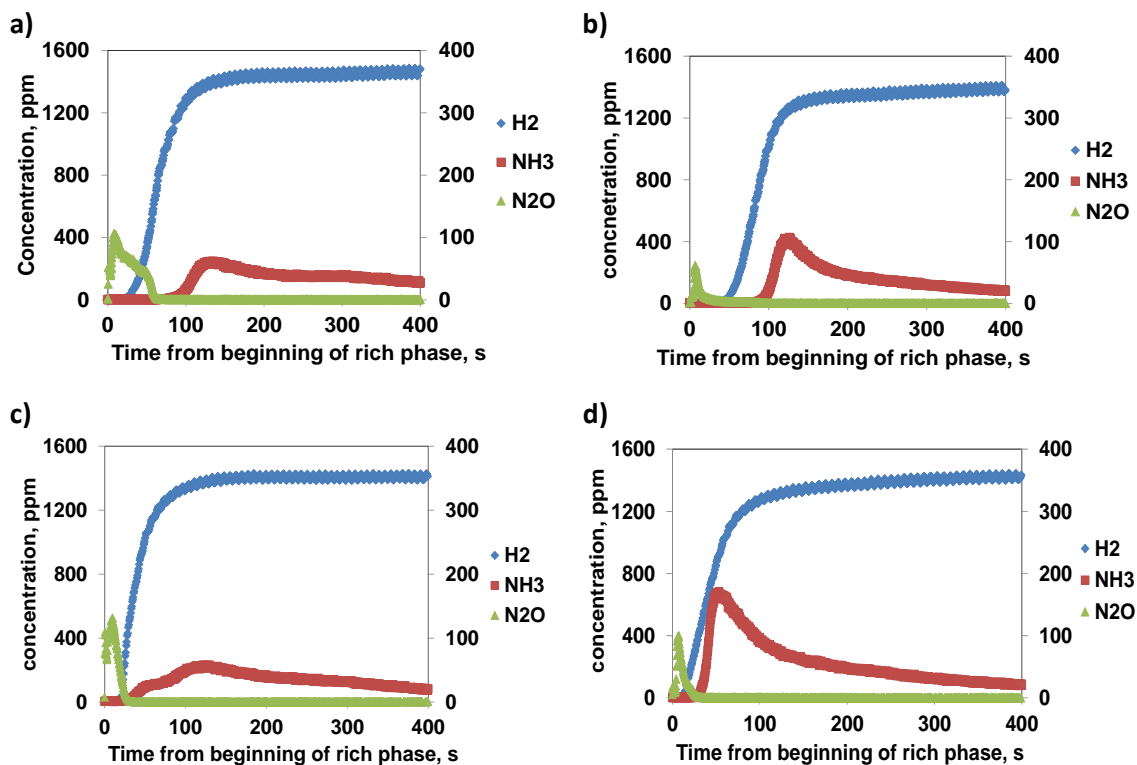


**Figure 6.4. Relationship between the break-through times of H<sub>2</sub>, NH<sub>3</sub>, and N<sub>2</sub>O for: a) B-225 DG at 200 °C, b) B-225 DG at 300 °C, c) B-225 AD at 200 °C, and d) B-225 AD at 300 °C.**

Considering that Xu et al. [38] stated that low H<sub>2</sub>:NO<sub>x</sub> ratios favor N<sub>2</sub>O production, and there exists for the B-225 catalyst at 200 °C over a 60 s delay after N<sub>2</sub>O release and before NH<sub>3</sub> release is present, the first reaction is more likely to occur at the lean to rich transition. As Choi et al. recently reported [97], the criteria for NO<sub>x</sub> release from the Ba sites back to the Pt crystallites and from the Ba sites located far from Pt is a net deficit of oxygen present in the monolith at a particular point.

As reported by many groups [35,36,38,40-46], a reductant front is present at the beginning of the rich phase at the front of the catalyst monolith. H<sub>2</sub> consumes any residual oxygen present in the gas stream as well as any oxygen chemisorbed on the catalyst surface. By consuming the oxygen present, the environment becomes oxygen deficient and NO<sub>x</sub> release begins. N<sub>2</sub>O is favored at the leading edge of the front since

any H<sub>2</sub> present reacts with either stored oxygen or NO<sub>x</sub>. N<sub>2</sub>O production continues until enough H<sub>2</sub> is present in the reductant front to increase the H<sub>2</sub>:NO<sub>x</sub> ratio to levels that favor NH<sub>3</sub> (2.5) [38,40]. Because the hydrogen is consumed at the leading edge of the front, N-species such as N<sub>2</sub>O and unreacted NO and NO<sub>2</sub> are capable of traveling downstream in the monolith. The N<sub>2</sub>O passes through unreacted while NO and NO<sub>2</sub> can be readsorbed at sites located further along the axis of the monolith.

Eventually, as the regeneration phase continues, the chemisorbed oxygen at the Pt sites is consumed and the amount of hydrogen present at the Pt/Ba interface increases. The actual amount of hydrogen present at this time is dependent on the rate of diffusion of NO<sub>x</sub> from Ba to the Pt sites. At 200 °C, the kinetics of the following reaction is slow enough that the rate of diffusion is controlling:



The delay between H<sub>2</sub> and NH<sub>3</sub> in the effluent as shown in Fig 6.4a supports the necessity of a high ratio of H<sub>2</sub>:NO<sub>x</sub> for NH<sub>3</sub> production [35-40]. Before NH<sub>3</sub> reaches the effluent, NO<sub>x</sub> stored downstream in the catalyst must be consumed or NH<sub>3</sub> will react with NO<sub>x</sub> as follows:



The yield and the selectivity of NH<sub>3</sub> increases along the length of the catalyst as shown in Fig. 6.5, because as one moves downstream, less NO<sub>x</sub> is available to react with NH<sub>3</sub> [35,36,41,57,101-103].

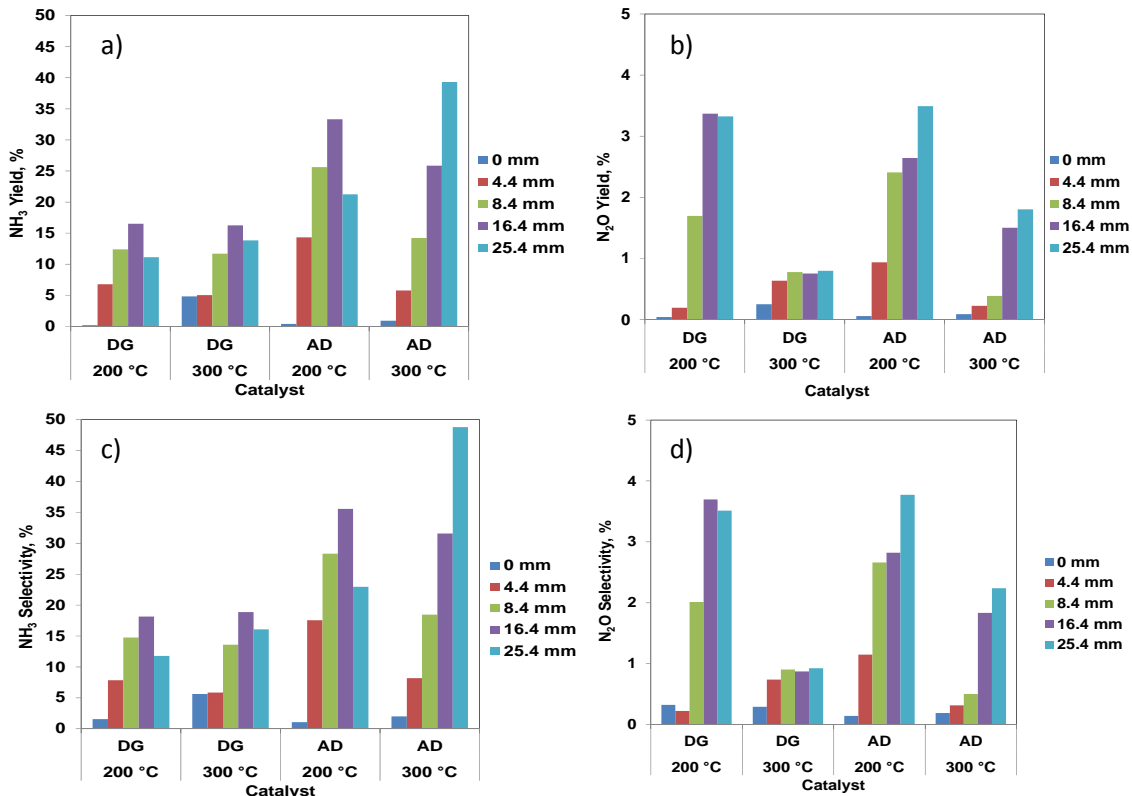


**Figure 6.5. Comparison of yield and selectivity for B-225 DG and AD catalysts. a) NH<sub>3</sub> Yield, %, b) N<sub>2</sub>O Yield, %, c) NH<sub>3</sub> Selectivity, %, d) N<sub>2</sub>O Selectivity.**

Using the assumption that NO<sub>x</sub> is stored as a monolayer and considering the results of the NO<sub>x</sub> storage during the lean phase in Fig 6.3, it is evident that the entire length of LNT is involved in NO<sub>x</sub> storage. This situation is different than the experiments reported by Easterling et al. [47] where for the degreened B-225 catalyst, only the front portion of the catalyst was used for NO<sub>x</sub> storage. As reported for that experiment, the maximum in NH<sub>3</sub> selectivity occurred after the NO<sub>x</sub> storage zone. This spatial relationship is present again in these experiments except the NO<sub>x</sub> storage zone encompasses the entire length of the catalyst.

When the temperature of the experiment is increased to 300 °C, the controlling regime during regeneration changes from diffusion to H<sub>2</sub> feed limited. By noticing the greater time lag before H<sub>2</sub> appears in the effluent at 300 °C in Figure 6.4a compared to 200 °C in Figure 6.4b, this transition between control regimes becomes apparent. N<sub>2</sub>O again



appears shortly after the switch to rich conditions, but at 300 °C the length of time for which N<sub>2</sub>O is present in the effluent is much shorter than at 200 °C. The production of N<sub>2</sub>O continues until H<sub>2</sub> begins to be present at 200 °C, while at 300 °C, N<sub>2</sub>O production ends well before H<sub>2</sub> is observed. The conditions that are favorable to N<sub>2</sub>O exist for a shorter time in this case (H<sub>2</sub>:NO<sub>x</sub> < 1) [38,40]. Additionally, as reported in the literature [36,39,41,42,46] lower temperatures (T < 200 °C) are more favorable for N<sub>2</sub>O production. As the amount of H<sub>2</sub> present at the Pt/Ba interface increases, N<sub>2</sub> is produced until the ratio is great enough to favor NH<sub>3</sub>. The production of N<sub>2</sub> has been reported by [39,41] to be favored at a ratio of H<sub>2</sub>:NO<sub>x</sub> equal to ~1.

#### 6.4.2.2. B-225 AD.

Although a direct comparison between the degreened and aged catalysts cannot be made since the amount of NO<sub>x</sub> stored was not the same, the following remarks are applicable. Aging of the catalyst results in less Pt crystallites per length of catalyst (lower dispersion) with a larger particle diameter. In terms of the rate at which the reduction front propagates, after the catalyst has been aged, the H<sub>2</sub> front propagates along the length of the catalyst faster than the rate observed with the degreened catalyst. This increased rate of travel is shown in Fig. 6.4c where H<sub>2</sub> breakthrough is observed ~15 s quicker for the aged catalyst than for the degreened catalyst shown in Fig. 6.4a. Because there are fewer Pt crystallites, less chemisorbed oxygen and less stored NO<sub>x</sub> is present per length of the catalyst to consume the H<sub>2</sub> in the reduction front as it travels along the catalyst.

The other effect of sintering is apparent in the yield and selectivity of NH<sub>3</sub> and N<sub>2</sub>O in Fig 6.5. Although twice as much NO<sub>x</sub> was stored on the degreened catalyst as compared to the aged catalyst (Table 6.2), the NH<sub>3</sub> yield and selectivity are much greater for the aged catalyst than for the degreened catalyst. Additionally, the time between H<sub>2</sub> and NH<sub>3</sub> breakthrough is decreased for the aged catalysts. With fewer sites per length of catalyst, the stored NO<sub>x</sub> at the Ba sites must travel farther to reach the Pt sites during regeneration. Although the intrinsic rate of diffusion is the same, the increased distance results in an increase in diffusion time. By the time the NO<sub>x</sub> reaches the Pt sites, the ratio of H<sub>2</sub>:NO<sub>x</sub> is expected to be higher and at a value that favors NH<sub>3</sub> formation. Also contributing to

NH<sub>3</sub> selectivity is the possibility of reduced rates of NO<sub>x</sub>-NH<sub>3</sub> SCR and NH<sub>3</sub>-O<sub>2</sub> reactions after aging [39]. If these rates of reaction are significantly reduced, the probability of NH<sub>3</sub> consumption downstream in the catalyst by these reactions increases, and therefore leads to increased NH<sub>3</sub> concentrations in the effluent from the monolith.

#### *6.4.3 Modeling Results.*

The main focus of this work was to determine the ability of a model developed by Bhatia et al. [44] to predict the NH<sub>3</sub> selectivity of LNT catalysts that included Rh. Another variation between this study and the study by Bhatia et al. is the amount of fixed NO<sub>x</sub> stored on each catalyst and the residence time in the catalyst. As reported by Easterling et al. [47], the NO<sub>x</sub> storage capacity and oxygen storage capacity varies between degreened and aged catalysts. Whereas Bhatia et al. and Clayton et al. [44,46] varied Pt dispersion by adjusting the Pt loading of the catalysts, the dispersions in this experiment were varied by exposing the catalysts to aging conditions which which sintering of the Pt occurred. The residence time in the catalyst was adjusted by using a GHSV of 30,000 h<sup>-1</sup> instead of 60,000 h<sup>-1</sup>. This adjustment in GHSV is instructive in modeling the regeneration events since the residence time will vary in real world applications as the engine operates under various loads.

##### *6.4.3.1 Model vs. Experimental Results: B-225 DG.*

Simulations using the dispersion model were performed to predict the NH<sub>3</sub> production during regeneration of the two catalysts after a fixed level of NO<sub>x</sub> was stored. Table 6.3 lists the parameters used to fit the data. The only variation in parameters from the values used by Bhatia et al. [44] was the surface diffusivity of NO<sub>x</sub>, D<sub>A</sub>, traveling from Ba to the Pt sites. Since the model is based on PGM dispersion, the parameters that have the most impact on the model data are D<sub>A</sub> and the measured value of the PGM dispersion. While Bhatia used values of 5x10<sup>-19</sup> m<sup>2</sup>/s and 5x10<sup>-18</sup> m<sup>2</sup>/s for D<sub>A</sub> at 160 °C and 230 °C, respectively, a value of 9x10<sup>-18</sup> m<sup>2</sup>/s was used for 200 °C. As mentioned in the experimental section, values for D<sub>A</sub> are not available in the literature.

**Table 6.3 a. Values of  $N_c$ ,  $R_c$ , and  $R_{eff}$  for various Pt dispersions.**

Catalyst		Pt Dispersion (%)	$N_c$	$R_c$ (m)	$R_{eff}$ (m)
B-225	Degreened	15.6	$2.95 \times 10^{14}$	$2.22 \times 10^{-9}$	$1.77 \times 10^{-8}$
B-225	Aged	3.34	$2.95 \times 10^{14}$	$1.03 \times 10^{-8}$	$1.32 \times 10^{-7}$
B-225	Aged*	15.5	$1.02 \times 10^{14}$	$2.23 \times 10^{-9}$	$2.24 \times 10^{-8}$

\* Using the physical properties of Rh instead of Pt (see section 6.4.3.2. for explanation)

**Table 6.3 b. Parameter values to estimate  $N_c$  and  $R_{eff}$ .**

Pt		Rh	
$A_{PF}$	0.74	$A_{PF}$	0.74
$D_{Pt}$ (m)	$2.78 \times 10^{-10}$	$D_{Rh}$ (m)	$2.70 \times 10^{-10}$
$M_{PtT}$ (mol/channel)	$7.42 \times 10^{-7}$	$M_{RhT}$ (mol/channel)	$2.81 \times 10^{-7}$
$n_{ch}$	125	$n_{ch}$	125
$N_{av}$	$6.022 \times 10^{23}$	$N_{av}$	$6.022 \times 10^{23}$
$S_{BaO}$ (BaO molecules/m <sup>2</sup> exposed BaO)	$1.89 \times 10^{18}$	$S_{BaO}$ (BaO molecules/m <sup>2</sup> exposed BaO)	$1.89 \times 10^{18}$

**Table 6.3 c. Variation of  $M_{NO_x}$ (mol) with monolith length, assuming uniform, axial  $NO_x$  storage.**

Catalyst		25.4 mm	16.4 mm	8.4 mm	4.4 mm	0.0 mm
B-225	Degreened	$2.26 \times 10^{-4}$	$1.46 \times 10^{-4}$	$7.46 \times 10^{-5}$	$3.91 \times 10^{-5}$	$8.89 \times 10^{-6}$
B-225	Aged	$2.26 \times 10^{-4}$	$8.07 \times 10^{-5}$	$4.13 \times 10^{-5}$	$2.17 \times 10^{-5}$	$4.92 \times 10^{-6}$

The comparisons of the experimental and model predicted data for the B-225 DG catalyst at 200 °C are shown in Fig 6.6a and b. The quality of the fit of the model was judged by comparing the spatiotemporal data as well as the relative amounts of  $NH_3$  measured at each of the positions along the length of the catalyst. With these parameters (Table 6.3), the fit of the data with respect to time from the beginning of regeneration was reasonable. The model captures the delay before the onset of  $NH_3$  at each of the positions. At the front of the catalyst, a value of 0.1 mm was used in the calculations for the parameters to ensure that the capillary was in a channel. Both sets of data show an increase in  $NH_3$  concentrations from the front position to the remaining locations. As previously reported

[47], the decrease in NH<sub>3</sub> concentration at the rear position (25.4 mm) was most likely due to a slight over-sampling present in the experimental setup.

Considering the maximum values of the NH<sub>3</sub> concentrations attained, the model over-predicted the values. As stated previously, the model assumes that NH<sub>3</sub> does not readsorb downstream on the catalyst surface. In order to provide a better fit of the data, the values for the reaction rates were systematically varied. The result of this effort was that the peak values for NH<sub>3</sub> were decreased while changing the shape of the curve from a sharp peak to more rounded curve when the reaction rate constant of NH<sub>3</sub> generation from the reduction of NO<sub>x</sub> with H<sub>2</sub> was changed from  $1 \times 10^{-3} \text{ m}^4/\text{mol} \cdot \text{s}$  to  $1 \times 10^{-5} \text{ m}^4/\text{mol} \cdot \text{s}$  as shown in Fig. 6.7b. Lastly, it is apparent that a tailing effect is present in the NH<sub>3</sub> measurements. This tailing is due to the polarity displayed by NH<sub>3</sub> in the capillary. Although steps were taken to minimize this effect by using resistance heating to keep the temperature of the capillary high from inside the catalyst to the sample cell of the mass spectrometer, there is always a slight hold up of NH<sub>3</sub> in this type of measurement.

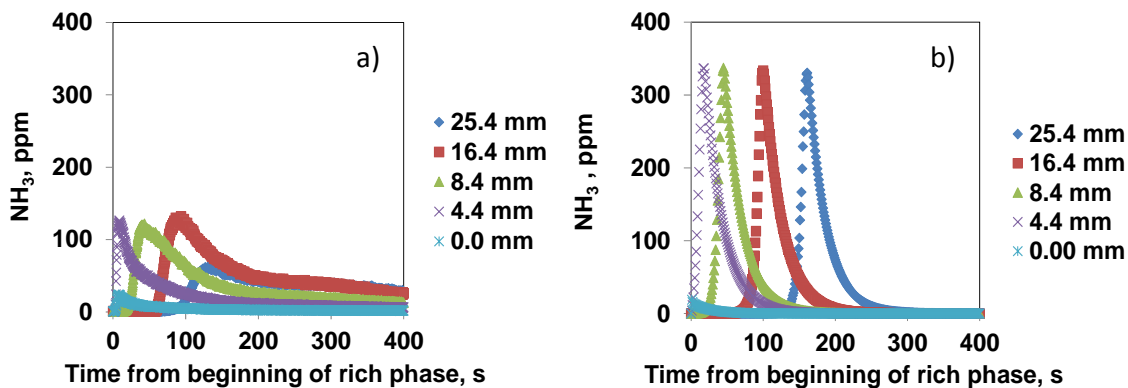


**Figure 6.6. Comparison between the a) experimental data and b) model predicted data for the B-225 DG catalyst at 200 °C.**

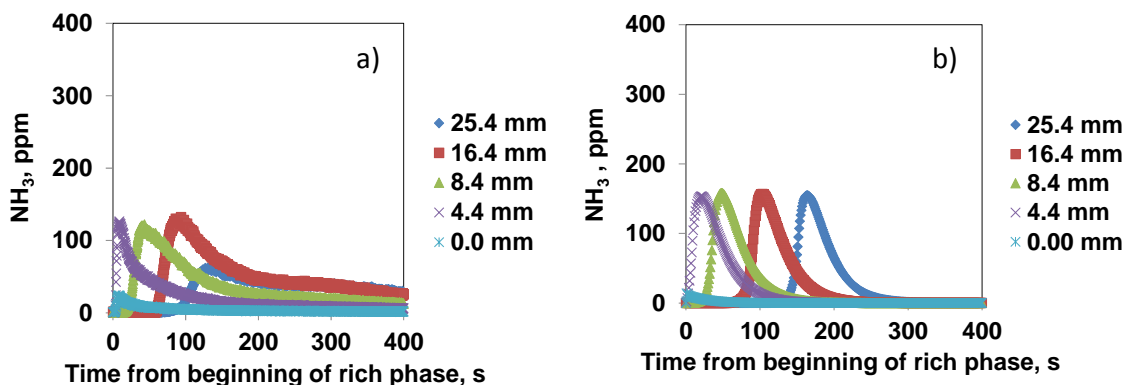


**Figure 6.7. Comparison between the a) experimental data and b) model predicted data for the B-225 DG catalyst at 200 °C with  $k_1 = 1 \times 10^{-5} \text{ m}^4/\text{mol}\cdot\text{s}$  instead of  $1 \times 10^{-3} \text{ m}^4/\text{mol}\cdot\text{s}$ .**

When the model was used to generate the  $\text{NH}_3$  data at 300 °C, a different regime controlled the  $\text{NH}_3$  selectivity. Whereas the process was diffusion controlled at 200 °C, the process is  $\text{H}_2$  feed-limited at 300 °C. A value of  $9 \times 10^{-17} \text{ m}^2/\text{s}$  was used for  $D_A$  at 300 °C since the model increases the diffusivity by an order of magnitude for every 100 °C temperature increase. This value of  $D_A$  is almost the same as the value used by Bhatia at 300 °C,  $5 \times 10^{-17} \text{ m}^2/\text{s}$  [44]. The experimental and model data are shown in Fig. 6.8a and b.

While the peak concentrations in the model data are close to experimental values, the delay before the onset of  $\text{NH}_3$  release into the gas stream is overestimated in the data provided by the model. The experimental data at 300 °C displays a sharper peak shape than the 200 °C data, and this characteristic is captured in the model data at 300 °C. The differences between a situation where  $\text{NO}_x$  diffusion is controlling and one limited by the rate  $\text{H}_2$  is fed to process become more visible at the measurement locations further along the length of the catalyst. At all of the locations in the experimental data,  $\text{NH}_3$  release begins less than 100 s after conditions are changed to rich. However, for the model the  $\text{NH}_3$  release for the 16.4 mm and 25.4 mm positions does not begin until after 100 s.

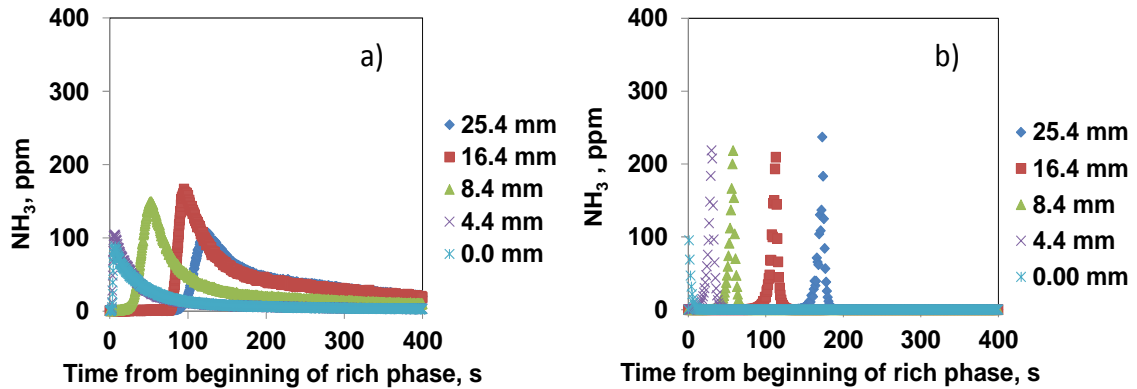


**Figure 6.8. Comparison between the a) experimental data and b) model predicted data for the B-225 DG catalyst at 300 °C.**

For consistency, the data were also generated using a value for  $k_1$  of  $1 \times 10^{-5} \text{ m}^4/\text{mol} \cdot \text{s}$ , the results being presented in Fig. 6.9a and b. This parameter adjustment did not provide an improvement in the predicted model data. The result of this change was a decrease in the peak  $\text{NH}_3$  concentration. Although the reaction rate constants do not compensate for temperature in the model, based on the fits displayed in Fig. 6.7 and 6.8, a case can be made that  $k_1$  does vary with the temperature from 200 °C to 300 °C. This change in rate constant could also be accounting for a process which was not accounted for by the model, i.e.,  $\text{NH}_3$  readsorption.

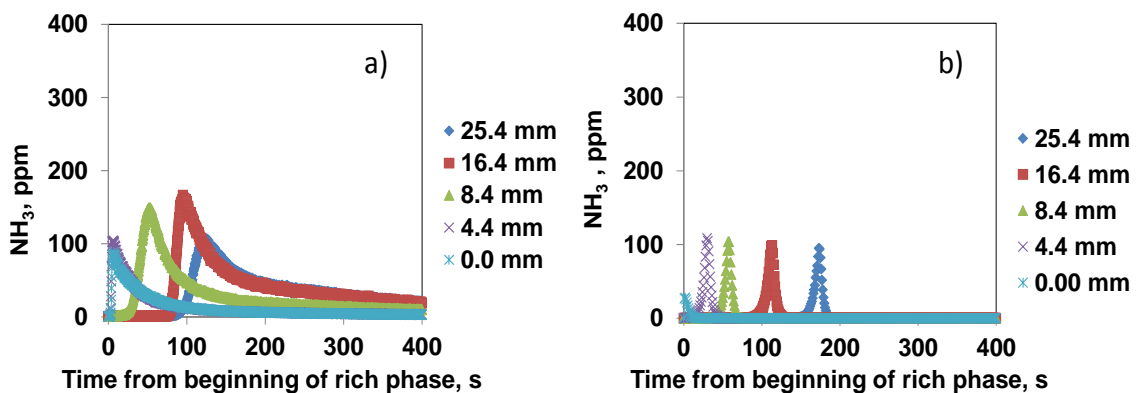


**Figure 6.9. Comparison between the a) experimental data and b) model predicted data for the B-225 DG catalyst at 300 °C with  $k_1 = 1 \times 10^{-5}$  instead of  $1 \times 10^{-3}$ .**

#### 6.4.3.2. Model vs. Experimental Results: B-225 AD.

As discussed for the experimental data, the most prevalent change that occurs with a catalyst that has undergone aging is the reduction in the time or delay before  $\text{NH}_3$  release is measured at the positions along the length of the catalyst. Using the parameters listed in Table 6.4, a comparison was made between the experimental and model data for aged B-225 catalyst at 200 °C (see Fig. 6.10a and b). The average radius of the Pt crystallites and the average radius of stored  $\text{NO}_x$  around the crystallite both increased as expected after aging. The reduced lag before  $\text{NH}_3$  release occurs in the aged catalyst compared to the degreened catalyst is captured by the model. Additionally, the shape of the  $\text{NH}_3$  curves (sharp peaks) is also captured in the model data. However, a problem exists concerning the parameters used to predict this set of data. As mentioned earlier, the dispersion and the diffusivity values are the parameters that have the greatest effect on the data predicted by the model. Using a  $D_A$  value of  $9 \times 10^{-18} \text{ m}^2/\text{s}$  as with the degreened data generates data that do not agree with the experimental data. The flaw in the model data set is that all of the onset of  $\text{NH}_3$  releases occur at the instant conditions are switched from lean to rich in the catalyst. Although this delay is reduced after the catalyst is aged, nevertheless, a delay still exists in the experimental data for this case.

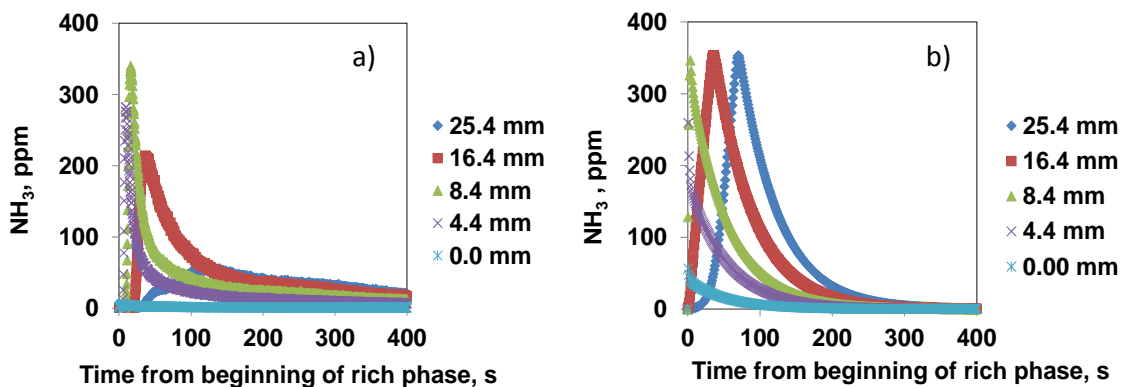


**Figure 6.10. Comparison between the a) experimental data and b) model predicted data for the B-225 AD catalyst at 200 °C with  $D_A = 9 \times 10^{-18} \text{ m}^2/\text{s}$ .**

To obtain a better fit of the data,  $D_A$  was increased to  $9 \times 10^{-16} \text{ m}^2/\text{s}$ , and this comparison is shown in Fig. 6.11a and b. While an improved fit is obtained from changing the value for  $D_A$ , an increase in the diffusivity is counter intuitive for aged catalysts since the sintering should result in phase segregation between Pt and Ba speices.

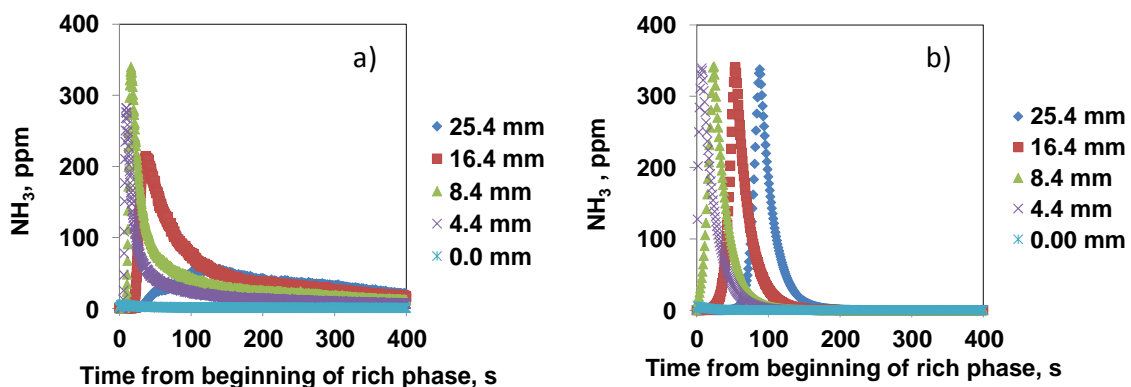


**Figure 6.11.** Comparison between the a) experimental data and b) model predicted data for the B-225 AD catalyst at 200 °C with with  $D_A = 9 \times 10^{-16} \text{ m}^2/\text{s}$ .

As a way to provide a better fit, the parameters used in the model for the aged catalyst were calculated using Rh instead of Pt. When Rh is used in a Pt/Rh alloy, catalysts have been reported to be more resistant to sintering [63]. Moreover, as discussed earlier, Rh is less prone to sintering than Pt in the first place, due to the lower vapor pressure of both the metal and the oxide, as compared to Pt [64]. In addition, Rh has been reported to be a more effective reduction catalyst than Pt [59,60]. Hence, it is reasonable to assume that after aging, Rh/Pt particles are primarily responsible for the  $\text{NO}_x$  reduction activity of the catalyst. For this set of generated data, the dispersion of PGM was adjusted so that the radii of the crystallites using properties of Rh were equal to the values using Pt.

With the value of  $D_A$  again at  $9 \times 10^{-18} \text{ m}^2/\text{s}$ , Fig. 6.12a and b shows the comparison between experimental and model data for B-225 AD at 200 °C. The changes in the parameters involved in the model are displayed in Table 6.4a and b. The result of using Rh to predict the properties of the PGM crystallites is an improved fit of the data with regards to both the delay before the onset, peak concentration, and shape of the release curves of  $\text{NH}_3$ . For the experimental data, almost no delay exists for the beginning of



NH<sub>3</sub> release at the 0.0 mm, 4.4 mm, and 8.4 mm positions. As discussed, this is an expected result of a decrease in PGM dispersion due to sintering. Fewer crystallites per unit length of catalyst lead to an increase in the rate of propagation of the H<sub>2</sub> front in the catalyst. This increase also decreases the time required for H<sub>2</sub>:NO<sub>x</sub> ratios to reach levels that favor NH<sub>3</sub> selectivity. However, the model fails to capture the decrease in maxima of NH<sub>3</sub> observed at the 16.4 mm and 25.4 mm positions. Although the decrease at 25.4 mm may be attributed to the method of sampling the gas species within the channel of the monolith using SpaciMS, the decrease observed at 16.4 mm leads one to conclude either that the NH<sub>3</sub> is readsorbed on the catalyst surface or consumed by NO<sub>x</sub> downstream in the catalyst.

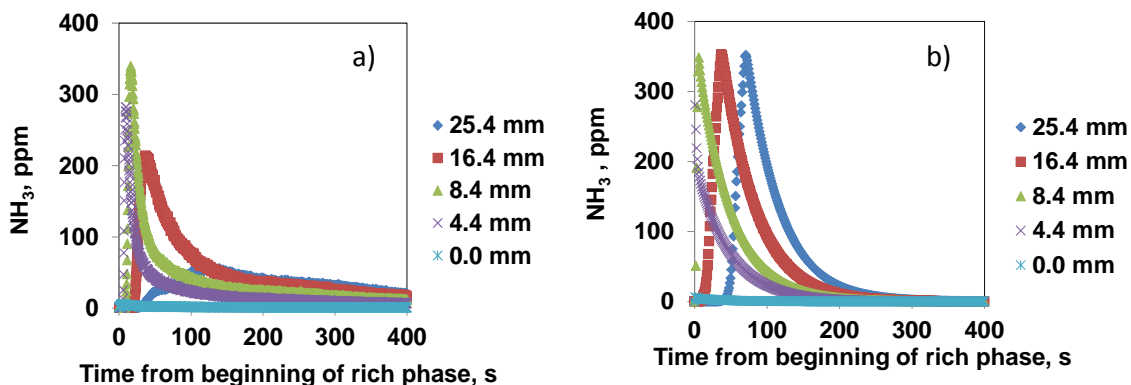


**Figure 6.12. Comparison between the a) experimental data and b) model predicted data for the B-225 AD catalyst at 200 °C.**

The same shortcomings exist in using Pt crystallites parameters for the modeling at 300 °C as at 200 °C. Again Rh was used for parameter evaluation for this data set as shown in Fig. 6.13a and b. Although this correction does provide an improved fit in terms of the spatiotemporal nature of the data, as with the degreened catalyst at 300 °C, the data from the model fails to capture all of the characteristics of the experimental data such as shape of the curves and maximum concentrations. This shortcoming is again the result of the process becoming H<sub>2</sub> feed limited at the higher temperature.

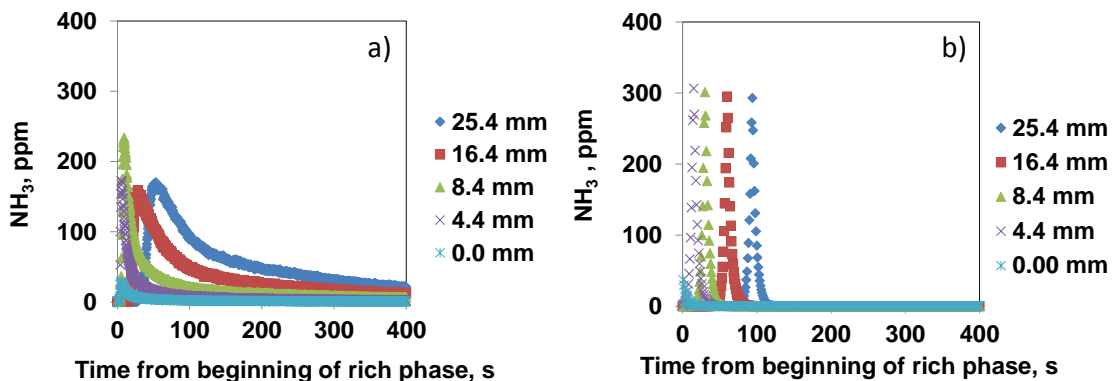


**Figure 6.13. Comparison between the a) experimental data and b) model predicted data for the B-225 AD catalyst at 300 °C.**

An intriguing feature of the comparison between the degreened and aged data concerns the maximum concentration of  $\text{NH}_3$  measured at any of the points along the catalyst. Whereas the model did predict lower  $\text{NH}_3$  levels at 200 °C than at 300 °C ( Fig 6.12 and Fig 6.13) as seen for the experimental aged data, this was not the case for the degreened data (Fig 6.6 and 6.7). The model predicted a higher, maximum concentration of  $\text{NH}_3$  for the 200 °C data as compared to the data at 300 °C, whereas the experimental data possessed the opposite trend. In fact, the slight increase selectivity as suggested by the peak  $\text{NH}_3$  concentrations in the experimental data for the higher temperature is in agreement with the findings as reported by Bhatia et al. and Clayton et al. [44,46]. If the degreened catalyst is compared to the results Bhatia and Clayton reported for their 8% dispersion catalyst, the experimental data presented here is agreement with their results that  $\text{NH}_3$  release increases with increasing temperature to 300 °C, while the model data presented here is contrary to their results. Similarly, if the aged data presented here is compared to Bhatia and Clayton’s data for the 3% dispersion catalyst, the trends in the experimental and model predicted data agree with their trends for the low dispersion catalyst that net  $\text{NH}_3$  increases with increasing temperature. The slight increase in the experimental data for the higher temperature is contrary to the expected trends based on LNT catalysts usually displaying increased selectivity to  $\text{NH}_3$  at temperatures below 250 °C.

### 6.5. Conclusions.

The crystallite-scale model developed by Bhatia [44] has been employed to predict the selectivity of  $\text{NH}_3$  in experiments in which degreened and aged Pt/Rh/Ba/ $\text{Al}_2\text{O}_3$  LNT catalysts underwent regeneration after a fixed amount of  $\text{NO}_x$  was stored. Experiments included two catalysts at two different temperatures, whose PGM dispersions were varied by subjecting one of the catalysts to aging under lean conditions at elevated temperatures. The results from the experiments were consistent with the species observed during regeneration being a function of the PGM dispersion and the ratio of  $\text{H}_2:\text{NO}_x$  at the Pt/Ba interface. As reported in the literature [35,38,41-47], a reductant front travels down the length of the catalyst during regeneration in which the ratio of reductant to stored  $\text{NO}_x$  varies based on time and position.  $\text{N}_2\text{O}$  is favored at low ratios of  $\text{H}_2:\text{NO}_x$  (at the leading edge of the front) and  $\text{NH}_3$  is favored at higher ratios of  $\text{H}_2:\text{NO}_x$  (behind the reduction front).

The modeling results indicated the use of a diffusion-based model with temperature dependent diffusivities is capable of capturing the spatiotemporal trends associated with  $\text{NH}_3$  release from the LNT at low temperatures and high dispersions. The model accurately predicted the individual delay at each position before the onset of  $\text{NH}_3$  release. The model was also able to predict these trends for the aged data after the parameters were adjusted using the values for the physical properties of Rh instead of Pt. This change was justified not only by the results, but also by the fact that Rh is a superior reduction catalyst and more resilient to sintering than Pt; hence, Rh is expected to be the main catalytic species active in the reduction of  $\text{NO}_x$  in the aged catalyst, particularly at lower temperatures (e.g. 200 °C).

Further refinement of the model is required to account for the over prediction of the amounts of  $\text{NH}_3$  measured at each location for two catalysts. The increased amounts of  $\text{NH}_3$  predicted by the model are most likely due to a combination of the lack of accounting for  $\text{NH}_3$  readsorption on the catalyst after it is released, and the assumption of a uniform storage of  $\text{NO}_x$  along the length of the catalyst. An improved storage model that could capture the gradients in the amount of  $\text{NO}_x$  stored from the front to the rear of

the monolith would be valuable to predict the phenomena observed during regeneration. Lastly, if a SpaciMS study were performed in which the amounts of reductant present at each measurement location were measured, it would be beneficial in providing insight into the conditions influencing  $\text{NH}_3$  selectivity.

### 6.6. References.

- [1] N. Miyoshi, S. Matsumoto, K. Katoh, T. Tanaka, J. Hardara, N. Takashi, K. Yokota, M. Sugiura, K. Kasahara, Development of New Concept Three-Way Catalyst for Automotive Lean-Burn Engines. SAE Technical Paper Series 950809 (1995).
- [2] N. Takahashi, H. Shinjoh, T. Iijima, T. Suzuki, K. Yamazaki, K. Yokota, H. Suzuki, N. Miyoshi, S. Matsumoto, T. Tanizawa, T. Tanaka, S. Tateishi, K. Kasahara, The New Concept 3-Way Catalyst for Automotive Lean-Burn Engine: NO<sub>x</sub> Storage and Reduction Catalyst. *Catalysis Today* 27 (1996) 63-69.
- [3] J.G.E. Cohn, D.R. Steele and H.C. Andersen, Selective Removal of Nitrogen Oxides from Oxygen-Containing Gases, Especially from Nitric Acid Production from Ammonia. US Patent No. 2975025 (1961).
- [4] W.S. Epling, L.E. Campbell, A. Yezerets, N.W. Currier, J.E. Parks II, Overview of the Fundamental Reactions and Degradation Mechanisms of NO<sub>x</sub> Storage/Reduction Catalysts. *Catalysis Reviews* 46 (2004) 163-246.
- [5] R.Q. Long, R.T. Yang, Superior Fe-ZSM-5 Catalyst for Selective Catalytic Reduction of Nitric Oxide by Ammonia. *Journal of the American Chemistry Society* 121 (1999) 5595-5596.
- [6] A.Z. Ma, W. Grunert, Selective Catalytic Reduction of NO by Ammonia over Fe-ZSM-5 Catalysts. *Chemical Communications (Cambridge)* 1 (1999) 71-72.
- [7] U.S. Patent Appl. US2004/0076565, and U.S. Patents 7332135, 7485273, 7640730, and 7674743.
- [8] J. Theis, E. Gulari, A LNT+SCR System for Treating the NO<sub>x</sub> Emissions from a Diesel Engine. SAE Technical Paper Series 2006-01-0210 (2006).

- [9] R. Snow, D. Dobson, R. Hammerle, S. Katare, Robustness of a LNT-SCR System to Aging Protocol. SAE Technical Paper Series 2007-01-0469 (2007).
- [10] R. Snow, G. Cavataio, D. Dobson, C. Montreuil, R. Hammerle, Calibration of a LNT-SCR Diesel Aftertreatment System. SAE Technical Paper Series 2007-01-1244 (2007).
- [11] H. Shinjoh, N. Takahashi, K. Yokota, Synergic Effect of Pd/ $\gamma$ -alumina and Cu/ZSM-5 on the Performance of NO<sub>x</sub> Storage Reduction Catalyst. Topics in Catalysis 42/43 (2007) 215-219.
- [12] T. Nakatsuji, M. Matsubara, J. Rouistenmaki, N. Sato, H. Ohno, A NO<sub>x</sub> Reduction System Using Ammonia-storage Selective Catalytic Reduction in Rich/Lean Excursions. Applied Catalysis B: Environmental 77 (2007) 190-201.
- [13] E.C. Corbos, M. Haneda, X. Courtois, P. Marecot, D. Duprez, H. Hamada, Cooperative Effect of Pt–Rh/Ba/Al and CuZSM-5 Catalysts for NO<sub>x</sub> Reduction during Periodic Lean-Rich Atmosphere. Catalysis Communications 10 (2008) 137.
- [14] P. Forzatti, L. Lietti, The Reduction of NO<sub>x</sub> Stored on LNT and Combined LNT–SCR Systems. Catalysis Today 155 (2010) 131-139.
- [15] L. Xu, R. McCabe, W. Ruona, G. Cavataio, Impact of a Cu-zeolite SCR Catalyst on the Performance of a Diesel LNT+SCR System. SAE Technical Paper Series 2009-01-0285 (2009).
- [16] E.C. Corbos, M. Haneda, X. Courtois, P. Marecot, D. Duprez, H. Hamada, NO<sub>x</sub> Abatement for Lean-Burn Engines under Lean–Rich Atmosphere over Mixed NSR-SCR Catalysts: Influences of the Addition of a SCR Catalyst and of the Operational Conditions. Applied Catalysis A: General. 365 (2009) 187-193.

- [17] J. Parks, V. Prikhodko, Ammonia Production and Utilization in a Hybrid LNT+SCR System. SAE Technical Paper Series 2009-01-2739 (2009).
- [18] J.R. Theis, J.A. Ura, R.W. McCabe, The Effects of Sulfur Poisoning and Desulfation Temperature on the NO<sub>x</sub> Conversion of LNT+SCR Systems for Diesel Applications. SAE Technical Paper Series 2010-01-0300 (2010).
- [19] J. McCarthy Jr., T. Korhumel Jr., A. Marougy, Performance of a Fuel Reformer, LNT and SCR Aftertreatment System Following 500 LNT Desulfation Events. SAE Technical Paper Series 2009-01-2835 (2009).
- [20] L. Xu, R. McCabe, M. Dearth, W. Ruona, Laboratory and Vehicle Demonstration of “2nd-Generation” LNT + in-situ SCR Diesel NO<sub>x</sub> Emission Control Systems SAE Technical Paper Series 2010-01-0305 (2010).
- [21] A. Lindholm, A. Sjövall, L. Olsson, Reduction of NO<sub>x</sub> over a Combined NSR and SCR System. Applied Catalysis B: Environmental 98 (2010) 112-121.
- [22] R. Bonzi, L. Lietti, L. Castoldi, P. Forzatti, NO<sub>x</sub> Removal over a Double-Bed NSR-SCR Reactor Configuration Catalysis Today 151 (2010) 376-385.
- [23] L. Xu, R. McCabe, P. Tennison, H-W. Jen, Laboratory and Vehicle Demonstration of “2nd-Generation” LNT + in-situ SCR Diesel Emission Control Systems. SAE Technical Paper Series 2011-01-0308 (2011).
- [24] J.R. Theis, M. Dearth, R. McCabe, LNT+SCR Catalyst Systems Optimized for NO<sub>x</sub> Conversion on Diesel Applications. SAE Technical Paper Series 2011-01-0305 (2011).

- [25] L. Castoldi, R. Bonzi, L. Lietti, P. Forzatti, S. Morandi, G. Ghiotti, S. Dzwigaj, Catalytic Behaviour of Hybrid LNT/SCR Systems: Reactivity and in situ FTIR study. *Journal of Catalysis* 282 (2011) 128-144.
- [26] L. Xu, R.W. McCabe, H.S. Gandhi, C.N. Montreuil, U.S. Patent allowed, July, 2011.
- [27] M. Weibel, N. Waldbüßer, R. Wunsch, D. Chatterjee, B. Bandl-Konrad, B. Krutzsch, A Novel Approach to Catalysis for NO<sub>x</sub> Reduction in Diesel Exhaust Gas. *Topics in Catalysis* 52 (2009) 1702-1708.
- [28] T. Johnson, Diesel Engine Emissions and Their Control. *Platinum Metals Review* 52 (2008) 23-37.
- [29] L. Xu, R.W. McCabe, LNT + *in situ* SCR Catalyst System for Diesel Emissions Control. *Catalysis Today* 184 (2012) 83-94.
- [30] A. Kato, S. Matsuda, T. Kamo, F. Nakajima, H. Kuroda, T. Narita, Reaction between NO, and NH<sub>3</sub>, on Iron Oxide-Titanium Oxide Catalyst. *Journal of Physical Chemistry* 85 (1981) 4099-4102.
- [31] M. Koebel, M. Elsener, G. Madia, Reaction Pathways in the Selective Catalytic Reduction Process with NO and NO<sub>2</sub> at Low Temperatures. *Industrial Engineering Chemical Research* 40 (2001) 52-59.
- [32] J. Wang, Y. Ji, Z. Hea, M. Crocker M. Dearth, R.W. McCabe, A Non-NH<sub>3</sub> Pathway for NO<sub>x</sub> Conversion in Coupled LNT-SCR Systems. *Applied Catalysis B: Environmental* 111– 112 (2012) 562– 570.
- [33] J.A. Ura, C.T. Goralski, Jr., G.W. Graham, R.W. McCabe, Laboratory Study of Lean NO<sub>x</sub> Trap Desulfation Strategies. *SAE Technical Paper Series* 2005-01-1114 (2005).



- [34] T. Morita, N. Suzuki, N. Satoh, K. Wada and H. Ohno, Study on Low NO<sub>x</sub> Emission Control Using Newly Developed Lean NO<sub>x</sub> Catalyst for Diesel Engines. SAE Technical Paper Series 2007-01-0239 (2007).
- [35] J.A. Pihl, J.E. Parks, C. Stuart Daw, T.W. Root, Product Selectivity During Regeneration of Lean NO<sub>x</sub> Trap Catalyst. SAE Tech. Paper 2006-01-3441, 2006.
- [36] L. Cumaranatunge, S.S. Mulla, A. Yezerets, N.W. Currier, W.N. Delgass, F.H. Ribeiro, Ammonia is a Hydrogen Carrier in the Regeneration of Pt/BaO/Al<sub>2</sub>O<sub>3</sub> NO<sub>x</sub> traps with H<sub>2</sub>. *Journal of Catalysis* 246 (2007) 29–34.
- [37] I. Nova, L. Castoldi, L. Lietti, E. Tronconi, and P. Forzatti, How to Control the Selectivity in the Reduction of NO<sub>x</sub> with H<sub>2</sub> over Pt-Ba/Al<sub>2</sub>O<sub>3</sub> Lean NO<sub>x</sub> Trap Catalysts. *Topics in Catalysis* 42–43, (2007) 21-25.
- [38] J. Xu, R. Clayton, V. Balakotaiah, M.P. Harold, Experimental and Microkinetic Modeling of Steady-State NO Reduction by H<sub>2</sub> on Pt/BaO/Al<sub>2</sub>O<sub>3</sub> Monolith Catalysts. *Applied Catalysis B: Environmental* 77 (2008) 395–408.
- [39] J. Wang, Y. Ji, V. Easterling, M. Crocker, M. Dearth, R.W. McCabe, The Effect of Regeneration Conditions on the Selectivity of NO<sub>x</sub> Reduction in a Fully Formulated Lean NO<sub>x</sub> Trap Catalyst. *Catalysis Today* 175 (2011) 83-92.
- [40] R.D. Clayton, M.P. Harold, V. Balakotaiah, Selective Catalytic Reduction of NO by H<sub>2</sub> in O<sub>2</sub> on Pt/BaO/Al<sub>2</sub>O<sub>3</sub> Monolith NO<sub>x</sub> Storage Catalysts. *Applied Catalysis. B* 81 (2008) 161-181.
- [41] S.S. Mulla, S.S. Chaugule, A. Yezerets, N.W. Currier, W.N. Delgass, F.H. Ribeiro, Regeneration Mechanism of Pt/BaO/Al<sub>2</sub>O<sub>3</sub> Lean NO<sub>x</sub> Trap Catalyst with H<sub>2</sub>. *Catalysis Today* 136 (2008) 136-145.

- [42] W.P. Partridge, J.-S. Choi, NH<sub>3</sub> Formation and Utilization in Regeneration of Pt/Ba/Al<sub>2</sub>O<sub>3</sub> NO<sub>x</sub> Storage-Reduction Catalyst with H<sub>2</sub>. *Applied Catalysis B: Environmental* 91 (2009) 144-151.
- [43] P. Forzatti, L. Lietti, N. Gabrielli, A Kinetic Study of the Reduction of NO<sub>x</sub> Stored on Pt-Ba/Al<sub>2</sub>O<sub>3</sub> Catalyst. *Applied Catalysis B: Environmental* 99 (2010) 145–155.
- [44] D. Bhatia, M.P. Harold, V. Balakotaiah, A Global Kinetic Model for NO<sub>x</sub> Storage and Reduction on Pt/BaO/Al<sub>2</sub>O<sub>3</sub> Monolithic Catalysts. *Catalysis Today* 151 (2010) 314-329.
- [45] R.D. Clayton, M.P. Harold, V. Balakotaiah, NO<sub>x</sub> Storage and Reduction with H<sub>2</sub> on Pt/BaO/Al<sub>2</sub>O<sub>3</sub> Monolith: Spatio-Temporal Resolution of Product Distribution. *Applied Catalysis B: Environmental* 84 (2008) 616-630.
- [46] R.D. Clayton, M.P. Harold, V. Balakotaiah, C.Z. Wan, Pt Dispersion Effects During NO<sub>x</sub> Storage and Reduction on Pt/BaO/Al<sub>2</sub>O<sub>3</sub> Catalysts. *Applied Catalysis B: Environmental* 90 (2009) 662-676.
- [47] V. Easterling, Y. Ji, M. Crocker, M. Dearth, R.W. McCabe, Application of SpaciMS to the Study of Ammonia Formation in Lean NO<sub>x</sub> Trap Catalysts. *Applied Catalysis B: Environmental* 123–124 (2012) 339–350.
- [48] I. Nova, L. Lietti, L. Castoldi, E. Tronconi, P. Forzatti, New Insights in the NO<sub>x</sub> Reduction Mechanism with H<sub>2</sub> Over Pt-Ba/γ-Al<sub>2</sub>O<sub>3</sub> Lean NO<sub>x</sub> Trap Catalysis Under Near-Isothermal Conditions. *Journal of Catalysis* 239 (2006) 244-254.
- [49] I. Nova, L. Castoldi, L. Lietti, E. Tronconi, P. Forzatti, F. Prinetto, G. Ghiotti, SAE Technical Paper, 2005-01-1085.

- [50] N.W. Cant, I.O.Y. Liu, M.J. Patterson, The Effect of Proximity Between Pt and BaO on Uptake, Release, and Reduction of NO<sub>x</sub> on Storage Catalysts. *Journal of Catalysis* 243 (2006) 309-317.
- [51] R. Büchel, R. Strobel, A. Baiker, S. E. Pratsinis, Effect of the Proximity of Pt to Ce or Ba in Pt/Ba/CeO<sub>2</sub>. Catalysts on NO<sub>x</sub> Storage–Reduction Performance. *Topics in Catalysis* 52 (2009) 1709–1712.
- [52] U. Tuttlies, V. Schmeißer, G. Eigenberger, A Mechanistic Simulation Model for NO<sub>x</sub> Storage Catalyst Dynamics. *Chemical Engineering Science* 59 (2004) 4731–4738.
- [53] V. Schmeißer, D. Chatterjee, M. Weibel, Towards a Realistic Simulation Model for NO<sub>x</sub>-Storage Catalyst Dynamics. *Topics in Catalysis* 42–43, (2007) 77-81.
- [54] V. Balakotaiah, N. Gupta, D.H. West, A Simplified Model for Analyzing Catalytic Reactions in Short Monoliths, *Chemical Engineering Science* 55 (22) (2000) 5367–5383.
- [55] R.S. Larson, J.A. Pihl, V. Kalyana Chakravarthy, T.J. Toops, C.S. Daw, Microkinetic Modeling of Lean NO<sub>x</sub> Trap Chemistry under Reducing Conditions. *Catalysis Today* 136 (2008) 104–120.
- [56] <http://www.cleers.org>. Downloaded 11/20/12.
- [57] A. Lindholm, N.W. Currier, J. Li, A. Yezerets, L. Olsson, Detailed Kinetic Modeling of NO<sub>x</sub> Storage and Reduction with Hydrogen as the Reducing Agent and in the Presence of CO<sub>2</sub> and H<sub>2</sub>O over a Pt/Ba/Al Catalyst. *Journal of Catalysis* 258 (2008) 273–288.

- [58] P. Kočí, F. Plát, J. Šěpánek, Š. Bártová, M. Marek, M. Kubček, V. Schmeißer, D. Chatterjee, M. Weibel, Global Kinetic Model for the Regeneration of NO<sub>x</sub> Storage Catalyst with CO, H<sub>2</sub> and C<sub>3</sub>H<sub>6</sub> in the Presence of CO<sub>2</sub> and H<sub>2</sub>O. *Catalysis Today* 147S (2009) S257–S264.
- [59] A. Amberntsson, E. Fridell, M. Skoglundh, Influence of Platinum and Rhodium Composition on the NO<sub>x</sub> Storage and Sulphur Tolerance of a Barium Based NO<sub>x</sub> Storage Catalyst. *Applied Catalysis B: Environmental* 46 (2003) 429-439.
- [60] H. Abdulhamid, E. Fridell, M. Skoglundh, The reduction phase in NO<sub>x</sub> Storage Catalysis: Effect of Type of Precious Metal and Reducing Agent. *Applied Catalysis B: Environmental* 62 (2006) 319-328.
- [61] T. Kobayashi, T. Yamada, K. Kayano, Study of NO<sub>x</sub> Trap Reaction by Thermodynamic Calculation. SAE Technical Paper Series 970745 (1997).
- [60] J.R. Theis, J.A. Ura, R.W. McCabe, The Effects of Platinum and Rhodium on the Functional Properties of a Lean NO<sub>x</sub> Trap. SAE Technical Paper Series 2007-01-1055 (2007).
- [63] G. Ertl, H. Knözinger, J. Weitkamp. *Environmental Catalysis*, Wiley-VCH, New York, 1999.
- [64] V. Easterling, Y. Ji, M. Crocker, J. Ura, J.R. Theis, R.W. McCabe, Effect of Ceria on the Desulfation Characteristics of Model Lean NO<sub>x</sub> Trap Catalysts. *Catalysis Today* 151 (2010) 338–346.
- [65] V. Perrichon, L. Retailleau, P. Bazin, M. Daturi, J.C. Lavalley, Metal Dispersion of CeO<sub>2</sub>-ZrO<sub>2</sub> Supported Platinum Catalysts Measured by H<sub>2</sub> or CO Chemisorption. *Applied Catalysis* 260 (2004) 1-8.

- [66] M. Bowker, P. Stone, R. Smith, E. Fourre, M. Ishii, N.H. de Leeuw, The Surface Structure of BaO on Pt(111): (2 x 2)-Reconstructed BaO(111). *Surface Science* 600 (2006) 1973–1981.
- [67] L. Castoldi, I. Nova, L. Lietti, P. Forzatti, Study of the Effect of Ba Loading for Catalytic Activity of Pt–Ba/Al<sub>2</sub>O<sub>3</sub> Model Catalysts. *Catalysis Today* 96 (2004) 43-52.
- [68] P.T. Fanson, M.R. Horton, W.N. Delgass, J. Lauterbach, FTIR Analysis of Storage Behavior and Sulfur Tolerance in Barium-Based NO<sub>x</sub> Storage and Reduction (NSR) Catalysts *Applied Catalysis B: Environmental* 46 (2003) 393-413.
- [69] J. Dawody, M. Skoglundh, S. Wall, E. Fridell, Role of Pt-Precursor on the Performance of Pt/BaCO<sub>3</sub>/Al<sub>2</sub>O<sub>3</sub>·NO<sub>x</sub> Storage Catalysts. *Journal of Molecular Catalysis A: Chemistry* 225 (2005) 259-269.
- [70] L. Lietti, P. Forzatti, I. Nova, E. Tronconi, NO<sub>x</sub> Storage Reduction Over Pt-Ba/γ-Al<sub>2</sub>O<sub>3</sub> Catalyst. *Journal of Catalysis* 204 (2001) 175-191.
- [71] H. Mahzoul, J.F. Brilhac, P. Gilot, Experimental and Mechanistic Study of NO<sub>x</sub> Adsorption over NO<sub>x</sub> Trap Catalysts. *Applied Catalysis B: Environmental* 20 (1999) 47-55.
- [72] L. Olsson, H. Persson, E. Fridell, M. Skoglundh, B. Andersson, A Kinetic Study of NO Oxidation and Storage on Pt/Al<sub>2</sub>O<sub>3</sub> and Pt/BaO/Al<sub>2</sub>O<sub>3</sub>. *Journal of Physical Chemistry B: Environmental* 105 (2001) 6895-6906.
- [73] I. Nova, L. Castoldi, L. Lietti, E. Tronconi, P. Forzatti, F. Prinetto, G. Ghiotti, NO<sub>x</sub> Adsorption Study Over Pt-Ba/Alumina Catalysts: FT-IR and Pulse Experiments. *Journal of Catalysis* 222 (2004). 377-388.

- [74] I. Nova, L. Castoldi, F. Prinetto, V. Dal Santo, L. Lietti, E. Tronconi, P. Forzatti, G. Ghiotti, R. Psaro, S. Recchia, NO<sub>x</sub> Adsorption Study over Pt–Ba/alumina Catalysts: FT-IR and Reactivity Study. *Topics in Catalysis* 30-31 (2004) 181-186.
- [75] P. Forzatti, L. Castoldi, L. Lietti, I. Nova, E. Tronconi, Identification of the Reaction Networks of the NO<sub>x</sub> Storage/Reduction in Lean NO<sub>x</sub> Trap Systems. *Studies in Surface Science and Catalysis* 171 (2007) 175-208.
- [76] W.S. Epling, J.E. Parks, G.C. Campbell, A. Yezerets, N.W. Currier, L.E. Campbell, Further Evidence of Multiple NO<sub>x</sub> Sorption Sites on NO<sub>x</sub> Storage/Reduction Catalysts. *Catalysis Today* 96 (2004) 21-30.
- [77] E. Fridell, A. Amberntsson, L. Olsson, A.W. Grant, M. Skoglundh, Platinum Oxidation and Sulphur Deactivation in NO<sub>x</sub> Storage Catalysts. *Topics in Catalysis* 30/31 (2004) 143-146.
- [78] F. Rodrigues, L. Juste, C. Potvin, J.F. Tempère, G. Blanchard, G. Djéga-Mariadassou, NO<sub>x</sub> Storage on Barium-Containing Three-Way Catalyst in the Presence of CO<sub>2</sub>. *Catalysis Letters* 72 (2001) 59-64.
- [79] B.R. Kromer, L. Cao, L. Cumaranatunge, S.S. Mulla, J.L. Ratts, A. Yezerets, N.W. Currier, F.H. Ribeiro, W.N. Delgass and J.M. Caruthers, Modeling of NO Oxidation and NO<sub>x</sub> Storage on Pt/BaO/Al<sub>2</sub>O<sub>3</sub> NO<sub>x</sub> traps. *Catalysis Today* 136 (2008) 93-103.
- [80] A.K. Datye, Q. Xu, K.C. Kharas, J.M. McCarty, Particle Size Distributions in Heterogeneous Catalysts: What Do They Tell Us About the Sintering Mechanism? *Catalysis Today* 111 (2006) 59-67.

- [81] B.-H. Jang, T.-H. Yeon, H.-S. Han, Y.-K. Park, J.-E. Yie, Deterioration Mode of Barium-Containing NO<sub>x</sub> Storage Catalyst. *Catalysis Letters* 77 (2001) 21-28.
- [82] C.-W. Yi, J.H. Kwak, C.H.F. Peden, C. Wang, J. Szanyi, Understanding Practical Catalysts Using a Surface Science Approach: The Importance of Strong Interaction between BaO and Al<sub>2</sub>O<sub>3</sub> in NO<sub>x</sub> Storage Materials. *Journal of Physical Chemistry C: Letters* 111 (2007) 14942-14944.
- [83] E.C. Corbos, X. Courtois, F. Can, P. Marécot, D. Duprez, NO<sub>x</sub> Storage Properties of Pt/Ba/Al Model Catalysts Prepared by Different Methods: Beneficial Effects of a N<sub>2</sub> Pre-Treatment Before Hydrothermal Aging. *Applied Catalysis B: Environmental* 84 (2008) 514-523.
- [84] J. Dawody, L. Eurenium, H. Abdulhamid, M. Skoglundh, E. Olsson, E. Fridell, Platinum Dispersion Measurements for Pt/BaO/Al<sub>2</sub>O<sub>3</sub>, NO<sub>x</sub> Storage Catalysts. *Applied Catalysis A: General* 296 (2005) 157-168.
- [85] J. Hepburn, E Thanasiu, D. Dobson, W. Watkins, Experimental and Modeling Investigations of NO<sub>x</sub> Trap Performance. SAE Technical Paper 962051 (1996).
- [86] M. Vaarkamp, J.T. Miller, F.S. Modica, G.S. Lane, D.C. Koningsberger, Sulfur Poisoning of a Pt/BaK-LTL Catalyst: A Catalytic and Structural Study Using Hydrogen Chemisorption and X-ray Absorption Spectroscopy. *Journal of Catalysis* 138 (1992) 675-685.
- [87] M. Vaarkamp, J.T. Miller, F.S. Modica, D.C. Koningsberger, On the Relation between Particle Morphology, Structure of the Metal-Support Interface, and Catalytic Properties of Pt/γ-Al<sub>2</sub>O<sub>3</sub>. *Journal of Catalysis* 163 (1996) 294-305.

- [88] N.A. Ottinger, T.J. Toops, K. Nguyen, B.G. Bunting, J. Howe, Effect of Lean/Rich High Temperature Aging on NO Oxidation and NO<sub>x</sub> Storage/Release of a Fully Formulated Lean NO<sub>x</sub> Trap. *Applied Catalysis B: Environmental* 101 (2011) 486-494.
- [89] R. Büchel, R. Ströbel, F. Krumeich, A. Baiker, S.E. Pratsinis, Influence of Pt Location on BaCO<sub>3</sub> or Al<sub>2</sub>O<sub>3</sub> During NO<sub>x</sub> Storage Reduction. *Journal of Catalysis* 261 (2009) 201-207.
- [90] S.S. Chaugule, A. Yezerets, N.W. Currier, F.H. Ribeiro, W.N. Delgass, 'Fast' NO<sub>x</sub> Storage on Pt/BaO/γ-Al<sub>2</sub>O<sub>3</sub> Lean NO<sub>x</sub> Traps with NO<sub>2</sub> + O<sub>2</sub> and NO + O<sub>2</sub>: Effects of Pt, Ba Loading. *Catalysis Today* 151 (2010) 291-303.
- [91] S.S. Chaugule, V.F. Kispersky, J.L. Ratts, A. Yezerets, N.W. Currier, F.H. Ribeiro, W.N. Delgass, Formation and Removal of Ba-Carbonates or Carboxylates on Pt/BaO/γ-Al<sub>2</sub>O<sub>3</sub> Lean NO<sub>x</sub> Traps. *Applied Catalysis B: Environmental* 107 (2011) 26-33.
- [92] U. Elizundia, R. López-Fonseca, I. Landa, M.A. Gutiérrez-Ortiz, J.R. González-Velasco, FT-IR study of NO<sub>x</sub> Storage Mechanism over Pt/BaO/Al<sub>2</sub>O<sub>3</sub> Catalysts. Effect of the Pt-BaO Interaction. *Topics in Catalysis* 42–43 (2007) 37-41.
- [93] X. Chen, J. Schwank, J. Li, W.F. Schneider, C.T. Goralski Jr., P.J. Schmitz, Thermal Decomposition of Dispersed and Bulk-Like NO<sub>x</sub> Species in Model NO<sub>x</sub> Trap Materials. *Applied Catalysis B: Environmental* 61 (2005) 164-175.
- [94] X. Wei, X. Liu, M. Deeba, Characterization of Sulfated BaO-Based NO<sub>x</sub> Trap. *Applied Catalysis B: Environmental* 58 (2005) 41-49.
- [95] J.-S. Choi, W.P. Partridge, J.A. Pihl, C.S. Daw, Sulfur and Temperature Effects on the Spatial Distribution of Reactions Inside a Lean NO<sub>x</sub> Trap and Resulting Changes in Global Performance. *Catalysis Today* 136 (2008) 173-182.



- [96] J.-S. Choi, W.P. Partridge, C.S. Daw, Sulfur Impact on NO<sub>x</sub> Storage, Oxygen Storage, and Ammonia Breakthrough During Cyclic Lean/Rich Operation of a Commercial Lean NO<sub>x</sub> Trap. *Applied Catalysis B* 77 (2007) 145-156.
- [97] J.-S. Choi, W.P. Partridge, J.A. Pihl, M.-Y. Kim, P. Kočí, C.S. Daw, Spatiotemporal Distribution of NO<sub>x</sub> Storage and Impact NH<sub>3</sub> and N<sub>2</sub>O Selectivities During Lean/Rich Cycling of a Ba-Based Lean NO<sub>x</sub> Trap Catalyst. *Catalysis Today*, 184 (2012) 20-26.
- [98] L. Letti, I. Nova, P. Forzatti, Journal of Catalysis Role of Ammonia in the Reduction by Hydrogen of NO<sub>x</sub> Stored over Pt–Ba/Al<sub>2</sub>O<sub>3</sub> lean NO<sub>x</sub> trap Catalysts. 257 *Journal of Catalysis* (2008) 270-282.
- [99] I. Nova, L. Lietti, P. Forzatti, Mechanistic Aspects of the Reduction of Stored NO<sub>x</sub> over Pt-Ba/Al<sub>2</sub>O<sub>3</sub> Lean NO<sub>x</sub> Trap Systems. *Catalysis Today* 136 (2008) 128-135.
- [100] L. Lietti, N. Artioli, L. Righini, L. Castoldi, P. Forzatti, Pathways for N<sub>2</sub> and N<sub>2</sub>O Formation during the Reduction of NO<sub>x</sub> over Pt–Ba/Al<sub>2</sub>O<sub>3</sub> LNT Catalysts Investigated by Labeling Isotopic Experiments. *Industrial Engineering and Chemistry Research* 51 (2012) 7597–7605.
- [101] P. Forzatti, L. Lietti, I. Nova, On Board Catalytic NO<sub>x</sub> Control: Mechanistic Aspects of the Regeneration of Lean NO<sub>x</sub> Traps with H<sub>2</sub>. *Energy & Environmental Science* 1 (2008) 236–247.
- [102] P. Koci, F. Plat, J. Stepanek, M. Kubicek, M. Marek, Dynamics and Selectivity of NO<sub>x</sub> Reduction in NO<sub>x</sub> Storage Catalytic Monolith. *Catalysis Today* 137 (2008) 253–260.

[103] A. Lindholm, N.W. Currier, E. Fridell, A. Yezerets, L. Olsson, NO<sub>x</sub> Storage and Reduction over Pt Based Catalysts with Hydrogen as the Reducing Agent: Influence of H<sub>2</sub>O and CO<sub>2</sub>. *Applied Catalysis B-Environmental* 75 (2007) 78–87.

## Chapter 7. Significant Findings and Recommendations for Future Work.

The purpose of this dissertation was to determine the effects of ceria addition on the aging and sulfation characteristics of LNT catalysts for stand-alone and LNT-SCR applications. The methodology for achieving this goal was as follows:

- Investigation of the effects of ceria addition on LNT desulfation behavior using powder catalysts and fully formulated monolithic LNT catalysts.
- Elucidation of the effect of washcoat composition on LNT aging characteristics, employing fully formulated monolithic LNT catalysts containing varying amounts of Pt, Rh, and BaO after subjection to accelerated aging on a bench reactor.
- Employment of SpaciMS to understand the factors influencing the selectivity of NO<sub>x</sub> reduction in two fully formulated LNT catalysts, both degreened and thermally aged.
- Application of a model to predict experimental SpaciMS data pertaining to NH<sub>3</sub> selectivity during regeneration of degreened and aged LNT catalysts possessing fixed NO<sub>x</sub> storage amounts that approximated complete surface storage.

The impetus for this research was provided by the demands of consumers and auto makers alike for improved fuel economy from lean burn engines, while attaining reduced exhaust emissions, particularly NO<sub>x</sub> (NO + NO<sub>2</sub>).

### *7.1. Significant Findings.*

#### *7.1.1. Effect of Ceria on the Desulfation Characteristics of Model Lean NO<sub>x</sub> Trap Catalysts.*

- Ceria can function as a sulfur sink in LNT catalysts, thereby helping to protect the main Ba NO<sub>x</sub> storage phase from sulfation.
- Pt and Ba proximity: when Pt and Ba are physically separated, the desulfation temperature of the surface BaSO<sub>4</sub> is shifted by 20-40 °C towards higher temperature, i.e., towards the position characteristic of bulk BaSO<sub>4</sub>
- Addition of La-stabilized CeO<sub>2</sub> or CeO<sub>2</sub>-ZrO<sub>2</sub>:

- Greater resistance to deactivation during sulfation (as reflected by the NO<sub>x</sub> storage efficiency)
- Required lower temperatures to restore the NO<sub>x</sub> storage efficiency to its pre-sulfation value.
- Precious metal loadings can significantly impact desulfation efficiency, both high Rh and Pt loadings being beneficial for catalyst desulfation.

*7.1.2. Effect of Aging on the NO<sub>x</sub> Storage and Regeneration Characteristics of Fully Formulated Lean NO<sub>x</sub> Trap Catalysts.*

- According to H<sub>2</sub> chemisorption and TEM data, Pt sintering occurred and resulted in decreased contact between the Pt and Ba phases, this contributed to decreased first cycle NSE due to less efficient NO<sub>x</sub> spillover from Pt to Ba during NO<sub>x</sub> adsorption.
- TEM and XRD data indicate the accumulation of sulfur in the washcoat, present as BaSO<sub>4</sub> (30% of the Ba present) providing an additional explanation for the loss in initial and cycle-averaged NSE after catalyst aging.
- Given the importance of the Pt-Ba interface, it follows that high Pt loadings are beneficial for catalyst performance since they provide one means of ensuring a high degree of Pt-Ba contact.

*7.1.3. Application of SpaciMS to the Study of Ammonia Formation in Lean NO<sub>x</sub> Trap Catalysts.*

- Losses in surface area, accompanied by segregation of the Pt/Rh sites and BaO storage sites, account for the decreased NO<sub>x</sub> storage efficiency of the aged catalysts.
- During lean phase NO<sub>x</sub> storage on aged catalysts, NO and NO<sub>2</sub> were required to travel further to reach storage sites due to the decreased storage site concentration. Consequently, after aging the NO<sub>x</sub> storage-reduction zone was elongated.
  - Stretching of the NSR zone results in an increase of the NO<sub>x</sub> “puff” that appears during the onset of the rich front as it travels along the length of the catalyst

- Since  $\text{NO}_x$  release from the catalyst tracks the NSR zone, for an aged catalyst the  $\text{NO}_x$  concentration peaks closer to the rear of the catalyst; hence, the probability that  $\text{NO}_x$  can re-adsorb downstream of the reduction front and subsequently undergo reduction by  $\text{NH}_3$  is diminished, and consequently the  $\text{NO}_x$  emission is higher.
- Stretching of the NSR zone causes the  $\text{NH}_3$  selectivity of an aged catalyst to increase.
- Loss of OSC and  $\text{NO}_x$  storage sites leads to an increase in the rate of propagation of the reductant front in the aged catalyst compared to the degreened catalyst.
- $\text{NO}_x$  is released more slowly from storage sites (due to Pt-Ba phase segregation), such that for the aged catalysts the kinetics of  $\text{NO}_x$  reduction are controlled by the rate of  $\text{NO}_x$  diffusion to the Pt sites (rather than being feed limited).

*7.1.4. An Investigation into the Validity of a Crystallite-Scale Model to Predict the  $\text{NH}_3$  Regeneration of a Pt/Rh/BaO/ $\text{Al}_2\text{O}_3$  Lean  $\text{NO}_x$  Trap Catalyst.*

- Results from the experiments were consistent with the species observed during regeneration being a function of the PGM dispersion and the ratio of  $\text{H}_2:\text{NO}_x$  at the Pt/Ba interface.
- $\text{N}_2\text{O}$  is favored at low ratios of  $\text{H}_2:\text{NO}_x$  (at the leading edge of the front) and  $\text{NH}_3$  is favored at higher ratios of  $\text{H}_2:\text{NO}_x$  (behind the reduction front).
- Modeling results indicated the use of a diffusion-based model with temperature dependent diffusivities is capable of capturing the spatiotemporal trends associated with  $\text{NH}_3$  release from the LNT at low temperatures and high dispersions.
- The model accurately predicted the individual delay at each position before the onset of  $\text{NH}_3$  release.
- The model was also able to predict these trends for the aged data after the parameters were adjusted using the values for the physical properties of Rh instead of Pt.

### *7.2 Suggestions for Future Research.*

Although the work presented in this study of LNT catalysts as a capable technology for reducing  $\text{NO}_x$  and  $\text{NH}_3$  emissions (while delivering increased fuel economy resulting from the use of lean-burn engines compared to stoichiometric engines), several challenges will influence the penetration of LNT technology into the marketplace. As engines become more efficient, the resulting exhaust temperatures become cooler. In typical lean burn applications, exhaust temperatures are generally in the temperature range of 150 to 400 °C. The next generation of engines currently under development for real world use possesses exhaust temperatures as low as 100 °C. Exhaust temperatures lower than 200 °C are problematic since the activity of the PGMs are significantly reduced in regards to  $\text{NO}_x$  oxidation during storage and  $\text{NO}_x$  reduction to  $\text{NH}_3$  and  $\text{N}_2$  during catalyst regeneration. Catalyst materials besides traditional Pt, Rh, and Pd must be developed to meet this demand.

It has become apparent from the data gathered using the SpaciMS that a need exists for the capability to measure reductants in addition to the products generated from  $\text{NO}_x$  reduction. For the successful implementation of an LNT-SCR system,  $\text{NH}_3$  production must be tuned to the amount of  $\text{NO}_x$  that slips from the LNT to the SCR catalyst. Since  $\text{NH}_3$  selectivity is a function of the relative amounts of  $\text{H}_2:\text{NO}_x$  present at the PGM sites, the  $\text{H}_2$  concentration would be an effective measurement tool in determining the  $\text{H}_2:\text{NO}_x$  ratios present at different locations in the catalyst rather than just measuring the N-species present (i.e.,  $\text{N}_2$ ,  $\text{NH}_3$ , and  $\text{N}_2\text{O}$ ). Additionally, the capability to measure  $\text{H}_2$  is advantageous because  $\text{H}_2$  is produced from hydrocarbons and CO during regeneration due to steam reforming and the water gas-shift reaction. An ideal SpaciMS apparatus would have the ability to measure  $\text{NO}_x$  storage and regeneration with both low ( $\text{NO}$ ,  $\text{NO}_2$ ,  $\text{O}_2$ ,  $\text{CO}$ ,  $\text{CO}_2$ ,  $\text{H}_2\text{O}$ ) and medium ( $\text{N}_2\text{O}$ ,  $\text{N}_2$ ,  $\text{O}_2$ ) energy sources while simultaneously measuring  $\text{H}_2$  concentrations. A system with three capillary probes attached to two chemical ionization mass spectrometers and one electron pulse ionization mass spectrometer would be able to accomplish this aim.

In regards to modeling the storage and reduction processes, the following improvements would provide a better predictive capability in LNT-SCR design. One of the assumptions used in predicting the  $\text{NH}_3$  selectivity during regeneration from a LNT with a fixed amount of  $\text{NO}_x$  stored was an assumed value for the diffusivity of  $\text{NO}_x$  stored on the surface of the catalyst. While this value was adjusted with temperature, the discussion in Chapter 6 demonstrated that unaccounted processes such as  $\text{NH}_3$  readsorption most likely occur during regeneration. Additional complications arise during aging when sintering of the PGM component occurs, resulting in changes in the diffusion of  $\text{NO}_x$ .

Another assumption was that  $\text{NO}_x$  was stored uniformly along the axis of the monolith catalyst. While a uniform distribution of stored  $\text{NO}_x$  would provide a beneficial, desired proximity to PGMs essential for efficient  $\text{NO}_x$  storage and reduction, this situation does not exist on the surface of the LNT catalyst, especially after aging. As mentioned in the preceding discussion, the distribution of the various catalyst components determines the surface area of Pt/Ba proximity which in turn governs  $\text{NO}_x$  storage gradients, the rate of the propagation of the reductant front during regeneration, and ultimately the selectivity of the various N-species produced during regeneration of the LNT catalyst. A model capable of predicting the chromatographic-like nature of  $\text{NO}_x$  storage existing on the surface would attain a better fit of the experimental data.

## Appendix A.1. Nomenclature.

1/1 cycles: One min lean periods to one min rich periods.

5/3 cycles: Five min lean periods to three min rich periods.

$a$ : Width/hydraulic diameter of the channel (m)

$A_{PF}$ : Atomic packing factor

AD: Aged catalyst.

B-225: Catalyst sample where 225 refers to the washcoat loading in g/L.

BET: Surface measurement technique named after the last names of Stephen Brunauer, Paul Hugh Emmett, and Edward Teller.

$C_A$ : Surface concentration of stored  $\text{NO}_x$  ( $\text{mol}/\text{m}^2$  exposed BaO).

$C_{AO}$ : Surface concentration of stored  $\text{NO}_x$  before start of regeneration ( $\text{mol}/\text{m}^2$  exposed BaO).

$C_A^*$ : Dimensionless concentration of stored  $\text{NO}_x$ .

$C_j^{in}$ : Inlet concentration of species  $j$  in the fluid phase ( $\text{mol}/\text{m}^3$ ).

$C_j^{in*}$ : Dimensionless inlet concentration of species  $j$  in the fluid phase.

$C_{jm}$ : Cup-mixing concentration of species  $j$  in the fluid phase ( $\text{mol}/\text{m}^3$ ).

$C_{jm}^*$ : Dimensionless cup-mixing concentration of species  $j$  in fluid phase.

$C_{jwc}$ : Concentration of species  $j$  at the fluid–washcoat interface ( $\text{mol}/\text{m}^3$ ).

$C_{jwc}^*$ : Dimensionless concentration of species  $j$  at fluid–washcoat interface.

$c_{Pt}$ : Surface concentration of Pt (moles exposed Pt/ $\text{m}^2$  exposed Pt).

CAFE: Corporate Average Fuel Economy.

CDC: Centers for Disease Control.

CI-MS: Chemical ionization mass spectrometer.

$d$ : Diameter of monolith sample (cm).

$d$ : Pt dispersion (%)

$D_A$ : Diffusivity of stored  $\text{NO}_x$  in the Ba phase ( $\text{m}^2/\text{s}$ ).

$D_{jm}$ : Diffusivity of species  $j$  in the fluid phase ( $\text{m}^2/\text{s}$ ).

$D_{Pt}$ : Diameter of a Pt atom (m).

DOC: Diesel oxidation catalysts.

DG: Degreened catalyst



DPF: Diesel particulate filter.

DRIFTS: Diffuse reflectance infrared Fourier transform spectroscopy.

EELS: Electron energy loss spectroscopy.

EIMS: Electron pulse ionization mass spectrometer.

EM: Electron microscopy.

ER: Eley-Rideal.

FTP: Federal testing procedure.

GHSV: Gas hourly space velocity ( $\text{h}^{-1}$ ).

GVWR: Gross vehicle weight rating.

H\*: Hydrogen species associated with Pt.

HC: Hydrocarbons.

HC-SCR: Selective catalytic reduction of  $\text{NO}_x$  with hydrocarbon reductants.

HRTEM-EELS: High-resolution transmission electron microscopy-electron energy loss spectroscopy.

$I_p$ : Perimeter of Pt/Ba interface per channel (m).

$k_1$ : Rate constant for  $\text{NO}_x$  regeneration by  $\text{H}_2$  ( $\text{m}^4/\text{mol s}$ ).

$k_2$ : Rate constant for  $\text{NO}_x$  regeneration by  $\text{NH}_3$  ( $\text{m}^4/\text{mol s}$ ).

$k_3$ : Rate constant for consumption of  $\text{H}_2$  by chemisorbed oxygen ( $\text{m}^3/\text{mol s}$ ).

$k_{c,j}$ : Mass transfer coefficient of species  $j$  (m/s).

$l$ : Length of monolith sample (m).

$L$ : Length of the monolith (m)

LH: Langmuir-Hinshelwood.

LNT: Lean  $\text{NO}_x$  trap.

LNT-SCR: Lean  $\text{NO}_x$  trap coupled with a selective catalytic reduction catalyst.

LDDs: Light duty diesels.

$m_{wc}$ : Mass of washcoat (g).

$M_{\text{NO}_x}$ : Total moles of  $\text{NO}_x$  stored on the catalyst.

$M_{Pt_T}$ : Total moles of Pt in the washcoat per channel.

$n_{ch}$ : Total number of channels in the catalyst.

$N_{av}$ : Avogadro number.

$N_c$ : Number of crystallites per channel.

$N_{Pt}$ : Number of atoms in a Pt particle.  
 $N_{Pt_s}$ : Number of surface atoms.  
 $N_T$ : Number of Pt atoms in the Pt crystallite.  
 NSC:  $NO_x$  storage capacity.  
 NSE:  $NO_x$  storage efficiency.  
 $NO_x$ : Oxides of nitrogen.  
 NSR:  $NO_x$  storage and reduction.  
 $O^*$ : Oxygen species associated with Pt sites.  
 $O^{*'}$ : Poorly active oxygen species.  
 ORNL: Oak Ridge National Laboratory.  
 OSC: Oxygen storage capacity.  
 PBA: Pt/BaO/ $Al_2O_3$  catalyst.  
 PBAC: Catalyst containing Pt/BaO/ $Al_2O_3$  and Pt/ $CeO_2$  powders in a 76:24 weight ratio.  
 PM: Particulate matter.  
 PGM: Platinum group metals (Ru, Rh, Pd, Os, Ir, Pt).  
 $r$ : Radial coordinate (m).  
 $r^*$ : Dimensionless radial coordinate.  
 $R_c$ : Radius of the crystallite (m).  
 $R_{eff}$ : Radius over which  $NO_x$  is stored on exposed BaO (m).  
 $R_\Omega$ : Effective transverse length scale (m)  
 $S_{BaW}$ : Total surface area of active BaO per unit mass of washcoat ( $m^2/g$  washcoat)  
 $S_{BaO}$ : Surface density of BaO (BaO molecules/ $m^2$  exposed BaO surface)  
 $S_E$ : Exposed Pt surface area per channel ( $m^2$ )  
 SCR: Selective catalytic reduction.  
 SFTP: Supplementary federal testing procedures.  
 SpaciMS: Spatially resolved capillary inlet mass spectrometry.  
 STEM: Scanning transmission electron microscopy.  
 $t$ : Time during the regeneration (s).  
 TAP: Temporal analysis of products reactor.  
 TCD: Thermal conductivity detector.  
 TEM: Transmission electron microscopy.

TPR: Temperature programmed reduction.

TWC: Three-way catalytic converter.

$\bar{u}$ : Average fluid velocity in the fluid phase (m/s).

$W_a$ : Atomic weight.

WGS: Water gas shift reaction.

$x$ : Axial coordinate (m).

XRD: X-ray diffraction.

XPS: X-ray photoelectron spectroscopy.

$z$ : dimensionless axial coordinate.

$\delta_c$ : Thickness of the washcoat on a monolith catalyst (m).

$\epsilon_{wc}$ : Porosity within the washcoat.

$\theta_v$ : Fractional surface coverage of vacant sites on Pt.

$\theta_{O-Pt}$ : Fractional surface coverage of chemisorbed oxygen on Pt.

$\lambda$ : Dimensionless radial distance.

$\lambda_{Pt}$ : Total interfacial perimeter per gram of Pt.

$\sigma$ : particle density ( $\text{g}/\text{nm}^3$ )

$\tau$ : Dimensionless time.

$\omega$ : Average atom density of Pt particle surface.

$\Sigma_p$ : Number of particles per gram of Pt.

## Appendix A.2. Development of the Material Balances Used the Dispersion Model.

This is the model developed by Bhatia et al [1]. The model has been modified for this study.

### A.2.1. Parameter Development.

Assumption #1: stored  $\text{NO}_x$  species (represented by 'A' here) undergoes reverse-spillover via diffusion in the Ba phase towards the Pt/Ba interface, where it is reduced by  $\text{H}_2$  as well as the reaction network intermediate,  $\text{NH}_3$ .

Figure A.2.1 shows the Pt crystallite and the  $\text{NO}_x$  stored around it. Figure A.1. is a bird-eye's view.  $R_c$  is the radius of the crystallite, and  $R_{\text{eff}}$  is the radius of  $\text{NO}_x$  stored around the crystallite.

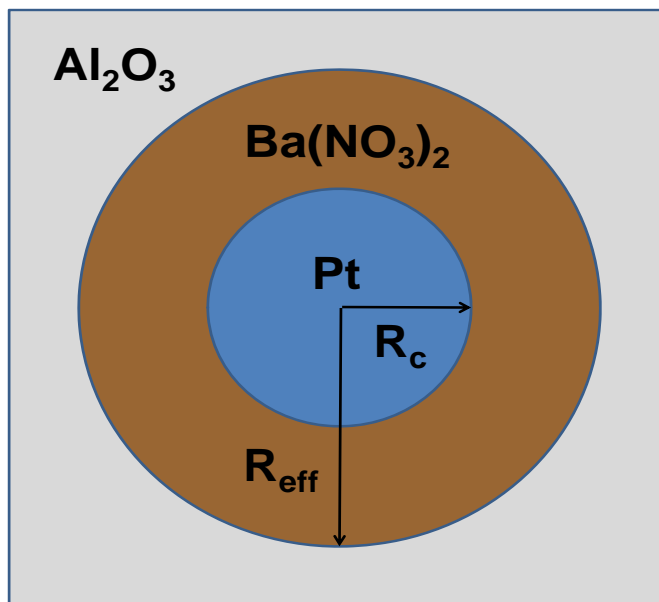


Figure A.2.1. Illustration of down-looking view of Pt on exposed BaO supported on  $\text{Al}_2\text{O}_3$ .

Assumption #2: the Pt crystallites have a hemispherical shape.

Let  $N_T$  be the total number of Pt atoms in the Pt crystallite.

$$N_T = \frac{\text{volume of Pt crystallite (hemisphere)} * A_{PF}}{\text{volume of Pt atom}} = \frac{1/2 * 4/3 \pi R_C^3 A_{PF}}{4/3 \pi (D_{Pt}/2)^3} = \frac{2/3 \pi R_C^3 A_{PF}}{1/6 \pi D_{Pt}^3} \quad (\text{A.2.1})$$

where  $A_{PF}$  is the atomic packing factor. For Pt with a FCC structure,  $A_{PF}$  is equal to 0.74.  $D_{Pt}$  is the diameter of the Pt atom.

Using equation (A.1), the number of crystallites in a monolith channel,  $N_C$ , is calculated from:

$$N_C = \frac{M_{Pt_T} N_{AV}}{N_T} \quad (\text{A.2.2})$$

where  $M_{Pt_T}$  is the total number of moles of Pt in the washcoat per channel, and  $N_{AV}$  is Avogadro's number. Substituting (A.2.1) into (A.2.2):

$$N_C = \frac{M_{Pt_T} N_{AV} 1/6 \pi D_{Pt}^3}{2/3 \pi R_C^3 A_{PF}} = \frac{M_{Pt_T} N_{AV} D_{Pt}^3}{4 R_C^3 A_{PF}} \quad (\text{A.2.3})$$

The total exposed surface area,  $S_E$ , is equal to:

$$S_E = 1/2 \text{ surface area (sphere)} N_C = 1/2 4\pi R_C^2 N_C = 2\pi R_C^2 N_C \quad (\text{A.2.4})$$

The total Pt/Ba interfacial perimeter for a single channel,  $I_p$ :

$$I_p = \text{perimeter (circle)} * N_C = 2\pi R_C N_C \quad (\text{A.5})$$

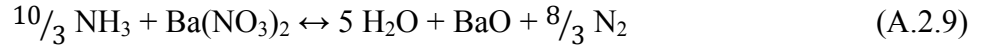
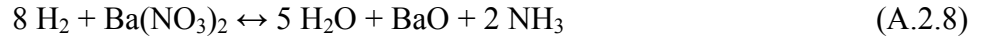
Substituting (A.2.3) into (A.2.4) and (A.2.5):

$$S_E = \frac{M_{PtT} N_{AV} D_{Pt}^3 \pi}{2 A_{PF} R_C} \quad (A.2.6)$$

$$I_P = \frac{M_{PtT} N_{AV} D_{Pt}^3 \pi}{2 A_{PF} R_C^2} \quad (A.2.7)$$

The overall catalytic reactions occurring at the Pt/Ba interface are:

Assumption #3: NO<sub>x</sub> is stored in the form of nitrates



In addition, some of the H<sub>2</sub> is consumed by chemisorbed oxygen on the Pt crystallites:



Assumption #4: One-dimensional diffusion of NO<sub>x</sub> within the Ba phase ( $R_C \leq r \leq R_{eff}$ ).

A localized material balance for stored NO<sub>x</sub> gives:

input – output + generation = accumulation

$$P N_A|_r - P N_A|_{r+\Delta r} + 0 = \frac{\partial n_A}{\partial t} \quad (A.2.11)$$

where P is the perimeter and equal to  $P = 2\pi r$ ,  $N_A$  is the flux of NO<sub>x</sub>, and  $n_A$  is the moles of NO<sub>x</sub> present. Utilizing  $n_A = C_A P \Delta r$  where  $C_A$  is the concentration of NO<sub>x</sub>. The above equation reduces to  $\frac{\partial N_A}{\partial r} = \frac{\partial n_A}{\partial t}$ . Substituting  $N_A = D_A \frac{\partial C_A}{\partial r}$  where  $D_A$  is the diffusivity of NO<sub>x</sub> into (A.2.11):

$$\begin{aligned}
P N_A|_r - P N_A|_{r+\Delta r} &= \frac{\partial C_A P \Delta r}{\partial t} \\
\frac{\partial}{\partial r} (N_A P) &= \frac{\partial C_A P}{\partial t} \\
2\pi \frac{\partial}{\partial r} \left( r D_A \frac{\partial C_A}{\partial r} \right) &= 2\pi r \frac{\partial C_A}{\partial t} \\
\frac{\partial C_A}{\partial t} &= \frac{D_A}{r} \frac{\partial}{\partial r} \left( r \frac{\partial C_A}{\partial r} \right) \quad R_C \leq r \leq R_{\text{eff}} \quad (\text{A.2.12})
\end{aligned}$$

The following conditions apply to (A.2.12):

$$\text{I.C. at } t = 0, C_A = C_{A0}(r) \text{ for } R_C \leq r \leq R_{\text{eff}} \quad (\text{A.2.13})$$

B.C. 1. Assumption #5, diffusional limitations in the washcoat (transverse to axial flow) are negligible, and the diffusive flux of stored  $\text{NO}_x$  at the Pt/Ba interface is equal to consumption of  $\text{NO}_x$  by  $\text{NH}_3$  and  $\text{H}_2$ :

$$N_A = D_A \frac{\partial C_A}{\partial r} = k_1 C_A C_{\text{H}_2, \text{WC}} + k_2 C_A C_{\text{NH}_3, \text{WC}} \quad (\text{A.2.14})$$

where  $k_1$  is rate constant for  $\text{NO}_x$  regeneration by  $\text{H}_2$  ( $\text{m}^4/\text{mol s}$ ), and  $k_2$  is rate constant for  $\text{NO}_x$  regeneration by  $\text{NH}_3$  ( $\text{m}^4/\text{mol s}$ ). The rate expression is derived from the fact that the consumption at the interface is dependent on the amount of  $\text{NO}_x$  at the surface and the amount of  $\text{H}_2$  or  $\text{NH}_3$  present.

$$\text{B.C.2. at } r = R_{\text{eff}}, \frac{\partial C_A}{\partial r} = 0 \quad (\text{A.2.15})$$

Assumption #6,  $\text{NO}_x$  is stored uniformly in the washcoat as a monolayer of BaO and all  $\text{Al}_2\text{O}_3$  sites are covered.

$R_{eff}$  is an estimate of the BaO that is utilized for  $NO_x$  storage.  $R_{eff}$  is determined from equating the total moles of  $NO_x$  stored on the catalyst ( $M_{NO_x}$ ) to 2x the number of moles of exposed area around the Pt crystallite  $[\pi * (R_{eff}^2 - R_c^2)]$ .

$$M_{NO_x} = \frac{2 n_{ch} N_c S_{BaO} \pi (R_{eff}^2 - R_c^2)}{N_{av}} \quad (A.2.16)$$

Substituting the expression for  $N_c$  (A.2.3) into (A.2.16), the value for  $R_{eff}$  is:

$$R_{eff} = R_c \sqrt{1 + \frac{2 A_{PF} M_{NO_x} R_c}{n_{ch} \pi S_{BaO} D_{Pt}^3 M_{PtT}}} \quad (A.2.17)$$

where  $S_{BaO}$  surface density of BaO (BaO molecules/ $m^2$  exposed BaO surface). The total surface area of active BaO per unit mass of washcoat,  $S_{BaW}$ , is:

$$S_{BaW} = \frac{n_{ch} N_c \pi (R_{eff}^2 - R_c^2)}{m_{wc}} \quad (A.2.18)$$

where  $m_{wc}$  is the mass of the washcoat loading (g).

Using (A.2.16) and (A.2.18), we can relate the active BaO surface area to mol of  $NO_x$  stored:

ratio of  $\frac{S_{BaW}}{M_{NO_x}} = \frac{N_{av}}{2m_{wc}S_{BaO}} \rightarrow S_{BaW} = \frac{M_{NO_x} N_{av}}{2m_{wc}S_{BaO}} \quad (A.2.19)$



### A.2.2. Species Balance.

For a transient diffusion-reaction model of a porous catalyst with reaction, an overall mole balance gives:

$$F_{jx} \Big|_x - F_{jx} \Big|_{x+\Delta x} - RA_{\Omega_1} \Delta x = \frac{\partial n_j}{\partial t} \quad (\text{A.2.20})$$

where  $F_{jx} \Big|_x$  is the molar rate in, mol/s

$F_{jx} \Big|_{x+\Delta x}$  is the molar rate out, mol/s

$R$  is the molar rate of disappearance of component  $j$ . mol/m<sup>3</sup> catalyst

$A_{\Omega_1}$  is the cross sectional area of the fluid phase, m<sup>2</sup>

$x$  is the axial coordinate

$n_j$  is the mol of  $j$

Using  $n_j = c_j A_{\Omega_1} \Delta x \varepsilon_{wc}$ , dividing by  $A_{\Omega_1} \Delta x$ , and taking the limit as  $\Delta x \rightarrow 0$ :

$$\frac{1}{A_{\Omega_1}} \left( -\frac{\partial F_{jx}}{\partial x} \right) - R = \varepsilon_{wc} \frac{\partial c_j}{\partial t} \quad (\text{A.2.21})$$

where  $\varepsilon_{wc}$  is the porosity of the washcoat. If we assumed that the amount of material transported by diffusion in the axial direction is negligible compared with bulk flow (Knudsen diffusion):

$$\frac{\partial F_{jx}}{\partial x} = \bar{u} A_{\Omega_1} \frac{\partial c_j}{\partial x} \quad (\text{A.2.22})$$

so (A.2.21) becomes

$$\varepsilon_{wc} \frac{\partial c_j}{\partial t} = -\bar{u} \frac{\partial c_j}{\partial x} - R \quad (\text{A.2.23})$$

*A.2.2.1. Gas Phase Species Balance (Diffusion from the Bulk to the Interface).*

Assumption #7: Assuming the entire resistance for mass transfer in the gas phase resides in a stagnant film of a certain thickness, a balance for the diffusion of component  $j$  from the bulk phase to the fluid washcoat interface gives:

$$A_{\Omega_1} \bar{u} C_{jm}|_x - A_{\Omega_1} \bar{u} C_{jm}|_{x+\Delta x} - P_{\Omega} \Delta x k_{c,j}(x) (c_{jm} - c_{s,avg}) = 0 \quad (\text{A.2.24})$$

where  $A_{\Omega_1}$  = cross-sectional area of the fluid phase,  $\text{m}^2$

$c_{jm}$  = cup-mixing concentration in the fluid phase,  $\text{mol}/\text{m}^3$

$c_{s,avg}$  = circumferentially averaged concentration at the fluid-washcoat interface,  $\text{mol}/\text{m}^3$

$P_{\Omega}$  = the wetted fluid-washcoat interfacial perimeter,  $\text{m}$

$k_{me}(x)$  = position dependent mass transfer coefficient from the bulk of the fluid to the fluid-washcoat interface,  $\text{m}/\text{s}$

$\bar{u}$  = average fluid velocity,  $\text{m}/\text{s}$

Dividing by  $A_{\Omega_1} \Delta x$  and taking the limit as  $\Delta x \rightarrow 0$ :

$$\bar{u} \frac{\partial c_j}{\partial x} = -\frac{1}{R_{\Omega_1}} k_{me}(x) (c_{jm} - c_{s,avg}) \quad (\text{A.2.25})$$

and  $R_{\Omega_1}$  is the effective transverse diffusion length for the fluid phase,  $\text{m}$  ( $R_{\Omega_1} = \frac{A_{\Omega_1}}{P_{\Omega}}$ )

### A.2.2.2. Washcoat Species Balance.

Assumptions #8 and #9: Assuming a hypothetical film in the washcoat describes the intra-phase or internal mass transfer resistance and no diffusional limitations exist in the bulk washcoat (the concentration of  $j$  drops from  $c_{s,avg}$  to constant value of  $c_{j,wc}$ , we get the following:

$$P_{\Omega}\Delta x k_{mi}(x)(c_{s,avg} - c_{j,wc}) = R_{\Omega_2}R(c_{j,wc}) \quad (\text{A.2.26})$$

$k_{me}(x)$  = position dependent internal mass transfer coefficient between the interior of the washcoat and fluid-washcoat interface, m/s

$c_{j,wc}$  is the volume-averaged concentration in washcoat weighed with respect to activity, mol/m<sup>3</sup>

$A_{\Omega_2}$  = cross-sectional area of the washcoat, m<sup>2</sup>

$R_{\Omega_2}$  is the effective transverse diffusion length for the washcoat, m ( $R_{\Omega_2} = \frac{A_{\Omega_2}}{P_{\Omega}}$ )

$R$ , reaction rates evaluated at  $c_{j,wc}$ .

Dividing (A.2.26) by  $P_{\Omega}\Delta x$  and taking the limit  $\Delta x \rightarrow 0$ :

$$k_{mi}(x)(c_{s,avg} - c_{j,wc}) = R_{\Omega_2}R(c_{j,wc}) \quad (\text{A.2.27})$$

### A.2.2.3. Interface between the Fluid Phase and Washcoat.

At the interface between the fluid phase and the catalyst washcoat, no accumulation of mass can occur. This means that the external mass flux from the bulk gas phase to the interface must be the same as the interface to the bulk.

$$k_{me}(x)(c_{jm} - c_{s,avg}) = k_{mi}(x)(c_{s,avg} - c_{j,wc}) \quad (\text{A.2.28})$$

Using the idea of the overall, position dependent mass transfer coefficient,  $k_{c,j}(x)$  is equal to the total individual resistances:

$$\frac{1}{k_{c,j}(x)} = \frac{1}{k_{me}(x)} + \frac{1}{k_{mi}(x)} \quad (\text{A.2.29})$$

Using (A.2.29) in (A.2.25) and (A.2.28), the  $c_{s,avg}$  term can be eliminated. So (A.2.28) into (A.2.25):

$$\bar{u} \frac{\partial c_j}{\partial x} = -\frac{1}{R_{\Omega_1}} k_{c,j}(x) (c_{jm} - c_{j,wc}) \quad (\text{A.2.30})$$

and (A.2.29) into (A.2.28):

$$k_{c,j}(x) (c_{jm} - c_{j,wc}) = R_{\Omega_2} R (c_{j,wc}) \quad (\text{A.2.31})$$

or

$$R (c_{j,wc}) = \frac{k_{c,j}(x)}{R_{\Omega_2}} (c_{jm} - c_{j,wc}) = \quad (\text{A.2.32})$$

#### A.2.2.4. The Species Balance for Component $j$ in the Fluid Phase.

The final expression for the species balance for component  $j$  in the fluid phase is obtained by substituting (A.2.31) and (A.2.32) into (A.2.23):

$$\frac{\partial c_j}{\partial t} = -\bar{u} \frac{\partial c_{jm}}{\partial x} - \frac{k_{c,j}(x)}{R_{\Omega}} (c_{jm} - c_{j,wc}) \quad (\text{A.2.33})$$

where the fluid velocity (m/s) and the transverse diffusion length scale (m) are represented by  $\bar{u}$  and  $R_{\Omega}$ , respectively. The position-dependent mass-transfer coefficients for each species  $j$ , represented by  $k_{c,j}(x)$ , are used to account for the transverse gradients. The position dependence obtained from Ramanathan et al. [2] is used here for a square channel of uniform washcoat thickness (Figure A.2), its development is described in Section A.3.5.

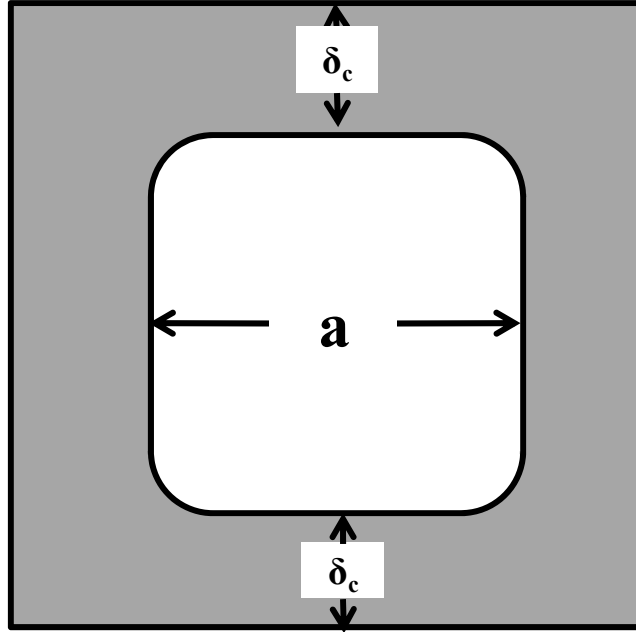


**Figure A.2.2. Square channel of uniform washcoat thickness.**

$$R_{\Omega_1} = \frac{\text{flow area } (A_{\Omega_1})}{\text{fluid washcoat perimeter } P_{\Omega}} = \frac{R}{2} \quad (\text{A.2.34})$$

and

$$R_{\Omega_2} = \frac{\text{washcoat cross-sectional area } (A_{\Omega_2})}{\text{interfacial perimeter } P_{\Omega}} = \frac{(a+2\delta_c)^2 - a^2}{4a} = \frac{\delta_c(a+\delta_c)}{a} \quad (\text{A.2.35})$$

where

$R_{\Omega_1}$  = effective transverse length scale (m) in the fluid phase, m

$R_{\Omega_2}$  = effective transverse length scale (m) in the washcoat, m

$a$  = width/hydraulic diameter of the channel, m

$\delta_c$  = thickness of the washcoat (m)

The reaction rate term,  $R(c_{j,wc})$ , is comprised of the reactions that occur at the fluid-washcoat interface and the catalyst surface.

At the interface (1):

$$R(c_{j,wc}) = \text{interfacial reaction rate} * \frac{I_P}{\text{surface area } R_{\Omega_1}} \quad (\text{A.2.36})$$

At the surface (2):

$$R(c_{j,wc}) = \text{surface reaction rate} * \frac{I_P}{\text{surface area } R_{\Omega_1}} \quad (\text{A.2.37})$$

where  $S_E$  and  $I_P$  are defined in (A.2.4) and (A.2.5).

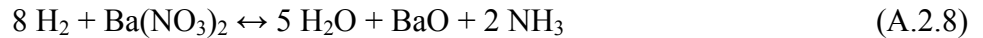
### A.2.3. Washcoat Species Balance.

#### A.2.3.1. Hydrogen Surface Balance.

For a square channel of uniform cross-section, the species balance for  $H_2$  is given by:

$$\varepsilon_{wc} \frac{\delta c_{H_2,wc}}{\delta t} = \frac{k_{c_{H_2}}(x)}{R_{\Omega_2}} k_{c,j}(x) (c_{H_2m} - c_{H_2,wc}) - R_{\Omega_2} R(c_{H_2,wc}) \quad (\text{A.2.38})$$

The reaction rate of  $H_2$  reacting with stored  $NO_x$  at the Pt/Ba interface (A.8),  $r=R_c$ , is given by:



$$R(c_{wc}) = 4k_1 c_A|_{r=R_c} c_{H_2,wc} * \frac{N_c 2\pi R_c}{4aLR_{\Omega_2}} \quad (\text{A.2.39})$$

For  $H_2$  reacting with chemisorb oxygen on the surface of the Pt crystallite (A.2.10):



$$R(c_{wc}) = k_3 c_{Pt} \theta_{O-Pt} c_{H_2,wc} * \frac{N_c 2\pi R_c^2}{4aLR_{\Omega_2}} \quad (\text{A.2.40})$$

The total reaction rate expression for the consumption of H<sub>2</sub>:

$$R(c_{wc}) = \frac{c_{H_2wc} N_c 2\pi R_c}{\delta_c (a + \delta_c)} * (4k_1 c_A|_{r=R_c} + k_3 c_{Pt} \theta_{O-Pt} R_c) \quad (\text{A.2.41})$$

The diffusion of H<sub>2</sub> is expressed as:

$$\frac{k_{C_{H_2}}(x)}{R_{\Omega_2}} (c_{H_2m} - c_{H_2,wc}) = \frac{a}{\delta_c (a + \delta_c)} k_{C_{H_2}}(x) (c_{H_2m} - c_{H_2,wc}) \quad (\text{A.2.42})$$

Substituting (A.40) and (A.41) into (A.37):

$$\frac{\delta c_{H_2,wc}}{\delta t} = \frac{1}{\varepsilon_{wc} \delta_c (a + \delta_c)} \left[ \frac{a k_{C_{H_2}}(x) (c_{H_2m} - c_{H_2,wc}) - \frac{c_{H_2,wc} N_c 2\pi R_c}{4L} (4k_1 c_A|_{r=R_c} + k_3 c_{Pt} \theta_{O-Pt} R_c) \right] \quad (\text{A.2.43})$$

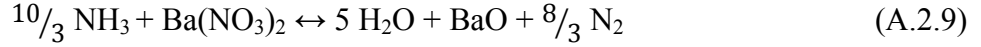
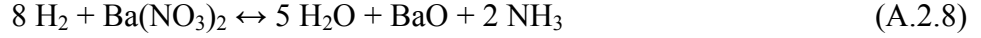
Assumption #10: (A.2.43) assumes the reaction rate between H<sub>2</sub> and the stored NO<sub>x</sub> is proportional to the perimeter of the Pt/Ba interface, whereas the reaction between H<sub>2</sub> and chemisorbed O<sub>2</sub> is proportional to the surface area of exposed Pt atoms. Hence, the term “4k<sub>1</sub>c<sub>A</sub>|<sub>r=R<sub>c</sub></sub>” represents the consumption of H<sub>2</sub> by NO<sub>x</sub>, whereas the term “k<sub>3</sub>c<sub>Pt</sub>θ<sub>O-Pt</sub>R<sub>c</sub>” represents the consumption of H<sub>2</sub> by chemisorbed oxygen on the exposed Pt surface.

#### A.2.3.2. NH<sub>3</sub> Surface Balance.

The diffusion of NH<sub>3</sub> on the surface is similar to that of H<sub>2</sub>:

$$\frac{k_{C_{NH_3}}(x)}{R_{\Omega_2}} (c_{NH_3m} - c_{NH_3,wc}) \quad (\text{A.2.44})$$

As for the reaction rate expression, NH<sub>3</sub> only reacts at the Pt/Ba interface and not on the Pt surface. NH<sub>3</sub> is produced in (A.2.8) and consumed in (A.2.9):



The rate expression for (A.2.8):

$$R(c_{wc}) = k_1 c_A|_{r=R_c} c_{H_2wc} * \frac{N_c 2\pi R_c}{4aLR_{\Omega_2}} \quad (\text{A.2.45})$$

The rate expression for (A.2.9)

$$R(c_{wc}) = -\left(\frac{5}{3}\right) k_2 c_A|_{r=R_c} c_{NH_3wc} * \frac{N_c 2\pi R_c}{4aLR_{\Omega_2}} \quad (\text{A.2.46})$$

Using the expression for  $R_{\Omega_2}$  (A.2.34), the total rate of reaction for NH<sub>3</sub> is:

$$\text{total } R(c_{wc}) = k_1 c_{H_2wc} * \frac{c_A|_{r=R_c} N_c 2\pi R_c}{4L} \frac{1}{\delta_c(a+\delta_c)} \left[ k_1 c_{H_2wc} - \left(\frac{5}{3}\right) k_2 c_{NH_3wc} \right] \quad (\text{A.2.47})$$

Substituting (A.2.36), (A.2.37), (A.2.44), and (A.2.47) into (A.2.33):

$$\frac{\delta c_{NH_3,wc}}{\delta t} = \frac{1}{\varepsilon_{wc} \delta_c (a+\delta_c)} \left\{ \begin{aligned} & a k_{c_{NH_3}}(x) (c_{NH_3m} - c_{NH_3,wc}) + \\ & \frac{c_A|_{r=R_c} N_c 2\pi R_c}{4L} \left[ k_1 c_{H_2wc} - \left(\frac{5}{3}\right) k_2 c_{NH_3wc} \right] \end{aligned} \right\} \quad (\text{A.2.48})$$

Assumption #11: NH<sub>3</sub> does not react with chemisorbed oxygen on Pt. The term “ $k_1 c_{H_2wc}$ ” is the generation of NH<sub>3</sub>, whereas “ $\left(\frac{5}{3}\right) k_2 c_{NH_3wc}$ ” is the consumption of NH<sub>3</sub> by stored NO<sub>x</sub>.

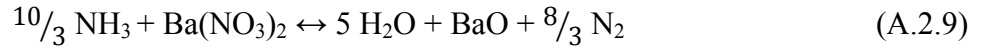


### A.2.3.3. $N_2$ Surface Balance.

The diffusion of  $N_2$  on the surface is similar to that of  $H_2$  and  $NH_3$ :

$$\frac{k_{c_{N_2}}(x)}{R_{\Omega_2}}(c_{N_{2m}} - c_{N_{H_3,wc}}) \quad (A.2.49)$$

The reaction rate expression for the generation of  $N_2$  at the interface is (A.2.9):



$$R(c_{wc}) = (4/3)k_2c_A|_{r=R_c}c_{NH_3wc} * \frac{N_c2\pi R_c}{4aLR_{\Omega_2}} \quad (A.2.50)$$

Using the expression for  $R_{\Omega_2}$  (A.2.34):

$$R(c_{wc}) = * \frac{k_2c_A|_{r=R_c}c_{NH_3wc}N_c2\pi R_c}{3L\delta_c(a+\delta_c)} \quad (A.2.51)$$

Substituting (A.2.49) and (A.2.51) into (A.2.25):

$$\frac{\delta c_{N_2,wc}}{\delta t} = \frac{1}{\varepsilon_{wc}\delta_c(a+\delta_c)} \left[ ak_{c_{H_2}}(x)(c_{N_{2m}} - c_{N_2,wc}) + \frac{N_c2\pi R_c k_2 c_A|_{r=R_c} c_{NH_3wc}}{3L} \right] \quad (A.2.52)$$

### A.2.3.4. Vacant Site Balance.

Lastly, a vacant site balance is required using (A.2.10):



Here, generation is equal to accumulation:

$$\frac{\partial \theta_v}{\partial t} = k_3 c_{H_2wc} \theta_{O-Pt} \quad (A.2.53)$$

The initial and boundary conditions for (A.2.43), (A.2.48), (A.2.52), and (A.2.53):

$$\text{I.C. } @ t = 0, \quad c_{j,m} = 0, \quad c_{jwc} = 0, \quad \theta_v = 0 \text{ for } 0 < x \leq L \quad (\text{A.2.54})$$

$$\text{B.C. } @ x = 0, \quad c_{j,m} = c_j^{in} \quad (\text{A.2.55})$$

where  $c_j^{in}$  is the inlet concentration of species  $j$  in the fluid phase, mol/m<sup>3</sup>.

#### A.2.4. Dimensionless Expression for Use in the Model.

The above expressions are non-dimensionalized for their use in the model using the following expressions:

$$\text{Dimensionless axial coordinate} \quad z = \frac{x}{L} \quad (\text{A.2.56})$$

$$\text{Dimensionless radial coordinate} \quad r^* = \frac{r-R_c}{R_{eff}-R_c} \quad (\text{A.2.57})$$

$$\text{Dimensionless time} \quad \tau = \frac{tD_A}{(R_{eff}-R_c)^2} \quad (\text{A.2.58})$$

$$\text{Dimensionless radial distance} \quad \lambda = \frac{R_c}{R_{eff}-R_c} \quad (\text{A.2.59})$$

$$\text{Using } \lambda, r^* \text{ becomes} \quad r^* = \frac{r}{R_{eff}-R_c} - \lambda \quad (\text{A.2.60})$$

Dimensionless cup-mixing concentration of species  $j$  in the fluid phase

$$C_{jm}^* = \frac{c_{jm}}{c_{H_2}^{in}} \quad (\text{A.2.61})$$

Dimensionless cup-mixing concentration of species  $j$  in the fluid-washcoat interface

$$C_{jwc}^* = \frac{c_{jwc}}{c_{H_2}^{in}} \quad (\text{A.2.62})$$

Dimensionless concentration of stored NO<sub>x</sub>

$$C_A^* = \frac{C_A}{C_{AO}} \quad (\text{A.2.63})$$

With this expressions, the following expressions can be non-dimensionalized:

A localized material balance for stored  $\text{NO}_x$ :

$$\frac{\partial C_A}{\partial t} = \frac{D_A}{r} \frac{\partial}{\partial r} \left( r \frac{\partial C_A}{\partial r} \right) \quad (\text{A.2.12})$$

$$\frac{\partial C_A^*}{\partial \tau} = \frac{\partial^2}{\partial r^{*2}} + \left( \frac{1}{r^{*+\lambda}} \right) \frac{\partial C_A^*}{\partial r^*} \quad (\text{A.2.64})$$

$$\text{I.C. at } \tau = 0, \quad C_A^* = 1, \quad 0 \leq r^* \leq 1 \quad (\text{A.2.65})$$

B.C.1. at  $r^* = 0$ ,

$$\frac{\partial C_A^*}{\partial r^*} = \frac{(R_{eff} - R_c) C_{H_2}^{in}}{D_A} (k_1 C_{H_2wc}^* + k_2 C_{NH_3wc}^*) \quad (\text{A.2.66})$$

$$\text{B.C.2. at } r^* = 1, \quad \frac{\partial C_A^*}{\partial r^*} = 0 \quad (\text{A.2.67})$$

Washcoat Species Balance (A.2.25) becomes:

$$\frac{\partial C_{jm}^*}{\partial \tau} = \frac{(R_{eff} - R_c)^2}{D_A} \left[ -\frac{\bar{u}}{L} \frac{\partial C_{jm}^*}{\partial z} - \frac{k_{c,j}(z)}{R_\Omega} (C_{jm}^* - C_{jwc}^*) \right] \quad (\text{A.2.68})$$

The  $\text{H}_2$  surface balance (A.2.43) becomes:

$$\frac{\partial C_{H_2wc}^*}{\partial \tau} = \frac{(R_{eff} - R_c)^2}{D_A \epsilon_{wc} \delta_c (a + \delta_c)} \left[ \frac{a k_{cH_2}(z) (C_{H_2in}^* - C_{H_2wc}^*) - C_{H_2wc}^* N_c 2\pi R_c}{4L} (4k_1 C_{AO} C_A^*|_{r^*=0} + k_3 c_{Pt} \theta_{O-Pt} R_c) \right] \quad (\text{A.2.69})$$

The  $\text{NH}_3$  surface balance (A.2.48) becomes:

$$\frac{\partial C_{NH_3wc}^*}{\partial \tau} = \frac{(R_{eff} - R_c)^2}{D_A \epsilon_{wc} \delta_c (a + \delta_c)} \left[ \frac{a k_{cNH_3}(z) (C_{NH_3in}^* - C_{NH_3wc}^*) + N_c 2\pi R_c C_A^*|_{r^*=0}}{4L} (k_1 C_{H_2wc}^* - (5/3) k_2 C_{NH_3wc}^*) \right] \quad (\text{A.2.70})$$

The  $N_2$  surface balance (A.2.52) becomes:

$$\frac{\partial C_{N_2wc}^*}{\partial \tau} = \frac{(R_{eff} - R_c)^2}{D_A \epsilon_{wc} \delta_c (a + \delta_c)} \left[ a k_{cN_2}(z) (C_{N_2in}^* - C_{N_2wc}^*) + \frac{N_c 2\pi R_c C_{AO} C_A^* |_{r^*=0} C_{NH_3wc}^*}{3L} \right] \quad (A.2.71)$$

Finally, the vacant site balance (A.2.53) becomes:

$$\frac{\partial \theta_v}{\partial \tau} = \frac{(R_{eff} - R_c)^2}{D_A} k_3 C_{H_2}^{in} C_{H_2wc}^* \theta_{O-Pt} \quad (A.2.72)$$

The initial and boundary conditions for the species balances become:

$$\text{I.C.} \quad \text{at } \tau = 0, \quad C_{jm}^* = 0, \quad C_{jwc}^* = 0, \quad \theta_v = 0 \quad \text{for } 0 < z \leq 1 \quad (A.2.73)$$

$$\text{B.C.} \quad \text{at } z = 0, \quad C_{jm}^* = C_j^{in*} \quad (A.2.74)$$

where  $C_j^{in*}$  is the dimensionless inlet concentration of species  $j$

#### A.2.5. Determination of the Overall Mass Transfer Coefficient.

From Ramanathan et al. [2], position dependent mass transfer coefficient for species  $j$  at axial position  $x$ ,  $k_{c,j}(x)$ , is calculated for the case of fully developed laminar flow with the velocity field developing along with the concentration boundary layer using the following expression:

$$Sh_{\Omega}(x) = \frac{k_{c,j}(x) R_{\Omega}}{D_{me}(j)} \quad (A.2.75)$$

If

$$z(j) < \frac{R_{\Omega_2} \bar{u}}{D_{me}(j) Sc^{1/3}} \left( \frac{1.4}{Sh_{i\infty}} \right)^2 \quad (\text{A.2.76})$$

then:

$$k_{c,j}(x) = \frac{0.35 D_{me}(j)}{R_{\Omega} Sc(j)^{1/6}} \left( \frac{R_{\Omega}^2 \bar{u}}{z(j) D_{me}(j)} \right)^{1/2} \quad (\text{A.2.77})$$

else:

$$k_{c,j}(x) = \frac{D_{me}(j)}{R_{\Omega} \left( \frac{Sh_{i\infty}}{4} \right)} \quad (\text{A.2.78})$$

where:

$Sh_{\Omega}(x)$  = Sherwood Number, defined by (A.2.75)

$k_{c,j}(x)$  = position dependent mass transfer coefficient for species  $j$  at axial position  $x$  (m/s)

$R_{\Omega}$  = effective transverse length scale in the fluid phase (m), in this case: one-half the channel hydraulic radius (m) (A.2.34)

$D_{me}(j)$  = diffusion coefficient in the fluid phase (m<sup>2</sup>/s)

$z(i)$  = dimensionless coordinate along the length of the channel

$R_{\Omega_2}$  = effective transverse length scale in the washcoat (m) (A.2.35)

$\bar{u}$  = average fluid velocity (m/s)

$Sc$  = Schmidt Number =  $\frac{v}{D_{me}(j)}$

$\nu$  = kinematic viscosity (m<sup>2</sup>/s) =  $\frac{\mu}{\rho}$

$\mu$  = dynamic viscosity (kg/m\*s)

$\rho$  = density (kg/m<sup>3</sup>)

$Sh_{i\infty}$  = asymptotic Sherwood(Nusselt) numbers for the channel (with constant flux boundary condition). Here  $Sh_{i\infty} = 3.608$  [2]

*A.2.6.References.*

- [1] D. Bhatia, M.P. Harold, V. Balakotaiah, A Global Kinetic Model for NO<sub>x</sub> Storage and Reduction on Pt/BaO/Al<sub>2</sub>O<sub>3</sub> Monolithic Catalysts. *Catalysis Today* 151 (2010) 314-329.
- [2] K. Ramanathan, V. Balakotaiah, D.H. West, “Light-Off Criterion and Transient Analysis of Catalytic Monoliths.” *Chemical Engineering Science* 58 (2003) 1381 – 1405.

## **Bibliography**

<http://www.arb.ca.gov/ch/educational/definition.htm>. Downloaded 5/23/12.

<http://www.cleers.org>. Downloaded 11/20/12.

<http://cta.ornl.gov/data/chapter12.shtml>. Downloaded 5/23/12.

<http://www.dieselnet.com/standards/cycles/ftp75.php>. Downloaded 5/25/12.

[http://www.dieselnet.com/standards/us/ld\\_t2.php](http://www.dieselnet.com/standards/us/ld_t2.php). Downloaded 5/25/12.

<http://www.ebullionguide.com/>. Downloaded 10/24/12.

<http://www.epa.gov/lawsregs/laws/caa.html>. Downloaded 5/23/12.

<http://www.epa.gov/oig/reports/2004/20040929-2004-P-00033.pdf>. Downloaded 5/23/12

<http://epa.gov/otaq/invtory/overview/results/longdesc-all.htm#hc>. Downloaded 5/25/12.

[http://www.fhwa.dot.gov/environment/air\\_quality/publications/fact\\_book/page14.cfm](http://www.fhwa.dot.gov/environment/air_quality/publications/fact_book/page14.cfm).  
Downloaded 5/23/12.

<http://www.greenercars.org/LEED2012.xls>. Downloaded 10/24/12.

<http://www.wtrg.com/prices.htm>. Downloaded 5/25/12.

[http://www.pscleanair.org/images/chart\\_sources.gif](http://www.pscleanair.org/images/chart_sources.gif). Downloaded 5/23/12

<http://www.epw.senate.gov/enlaws/cleanair.pdf>. Downloaded 2/5/13.

H. Abdulhamid, E. Fridell, M. Skoglundh, Top. Catal. 30-31 (2004) 161.

- H. Abdulhamid, E. Fridell, J. Dawody, M. Skoglundh, *J. Catal.* 241 (2006) 200.
- H. Abdulhamid, E. Fridell, M. Skoglundh, *Appl. Catal. B: Env.* 62 (2006) 319.
- M. Abul-Milh, H. Westberg, *Top. Catal.* 42-43 (2007) 209.
- K. Adams, G. Graham, *Appl. Catal. B: Env.* 80 (2008) 343.
- A. Amberntsson, H. Persson, P. Engstrom, B. Kasemo, *Appl. Catal. B: Env.* 31 (2001) 27.
- A. Amberntsson, E. Fridell, M. Skoglundh, *Appl. Catal. B: Env.* 46 (2003) 429.
- A. Ambertsson, M. Skoglundh, S. Ljungström, E. Fridell, *J. Catal.* 217 (2003) 253.
- J.A. Anderson, B. Bachiller-Baeza, M. Fernández-García, *Physi. Chem. Chem. Phys.* 5 (2003) 4418.
- C. Apestegua, T. Garetto, A. Borgna, *J. Catal.* 106 (1987) 73.
- V. Balakotaiah, N. Gupta, D.H. West, *Chem. Eng. Sci.* 55 (22) (2000) 5367–5383.
- M. E. Bartram, R. G. Windham, B. E. Koel, *Langmuir* 4 (1988) 240.
- P. Bazin, O. Saur, J. Lavalley, G. Blanchard, V. Visciglio, O. Touret, *Appl. Catal. B: Env.* 13 (1997) 265.
- P. Bazin, O. Saur, F.C. Meunier, M. Daturi, J.C. Lavalley, A.M. Le Govic, V. Harlé, G. Blanchard, *Appl. Catal. B* 90 (2009) 368.
- B. Béguin, E. Garbowski, M. Primet, *Appl. Catal.* 75 (1991) 119.



- D. Bhatia, R.D. Clayton, M.P. Harold, V. Balakotaiah, *Catal. Today* 147 (2009) S250.
- D. Bhatia, R.W. McCabe, M.P. Harold, V. Balakotaiah, *J. of Catal.* 266 (2009) 106.
- D. Bhatia, M.P. Harold, V. Balakotaiah, *Catal. Today* 151 (2010) 314.
- S. Benard, L. Retailleau, F. Gaillard, P. Vernoux, A. Giroir-Fendler, *Appl. Catal. B: Env.* 55 (2005) 11.
- R. Bonzi, L. Lietti, L. Castoldi, P. Forzatti, *Catal. Today* 151 (2010) 376.
- M. Bowker, P. Stone, R. Smith, E. Fourre, M. Ishii, N.H. de Leeuw, *Surf. Sci.* 600 (2006) 1973.
- J. Breen, M. Marella, C. Pistarino, J. Ross, *Catal. Lett.* 80 (2002) 123.
- R. Büchel, R. Ströbel, A. Baiker, S.E. Pratsinis, *Top. Catal.* 52 (2009) 1709.
- R. Büchel, R. Strobel, F. Krumeich, A. Baiker, S.E. Pratsinis, *J. of Catal.* 261 (2009) 201.
- R. Burch, T. Watling, *Catal. Lett.* 37 (1996) 51.
- R. Burch, T. Watling, *Appl. Catal. B: Env.* 11 (1997) 207.
- R. Burch, *Top. Catal.* 24 (2003) 97.
- R. Burch, S.T. Daniells, P. Hu, *J. Chem. Phys.* 121 (2004) 2737.
- N.W. Cant, M. Patterson, *Catal. Today* 73 (2002) 271.
- N.W. Cant, I.O.Y. Liu, M.J. Patterson, *J. of Catal.* 243 (2006) 309.

- M. Casapu, J. Grunwaldt, M. Maciejewski, M. Wittrock, U. Göbel, A. Baiker, Appl. Catal. B: Env. 63 (2006) 232.
- M. Casapu, J.-D. Grunwaldt, M. Maciejewski, A. Baiker, S. Eckhoff, U. Göbel, M. Wittrock, J. of Catal. 251 (2007) 28.
- M. Casapu, J. Grunwaldt, M. Maciejewski, A. Baiker, M. Wittrock, U. Göbel, S. Eckhoff, Top. Catal. 42-43 (2007) 3.
- L. Castoldi, I. Nova, L. Lietti and P. Forzatti, Catal. Today 96 (2004) 43.
- L. Castoldi, L. Lietti, R. Matarrese, P. Forzatti, Top. Catal. 52 (2009) 1713.
- L. Castoldi, R. Bonzi, L. Lietti, P. Forzatti, S. Morandi, G. Ghiotti, S. Dzwigaj, J. Catal. 282 (2011) 128.
- D. Chatterjee, P. Koči, V. Schmeißer, M. Marek, M. Weibel, B. Krutzsch, Catal. Today 151 (2010) 395.
- S.S. Chaugule, V.F. Kispersky, J.L. Ratts, A. Yezerets, N.W. Currier, F.H. Ribeiro, W.N. Delgass, Appl. Catal. B: Env. 107 (2011) 26.
- S.S. Chaugule, A. Yezerets, N.W. Currier, F.H. Ribeiro, W.N. Delgass, Catal. Today 151 (2010) 291.
- X. Chen, J. Schwank, J. Li, W.F. Schneider, C.T. Goralski Jr., P.J. Schmitz, Appl. Catal. B: Env. 61 (2005) 164.
- J.-S. Choi, W.P. Partridge, C.S. Daw, Appl. Catal. A: Gen. 293 (2005) 24.

- J.-S. Choi, W.P. Partridge, W.S. Epling, N.W. Currier, T. M. Yonushonis, *Catal. Today* 114 (2006) 102.
- J.-S. Choi, W.P. Partridge, C.S. Daw, *Appl. Catal. B* 77 (2007) 145.
- J.-S. Choi, W.P. Partridge, J.A. Pihl, C.S. Daw, *Catal. Today* 136 (2008) 173.
- J.-S. Choi, W.P. Partridge, M.J. Lance, L.R. Walker, J.A. Pihl, T.J. Toops, C.E.A. Finney, C.S. Daw, *Catal. Today* 151 (2010) 354.
- J.-S. Choi, W.P. Partridge, J.A. Pihl, M.-Y. Kim, P. Kočí, C.S. Daw, *Catal. Today*, 184 (2012) 20.
- R.D. Clayton, M.P. Harold, V. Balakotaiah, *Appl. Catal. B: Env.* 81 (2008) 161.
- R.D. Clayton, M.P. Harold, V. Balakotaiah, *Appl. Catal. B: Env.* 84 (2008) 616.
- R.D. Clayton, M.P. Harold, V. Balakotaiah, *AIChE J.* 55 (2009) 687.
- R.D. Clayton, M.P. Harold, V. Balakotaiah, C.Z. Wan, *Appl. Catal. B: Env.* 90 (2009) 662.
- J.G.E. Cohn, D.R. Steele and H.C. Andersen, US Patent No. 2975025 (1961).
- E. Corbos, S. Elbouazzaoui, X. Courtois, N. Bion, P. Marecot, D. Duprez, *Top. Catal.* 42-43 (2007) 9.
- E. Corbos, X. Courtois, N. Bion, P. Marecot, D. Duprez, *Appl. Catal. B: Env.* 80 (2008) 62.
- E.C. Corbos, X. Courtois, F. Can, P. Marécot, D. Duprez, *Appl. Catal. B: Env.* 84 (2008) 514.

- E.C. Corbos, M. Haneda, X. Courtois, P. Marecot, D. Duprez, H. Hamada, *Catal. Comm.* 10 (2008) 137.
- E.C. Corbos, M. Haneda, X. Courtois, P. Marecot, D. Duprez, H. Hamada, *Appl. Catal. A: Gen.* 365 (2009) 187.
- C. Courson, A. Khalfi, M. Mahzoul, S. Hodjati, N. Moral, A. Kiennemann, P. Gilot, *Catal. Comm.* 3 (2002) 471.
- L. Cumaranatunge, S.S. Mulla, A. Yezerets, N.W. Currier, W.N. Delgass, F.H. Ribeiro, *J. Catal.* 246 (2007) 29.
- A.K. Datye, Q. Xu, K.C. Kharas, J.M. McCarty, *Catal. Today* 111 (2006) 59.
- S.C. Davis, S.W. Diegel. U.S. Department of Energy, Office of Energy Efficiency and Renewal Energy. *Transportation Energy Data Book: Edition 24*, ORNL-6973. December 2004.
- J. Dawody, L. Eurenus, H. Abdulhamid, M. Skoglundh, E. Olsson, E. Fridell, *Appl. Catal. A: Gen.* 296 (2005) 157.
- J. Dawody, M. Skoglundh, S. Wall, E. Fridell, *J. Molec. Catal. A: Chem.* 225 (2005) 259.
- P. Denton, A. Giroir-Fendler, H. Praliaud, M. Primet, *J. Catal.* 189 (2000) 410.
- V. Easterling, Y. Ji, M. Crocker, J. Ura, J.R. Theis, R.W. McCabe, *Catal. Today* 151 (2010) 338.
- V. Easterling, Y. Ji, M. Crocker, M. Dearth, R.W. McCabe, *Appl. Catal. B: Env.* 123-124 (2012) 339.

- P. Eastwood. *Critical Topics in Exhaust Gas Aftertreatment Research* Studies Press, Ltd., Baldock, Hertfordshire, England, 2000 p.231.
- S. Elbouazzaoui, X. Courtois, P. Marecot, D. Duprez, *Top. Catal.* 30/31 (2004) 493.
- S. Elbouazzaoui, E.C. Corbos, X. Courtois, P. Marecot, D. Duprez, *Appl. Catal. B: Env.* 61 (2005) 236.
- U. Elizundia, R. López-Fonseca, I. Landa, M.A. Gutiérrez-Ortiz, J.R. González-Velasco, *Top. Catal.* 42–43 (2007) 37.
- W.S. Epling, G.C. Campbell, J.E. Parks, *Catal Lett* 90, (2003) 45.
- W.S. Epling, L.E. Campbell, A. Yezerets, N.W. Currier, J.E. Parks II, *Catal. Rev.* 46 (2004) 163.
- W.S. Epling, J.E. Parks, G.C. Campbell, A. Yezerets, N.W. Currier, L.E. Campbell, *Catal. Today* 96 (2004) 21.
- W.S. Epling, A. Yezerets, N.W. Currier, *Catal. Lett.* 110 (2006) 143.
- W.S. Epling, A. Yezerets, N.W. Currier, *Appl. Catal. B: Env.* 74 (2007) 117.
- S. Erkfeldt, E. Jobson, M. Larrson, *Top. Catal.* 16/17 (2001) 127.
- G. Ertl, H. Knözinger, J. Weitkamp. *Environmental Catalysis*, Wiley-VCH, New York, 1999.
- P.T. Fanson, M.R. Horton, W.N. Delgass, J. Lauterbach, *Appl. Catal. B: Env.* 46 (2003) 393.

- N. Fekete, R. Kemmler, D. Voigtländer, B. Krutzsch, E. Zimmer, G. Wenninger, W. Strehlau, J. van den Tilaart, J. Leyrer, E. Lox, W. Müller, SAE Technical Paper Series 970746 (1997).
- F. Fajardie, J.-F. Tempere, J.-M. Manoli, O. Touret, G. Djéga-Mariadassou, Catal. Lett. 54 (1998) 187.
- P. Forzatti, L. Castoldi, I. Nova, L. Lietti, E. Tronconi, Catal. Today 117 (2006) 316.
- P. Forzatti, L. Castoldi, L. Lietti, I. Nova, E. Tronconi, Stud. Surf. Sci. Catal. 171 (2007) 175.
- P. Forzatti, L. Lietti, I. Nova, Energy & Env Sci. 1 (2008) 236.
- P. Forzatti, L. Lietti, Catal. Today 155 (2010) 131.
- P. Forzatti, L. Lietti, N. Gabrielli, Appl. Catal. B: Env. 99 (2010) 145.
- E. Fridell, M. Skoglundh, S. Johansson, H. Persson, B. Westerberg, A. Törncrena, G. Smedler, Stud. Surf. Sci. Catal. 116 (1998) 537.
- E. Fridell, H. Persson, B. Westerberg, L. Olsson, M. Skoglundh, Catal. Lett. 66 (2000) 71.
- E. Fridell, H. Persson, L. Olsson, B. Westerberg, A. Amberntsson, M. Skoglundh, Top. Catal. 16/17 (2001) 133.
- E. Fridell, A. Amberntsson, L. Olsson, A.W. Grant, M. Skoglundh, Top. Catal. 30/31 (2004) 143.
- L.J. Gill, P.G. Blakeman, M.V. Twigg, A.P. Walker, Top. Catal. 28 (2004) 157.

- G.W. Graham, H.-W. Jen, W. Chun, R.W. McCabe, *J. Catal.* 182 (1999) 228.
- G. Graham, H. Jen, W. Chun, H. Sun, X. Pan, R. McCabe, *Catal. Lett.* 93 (2004) 129.
- C.G. Granqvist, R.A. Buhrman, *J. of Catal.* 42 (1976) 477.
- P.-H. Han, Y.-K. Lee, S.-M. Han, H.-K. Rhee, *Top. Catal.* 16/17 (2001) 165.
- R.H. Heck, R.J. Farrauto, *Appl. Catal A: General*, 221 (2001) 443.
- R.M. Heck, R.J. Farrauto. *Catalytic Air Pollution Control: Commercial Technology*, 2nd ed., John Wiley and Sons, Inc., New York, 2002.
- W.C. Hecker, A.T. Bell, *J. Catal.* 92 (1985) 247.
- J. Hepburn, E. Thanasiu, D. Dobson, W. Watkins, SAE Technical Paper 962051 (1996).
- H. Hirano, T. Yamada, K.I. Tanaka, J. Siera, P. Cobden, B.E. Nieuwenhuys, *Surf. Sci.* 262 (1992) 97.
- H. Hirano, T. Yamada, K.I. Tanaka, J. Siera, B.E. Nieuwenhuys, *Stud. Sci. Catal.* 75 (1993) 345.
- T.K.N. Hoang, L. Derimaeker, V.B. La, R. Finsy, R. Langmuir 20 (2004) 8966.
- S. Hodjati, C. petit, V. Pitchon, A. Kienneman, *Catal. Today* 59 (2000) 323.
- G. Jacobs, L. Williams, U. Graham, D. Sparks, B. Davis, *Appl. Catal., A: Gen.* 252 (2003) 107.
- D. James, E. Fourré, M. Ishii, M. Bowker, *Appl. Catal. B: Env.* 45 (2) (2003) 147.

B.-H. Jang, T.-H. Yeon, H.-S. Han, Y.-K. Park, J.-E. Yie, *Catal. Lett.* 77 (2001) 21.

Y. Ji, T.J. Toops, U.M. Graham, G. Jacobs, M. Crocker, *Catal. Lett.* 110 (2006) 29.

Y. Ji, T.J. Toops, M. Crocker, *Catal. Lett.* 119 (2007) 257.

Y. Ji, J.S. Choi, T.J. Toops, M. Crocker, M. Naseri, *Catal. Today* 136 (2008) 146.

Y. Ji, T.J. Toops, M. Crocker, *Catal. Lett.* 127 (2009) 55.

Y. Ji, T.J. Toops, J.A. Pihl, M. Crocker, *Appl. Catal. B: Env.* 91 (2009) 329.

Y. Ji, C. Fisk, V. Easterling, U. Graham, A. Poole, M. Crocker, J.-S. Choi, W. Partridge, K. Wilson, *Catal. Today* 151 (2010) 362.

Y. Ji, V. Easterling, U. Graham, C. Fisk, M. Crocker, J.-S. Choi, *Appl. Catal. B: Env.* 103 (2011) 413.

M.F.L. Johnson, *J. Catal.* 123 (1990) 245.

T. Johnson, *Platinum Metals Rev.* 52 (2008) 23.

P. Jozsa, E. Jobson, M. Larsson, *Top. Catal.* 30-31 (2004) 177.

K.S. Kabin, R.L. Muncrief, M.P. Harold, *Catal. Today* 96 (2004) 79.

K.S. Kabin, R.L. Muncrief, M.P. Harold, Y. Li, *Chem. Eng. Sci.* 59 (2004) 5319.

K.S. Kabin, P. Khanna, R.L. Muncrief, V. Medhekar, M.P. Harold, *Catal. Today* 114 (2006) 72.



- J. Kašpar, P. Fornasiero, M. Graziani, *Catal. Today* 50 (1999) 285.
- A. Kato, S. Matsuda, T. Kamo, F. Nakajima, H. Kuroda, T. Narita, *J. Phys. Chem.* 85 (1981) 4099.
- S. Kikuyama, I. Matsukuma, R. Kikuchi, K. Sasaki, K. Eguchi, *Appl. Catal. A: Gen.* 226 (2002) 23.
- D. Kim, Y. Chin, J. Kwak, J. Szanyi, C.H.F. Peden. *Catal. Letters* 105 (2005) 259.
- D. Kim, Y. Chin, G. Muntean, A. Yereretz, N. Currier, W. Epling, H. Chen, H. Hess, C.H.F Peden, *Ind. Eng. Chem. Res.* 45 (2006) 8815.
- D.H. Kim, J. Szanyi, J.H. Kwak, T. Szailer, J. Hanson, C.M. Wang, C.H.F. Peden, *J. Phys. Chem. B* 110 (2006) 10441.
- D.H. Kim, J.H. Kwak, J. Szanyi, S.D. Burton, C.H.F. Peden, *Appl. Catal. B: Env.* 72 (2007) 233.
- D.H. Kim, Y.-H. Chin, J.H. Kwak, C.H.F. Peden, *Catal. Lett.* 124 (2008) 39.
- D. Kim, J. Kwak, X. Wang, J. Szanyi, C.H.F. Peden, *Catal. Today* 136 (2008) 183.
- D. Kim, J. Kwak, J. Szanyi, S. Cho, C.H.F. Peden. *J. of Phys. Chem.* 112 (2008) 2981.
- T. Kobayashi, T. Yamada, K. Kayano, *SAE Technical Paper Series* 970745 (1997).
- T.P. Kobylinski, B.W. Taylor, *J. of Catal.* 33 (1974) 376.
- P. Kőci, F. Plat, J. Stepanek, M. Kubicek, M. Marek, *Catal. Today* 137 (2008) 253.

- P. Kočí, F. Plát, J. Šěpánek, Š. Bártoová, M. Marek, M. Kubček, V. Schmeißer, D. Chatterjee, M. Weibel, *Catal. Today* 147S (2009) S257.
- M. Koebel, M. Elsener, G. Madia, *Ind.Eng. Chem. Res.* 40 (2001) 52.
- B.R. Kromer, L. Cao, L. Cumarantunge, S.S. Mulla, J.L. Ratts, A. Yezerets, N.W. Currier, F.H. Ribeiro, W.N. Delgass and J.M. Caruthers, *Catal. Today* 136 (2008) 93.
- H. Kubicka, *J. of Catal.* 12 (1968) 223.
- A. Kumar, M.P. Harold, V. Balakotaiah, *J. Catal.* 270 (2010) 214.
- J.H. Kwak, D.H. Kim, T. Szailer, C.H.F. Peden, J. Szanyi, *Catal.Lett.*111 (2006) 119.
- J. Kwak, D. Kim, J. Szanyi, C.H.F. Peden, *Appl. Catal. B: Env.* 84 (2008) 545.
- L. Kylhammar, R. Carlsson, H. Ingelsten, H. Grönbeck, M. Skoglundh, *Appl.Catal. B: Env.* 84 (2008) 268.
- R.S. Larson, J.A. Pihl, V. Kalyana Chakravarthy, T.J. Toops, C.S. Daw, *Catal. Today* 136 (2008) 104.
- J.-H. Lee, H.H. Kung, *Catal. Lett.* 51 (1998) 1.
- T. Lesage, C. Verrier, P. Bazin, J. Saussey, S. Malo, C. Hedouin, G. Blanchard, M. Daturi, *Top. Catal.* 30/31 (2004) 31.
- T. Lesage, C. Verrier, P. Bazin, J. Saussey, M. Daturi, *Phys. Chem. Chem. Phys.* 5 (2003) 4435.

X. Li, M. Meng, P. Lin, Y. Fu, T. Hu, Y. Xie, J. Zhang, *Top. Catal.* 22 (2003) 111.

L. Lietti, P. Forzatti, I. Nova, E. Tronconi, *J. Catalysis* 204 (2001) 175.

L. Letti, I. Nova, P. Forzatti, *J. Catal.* 257 (2008) 270.

L. Lietti, N. Artioli, L. Righini, L. Castoldi, P. Forzatti, *Ind. Eng. Chem. Res.* 51 (2012) 7597.

L. Limousy, H. Mahzoul, J. Brilhac, F. Garin, G. Maire, P. Gilot, *Appl. Catal. B: Env.* 45 (2003) 169.

A. Lindholm, N.W. Currier, E. Fridell, A. Yezerets, L. Olsson, *Appl. Catal. B: Env.* 75 (2007) 78.

A. Lindholm, N.W. Currier, J. Li, A. Yezerets, L. Olsson, *J. of Catal.* 258 (2008) 273.

A. Lindholm, A. Sjövall, L. Olsson, *Appl. Catal. B: Env.* 98 (2010) 112.

L.F. Liotta, A. Macaluso, G.E. Arena, M. Livi, G. Centi, G. Deganello, *Catal. Today* 75 (2002) 439.

Z. Liu, J. Anderson, *J. Catal.* 224 (2004) 18.

Z. Liu, J. Anderson, *J. Catalysis* 228 (2004) 243.

R.Q. Long, R.T. Yang, *J. Amer. Chem. Society* 121 (1999) 5595.

J.-Y. Luo, M. Al-Harbi, M. Pang, W.S. Epling, *Appl. Catal. B: Env.* 106 (2011) 664.

A.Z. Ma, W. Grunert, *Chem. Comm. (Cambridge)* 1 (1999) 71.

- H. Mahzoul, J.F. Brilhac, P. Gilot, *Appl. Catal. B: Env.* 20 (1999) 47.
- H. Mahzoul, J. Brilhac, B. Stanmore, *Top. Catal.* 16/17 (2001) 293.
- D. Martin, D. Duprez, *J. Molec. Catal. A: Chem.* 118 (1997) 113.
- N. Macleod, R.M. Lambert, *Appl. Catal. B: Env.* 46 (2003) 483-495.
- E. Mamontov, T. Egami, R. Brezny, M. Koranne, S. Tyagi, *J. Phys. Chem. B* 104 (2000) 11110.
- A. Martínez-Arias, M. Fernández-García, A. Iglesias-Juez, A.B. Hungria, J.A. Anderson, J.C. Conesa, J. Soria, *Appl. Catal. B: Env.* 38 (2002) 151.
- S. Matsumoto, *CATTECH* 4 (2000) 102.
- J. McCarthy Jr., T. Korhumel Jr., A. Marougy, *SAE Technical Paper Series* 2009-01-2835 (2009).
- N. Miyoshi, S. Matsumoto, K. Katoh, T. Tanaka, J. Hardara, N. Takashi, K. Yokota, M. Sugiura, K. Kasahara, *SAE Technical Paper Series* 950809 (1995).
- T. Morita, N. Suzuki, N. Satoh, K. Wada and H. Ohno, *SAE Technical Paper Series* 2007-01-0239 (2007).
- S.S. Mulla, N. Chen, L. Cumarantunge, G.E. Blau, D.Y. Zemlyanov, W.N. Delgass, W.S. Epling, F.H. Ribeiro, *J. Catal* 241 (2006) 389.
- S.S. Mulla, S.S. Chaugule, A. Yezerets, N.W. Currier, W.N. Delgass, F.H. Ribeiro, *Catal. Today* 136 (2008) 136.
- R.L. Muncrief, R. Khanna, K.S. Kabin, M.P. Harold, *Catal. Today* 98 (2004) 393.

C.K. Narula, S.R. Nakouzi, R. Wu, C.T. Goralski Jr., L.F. Allard Jr., *AIChE J.* 47 (2001) 744.

T. Nakatsuji, M. Matsubara, J. Rouistenmaki, N. Sato, H. Ohno, *Appl. Catal. B: Env.* 77 (2007) 190.

K. Nguyen, H. Kim, B.G. Bunting, T.J. Toops, C.S. Yoon, *SAE Technical Paper Series* 2007-01-0470 (2007).

I. Nova, L. Castoldi, L. Lietti, E. Tronconi, P. Forzatti, *Catal. Today* 75 (2002) 431.

I. Nova, L. Castaldi, L. Lietti, E. Tronconi, P. Forzatti, F. Prinetto, G. Ghiotti, *J. Catal.* 222 (2004). 377.

I. Nova, L. Castoldi, F. Prinetto, V. Dal Santo, L. Lietti, E. Tronconi, P. Forzatti, G. Ghiotti, R. Psaro, S. Recchia, *Top. Catal.* 30-31 (2004) 181.

I. Nova, L. Castoldi, L. Lietti, E. Tronconi, P. Forzatti, F. Prinetto, G. Ghiotti, *SAE Technical Paper*, 2005-01-1085.

I. Nova, L. Lietti, L. Castoldi, E. Tronconi, P. Forzatti, *J. Catal.* 239 (2006) 244.

I. Nova, L. Castoldi, L. Lietti, E. Tronconi, P. Forzatti, *SAE Technical Paper Series* 2006-01-1368 (2006).

I. Nova, L. Castoldi, L. Lietti, E. Tronconi, and P. Forzatti, *Top. Catal.* 42–43, (2007) 21.

I. Nova, L. Lietti, P. Forzatti, *Catal. Today* 136 (2008) 128.

H. Ohtsuka, T. Tabata, *Appl. Catal. B: Env.* 29 (2001) 177.

H. Ohtsuka, *Appl. Catal. B: Env.* 33 (2001) 325.

- L. Olsson, B. Westerberg, H. Persson, E. Fridell, M. Skoglundh, B. Andersson, *J. Phys. Chem. B* 103 (1999) 10433.
- L. Olsson, H. Persson, E. Fridell, M. Skoglundh, B. Andersson, *J. Phys. Chemistry B* 105 (2001) 6895.
- L. Olsson, E. Fridell, M. Skoglundh, B. Andersson, *Catal. Today* 73 (2002) 263.
- L. Olsson, E. Fridell, *J. of Catal.* 210 (2002) 340..
- N.A. Ottinger, T.J. Toops, K. Nguyen, B.G. Bunting, J. Howe, *App. Catal. B: Env.* 101 (2011) 486.
- F. Oudet, P. Courtine, A. Vejux, *J. Catal.* 114 (1988) 112.
- D.H. Parker, B.E. Koel, *J. of Vacuum Sci. Tech. A: Vac. Surf. Films* 8 (1990) 2585.
- J. Parks, V. Prikhodko, SAE Technical Paper Series 2009-01-2739 (2009).
- W.P. Partridge, T.J. Toops, J.B. Green, T.R. Armstrong, *J. Power Sources* 160 (2006) 454.
- W.P. Partridge, J.-S. Choi, *Appl. Catal. B: Env.* 91 (2009) 144.
- V.I. Parvulescu, G. Grange, B. Delom, *Catal. Today* 46 (1998) 233.
- A.J. Paterson, D.J. Rosenberg, J.A. Anderson, *Stud. Surf. Sci. Catal.* 138 (2001) 429.
- M.A. Peralta, V.G. Milt, L.M. Cornaglia, C.A. Querini, *J. Catal.* 242 (2006) 118.
- V. Perrichon, L. Retailleau, P. Bazin, M. Daturi, J.C. Lavalley, *Appl. Catal.* 260 (2004) 1.

- A. Phatak, N. Koryabkina, S. Rai, J.L. Ratts, W. Ruettinger, R.J. Farrauto, G.E. Blau, W.N. Deglass, F.H. Ribeiro, *Catal. Today* 123 (2007) 224.
- M. Piacentini, M. Maciejewski, A. Baiker, *Top. Catal.* 42-43 (2007) 55.
- S. Phillip, A. Drochner, J. Kunert, H. Vogel, J. Theis, E. Lox, *Top. Catal.* 30/31 (2004) 235.
- J. Pihl, J. Parks, C. Daw, T. Root, SAE Technical Paper Series 2006-01-3441 (2006).
- M. Pijolat, M. Dauzat, M. Soustelle, *Solid State Ionics* 50 (1992) 31.
- S. Poulston, R. Rajaram, *Catal. Today* 81 (2003) 603.
- V.Y. Prikhodko, K. Nguyen, J.-S. Choi, C.S. Daw, *Appl. Catal. B: Env.* 92 (2009) 9.
- F. Prinetto, G. Ghiotti, I. Nova, L. Lietti, E. Tronconi, P. Forzatti, *J. Phys.Chem B* 105 (2001) 12732.
- K. Ramanathan, V. Balakotaiah, D.H. West, *Chem. Eng. Sci.* 58 (2003) 1381.
- F. Rodrigues, L. Juste, C. Potvin, J.F. Tempère, G. Blanchard, G. Djéga-Mariadassou, *Catal. Lett.* 72 (2001) 59.
- E. Rohart, V. Bellière-Baca, K. Yokota, Harlé, C. Pitois, *Top. Catal.* 42-43 (2007) 71.
- F. Rohr, S. Peter, E. Lox, M. Kögel, A. Sassi, L. Juste, C. Rigau, G. Belot, P. Gélina, M. Primet, *Appl. Catal. B: Env.* 56 (2007) 201.
- F. Rohr, U. Gobel, P. Kattwinkel, S. Philipp, P. Gelin, *Appl. Catal. B: Env.* 70 (2007) 189.

- S. Salasc, M. Skoglundh, E. Fridell, *Appl. Catal. B: Env.* 36 (2002) 145.
- H. Schaper, E.B.M. Doesburg, L.L. Van Reigen, *Appl. Catal.* 7 (1983) 211.
- H. Schaper, E.B.M. Doesburg, P.H.M. De Korte, L.L. Van Reijen, *Solid State Ionics* 16 (1985) 261.
- V. Schmeißer, D. Chatterjee, M. Weibel, *Top. Catal.* 42–43, (2007) 77.
- P.J. Schmitz, R.J. Baird, *J. Phys. Chem. B* 106 (2002) 4172.
- A. Scotti, I. Nova, E. Tronconi, L. Castaldi, L. Lietti, P. Forzatti, *Ind. Eng. Chem. Res.* 43 (2004) 4522
- C. Sedlmair, K. Seshan, A. Jentys, J.A. Lercher, *Catal. Today* 75 (2002) 413.
- C. Sedlmair, K. Seshan, A. Jentys, J.A. Lercher, *J. of Catal.* 214 (2003) 308.
- J. Segner, W. Vielhaber, G. Ertl, *Israel J. of Chem.* 22 (1982) 375.
- H. Shinjoh, N. Takahashi, K. Yokota, *Top. Catal.* 42/43 (2007) 215.
- E. Shustorovich and A.T. Bell, *Surf. Sci.* 289 (1993) 127.
- J. Sjöblom, K. Papadakis, D. Creaser, C.U. I. Odenbrand, *Catal. Today* 100 (2005) 243.
- M. Skoglundh, H. Johansson, L. Löwendahl, K. Jansson, L. Dahl, B. Hirschauer, *Appl. Catal. B: Env.* 7 (1996) 299.
- R. Snow, D. Dobson, R. Hammerle, S. Katare, *SAE Technical Paper Series* 2007-01-0469 (2007).



- R. Snow, G. Cavataio, D. Dobson, C. Montreuil, R. Hammerle, SAE Technical Paper Series 2007-01-1244 (2007).
- A. Stakheev, P. Gabrielsson, I. Gekas, N. Teleguina, G. Bragina, N. Tolkachev, G. Baeva, Top. Catal. 42-43 (2007) 143.
- H.G. Stenger Jr., J.S. Hepburn, Energy Fuels 1 (1987) 412.
- R. Strobel, F. Krumeich, S.E. Pratsinis, A. Baiker, J. Catal. 243 (2006) 229. M. Symalla, A. Drochner, H. Vogel, S. Phillip, U. Göbel, W. Müller, Top. Catal. 42-43 (2007) 199.
- T. Szailer, J. Kwak, D. Kim, J. Hanson, C. Peden, J. Szanyi, J. Catal. 239 (2006) 51.
- N. Takahashi, H. Shinjoh, T. Iijima, T. Suzuki, K. Yamazaki, K. Yokota, H. Suzuki, N. Miyoshi, S. Matsumoto, T. Tanizawa, T. Tanaka, S. Tateishi, K. Kasahara, Catal. Today 27 (1996) 63.
- N. Takahashi, A. Suda, I. Hachisuka, M. Sugiura, H. Sobukawa, H. Shinjoh, Appl. Catal. B: Env. 72 (2007) 187.
- M. Takeuchi, S. Matsumoto, Top. Catal 28 (2004) 151.
- J. Theis, J. Ura, C. Goralski, H. Jen, E. Thanasiu, Y. Graves, A. Takami, H. Yamada, S. Miyoshi, SAE Technical Paper Series 2003-01-1160.
- J. Theis, E. Gulari, SAE Technical Paper Series 2006-01-0210 (2006).
- J.R. Theis, J.A. Ura, R.W. McCabe, SAE Technical Paper Series 2007-01-1055 (2007).
- J.R. Theis, J.A. Ura, R.W. McCabe, SAE Technical Paper Series 2010-01-0300 (2010).

J.R. Theis, M. Dearth, R. McCabe, SAE Technical Paper Series 2011-01-0305 (2011).

] R.G. Tonkyn, R.S. Disselkamp, C.H.F. Peden, Catal. Today 114 (2006) 94.

J.R. Theis, E. Gulari, Appl. Catal. B: Env. 75 (2007) 39.

T.J. Toops, D.B. Smith, W.S. Epling, J.E. Parks, W.P. Partridge, Appl. Catal. B: Env. 58 (2005) 255.

T.J. Toops, B.G. Bunting, K. Nguyen, A. Gopinath, Catal. Today 123 (2007) 285.

T. Truex, SAE Technical Paper Series 1999-01-1543 (1999).

G. Tuenter, W.F. van Leeuwen, L.J. Sneyvangers, Ind. Eng. Chem. Res. Dev. 25 (1986) 633.

U. Tuttlies, V. Schmeißer, G. Eigenberger, Chem. Eng. Sci. 59 (2004) 4731.

J.A. Ura, C.T. Goralski, Jr., G.W. Graham, R.W. McCabe, SAE Technical Paper Series 2005-01-1114 (2005).

U.S. Patent Appl. US2004/0076565, and U.S. Patents 7332135, 7485273, 7640730, and 7674743.

D. Uy, A.E. O'Neill, J. Li, W.L.H. Watkins, Catal. Lett. 95 (2004) 191.

M. Vaarkamp, J.T. Miller, F.S. Modica, G.S. Lane, D.C. Koningsberger, J. Catal. 138 (1992) 675.

M. Vaarkamp, J.T. Miller, F.S. Modica, D.C. Koningsberger, J. Catal. 163 (1996) 294.

J. Wang, M. Crocker, unpublished data.

- J. Wang, Y. Ji, V. Easterling, M. Crocker, M. Dearth, R.W. McCabe, *Catal. Today* 175 (2011) 83.
- J. Wang, Y. Ji, U. Graham, C. Cesar Spindola de Oliveira, M. Crocker, *Chinese J. of Catal.* 32 (2011) 736.
- J. Wang, Y. Ji, Z. Hea, M. Crocker M. Dearth, R.W. McCabe, *Appl. Catal. B: Env.* 111–112 (2012) 562.
- M. Waqif, P. Bazin, O. Saur, J. Lavalley, G. Blanchard, O. Touret, *Appl. Catal. B* 11 (1997) 193.
- X. Wei, X. Liu, M. Deeba, *Appl. Catal. B: Env.* 58 (2005) 41.
- M. Weibel, N. Waldbüßer, R. Wunsch, D. Chatterjee, B. Bandl-Konrad, B. Krutzsch, *Top. in Catal.* 52 (2009) 1702.
- B. Westerberg, E. Fridell, *J. of Molec. Catal. A: Chem.* 165 (2001) 249.
- B. Westerberg, E. Fridell, *J. of Molec. Catal. A: Chem.* 165 (2001) 249.
- S. Xie, G. Mestl, M.P. Rosynek, J. H. Lunsford, *J. Amer. Chem. Soc.* 119 (1997) 10186.
- E. Xue, K. Seshan, J.R.H. Ross, *Roles of Supports*, *Appl. Catal. B: Env.* 11 (1996) 65.
- T. Yang, T. Chang, C. Yeh, *Jo. of Molec. Catal. A: Chem.* 115 (1997) 339.
- C.-W. Yi, J.H. Kwak, C.H.F. Peden, C. Wang, J. Szanyi, *J. of Phys. Chem. C: Lett.* 111 (2007) 14942.
- C.W. Yi, J.H. Kwak, J. Szanyi, *J. Phys. Chem. C.* 111 (2007) 15299.

- J. Xu, R. Clayton, V. Balakotaiah, M.P. Harold, Appl. Catal. B: Env. 77 (2008) 395.
- L. Xu, R. McCabe, W. Ruona, G. Cavataio, SAE Technical Paper Series 2009-01-0285 (2009).
- L. Xu, R. McCabe, M. Dearth, W. Ruona, SAE Technical Paper Series 2010-01-0305 (2010).
- L. Xu, R.W. McCabe, Catal. Today 184 (2012) 83.
- L. Xu, R. McCabe, P. Tennison, H-W. Jen, SAE Technical Paper Series 2011-01-0308 (2011).
- L. Xu, R.W. McCabe, H.S. Gandhi, C.N. Montreuil, U.S. Patent allowed, July, 2011.
- K. Yamamoto, R. Kikuchi, T. Takeguchi, K. Eguchi, J. Catal. 238 (2006) 449.
- M. Yang, Y. Li, J. Wang, M. Shen, J. Catal. 271 (2010) 228.
- H. Yoshida, Y. Yazawa, N. Takagi, A. Satsuma, T. Tanka, S. Yoshida, T. Hattori, J. Synchrotron Radiation 6 (1999) 471.
- G. Zhou, T. Luo, R.J. Gorte, Appl. Catal. B: Env. 64 (2006) 88.
- R. Zukerman, L. Vradman, M. Herskowitz, E. Liverts, M. Liverts, A. Massner, M. Weibel, J.F. Brilhac, P.G. Blakeman, L.J. Peace, Chem. Eng. J. 155 (2009) 419.

## VITA

**Vencon Glenn Easterling.**

### **Personal Information.**

Place of birth: Ashland, Kentucky

### **Education.**

University of Kentucky  
Lexington, KY U.S.A.  
Bachelor of Science Degree in Chemical Engineering (1999)  
Environmental Engineering Certificate Option

University of Kentucky.  
Center for Applied Energy Research / Department of Chemistry.  
Lexington, KY U.S.A.  
Doctoral studies (2006-2012).  
Advisor: Prof. Mark Crocker. Co-advisor: Prof. Stephen Rankin.

### **Professional positions**

AK Steel Corporation  
Ashland Works  
Amanda Blast Furnace  
Ashland, KY U.S.A.  
Process Engineer (June 1999 - November 2003)

McWane, Incorporated  
McWane Cast Iron Pipe Company  
Birmingham, AL U.S.A.  
Management Trainee (February 2004 - August 2004)

United States Steel Corporation  
Fairfield Works  
#8 Blast Furnace  
Blowing Foreman (August 2004 - September 2005)

### **Awards, Honors, and Scholarships:**

- Department of Energy (DOE) Award # DE-FC26-05NT42631, DE-EE0000205
- University of Kentucky Center for Applied Energy Research (UK CAER).  
Research Assistantship (2006-2012).
- Ford Motor Company  
University Research Program Awardee (2008-2011)
- North America Metal Catalysis Society (NAMS)

Richard J. Kokes Travel Award program of NACS, 21<sup>st</sup> NAM Conference, San Francisco, CA, June 7-12, 2009

- UK Now Interview with the University of Kentucky President, Dr. Lee Todd  
May 31, 2010

### **Publications:**

- Easterling, V., Ji, Y., Crocker, M., Dearth, M., McCabe, R.W. “An Investigation into the Validity of a Crystallite-Scale Model to Predict the NH<sub>3</sub> Regeneration of a Pt/Rh/BaO/Al<sub>2</sub>O<sub>3</sub> Lean NO<sub>x</sub> Trap Catalyst” In preparation.
- Easterling, V., Ji, Y., Crocker, M., Dearth, M., McCabe, R.W. “Application of SpaciMS to the Study of Ammonia Formation in Lean NO<sub>x</sub> Trap Catalysts” *Applied Catalysis B: Environmental*, 123-124, 339-350 2012, doi:10.1016/j.apcatb.2012.05.002.
- Wang, J.; Ji, Y.; Easterling, V.; Crocker, M.; Dearth, M.; McCabe, R. “The Effect of Regeneration Conditions on the Selectivity of NO<sub>x</sub> Reduction in a Fully Formulated Lean NO<sub>x</sub> Trap Catalyst” *Catalysis Today* (2011), doi:10.1016/j.cattod.2011.02.048.
- Ji, Y.; Easterling, V.; Graham, U.; Fisk, C.; Crocker, M.; Choi, J.-S. “Effect of Aging on the NO<sub>x</sub> Storage and Regeneration Characteristics of Fully Formulated NO<sub>x</sub> Trap Catalysts” *Applied Catalysis B: Environmental*, 103, 413-427, 2011.
- Easterling, V.; Ji, Y.; Crocker, M.; Ura, J.; Theis, J.R.; McCabe, R.W. “Effect of Ceria on the Desulfation Characteristics of Model lean NO<sub>x</sub> trap Catalysts” *Catalysis Today*, 151, 338-346, 2010.
- Ji, Y.; Fisk, C.; Easterling, V.; Graham, U.; Poole, A.; Crocker, M.; Choi, J.-S.; Partridge, W.; Wilson, K. “NO<sub>x</sub> Storage-Reduction Characteristics of Ba-Based Lean NO<sub>x</sub> Trap Catalysts Subjected to Simulated Road Aging” *Catalysis Today*, 151, 362-375, 2010.

### **Professional Conference Presentations (Poster/Oral):**

- Easterling, V.; Crocker, M.; Dearth, M.; McCabe, R.; “Ammonia Formation in Lean NO<sub>x</sub> Trap Catalysts Studied by SpaciMS.” 7<sup>th</sup> International Conference on Environmental Catalysis, September 5, Lyon, France, 2012. -Oral
- Easterling, V.; Crocker, M.; Dearth, M.; McCabe, R.; Harold, M. “A Spatio-temporal Study of Lean NO<sub>x</sub> Trap Regeneration.” 22<sup>nd</sup> North American Metal Catalysis Meeting, June 6, Detroit, MI, 2011. - Oral
- Crocker, M.; Easterling, V.; Wang, J. Dearth, M.; McCabe, R.; Theis, J. “Laboratory Product Speciation Studies of the LNT + in-situ SCR NO<sub>x</sub> Emission

Control Concept.” Directions in Engine-Efficiency and Emissions Research (DEER) Conference, September 27-30, Detroit, MI, 2010. -Oral

- Ji, Y.; Easterling, V.; Fisk, C.; Crocker, M.; Choi, J.-S. "Effect of Aging on the NO<sub>x</sub> Storage and Regeneration Characteristics of Fully Formulated Lean NO<sub>x</sub> Trap Catalysts," 6th International Conference on Environmental Catalysis, September 12-15, Beijing, China, 2010. -Oral
- Easterling, V.; Ji, Y.; Crocker, M.; Ura, J.; Theis, U.R.; McCabe, R.W. "Effect of ceria on the desulfation characteristics of model lean NO<sub>x</sub> trap catalysts," Tri-State Catalysis Society Spring Symposium, April 26, Covington, KY, 2010. - Poster
- Ji, Y.; Easterling, V.; Fisk, C.; Crocker, M.; Choi, J.S. "Effect of Ceria on the Aging Characteristics of Fully Formulated Lean NO<sub>x</sub> Trap Catalysts." Tri-State Catalysis Society Spring Symposium, April 26, Covington, KY, 2010. - Oral
- Ji, Y.; Easterling, V.; Fisk, C.; Graham, U.; Crocker, M.; Choi, J.-S. "Effect of Ceria on the Aging Characteristics of Fully Formulated Lean NO<sub>x</sub> Trap Catalysts." 2010 DOE Crosscut Workshop on Lean Emissions Reduction Simulation, April 20-22, Dearborn, MI, 2010. - Oral
- Easterling, V.; Ura, J.; Theis, J.; McCabe, R.; Crocker, M., "Effect of Ceria on the Desulfation Characteristics of Model Lean NO<sub>x</sub> Trap Catalysts." 21st North American Metal Catalysis Meeting, June 9, San Francisco, CA, 2009. - Poster
- Ji, Y.; Fisk, C.; Easterling, V.; Crocker, M.; Choi, J.S.; Partridge, W. "NO<sub>x</sub> Storage-Reduction Characteristics of Ba-based Lean NO<sub>x</sub> Trap Catalysts Subjected to Simulated Road Aging." 21st North American Metal Catalysis Meeting, June 9, San Francisco, CA, 2009. - Oral
- Easterling, V.; Crocker, M.; Ura, J.; Theis, J.; McCabe, R. "Effect of Ceria on the Sulfation and Desulfation Characteristics of Lean NO<sub>x</sub> Trap Catalysts." Tri-State Catalysis Society Symposium, April 20, Lexington, KY, 2009. - Poster
- Ji, Y.; Easterling, V.; Crocker, M.; Toops, T.J.; Theis, J.; Ura, J.; McCabe, R.W. "Effect of Ceria on the Sulfation and Desulfation Characteristics of Lean NO<sub>x</sub> Trap Catalysts." 5th International Conference on Environmental Catalysis, Aug. 31 - Sept. 3, Belfast, Northern Ireland, 2008. - Oral